



HAL
open science

Adjoint-based aerostructural sensitivity analysis for wing design

Imane Ghazlane

► **To cite this version:**

Imane Ghazlane. Adjoint-based aerostructural sensitivity analysis for wing design. Optimization and Control [math.OC]. Université Nice Sophia Antipolis, 2012. English. NNT : 01B0JJ0DEY6 . tel-00925210

HAL Id: tel-00925210

<https://theses.hal.science/tel-00925210>

Submitted on 7 Jan 2014

HAL is a multi-disciplinary open access archive for the deposit and dissemination of scientific research documents, whether they are published or not. The documents may come from teaching and research institutions in France or abroad, or from public or private research centers.

L'archive ouverte pluridisciplinaire **HAL**, est destinée au dépôt et à la diffusion de documents scientifiques de niveau recherche, publiés ou non, émanant des établissements d'enseignement et de recherche français ou étrangers, des laboratoires publics ou privés.

UNIVERSITE DE NICE-SOPHIA ANTIPOLIS - UFR Sciences
Ecole Doctorale de Sciences Fondamentales Appliquées (EDSFA)

THESE

pour obtenir le titre de
Docteur en Sciences
de l'Université de Nice-Sophia Antipolis
Discipline : **Mathématiques Appliquées**

présentée et soutenue par
Imane Ghazlane

Adjoint-based aerostructural sensitivity analysis for wing design

Thèse dirigée par **Jean-Antoine DESIDERI**
et encadrée par **Gérald Carrier** et **Antoine Dumont**
soutenue le 17/12/2012

Jury :

M. Juan Jose ALONSO	Stanford University	Rapporteur
M. Pierre-Alain BOUCARD	ENS Cachan - LMT	Rapporteur
M. Christophe BLONDEAU	ONERA	Examinateur
M. Antoine DUMONT	ONERA	Examinateur
M. Michel VISONNEAU	CNRS - Ecole Centrale de Nantes	Président
M. Gérald CARRIER	ONERA	Examinateur
Mme Anne GAZAIX	Airbus	Examinatrice
M. Jean-Antoine DÉSIDÉRI	INRIA - OPALE	Directeur

Abstract

This work addresses the development of numerical methods for optimal wing shape design based in compressible flow. It presents the development and the validation of a discrete aero-structural adjoint method for sensitivity analysis with respect to both planform and internal structural design parameters which affect the cost function, be it aerodynamic or structural.

The developments performed in this work are an extension from the aero-elastic adjoint developments performed by Marcelet and are implemented in the CFD code elsA. While the aero-elastic adjoint method assumes that the wing stiffness is frozen, the here developed aero-structural adjoint method allows to consider structural variations. This extension is performed via a structural module, InAirSsi, developed during this work to model the wing box structure. This module is linearized to supply the necessary terms to the adjoint system. The structural module has been validated via the gradient-based sizing of the structural wing box of an Airbus research configuration.

The adjoint solver in the CFD code elsA covers now both planform variations and internal structural variations and allows the gradient computation of either an aerodynamic cost function or a structural cost function. The gradient computed by the aero-structural adjoint method are validated systematically through a comparison with finite differences.

Résumé

Cette thèse a pour cadre le développement de méthodes numériques pour la conception optimale de forme de voilure en aérodynamique compressible. Ce travail a donné lieu au développement et à la validation d'un adjoint discret aéro-structure pour l'analyse de sensibilité par rapport aux paramètres de forme et de structure interne de l'aile dont dépend la fonction d'intérêt, qu'elle soit aérodynamique ou structurale. Les développements logiciels ont été réalisés dans le code de simulation numérique de mécanique des fluides elsA et font suite aux travaux de Marcelet portant sur l'adjoint aéro-élastique et dont ils sont une extension. Alors que pour l'adjoint aéro-élastique, on considère une aile flexible, de caractéristiques structurales constantes, pour l'adjoint aéro-structure, leur variations sont prises en compte. Pour cela, l'extension de la méthode adjointe s'est accompagnée du développement d'un module de modélisation de la structure interne de l'aile. Ce module est linéarisé et vient donc alimenter le système adjoint. Il a été validé par le dimensionnement de la structure primaire d'une configuration de recherche fournie par l'avionneur Airbus. Dans l'état actuel de développement de la méthode adjointe dans le code elsA, on peut donc désormais calculer les sensibilités d'une fonction aérodynamique ou d'une fonction structure par rapport aux paramètres de forme aérodynamique ou de structure interne de l'aile. Le calcul des gradients ainsi obtenus a été validé par des comparaisons systématiques aux différences finies.

Acknowledgements

Durant les trois dernières années, j'ai souvent été curieuse de lire les remerciements des manuscrits de thèse. J'y voyais la tonalité de ce qui allait suivre, l'intensité et le plaisir qu'on eu les auteurs pendant les années consacrées à leurs sujets de thèse. Je veux que la mienne, soit écrite en toute simplicité. Je veux tout d'abord y témoigner du plaisir que j'ai pris à travailler sur mon sujet, mais aussi je veux y exprimer ma gratitude envers mon entourage scientifique. Un entourage qui a été stimulant techniquement mais aussi humainement.

C'est tout d'abord à Monsieur **Daniel Destarac** que je voudrais dire merci. C'est durant mon stage de fin d'étude sur `ffd`¹, à l'étranger, que je me suis intéressée aux activités de l'Onera² sur l'optimisation et au développement de la méthode adjointe: `ffd` jouant un rôle important dans les développements de cette méthode dans le code `elsA`¹. Merci Monsieur Daniel Destarac pour votre disponibilité, pour vos conseils, pour la pertinence et la clarté de vos réponses et merci pour la finesse de votre humour.

Une thèse à l'Onera et en optimisation ne pouvait être -merveilleusement-dirigée que par Monsieur **Jean-Antoine Désidéri**. Merci pour la disponibilité et le temps que vous prenez pour chacun de vos doctorants, merci pour vos encouragements, et merci d'être un passionné des mathématiques.

¹Code d'extraction et de décomposition de traînée

²Office National d'Etudes et Recherche Aérospatiales

¹Ensemble logiciel développé par l'Onera pour la simulation des écoulements complexes externes et internes

Je remercie mes encadrants de thèse **Gérald Carrier** et **Antoine Dumont**. Merci **Gérald** pour tes propositions, ta disponibilité, et d'avoir toujours fait preuve d'optimisme scientifique peut importe le challenge. **Antoine** merci d'avoir toujours su poser LA question technique, celle qui permet de prendre du recul sur une idée, sur un travail, celle qui met les points sur les "H"... Merci pour ta présence professionnelle et amicale, pour tes encouragements, ton écoute et merci surtout de m'avoir laissé tant parler!

Merci également à mon chef d'Unité ACI² Monsieur **Joël Reneaux** de m'avoir accueilli et d'avoir mis tant d'énergie et de temps à résoudre les difficultés administratives que nous avons rencontrés.

MM. les Professeurs **Juan J. Alonso** et **Pierre-Alain** Boucard ont accepté d'être les rapporteurs de cette thèse, et je les en remercie, de même que pour leur participation au Jury. Ils ont également contribué par leurs nombreuses remarques et suggestions à améliorer la qualité de ce mémoire, et je leur en suis très reconnaissante. Je tiens également à remercier, avec gratitude, le Professeur **Michel Visonneau** d'avoir accepté de présider le Jury de soutenance. Merci à Monsieur **Christophe Blondeau** pour les discussions intéressantes et constructive que j'ai pu avoir avec lui au courant de ma thèse et d'avoir accepté de participer au Jury de soutenance. Madame **Anne Gazaix** m'a fait l'honneur de participer au Jury de soutenance; je l'en remercie profondément.

Merci à tous mes collègues de l'unité ACI avec qui ce fut agréable de travailler et d'échanger autour de la machine à café ou des croissants du Vendredi. En particulier, merci **Meryem Marcelet** d'avoir pris le temps de m'introduire à tes travaux de thèse. Merci **Didier Bailly** de m'avoir familiarisé durant les premier mois de ma thèse avec les techniques de RSM. Merci Michael Méheut pour ton aide sur SeanDef. Merci Itham Salah el Din (Issoum) pour ton aide sur LA chaine et puis tout simplement d'avoir

²Unité Avions Civiles

répondu à mes questions à de nombreuses occasions et merci de ta bonne humeur! **Jean-Luc hentrains-Gervois**, merci d'avoir mis à ma dispositions des outils qui m'ont beaucoup aidé pour coder InAirSsi. Je n'oublie pas que sans la précieuse aide de **Christophe Francois** sur le maillage, le chemin aurait été plus long! Merci **Phillipe Guillen** pour ton aide en informatique, celle qui m'a permit de dompter Madmax! Merci **Saloua Ben Khelil** pour ta sensibilité et pour tes sensibilités (celles de ffd!!) et d'avoir relu avec pertinence mon manuscrit. Et merci **Sophie Okerman** pour ta disponibilité et ta gentillesse.

Daigo Maruyama, ce fut fort agréable de t'avoir comme collègue de bureau, merci de nous avoir converti à Saint-Anne! je n'oublie pas mon second "colloc de bureau" **Aurélien Arntz**, merci. Merci à mes collègues avec qui j'ai partagé et avec qui je continue de partager des moments fort agréables: **Ludovic wiart, Mehdi Bordji, Stéphane Burguburu et Biel Ortun. Andrea Minelli**, mon collègue et ami, merci d'être Italien, merci pour ta gentillesse, ta bonne humeur, ta grande cuisine et de m'avoir écouté -sans bugger- parler de mes bugs c++ les derniers mois de thèse!

Un dernier et profond merci ira à mes amis et ma famille.

Un pensée pour ceux qui m'ont accompagné, inspiré et rassuré, sans le savoir, pendant les trois ans de thèse: Yehudi Menuhin, Itzhak Perlman, Pinchas Zukerman, Jascha heifetz et tant d'autres!

Contents

List of Figures	vii
List of Tables	xiii
1 Introduction	1
1.1 Context and Challenges	1
1.2 Our Approach	5
1.3 Organisation of the manuscript	7
2 Aero-structural wing design problem formulation	11
2.1 Preamble	11
2.2 Design space exploration techniques	13
2.2.1 Algorithms for global search	14
2.2.2 Algorithms for local search	17
2.2.3 Constrained optimisation	17
2.2.4 Multi-objective based approaches	19
2.3 The adjoint method in the context of wing shape design	21
2.3.1 Duality and adjoint	24
2.3.2 Discrete and continuous adjoint formulation: a comparison	25
2.4 Aerodynamic and structural trade-off via wing parametrization	28
2.4.0.1 Wing design parameters impact on aero-structural trade-off	31
2.5 Outcome	34

3	From aerodynamic design to aero-structural design using the adjoint method	37
3.1	Preamble	37
3.2	Numerical method for solving the governing flow equations	40
3.2.1	Governing flow equations	40
3.2.2	Finite Volume Discretization	41
3.2.3	Choice of scheme in space and time	42
3.3	Sensitivity analysis using the discrete aerodynamic adjoint method . . .	46
3.3.1	Accuracy of the gradients	48
3.4	Adjoint equations of the aero-elastic problem	50
3.4.1	Flexibility matrix approach	50
3.4.2	Numerical method for fluid and structure coupling	51
3.4.2.1	Aerodynamic load transfer to the structural mesh . . .	52
3.4.2.2	Structural displacement transfer to the CFD volume mesh	53
3.4.3	Flexibility matrix computation for aero-elastic analysis	55
3.4.4	Sensitivity analysis using the discrete aero-elastic adjoint method	62
3.5	Extension of the aeroelastic adjoint method to an aerostructural adjoint method	65
3.6	Outcome	68
4	Development of an adjoint-compatible structural model of the wing	69
4.1	Preamble	69
4.2	Structural model extraction	73
4.2.1	Primary structure elements	75
4.2.2	Elastic axis of the structural model	77
4.3	Wing box mechanical properties	78
4.4	Primary structure elements stress analysis	83
4.4.1	Load type on the wing box	83
4.4.2	Bending normal stress on wing box elements	85
4.4.3	Torsional shear stress on wing box elements	86
4.4.4	Shear stress in Euler-Bernoulli beam	86

4.5	Analytical wing structural weight estimation	87
4.5.1	Empirical methods	88
4.5.2	Analytical methods	88
4.5.3	Physics based methods	88
4.5.4	Wing weight estimation with InAirSsi	90
4.5.4.1	Constrained sizing for wing weight computation	92
4.6	Validation of InAirSsi	94
4.6.1	Computation with InAirSsi of the derivatives required for the adjoint formulation	95
4.6.2	Comparative sizing of four XRF1-based configurations coupling InAirSsi with gradient-based algorithm	98
4.6.3	Analysis of the effect of the parameter ρ for constraint aggregation	103
4.7	Outcome	114
5	From aero-elastic to aero-structural adjoint-based gradients: Detailed description	115
5.1	Preamble	115
5.2	Mathematical formulation	116
5.2.1	Gradient of an aerodynamic cost function w.r.t. α_{geom} :	117
5.2.2	Gradient of an aerodynamic cost function w.r.t. α_{struct} :	119
5.2.3	Gradient of a structural cost function w.r.t. α_{geom} :	120
5.2.4	Gradient of a structural cost function w.r.t. α_{struct} :	120
5.3	Implementation of the aero-structural adjoint method	121
5.3.1	Gradient of an aerodynamic cost function w.r.t. α_{geom} :	122
5.3.1.1	Sensitivity of R_f w.r.t. α_{geom}	122
5.3.1.2	Sensitivity of R_s w.r.t. α_{geom}	123
5.3.2	Gradient of an aerodynamic cost function w.r.t. α_{struct} :	124
5.3.2.1	Sensitivity of R_f w.r.t. α_{struct}	124
5.3.2.2	Sensitivity of R_s w.r.t. α_{struct}	124
5.3.3	Gradient of a structural cost function w.r.t. α_{geom} :	125
5.3.4	Gradient of a structural cost function w.r.t. α_{struct} :	126

5.3.5	Introduction of adjoint equations	126
5.4	Implementation of the derivatives appearing in the gradient of an aerodynamic cost function \mathcal{J}_{aero} and or structural cost function \mathcal{J}_{struct}	131
5.4.1	Terms appearing only in structural functions gradient	132
5.4.2	Terms appearing only in aerodynamic functions gradient	132
5.4.3	Terms appearing in the gradient formulation independently on the nature of the cost function	133
5.4.3.1	Sensitivities of \mathcal{X} , \mathcal{X}_{rig} , \mathcal{X}_{surf} , \mathcal{X}_b :	133
5.4.3.2	Sensitivities of aerodynamic loads L:	134
5.4.3.3	Sensitivities of the flexibility matrix:	137
5.4.3.4	Sensitivities of the structural properties I and J :	138
5.5	Outcome	138
6	Aerodynamic, aero-elastic and aero-structural adjoint-based gradients: results and comparison	141
6.1	Preamble	141
6.2	Test case description	141
6.3	Problem parametrization	142
6.4	Aerodynamic functions evaluation, decomposition and partial sensitivities of these functions with <i>ffd72</i>	147
6.5	Aerodynamic adjoint-based optimisations	147
6.5.1	Gradient validation	147
6.5.2	Application of the aerodynamic adjoint method to the optimisation of the test-case wing	148
6.5.2.1	Optimisation with first wing parametrisation: 5 twist control section + angle of attack	149
6.5.2.2	Optimisation with the second wing parametrisation: 10 twist control section + angle of attack	152
6.5.2.3	Optimization with the third wing parametrisation: 5 twist control section + 25 airfoil control points + angle of attack	155

6.6	Aero-elastic adjoint-based optimizations	159
6.6.1	Aero-elastic gradient validation	159
6.6.2	Application of the aero-elastic adjoint method to the elastic optimization of the test case wing	159
6.7	Aero-structural adjoint gradients	166
6.7.1	Aero-structural gradient validation	166
6.7.2	Remarks on difficulties linked to finite difference step convergence	166
6.7.3	Aero-structural gradient vs aero-elastic gradient	170
6.8	Outcome	172
7	Conclusion and perspectives	175
A	For the users of <i>elsA</i> BAG: module modifications	179
B	Structural sensivity with INAIRSSI	189
B.0.1	Calculation and validation of $\frac{dChord_{1aw}}{d\alpha_{geom}}$	189
C	Wing design	201
	Bibliography	203

List of Figures

1.1	Test-case configuration.	9
1.2	Aero-elastic deformation on the wing of the Airbus A320	10
2.1	Airbus milestones	29
2.2	Elliptic vs. aero-structural optimum lift distribution Source: Martins J., <i>A coupled-adjoint Method for high-fidelity aero-structural optimization</i>	30
2.3	Aircraft design process. Source: Mavris D.N., DeLaurentis D.	31
3.1	Load transfer at beam nodes.	54
3.2	Deflection and twist allocation to the CFD volume mesh points	56
4.1	Input-Output system of the structural module InAirSsi	73
4.2	The structural model of the wing	75
4.3	Primary structure elements in a wing cross section	76
4.4	Maximal thickness to chord ratio distribution on the AIRBUS XRF1 configuration	78
4.5	CATIA vs InAirSsi for I_{xx} of the XRF1 constructed primary structure	81
4.6	CATIA vs InAirSsi for I_{xx} of the full geometrical section of the XRF1 aerodynamic envelope	81
4.7	Bending and twist actions on primary wing box structure	84
4.8	Stress solicitation on primary wing box structure	84
4.9	Finite difference vs differentiation with InAirSsi for KS function	97
4.10	Finite difference vs differentiation with InAirSsi for the structural weight	97

4.11	Spanwise sensitivity of KS at the initial design point function with respect to the 42 thicknesses	97
4.12	Integrated aerodynamic load distributions on the four configurations (calculation at forced angle of attack corresponding to the cruise condition)	100
4.13	Cumulated F_z effort from the wing tip to the root at each spanwise position	101
4.14	Cumulated M_x moment from the wing tip to the root at each spanwise position	101
4.15	Cumulated M_y moment from the wing tip to the root at each spanwise position	101
4.16	Structural weight optimization history for the case conf 10/10	104
4.17	Structural weight optimization history for the case conf 8/8	104
4.18	Structural weight optimization history for the case conf 4/4	104
4.19	Structural weight optimization history for the case conf 4/0	104
4.20	$\rho = 50$: Initial span distribution of the ratio of the bending stress in $\{t_{c_{upp}} + t_{s_{upp}}\}$ to σ_{yield}	107
4.21	$\rho = 50$: Optimized span distribution of the ratio of the bending stress in $\{t_{c_{upp}} + t_{s_{upp}}\}$ to σ_{yield}	107
4.22	$\rho = 100$: Initial span distribution of the ratio of the bending stress in $\{t_{c_{upp}} + t_{s_{upp}}\}$ to σ_{yield}	107
4.23	$\rho = 100$: Optimized span distribution of the ratio of the bending stress in $\{t_{c_{upp}} + t_{s_{upp}}\}$ to σ_{yield}	107
4.24	$\rho = 200$: Initial span distribution of the ratio of the bending stress in $\{t_{c_{upp}} + t_{s_{upp}}\}$ to σ_{yield}	108
4.25	$\rho = 200$: Optimized span distribution of the ratio of the bending stress in $\{t_{c_{upp}} + t_{s_{upp}}\}$ to σ_{yield}	108
4.26	$\rho = 50$: Initial span distribution of the ratio of the torsion stress in $t_{c_{upp}}$ to τ_{yield}	108
4.27	$\rho = 50$: Optimized span distribution of the ratio of the torsion stress in $t_{c_{upp}}$ to τ_{yield}	108

4.28	$\rho = 100$: Initial span distribution of the ratio of the torsion stress in $t_{c_{upp}}$ to τ_{yield} .	109
4.29	$\rho = 100$: Optimized span distribution of the ratio of the torsion stress in $t_{c_{upp}}$ to τ_{yield} .	109
4.30	$\rho = 200$: Initial span distribution of the ratio of the torsion stress in $t_{c_{upp}}$ to τ_{yield} .	109
4.31	$\rho = 200$: Optimized span distribution of the ratio of the torsion stress in $t_{c_{upp}}$ to τ_{yield} .	109
4.32	$\rho = 50$: Initial span distribution of the ratio of the torsion stress in $t_{s_{low}}$ to τ_{yield} .	110
4.33	$\rho = 50$: Optimized span distribution of the ratio of the torsion stress in $t_{s_{low}}$ to τ_{yield} .	110
4.34	$\rho = 100$: Initial span distribution of the ratio of the torsion stress in $t_{s_{low}}$ to τ_{yield} .	110
4.35	$\rho = 100$: Optimized span distribution of the ratio of the torsion stress in $t_{s_{low}}$ to τ_{yield} .	110
4.36	$\rho = 200$: Initial span distribution of the ratio of the torsion stress in $t_{s_{low}}$ to τ_{yield} .	111
4.37	$\rho = 200$: Optimized span distribution of the ratio of the torsion stress in $t_{s_{low}}$ to τ_{yield} .	111
4.38	$\rho = 50$: Initial span distribution of the ratio of the torsion stress in t_{fs} to τ_{yield} .	111
4.39	$\rho = 50$: Optimized span distribution of the ratio of the torsion stress in t_{fs} to τ_{yield} .	111
4.40	$\rho = 100$: Initial span distribution of the ratio of the torsion stress in t_{fs} to τ_{yield} .	112
4.41	$\rho = 100$: Optimized span distribution of the ratio of the torsion stress in t_{fs} to τ_{yield} .	112
4.42	$\rho = 200$: Initial span distribution of the ratio of the torsion stress in t_{fs} to τ_{yield} .	112

4.43	$\rho = 200$: Optimized span distribution of the ratio of the torsion stress in t_{fs} to τ_{yield} .	112
5.1	Evaluation of $\frac{\partial L}{\partial \mathcal{X}_b}$ by finite differences VS linearization	136
6.1	Euler grid of the Airbus XRF1 wing-fuselage configuration	143
6.2	Zoom on the Euler grid of the Airbus XRF1 wing-fuselage configuration	144
6.3	Pressure distribution of the rigid configuration optimized for the C_{D_p} with CFDSQP algorithm. Parametrization with 5 twist control sections and the angle of attack	151
6.4	Pressure distribution of the rigid configuration optimized for the C_{D_p} with CFDSQP algorithm. Parametrization with 10 twist control sections and the angle of attack	153
6.5	Pressure distribution of the rigid configuration optimized for the C_{D_p} with CFDSQP algorithm. Parametrization with 5 twist control sections, 25 airfoil control points and the angle of attack	157
6.6	Twist angle on the control sections of the optimal elastic configuration	162
6.7	Mid-chord camber of control sections of the optimal elastic configuration	163
6.8	Summary of C_{D_p} <u>aerodynamic optimization</u> , performed with DOT algo- rithm. Parametrization with 5 control twist section, 5 camber sections and the angle of attack	164
6.9	Summary of C_{D_p} <u>aero-elastic optimization</u> , performed with DOT algo- rithm. Parametrization with 5 control twist section, 5 camber sections and the angle of attack	165
6.10	aero-structural adjoint-based gradient computation process	167
6.11	Convergence of the norm L_2 of the residual of first equation of the system 3.44 p. 64 (aero-elastic adjoint)	168
6.12	Convergence of the norm L_2 of the residual of first equation of the system 5.40 p. 129 (aero-structural adjoint)	168
B.1	Sensitivity of chord law with respect to twist	190

B.2	Sensitivity of the x-coordinates defining the chord law w.r.t twist	190
B.3	Sensitivity of the front spar web thickness with respect to twist	191
B.4	Sensitivity of lower wing thickness distribution with respect to twist . .	191
B.5	Sensitivity of first spar x-coordinate with respect to twist	192
B.6	Sensitivity of second spar x-coordinate with respect to twist	192
B.7	Sensitivity the leading edge mesh points with respect to twist	193
B.8	Sensitivity of the trailing edge mesh points with respect to twist	193
B.9	Sensitivity of thickness to chord ratio with respect to twist twist	194
B.10	Sensitivity beam node mesh with respect to twist	194
B.11	Sensitivity bending constant w.r.t twist parameter	195
B.12	Gradient of bending stiffness with resepect to skin thickness	196

List of Tables

2.1	Selection of global optimisation algorithms	16
2.2	Selection of local optimisation algorithms	18
4.1	Thickness distribution of the candidate configurations expressed as variations w.r.t. to the reference wing (0%)	99
4.2	Twist distribution of the candidate configurations	99
4.3	Initial structural weight and structural constraints aggregation	102
4.4	Structural weight and structural constraints aggregation at optimization convergence	103
4.5	Redesign results with different values of KS function parameter ρ	105
4.6	Redesign results with different values of the aggregation parameter ρ	106
6.1	Parametrisation dependency on the design problem: aerodynamic, aero-elastic or aero-structure	146
6.2	C_L and C_{D_p} gradient computation: aerodynamic adjoint and FD	148
6.3	Drag extraction and decomposition for both initial and optimised -in terms of C_{D_p} - configurations, $\alpha_{geom} \in \mathbb{R}^6$ (first wing parametrization)	150
6.4	Design parameters for the Initial point and optimized configuration by the CFSQP algorithm using the first parametrisation ($\alpha_{geom} \in \mathbb{R}^6$)	150
6.5	Design parameters for the Initial point and optimized configuration by the CFSQP algorithm using the first parametrisation ($\alpha_{geom} \in \mathbb{R}^{11}$)	152

6.6	Design parameters for the initial point and the optimized configuration by the CFSQP $\alpha_{geom} \in \mathbb{R}^{11}$	154
6.7	Drag extraction and decomposition: initial configuration, optimised NC (optimal in terms of C_{D_p}), $\alpha_{geom} \in \mathbb{R}^{31}$	156
6.8	Design parameters for the initial point and the optimized configuration by the CFSQP $\alpha_{geom} \in \mathbb{R}^{31}$	158
6.9	C_{L_p} and C_{D_p} gradient computation: aero-elastic adjoint and FD	160
6.10	Drag extraction and decomposition for initial, rigid and elastic optimal -in terms of C_{D_p} - configurations, $\alpha_{geom} \in \mathbb{R}^{11}$	161
6.11	C_{l_p} and C_{D_p} gradient computation: aero-structural adjoint and FD	169
6.12	FD step convergence for $\frac{dC_{l_p}}{d\alpha_i}$ computation	170
6.13	FD step convergence for $\frac{dC_{D_p}}{d\alpha_i}$ computation	170
6.14	Comparison of aero-elastic adjoint-based gradient and aero-structural adjoint-based gradient	171
6.15	Comparison of aero-elastic adjoint-based gradient and finite difference with a fixed structural model (to match the aero-elastic hypothesis	171

- \mathcal{A} : the enclosed area of the cross section.
- $D = D(\alpha)$ Displacement field on \mathcal{X}_b
- E Young modulus
- $F = F(I, J)$ Flexibility matrix
- G Shear modulus
- $I = I(\alpha_{struct})$ Bending stiffness of the structure
- $J = J(\alpha_{struct})$ Torsion stiffness of the structure
- \mathcal{J}_{geom} Aerodynamic cost function
- \mathcal{J}_{struct} Structural cost function
- $L = L(\mathcal{X}, \mathcal{X}_b, W^b)$ Aerodynamic loads reduced on \mathcal{X}_b
- n_b Structural mesh nodes
- $n_{\alpha_{geom}}$ Number of planform design variables
- $n_{\alpha_{struct}}$ Number of structural design variables
- n_{α} Number of total design variables
- n_f Number of aerodynamic cost functions
- n_{surf} Number of surface mesh cells
- n_{surf}^I Number of surface mesh cells within the influence area of load nodes
- n_s Number of structural cost functions
- $n_{\mathcal{X}_b}$ Number of structural mesh nodes
- $n_{\mathcal{X}}$ Number of mesh points
- n_{cell} Number of grid cells
- n_{cell}^I Number of grid cells at the interface fluid/structure
- p is the pressure
- Pr is the Prandtl number
- Pr_t is the turbulent Prandtl number
- p_{fs} : Position of the front spar web
- p_{rs} : Position of the rear spar web
- \mathbf{q} is the heat flux vector

- t_{fs} : Thickness of the front spar web
- t_{rs} : Thickness of the rear spar web
- t_{clow} : Thickness of the lower surface spar cap
- t_{cupp} : Thickness of the upper surface spar cap
- t_{slow} : Thickness of the lower surface skin
- t_{supp} : Thickness of the upper surface skin
- $W = W(\alpha)$ Aerodynamic conservative variables on \mathcal{X}
- $W^b = W^b(W, X)$ Aerodynamic conservative variables on \mathcal{X}_{surf}
- $\mathcal{X}_{rig} = \mathcal{X}_{rig}(\alpha_{geom})$ CFD volume mesh of the Jig shape configuration
- $\mathcal{X}_{surf} = \mathcal{X}_{surf}(\mathcal{X}_{rig}(\alpha_{geom}))$ CFD surface mesh
- $\mathcal{X}_b = \mathcal{X}_b(\mathcal{X}_{surf}, \alpha_{struct})$ structural mesh
- $\mathcal{X} = \mathcal{X}(\mathcal{X}_{rig}, \mathcal{X}_b, D)$ Current CFD volume mesh

- α_{geom} Aerodynamic shape design parameters
- α_{struct} Structural design parameters
- $\alpha = (\alpha_{geom}, \alpha_{struct})$
- μ is the viscosity coefficient
- μ_t is the turbulent viscosity coefficient
- τ is the stress tensor due to viscosity
- τ Torsional shearing stress

- CSM Computational Structural Mechanics
- CFD Computational Fluid Dynamics
- FD Finite Differences
- FE Finite Elements

1

Introduction

1.1 Context and Challenges

In 1997, Ilan Kroo writes with good reason (47): “When an aircraft designer hears that a new program will use multidisciplinary optimization, the reaction is often less than enthusiastic”. Fifteen years later, reactions are not altogether different.

The straightforward question that this statement raises is: why this lack of enthusiasm for multidisciplinary optimization? Is it because numerical optimization is entrusted to operate as a designer, or is it the complexity of managing multidisciplinary problems? One can wonder: is it because successful and complex multidisciplinary design optimization (MDO) results, conducted in a research¹ context, are not (easily?) transferable to an industrial context? Or is it simply an “cultural” problem due to the interaction of numerous disciplines? An interaction where each discipline intrudes on others and where the “degree of fidelity” that represents the discipline stands out as a priority over the problem itself.

Yet it is multidisciplinary that drove the evolution from the first² commercial airliner

¹A survey of Professor Holt Ashley (7) counts up between 1964 and 1980, 4550 papers on optimal control, 2142 on aerodynamic optimization and 1381 on structural optimization but mentions no industrial application.

²The concept of “first” depends on the definition we give to airliner: The first aircraft intended initially for commercial service is the *Sikorsky Ilya Muromets* (1913), which became the first four-engine bomber during the World War I and was able to carry 16 passenger. The Farman *Goliath*

to the most recently designed airliners such as the A380 or the B787. This aircraft evolution is the result of more than half a century of complex physical understanding and analysis that extends from aerodynamics and structures to turbo-machinery and includes acoustics, mathematics, etc.

In addition, this evolution is the result of innovative -yet mono-discipline- technologies that were coordinated together aiming at an overall performance. Unfortunately, it seems that this “multidisciplinary” harmony cannot be transposed easily to optimization nor numerical design. Nevertheless the time is right, the aviation sector is on a growing path, the time separating the development of two projects gets longer and the expected performance gain of a new project over its predecessor becomes higher. The design of a new aircraft may less and less rely solely on the experience acquired with the previous one. The incorporation of numerical multidisciplinary tools into design processes is a logical follow-up.

Despite this technological progress of aircraft, profitability of airline companies does not increase. Before developing shortly the reasons, we may already say that this restricted profitability certainly justifies the adoption of multidisciplinary numerical optimization by the aviation industry. There are two main reasons for the profitability restriction:

- (1) First, the last decade successful emergence of companies operating at very low costs.
- (2) Secondly, the continuous increase of oil price.

designed in 1918 as a heavy bomber at the end of the World War I was “recycled” as an airliner with a capacity of 14 passengers. The first all-metal airplane is the three-radial-engined *Tin Goose*, or the Ford Trimotor, developed with a capacity of carrying up to 12 passengers. The Ford Trimotor operates in the same time as The Fokker Trimotor, also an all-metal airplane, that dominated the American market in the 20’s until the crash of 1931. After the crash, the Fokker Trimotor was banned from commercial operations and two years later, the Boeing 247 had its first flight with 14 passengers. The Boeing 247 is probably the first commercial airliner that was intentionally designed for commercial transport and had an advanced design aiming at an aerodynamic performance, and also the first with a semi-monocoque construction. Boeing refused to sell the 247 to any company until United’s order for 60 aircraft was assured. To match the concurrence of United’s, Transcontinental and Western Airline (TWA) requested the development of the DC-2 from Douglas. The larger version of the DC-2, named the DC-3, was constructed 2 years later to replace the sleeper *Curtiss T-32 Condor II* at the request of Americans. The Douglas DC-3 remains the pre-war most popular airliner and cited as *first*.

The second reason stands out with the actual economic context. This also becomes increasingly meaningful in a time where environmental issues are entering the equation as an implicit economical parameter. The logical outcome of this is the focus of airlines and aircraft manufacturers on how to keep fuel consumption down without breaking the performance rise. An even greater stress is placed on the importance of fuel-burn reduction³ (64). Fuel-burn reduction can be achieved through engine efficiency, aerodynamic performance, lightweight materials, etc. But these solutions cannot be treated individually. Indeed, because the flight physics of the aircraft generates strong coupling between the different disciplines, designers are sooner or later faced with trade-offs: manoeuvrability vs stability, aerodynamics vs structural, nacelle drag vs bypass ratio, etc., all impacting the fuel consumptions and the range⁴ but in different manners. This work addresses one of the cited guiding trade-offs: aerodynamics vs structural⁵ performance. Aerodynamic performance is given in terms of drag and structural performance, in terms of structural weight. The present equation is simple, less drag and a lighter aircraft can be understood as less fuel consumption and a more efficient cruise, so that the aircraft can operate over an extended range and carry more payload, but the solution is not straightforward and even complex, because all parameters opened to the designer have direct and conflicting impacts on both disciplines, requiring these trade-offs. In addition, 10s of thousands of load cases must constrain the design of viable wings. However, less drag and lighter structures does not imply the convergence of the aero-structural problem; current aircraft developements with high aspect ratio wings and lighter structures are subject to dynamic aero-elastic problems (flutter, divergence, etc).

Multidisciplinary optimization can play a major role within the aircraft industry to efficiently and robustly find better designs with a higher level of confidence than cur-

³The A320 equipped with *sharklets* reduced their consumption by 3.5% corresponding to an annual CO2 reduction of 700 tones per aircraft

⁴Range=Aerodynamic efficiency×Propulsion efficiency×Structural efficiency

⁵For example: with an increased span, induced drag decreases, however the wing loading increases resulting in a structural weight increases

rently in-use conventions. This can be achieved by managing more efficiently -under the design engineer control- the different trade-offs involved in the design process.

If we need to give a simple definition of optimization -within the engineering context- then let us say that it is not a technique, which intends to offer a simple improvement, but rather a notion of exploitation of the design possibilities and alternatives. Optimization aims at making a design *as good as possible* and a solution *as cost-effective as possible*. All the design possibilities, optimal, worst and non-attractive ones, are embedded into a space (in the mathematical sense): the design space. What optimization is about, is to find the optimal solution among all the possibilities offered in this design space. There is a wide range of algorithms to explore the design space. However, the “fast and accurate” that drives industrial contexts (research context also...) imposes refinement over these methods.

MDO relies on efficient numerical analysis tools for each of the disciplines involved in the considered design process. For aerodynamic analysis, the cost of a single CFD (Computational Fluid Dynamics) evaluation is relatively affordable, but when it comes to optimization and more specifically to gradient-based optimization the cost increases⁶. However, CFD analysis is often concerned, several solutions exist to overcome the simulation time limitation, such as grid coarsening, multi-grid acceleration, use of massive parallel computing, etc. An alternative to the direct use of high fidelity CFD analysis can be the introduction of surrogate models. However this approach, which has received much attention these last years, has a strong limitation in terms of number of design parameters that can be allowed (The “curse of dimensionality”). Indeed, all the response surfaces methods have an accuracy which depends highly on the dimension of the design space. This design space dimension is what defines the richness of the possible solutions. As an illustration, a wing shape parametrized with only camber parameters will offer much less variety than a wing represented by its camber, span, twist, etc. The wider the design space, the more difficult it is for the algorithm to

⁶Interesting discussion on the limits of CFD optimization in terms of computer requirements is conducted by Thevenin in *Optimization and Computational Fluid Dynamics* (81)

converge toward an optimal solution.

The objective of this work is the development of a method used to compute the sensitivities of functions, involved in the design process, with respect to (w.r.t.) the design parameters, regardless of the design space dimension: The adjoint method. This means that the phases in which the optimization algorithm requires the sensitivity analysis will be noticeably shortened⁷. An attractive method in the context of large number sets of design parameters, where gradient-based optimization techniques have an advantage over other -global- optimization techniques, such as non-deterministic or surrogate based optimization techniques.

The developments concern the introduction of multidisciplinary -aerodynamic and structure- into the computation of the adjoint-based gradients. As mentioned previously, a special care has to be given to the aero-structural trade-off. The gradients of each single discipline cost function, computed with the adjoint method, have to take into account the dependence on the state variables of the other competing disciplines. In summary, the aero-structural adjoint method satisfies first, the need of incorporating multidisciplinary analysis and optimization in design cycle. Secondly, the need to converge in a short time toward a better aerodynamic and structural optimum.

1.2 Our Approach

Objectives

If the potential benefits from multidisciplinary optimization are clearly apparent, its actual and practical incorporation into a design process is less evident. Conceptual to preliminary design stages are ideal candidates for methods such the one developed in this work. For these early stages, we aim at developing a technique that can be incorporated into a MDO framework to permit the solution of aero-structural optimization. The problem to solve can be, for example, the weighted composite function of drag coefficient C_D and structural weight W : $C_D + \omega W$. Solving this problem,

⁷The sensitivity of a function \mathcal{J} with respect to n parameter, requires $2n$ evaluations of \mathcal{J} when -2nd order- Finite Difference are used while only one analysis and one adjoint state solution are required with the adjoint method

offers, the access to the evolution of the aero-structural trade-off via a higher -but not expensive- representation of what is currently performed at these stages by the industry.

New contributions

What this work is about is:

- (1) Development a fully parametric differentiable aero-structural analysis tool based on the ONERA CFD code *elsA* (standing for "ensemble logiciel de simulation en Aérodynamique) ; this involves a differentiated structural module that requires only few CPU seconds to build the structural model;
- (2) Enabling analytical calculation gradients, of any function involving both disciplines (aerodynamics and structure) w.r.t an aero-structural design space, available for gradient-based algorithms⁸.
- (3) Demonstration of this "gradient calculator" with representative problems.

Choice of the aero-structural models

This work builds on the adjoint CFD capability available in the software *elsA*. The physical modelling of aerodynamics can be performed with the Navier-stokes equations subset: Reynolds-averaged Navier-Stokes equation (RaNS) or Euler equations. We model the slender wing of a civil aircraft by a beam governed by the Euler-Bernoulli theory. Beam model proved to be suitable for aero-elastic wings (slender wings), thus it is important to bear in mind the fundamental difference between analysis methods to support the design opposed to analysis for design space investigation. The process of understanding and characterizing the behaviour of a well-defined configuration cannot be performed in the same manner as the process meant to assist the design by rapidly evaluating the performance and providing answers to design questions that arise. Giunta in (31) highlights: «*One drawback to using high fidelity analyses is numerical noise which occurs as a result of the incomplete convergence of iterative process[...] and the discrete representation of continuous physical objects*». This statement goes for both

⁸Both global and local optimization may require the information of the gradient

aerodynamic and structural criteria. However, the prediction of non-linear aerodynamics of transonic wings can not be performed without high-fidelity CFD, which is not a problem because we can easily afford the analysis cost of the aerodynamic performance that does not exceed one or two CPU hours (for “*every-day*” use cases). In addition, with an efficient mesh deformation tool that does not require any computational cost neither user interaction, both CFD analysis and aerodynamic sensitivity analysis are highly affordable.

The choice of our structural model is guided by the need to access the sensitivities of the wing aerodynamic and structural characteristics w.r.t planform and structural parameters easily at each iteration where the optimization algorithm requests sensitivity analysis. At early and intermediate design stages, the exact *absolute* structural performance is not necessarily required, whereas its sensitivity are.

1.3 Organisation of the manuscript

The development of the aero-structural adjoint method for sensitivity analysis used by gradient-based optimization algorithms denotes the need of predicting: (1) aerodynamic and structural analysis (2) aerodynamic and structural adjoint sensitivity analysis. The present manuscript describes the different steps of the development of the aero-structural adjoint-based gradient calculation and is organised as follows:

Chapter 2

The first section of this chapter formulates the problem we aim at solving: improvement of an aero-structural objective in an aero-structural solution space. The second section reviews the categories of optimization methods, and motivates the choice of the adjoint-based gradient technique. The principle of the adjoint method is presented in the third section and the last one is dedicated to highlight the importance of optimization in multidisciplinary design space through the parametrization.

Chapter 3

This chapter introduces the aero-structural adjoint method as an extension of the aerodynamic and the aero-elastic adjoints methods (90), (59), (56). The differences between the aerodynamic, aero-elastic and aero-structural adjoints are introduced.

Chapter 4

The functionality of the structural module developed in this work is validated in this chapter by a purely structural gradient-based sizing of the wing box of a selected wing-body test case. The outputs of the structural module provide the structural analysis and aero-structural sensitivity analysis used for the complete aero-structural gradient gathering.

Chapter 5

The development of the aero-structural adjoint is detailed in this chapter. The equations giving the gradient of aerodynamic or structural functions with respect to wing shape or internal structural design parameters are introduced. The different terms that compose these equations are described and their actual implementation presented.

Chapter 6

Application of the developed aero-structural adjoint method to a generic wing body configuration [Fig.1.1] is presented in this chapter. The comparison lays on the modelisation of the structure: rigid sensitivities computed with the aerodynamic adjoint method, then flexibility-free aero-elastic gradients performed by the aero-elastic adjoint and finally gradients with full aero-structural modelisation.

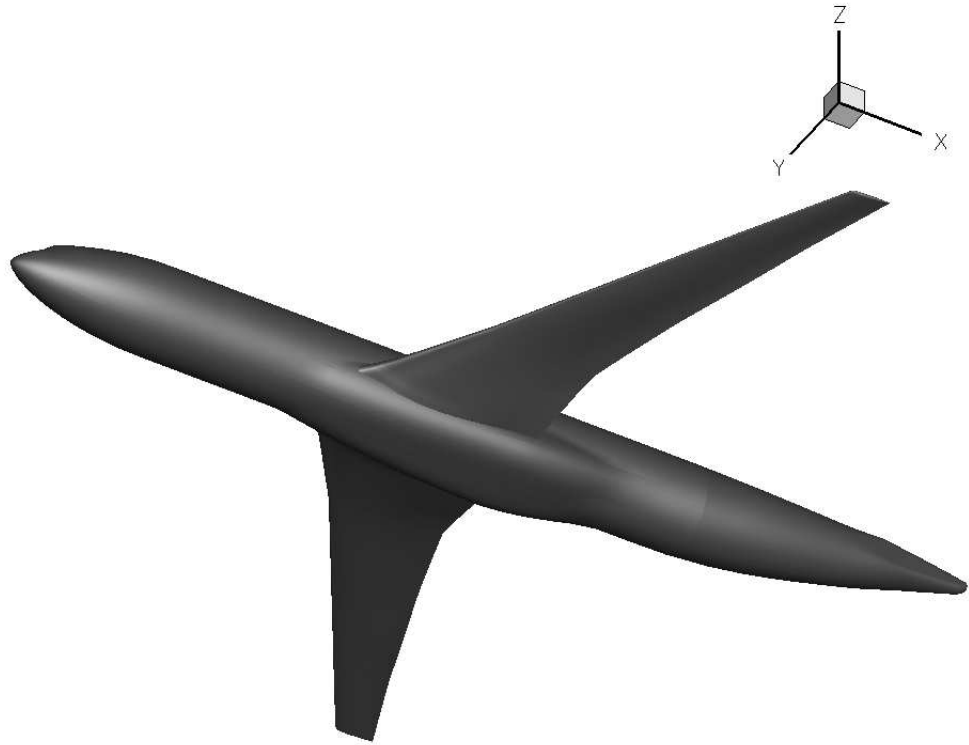


Figure 1.1: Test-case configuration.



Figure 1.2: Aero-elastic deformation on the wing of the Airbus A320

2

Aero-structural wing design problem formulation

2.1 Preamble

A transport aircraft is designed for maximum performance at specific flight condition points from its design envelope. These points are defined by the aircraft weight, the lift coefficient and the altitude (which translates into a given Mach and Reynolds number and a given angle of attack). At other flight conditions, the aircraft may lose its optimality. The benefit of multidisciplinary design optimisation (MDO) will come from the fact that:

- Without MDO the design space is necessarily restrained; For example, pure aerodynamic optimisation of planform parameters could be useless without consideration of the impact on the structure and therefore on weight.
- MDO is sine qua non for solving multi-point fuel-efficiency design problems which requires both global modifications (with an aero-structural impact) and the appropriate operating condition in terms of weight and aerodynamic performance.

We define the cost function \mathcal{J} of the target multidisciplinary and multipoint optimisation associated to wing design problem as the linear aggregation of the drag coefficient¹ at

¹The drag coefficient can be estimated through a far-field or near-field approach using the drag

the different cruise flight conditions and the structural weight:

$$\mathcal{J}(\alpha) = \sum_{i=1}^{n_f} \omega_i C_{D_i} + \omega C_{W_{box}}, \quad n_f \text{ flight cases}$$

$$\begin{cases} \alpha = \alpha_{j_{1 \leq j \leq n_{geom} + n_{struct}}} \\ \alpha_j = (\alpha_{geom}, \alpha_{struct}) \in \mathbb{R}^{n_{geom}} \times \mathbb{R}^{n_{struct}} \\ g_i(\alpha) \leq 0 \\ \sigma_k(\alpha) \leq 0, \quad k \text{ aero load case number} \end{cases}$$

\mathcal{J} is the weighted sum of drag coefficient C_{D_i} at the different flight conditions i and $C_{W_{box}} = \frac{W}{W_0}$ is the structural wing weight coefficient (wing box model), both aggregated with a weighting coefficient ω . The set of parameters, represented by the vector α , is necessarily aero-structural, and so the constraints (aerodynamic constraint g_i such as constraint on lift and pitching moment and structural constraints σ_k representing reserve factor or stresses in materials).

The decrease of \mathcal{J} and therefore of the aerodynamic drag and structural weight is constrained by the lift coefficient and by the allowable material stresses (stress analysis in this work is detailed in chapter 4) p. 69).

The manner we formulate the aero-structural optimisation problem is a choice guided by several reasons explained in this chapter. There exists other formulations of the aero-structural optimisation problem such as the BLISS approach (75), the collaborative optimisation (48), etc.

However, regardless of the method we adopt for the problem formulation, MDO consists fundamentally in evaluating the cost function (and constraints) at different points of the design space and methods for moving through the design space to improve the cost function(s). These design space points, candidate for functional evaluation, are selected by the search algorithm (optimisation algorithm).

Without an objective of addressing an exhaustive list of optimisation algorithms, section 2.2 p. 13 exemplifies some of the existing techniques, and evaluates -implicitly- the potential of the use of adjoint-based techniques within optimisation frameworks.

Section 2.3 p. 21 presents the adjoint method for gradient computation via the duality decomposition in FFD72 (22)

concept and gives briefly a comparison of the existing types of the adjoint formulation. The last section of this chapter highlights the importance of aero-structural trade-offs via the parametrisation and the great benefits of incorporating aero-structural adjoint-based techniques within design processes.

2.2 Design space exploration techniques

The problem presented in the previous section can be solved by different techniques. These techniques consist in algorithms that explore the design space aiming at an optimal improvement of the cost function, defined as:

$$\mathcal{J} : \mathbb{R}^n \mapsto \mathbb{R}^{n_g}$$

where \mathbb{R}^n is the design space and \mathbb{R}^{n_g} the solution space ($n_g = 1$ in our case). The search algorithms that explore the design space are classified as global (c.f. section 2.2.1 p. 14) or local (c.f. section 2.2.2 p. 17) algorithms.

These categories can be sub-classified depending on the function that drives the transition between an initial state and a final state. If the transition function is bijective, i.e. to a state i corresponds a unique state $i + 1$ then the algorithm is of a **deterministic nature**. When, to a current state corresponds more than one possible next state the algorithm is said to be **non-deterministic**. As it is mentioned by Liberti in (49), non-deterministic is not a synonym of stochastic. Algorithms are running in computers that are governed by deterministic processes and thus it can be shown that any non-deterministic process can be simulated by a deterministic process. Stochastic methods use randomness² of the iterates.

Optimisation algorithms move through the design space via two different methods: **Direct** or **Gradient-based**. The first category requires the evaluation of the function only. Gradient-based methods require, and use, the gradient information to build a

²The random elements can be either approximated by an algorithm, for example the PRNG (Pseudo random number generator) or generated based on physical methods which are based, essentially, on random atomic physics.

search direction and eventually to approximate the Hessian matrix used, for example, in the BFGS (Broyden-Fletcher-Goldfarb-Shanno) algorithm.

2.2.1 Algorithms for global search

The possible non-convex nature of “real-life” functions -brought by industrial engineering problems- adds complexity to the exploration of design spaces. Global optimisation comes as an answer to the presence of local-minima and to the challenges introduced by non-convex programming.

Global optimisation can be nature-inspired, physics inspired or purely mathematical methods. The mimic of the nature is recurring, through for example, *The River Formation Dynamics* that is inspired by the way waters forms rivers eroding the ground and depositing sediments. The biological social system also inspired the global optimisation like the flock of birds that is copied by the *Particle Swarm Algorithm*, or the *Ant Colony optimisation* that imitates an ant seeking food. Examples of the methods that copy the physics, are *The Rain Drop Method*, *The Simulated Annealing* (c.f. table 2.1 p. 16) or *Parallel Tempering*. The remaining class consists in algorithms that do not have any physical or nature link. One example is the pure *Random Search* which uses a uniform probability distribution to sample the entire search space. This algorithm is often used to seed another search technique such as the *Iterated Local Search* presented in table 2.1 p. 16 with other examples of the mentioned three classes.

Table 2.1 p. 16 does not aim at scanning the historic of global optimisations -out of the scope of this work- but rather exemplify the large number and variety of available techniques that illustrate the large efforts conducted by the optimisation community. Genetic algorithms (GA), that belongs to the evolutionary algorithms category, have been increasingly applied to aerospace problem: an interesting survey conducted by Anderson (2) reviews the trends of AIAA papers dedicated to GA based optimisations between 1996 and 2001. This growth is largely attributed to the growth in computer speed and, according to Anderson, because “*they have shown themselves to be superior to traditional design and analysis tools when complicated non-linear phenomena dominate the optimisation space*”.

This is certainly true and in addition, these global algorithms lay on a direct approach to scan the design space. This brings a significant simplification of the design framework since only analysis tools are required. But on the other hand it is commonly admitted that these methods have a prohibitive cost resulting from a slow convergence during the search for the global optimum, and thus are very demanding in term of number of functional evaluations which cannot be afforded in all contexts (industry...). In addition, global convergence is not guaranteed unless the problem is convex or in the case of solving nondegenerate problems via specific algorithms ??, or if we simply perform a Brute-force search technique.

Statistical techniques are commonly used to mitigate this expensive cost, for example Response Surface Modelling (RSM) methodologies combined with Design Of Experiments (DOE) techniques are enjoying increasing popularity. However, these methods depend highly on the discipline, the nature of the functional and its computation cost. In addition, building these surrogate models is complicated and expensive for high number of design parameters, which is likely the case in aero-structural optimisations. Indeed, if the wing planform geometry can be represented by less than 10 parameters -to simplify-, the detailed aerodynamic shape (airfoil geometry) and the structural components are far more demanding in term of parametrization.

Other methods that arose recently are the *hybridation* techniques which intend to gather both the efficiency and the robustness of direct global algorithms (providing the starting point) to the gradient based methods which benefits from the local refinement capabilities. At ONERA, the work of Wervaecke (88) exemplifies such formulation. She developed a hybrid algorithm based on the non-deterministic algorithm Covariance Matrix Adaptation Evolution Strategy (CMA-ES) (35) and the gradient-based CONMIN algorithm developed by Vanderplaats (83) and applied it to the optimisation of a 2D airfoil. The gradients for the local search part were computed by solving the aerodynamic adjoint problem.

Algorithm	Deterministic	Stochastic	About...
Branch and Bounds algorithms	×		The method “ branches ” the problem into sub-problems on which it computes the upper and lower bounds. The unpromising sub-problems can be eliminated using the bounds .
Evolutionary Computation (EC)^a		×	Defines all the algorithms that refine iteratively a set of design candidates called population, defined randomly, by evaluating their fitness ^b .
Simulated annealing		×	A Monte-Carlo ^c method that emulates heating and cooling of materials guiding the atoms towards a configuration with minimum internal energy.
Iterated local search		×	Applies local search to refine the broader neighbourhood of candidate solutions to their local minima.
Reactive Tabu Search		×	A short term memory of specific changes of recent moves within the search space is kept and defined as “tabu” areas (cycling is prevented). The algorithms reacts to the occurrence of cycles by adapting the tabu list size.

^aEvolutionary Strategy (ES), Genetic algorithms (GA)

^bReproduction capacity of an individual

^cThe method is named after the city where gambling is very popular. It is a non deterministic method that rely on repeated random sampling to compute an output

Table 2.1: Selection of global optimisation algorithms

2.2.2 Algorithms for local search

A local search algorithm searches an optimal solution locally, in the neighbourhood of the initial point. If global algorithms allow both decrease and increase of an objective function, local algorithms are favouring only its decreases (in the case of minimisation problems), restricting their search to the closest local optimum.

As mentioned previously, local algorithms are divided into methods that do not require any evaluation of the derivatives to explore the neighbourhood (Direct methods) and methods that require the evaluation of the gradients (Gradient-based methods). **Pattern search methods** is a family of direct algorithms fully exploitable on functions that are not continuous or differentiable.

When the gradient is available, numerous possibilities are given depending on the nature of the optimisation problem. For example, the **Quasi-Newton method**, that requires the approximation of the Hessian based on the gradient information, is effective for non-constrained problems. **Newton method** requires explicit computation of the Hessian matrix, which is not straightforward, and thus can be approximated from the gradients. Other iterative methods require “only” the evaluation of the gradients. The potential of these methods depends on the availability of the gradient information. The gradient can be computed via the Finite Differences, complex-step method or the adjoint method. This problematic, as an important part of this work, is further discussed throughout the present manuscript.

2.2.3 Constrained optimisation

The algorithms presented above are not all designed to optimize constrained problems, the extension has often to be performed later. This section introduces the methods by which constrained problems can be approached.

Let us consider the problem:

$$\begin{array}{ll} \text{Minimize} & \mathcal{J}(x) \text{ where } x \in \mathbb{R}^n \\ \text{Subject to} & g_i(x), i = 1, \dots, m \end{array}$$

Algorithm	Deterministic	Stochastic	About...
Steepest Descent	×		Is the most popular of gradient-based methods. the current step is taken in the direction of the negative gradient at the previous step approaching the minimum in a <i>zig-zag</i> manner.
Conjugate gradient method	×		The search is performed according to a direction which is a linear combination of the current and the past steepest descent vectors i.e the cost function is minimized within a hyperplane composed of all the previous search directions instead of following a unique line that points down the gradient.
Steepest-Ascent Hill Climbing	×		This method relies on the best neighbour approach
Stochastic Hill Climbing		×	A random selection is performed on the neighbour candidate solutions. The candidate is accepted only if \exists an improvement.

Table 2.2: Selection of local optimisation algorithms

The problem is parametrized by n variables and constrained by m inequalities linear or non linear. The methods for solving constrained optimisations problems -based on the theory of NLP³- differ in terms of the dimension of space that the search algorithm will explore.

The most intuitive way is to free the problem from the constrained formulation to simplify the design space exploration. Such approach is called *Penalty method*. It reformulates in a single function both objectives and constraints by introducing a penalty factor. It then solves the new unconstrained problem in n -dimensional space.

Lagrangian methods formulate the necessary conditions for optimality by introducing the so called Lagrange multipliers for equality constraint. This approach is generalized by the Karush–Kuhn–Tucker conditions (KKT), which can also take into account inequality constraints. It solves in a $(n + m)$ -dimensional space.

The primal methods, or *feasible direction methods* solve the initial problem, in a $(n - m)$ -dimensional space, by searching directly inside the feasible region. The main advantage is to converge towards a feasible point even if the optimality condition is not verified.

The dual formulation relaxes from the dimension of x and thus the algorithm works in a m -dimensional space (adjoint method...).

The most successful and popular approach for constrained optimisation is Sequential Quadratic Programming (SQP). It solves successively a set of linearly constrained quadratic approximation of the original non-linear problem. Each sub-problem optimizes a quadratic model of the cost function (assuming it is twice continuously differentiable). The explored points are not necessary feasible points. In this work, among other algorithms, CFSQP (16) algorithms was often used. It is a modified version of SQP that generates only feasible iterates.

2.2.4 Multi-objective based approaches

In this work, the aero-structural problem was formulated in a manner that the optimisation algorithm searches the solution space aiming at improving only one objective, that is actually the composition of aerodynamic and structural functions. There are

³Non Linear Programming

other approaches in which the different objectives are explicitly handled by the optimisation process.

When it comes to solving optimisation problems with competing objectives, appears the pareto optimality concept. A set of *non-dominated* design points that reveals the trade-offs between the involved disciplines. The robustness of these methods is evaluated according to their ability to reach this set, called the Pareto Front.

The method are themselves a Pareto set defined by the computation cost and the speed of search convergence. The use of evolutionary strategies (NSGA-II (19), MO-SHERPA) is widespread for Pareto front identification. If these methods show good results -as mentioned in the section 2.2.1 p. 14 - they also present weaknesses through their demanding computational resources associated to numerous design evaluations. The robustness of GA algorithms can even be questioned when the objective function(s) presents a noisy characteristic, or simply insufficiently converged CFD solutions for example. This may lead the GA to an non-exploitable design space area. In addition, it is not straightforward to specify a termination criterion, while a minima -local minima- is certainly reached at the convergence of the algorithms.

A comparative study of various multi-objectives evolutionary algorithms conducted in 2000 by Deb *et al.* can be found in (20), and more recently -in 2011- a comparison of these approaches is published by Zhou *et al.* in (109).

The work of Zerbinati and Désidéri (21) brings novelty to this topic by exploiting the gradient information when heading -cooperatively- to the Pareto Front. They introduced the Multiple Gradient Descent Algorithm (MGDA), that uses a clever combination of the gradients to find a descent direction common to all criteria.

Both global and local approaches -and their hybridation- present weaknesses well established and accepted. Concerning gradient-based approaches, they present a failure when the design space presents discontinuities, they are not able to deal with the non-convexity of design space, however as it is highlighted by Zingg (110): “ *in many*

engineering context, this is unlikely to be an issue, since the highly constrained nature of the design problem inhibits multi-modality ”.

2.3 The adjoint method in the context of wing shape design

The evaluation of aerodynamic quantities is performed via complex CFD tools -in use in the industry- that are often developed without a vision to be differentiated. Chapter 3 p. 37 is about the development of the adjoint method (with or without MDO) and its extension performed within the CFD software *elsA* (25).

When numerical optimisation was standardised, considerable efforts were made to access to the -adjoint based- sensitivities of aerodynamic quantities through the same code that performs the CFD analysis. We may cite the work of Jameson *et al.* at Princeton (39), Brezillon & Dwight *et al.* at the DLR (11), Peter , Renac, Dumont *et al.* at Onera (68)(72)(24), to name but a few. A well-written survey approach on numerical sensitivity analysis for aerodynamic optimisation is given in (69) and goes through the work of many research teams.

The benefits of the adjoint method for aerodynamic design through gradient-based algorithms were clearly perceptible (78), actually the exploitation of the local information during the design space search justified this enthusiasm. The local information given by sensitivity analysis are used to get a direction of improvement of the function that respects the constraint until the convergence is reached.

Of course, remains the question of whether or not using gradient-based or gradient-free algorithms, however the use of the derivative information requires this information to be available and at a reasonable expense. Genetic and evolutionary algorithms for example are -when not hybrid- gradient free methods. These methods access the local behaviour of the objective function by evaluating the cost function at different points of the design space. It is then obvious how these methods are resource-demanding in

high dimensional design spaces (see section 2.2.1 p. 14 and section 2.2.4 p. 19).

In the framework of aerodynamic shape optimisation, designers usually have a preconceived idea of what their optimal design should be, and this constitutes the starting point of the detailed design work. The efficiency of this method lays on the knowledge and the experience of the designers and has been demonstrated through the evolution of civil transport aircraft. The obtained aerodynamic shape is then an “extrapolation”, to simplify, of the existing aerodynamic aircraft shapes of the previous configuration. But what about the design of genuinely new configurations? What about the conceptual design, the design from scratch to analyse the feasibility of a project without past experience.

Are we able to improve these knowledge-based methods? How can we help the designer in exploring unknown region of the design space? Will the potential of the design space increase if we increase its degrees of freedom? How can we explore reliably a high dimensional design space, authorizing large evolutions of the design?

The optimisation of an existing configuration or the design of a new configuration cannot be done with a limited number of design variables: transonic aerodynamic performance requires a sufficient number of degrees of freedom to reach an optimum, considering the complex non-linear nature of the physics.

The critical point that justifies the thirty years of research and considerable efforts performed by the CFD community to widespread the utilization of adjoint-based gradient algorithm in industrial contexts is the cost-efficient computation of *accurate* gradients to allow the *exploitation* of the local information at a reasonable cost.

Sensitivity analysis cost and analysis accuracy

The derivatives of the objectives and constraints functions w.r.t. the design variables quantify the effect of each design parameter on the design and thus inform the

algorithm on the changes that have to be performed to reach a desired performance. Generally speaking, whatever the method used to calculate these sensitivities, the cost of the sensitivity analysis depends tremendously on the number of design parameters and/or on the number of objectives and constraints. In wing shape optimisation, the number of design variable exceeds the number of functions to be optimized and constraint to be verified. Although the number of functions and constraints influences the sensitivity analysis cost, there is no known method to reduce this impact, conversely, the powerful aspect of duality exploited by the adjoint method (see section 2.3.1 p. 24) relaxes sensitivity analysis of a cost function from the design space dimension.

The efficiency of any gradient-based methods depends on the computation -accuracy- of the gradient. These methods must be supported by a tool to compute the gradients of the objectives and constraints functions and quantify the sensitivities of the global performance w.r.t. the degrees of freedom of the problem.

Finite Difference (FD) is a way to compute these sensitivities. However, despite the increase of computational capabilities, this method requires at least a complete flow calculation for each design variable, which remains computationally costly. In addition, arises the necessary choice of the FD step. Sometimes a full step-convergence for each design variable -that are often not of the same order- is necessary. FD, besides being scientifically unchallenging, remains an unsatisfactory solution in terms of efficiency.

The adjoint method has a long history in optimal control theory and started with the work of Lions in 1971 (50). Pironneau introduced the adjoint method into fluid mechanics in 1984 (51), by applying it to flows governed by elliptic partial differential equations. The next section introduces the concept of duality exploited by the adjoint method.

2.3.1 Duality and adjoint

The adjoint method exploits the duality to make the resolution of any linear system fully independent of the dimension of the unknown.

Let us consider the known $\mathbb{R}^m \times \mathbb{R}^n$ matrix A and the known vectors $b \in \mathbb{R}^m$ and $c \in \mathbb{R}^n$. We would like to compute the vector product $c^T x$:

$$\text{compute } c^T x \quad \text{such as} \quad Ax = b$$

where $x \in \mathbb{R}^n$ is the unknown vector of the problem. The intuitive method is to solve the linear system $Ax = b$ for x and then substitute its value to compute the vector product $c^T x$.

Let us consider the same problem and introduce a vector $\lambda \in \mathbb{R}^m$, such as:

$$\lambda^T b = c^T x$$

The problem is reformulated as:

$$\text{compute } \lambda^T b \quad \text{such as} \quad A^T \lambda = c$$

To go further

Both systems are equivalent, and this is shown by:

$$\lambda^T b = \lambda^T Ax = (A^T \lambda)^T x = c^T x$$

Of course, this new linear system is not much easier to solve, the unknown of the first linear system is of dimension \mathbb{R}^n and the unknown of the second linear system is of dimension \mathbb{R}^m .

Imagine now that the known vector b is a matrix $B \in \mathbb{R}^m \times \mathbb{R}^p$ and the unknown vector x is a matrix $X \in \mathbb{R}^n \times \mathbb{R}^p$. This means, that if we chose to solve this linear system:

$$\text{compute } c^T X \quad \text{such as} \quad AX = B$$

a matrix of size $\mathbb{R}^n \times \mathbb{R}^p$ must be computed. But if we chose to solve this linear system

compute $\lambda^T B$ such as $A^T \lambda = c$

the dimension of the unknown remains \mathbb{R}^m . In other words, when the vector λ is introduced, the resolution of the linear system is independent of the dimension of the unknown.

The advantage of the linear duality is clearly visible. The former problem, that can be named as the primal problem, requires solving a linear system for the unknown matrix X , while the solution of the latter linear system, named the dual problem is independent on the nature and the dimension of the unknown and requires solving a linear system only for a vector, no matter what the dimension of the matrix X is.

This is the powerful aspect of duality that is exploited to solve linear systems independently of the dimension of the unknowns. The adjoint method is about exploiting the property of duality to compute the sensitivity of an output function $f(W)$ of the state variables W , by relaxing the resolution of the linear system from the computation of expensive terms (dimension dependent terms).

2.3.2 Discrete and continuous adjoint formulation: a comparison

The adjoint method comes in two distinct approaches, namely the continuous and the discrete. Both approaches result in a set of discrete adjoint equations and the way this set of equations is derived starting from the state variables defines the difference between the continuous and the discrete adjoint approaches.

The first step in the discrete adjoint is the discretization of the non-linear Partial Differential Equation (PDE) followed by the differentiation of the discretized equation, while the discretization is the last performed step in the continuous approach. One starts with the differentiation and forms the adjoint equations. With the discrete formulation, the adjoint solver is tightly linked to the direct state equations solver, since it implements an exact linearisation of it. The same code is usually used to solve the state equations and the discrete adjoint state equations.

The continuous adjoint formulation gives a discrete approximation to the gradient of an analytic function. While the discrete adjoint provides the exact gradient of the discrete approximation of the analytic function. These values will not be equal, or within the limit of infinitely fine discretization. The fact that the discrete approach gives the exact gradient of the discrete function represents a solid basis for validation, while the known inconsistency of the continuous approach makes difficult to know whether or not a slight discrepancy is due to the inexact value of the gradient or to a programming error. It has been shown that the accuracy of the continuous approach relies upon:

- the discretization scheme;
- the grid quality and resolution. The differences between both adjoints reduce as the mesh size increases;
- an appropriate check for the discretization scheme. The discrete formulation is often consulted to choose an appropriate discretization scheme.

For a non-smooth problem, i.e. with discontinuities like shocks, the continuous approach requires a specific boundary condition treatment, as described next: For shocked Euler flows, the continuous adjoint approach imposes to treat⁴ the discontinuities of the shock such as the adjoint variables are continuous across the shock. The implementation of boundary conditions must be imposed along the shock, and this of course implies, besides the mathematical difficulties, to detect the location of the shock. Although most of applications lays on CFD codes numerical dissipation to free from imposing internal shock boundary conditions, several teams worked in introducing methodologies to deal with nonsmooth flows in particular Giles and Pierce (28), Matsuzawa and Hafez (54).

For a 1-D quasi-Euler case, Giles and Pierce show in 1998 (29) that both formulations converge to the analytic solution, although no specific boundary conditions were

⁴Rankine-Hugoniot shock jump

enforced at the shock location. In this 1-D case, it was explained by the effect of numerical smoothing, on the assumption that the analytic solution is the only smooth solution at the shock, but in 2D and 3D cases, there is no proof of second order accuracy of aerodynamic quantities.

An important advantage of the continuous adjoint version that worth to be mentioned is that surface sensitivities can be available without the need to ever calculate the mesh sensitivities, necessary for the discrete version of the adjoint.

The development of the discrete adjoint program is reported to be less complicated than the continuous formulation, although more tedious when linearisation is performed normally *by hand*. When the analysis software has a simple academic structure or is architecturally complex but has been written in the perspective to be linearised, the powerful Automatic Differentiation (AD) tool ⁵ can be used explicitly to generate the adjoint code, totally or partially. Otherwise, the utilisation of AD become less straightforward and in this case the choice of AD may be revised. The interest of Automatic Differentiation to produce the discrete adjoint has been proven through the work of several teams in particular Mader, Martins and Alonso (65) (65), Cusdin and Mueller (17).

Both formulations have been advocated and preferred for their conceptual differences. In 1988, Jameson presented the first application of the continuous adjoint formulation to aerodynamic shape design through the inverse design of airfoils in transonic and inviscid flow (42). The continuous adjoint approach using Navier-Stokes equations was treated for the first time in (43). Giles, a firm advocate of the fully discrete formulation, used with Suli the discrete adjoint to analyse numerical errors in integral function (lift, drag...) (30). In the so-called “one shot” method that was first published in (80), the flow, the adjoint equation and the shape optimality equations are solved simultaneously in one shot. The adjoint method, in both formulations has been also applied to a wide variety of design problems subjects, e.g. McNamara et al. used the adjoint method for

⁵A widely used tool for Automatic Differentiation is TAPENADE, developed by INRIA. TAPENADE puts a particular emphasis on the adjoint differentiation

controlling physics-based fluid simulations applied to 3-D graphics animation (108).

The adjoint based optimisation methods are powerful and efficient for the CFD community. However we must still recognise that their application to design complex industrial shapes, often associated to poor grid quality, still suffers from weaknesses. There are still numerical ingredients besides numerical and physical assumptions that impact the adjoint-based gradients, and do not facilitate their integration into industrial context:

- the dependency on the convergence of the state equations;
- the exact linearisation of all terms;
- the difficulty to solve the full RaNS adjoint system that requires the challenging linearisation of turbulence models;
- the tedious efforts to produce complete adjoint optimisation system.
- the fact that the adjoint can not be used as a result of a *push-button* processes and requires user expertise ⁶

The developments of the adjoint method in the CFD software *elsA* will be addressed in chapter in chapter 3 p. 37.

2.4 Aerodynamic and structural trade-off via wing parametrization

Wing design takes part in the entire process of aircraft design. Figure 2.1 p.29 summarizes the traditional industrial milestones model of complete aircraft design and manufacturing process that go from M_0 to M_{15} . M_0 corresponds to the conceptual idea of the project and M_{15} is the final stage of the program.

⁶Of course, some commercial codes like ANSYS/FLUENT already have a working version of the adjoint for their products, however this does not imply that the adjoint method will be used in a daily basis in the environment where it is deployed



Figure 2.1: Airbus milestones

Once feasibility studies prove the interest of a new aircraft, the design of the wing undergoes two major phases: a preliminary and conceptual phase followed by a detailed phase. Depending on the nature of the project, the experience and the creativity of the engineers, the first phase (M_0 to M_5) converges to a design that represents the input of the second detailed phase.

Of course, the cost of the development of the aircraft depends on other important factors, some of them completely far from technical considerations, but it is important to keep, as much and as late as possible in the design process, the possibility for the engineers and the designers to innovate. The more advanced is the aircraft program, the more the innovation is “constrained”. The figure 2.3 p.31 presented by Mavris *et al* (62) confronts the actual and the target ease of design change evolution and system knowledge during the aircraft development process. This clearly highlights the importance of incorporating more disciplines earlier in design to control its process.

The benefits from the early stages (including conceptual stages) of the design are well established, the focus now is to enrich them with more physically relevant results based on higher fidelity analysis, without losing their important characteristic of being low in cost.

In this purpose, using MDO at this early stages will decrease the total cost of the production cycle and provide better design with more confidence. In fact, multidisciplinary interactions trades matter in the preliminary design stage, since all the taken design decision will impact further stages.

Among the different disciplines impacting aircraft performance, aerodynamic and structures are of prime importance. Moreover, the wing is probably the aircraft component

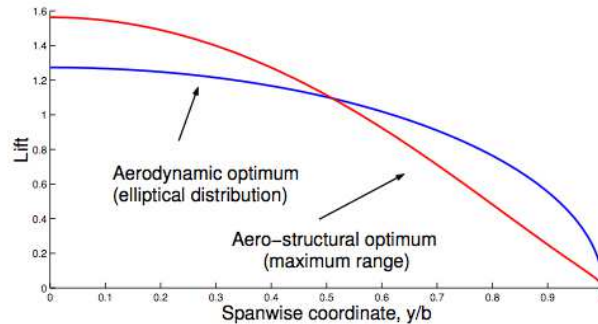


Figure 2.2: Elliptic vs. aero-structural optimum lift distribution Source: Martins J., *A coupled-adjoint Method for high-fidelity aero-structural optimization*

which has the largest impact on this performance (wing weight $\simeq 25\%$ OEW⁷, most of the lift, induced drag...) justifying the invested effort on wing aero-structural design tools.

The aero-structural wing performance depends first on the aerodynamic shape design that defines the aerodynamic envelope of the wing, and secondly on the structural sizing of the internal structural elements of the wing, the material properties and possibly the structural topology (or layout).

There are two major approaches to design a wing.

- A first approach that aims at finding a desired lift distribution by adapting the twist, taper ratio, and airfoil thickness distributions to find a targeted lift distribution. This approach is motivated by the importance of lift distribution in wing design since it affects the drag coefficient, through the induced drag component, the structural weight through the load distribution and thus the material constraints and finally the stalling characteristics. But it assumes the *a priori* knowledge of an optimal wing loading yielding to an optimal “aero-structural” trade-off [Fig. 2.2, p. 2.2] (57).

To illustrate the aero-structural trade-offs and stress the importance of incorporating multidisciplinary in design exploration, the next section summarizes the effects of some global planform parameters on both disciplines.

⁷Operating Empty Weight

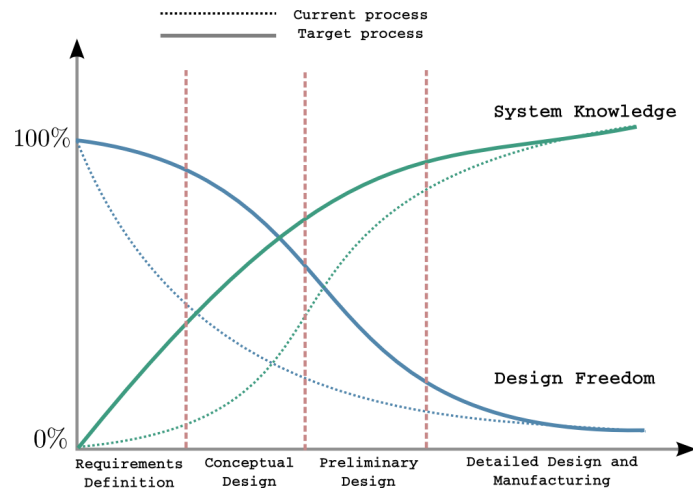


Figure 2.3: Aircraft design process. Source: Mavris D.N., DeLaurentis D.

- In the second approach, one directly searches the planform, the internal structure and the twist that improves aero-structural performances in terms of drag, structural weight and maximum lift constraint.

The second approach, less dependant on *a priori* hypothesis, is often combined with numerical optimization and can be used in both preliminary and latter stages of wing design.

2.4.0.1 Wing design parameters impact on aero-structural trade-off

Span

From a purely aerodynamic point of view, the increase of span decreases the induced drag. However in most cases of transport aircraft, the span modifications are mainly constrained by aero-structural (flutter, etc) and fuel volume considerations. There are other limitations of the span: it still has to meet the ground and airport facilities constraints and the impact on the structural weight which increases due to a higher bending moment to be carried out through the wing box.

Wing area

The wing area is the surface of the projection of the wing planform onto a horizontal plan. It is the area used to define all aerodynamic coefficients: C_L , C_D . If we think of the wing area as being an important drag factor, it is important to define correctly the area involved in the analysis, for example the total friction drag issued from the friction forces applied by the air on the aircraft body is affected by its total wetted area, and therefore by the wing area. Other characteristics that define the choice of the wing area are the low speed, maximum lift coefficient, the fuel volume and the structural weight. Having a large area to manage the stalling speed, comes at the expense of higher drag and higher structural weight.

Sweep angle

Wing sweep is strongly correlated to the wing speed. The main desirable effect of non-straight wing with a sweep angle Λ is a higher cruise Mach number that comes with a slight drag compressible penalty. In fact swept wings permit transonic airfoils -fixed thickness to chord ratio- to be used at higher Mach numbers, while the local effective normal Mach number is reduced: $M_{local} = M_{\infty} \cos(\Lambda)$. Since the dependence is in cosine, the same results are expected from negative sweep angle as it can be seen in memorable aircraft such as the *Junkers Ju 287*. Although this is not the scope of this work, the fact that the unconventional forward swept wing has to deal with unconventional aero-elastic effect such as static divergence and other issues linked to yaw and stall instability would introduce a direct interest of MDO in conceptual stage.

The effect of sweep are not strictly limited to the few lines above, additional important effects induced by sweep angle (on pitching moment, on lift coefficient, on flow streamlines, etc...) can be found in the book of Sadraey *Aircraft Design: A Systems Engineering Approach* presented in an introductory and pedagogic manner.

What we want to stress out is the importance of multidisciplinary design and analysis even in early stages of the design process, when it comes to make decisions on planform parameters such as the sweep angle which has a direct impact on several disciplines.

To sum up, the sweep angle affects the transonic wave drag (through the local mach

number effect) and the structural weight through the displacement of the center of gravity of the wing and the elastic axis, and requires a multidisciplinary approach to be explored during the wing design.

Twist

The most known effect of twist is first the spanwise redistribution of lift and thus a possible positive effect on the induced drag. Secondly, it prevents the stalling of the wing tip to occur before the wing root which would lead to a loss of aileron authority to control the aircraft. Another effect of twist is the modification of bending moment distribution in the wing and thus -via the skin- the stress level in the wing structural elements (spars mainly) which directly impact the structural sizing.

We may distinguish between two types of twist: the geometric twist and the aerodynamic twist. The twist is said to be geometric when the incidence angle varies along the span from the root to the wing tip and it is defined as aerodynamic when different airfoils sections are used along the span. For example, the Boeing 767 has a thickness-to-chord ratio of 15.1% at the root and 10.3% at the tip generating an aerodynamic twist. The Gulfstream IV has a wing incidence of $+3.5^\circ$ at the wing root and -2° at the tip, resulting in a -5.5° geometrical twist. Generally manufacturing difficulties arises from the geometric twist use.

There is also the twist induced by the aero-elastic effects. This twist results from the combination of torsion and bending deformations of the wing and is the direct response of the structure to the aerodynamic loads. It depends on many parameters, some of which are the wing structural material characteristics.

What must be retained from the previous lines is first the direct effect of twist on aerodynamics and its indirect effect -through the loads- on the structures. Another point that justifies the need of multidisciplinary and multi-objective design processes.

Taper ratio

The taper, defined as the ratio between the chord at the wing root and the chord at wing tip, can be used to tailor the spanwise lift distribution. Lowering the taper has positive

impact on the structural weight since the wing center of pressure will move inboard toward the center line of the fuselage and this results in a lower bending moment at the wing root which is beneficial to wing weight.

2.5 Outcome

This chapter presents the context of this work through a global and summarised review of different possible approaches to solve the aero-structural wing optimisation problem. Concerning the characterisation of the search algorithm, the local information given by the gradient is highly valuable and can be exploited in a global, local or hybrid approach for design space exploration. More than that, we see in the availability of sensitivity information a valuable input for the designer at all design stages. Not only for optimisation processes, but also to evaluate the evolution of the sensitivity of targeted performance w.r.t. the decision parameters between the pre-optimisation and post-optimisation stages. In a *traditional* design approach, the global geometrical parameters that define the wing (sweep, span, area...) are first defined -then optimized- by the designer, followed then by the optimisation of the aerodynamic local design variables (camber, twist...) and by the structural fitting and sizing. All the interest of our approach is about accessing -at stages where the first parameters category are defined- the targeted performance sensitivity information w.r.t. to all these parameters that usually appear later in the design process. This implies the necessity of introducing multidisciplinary and physical models to represent both global and local (disciplinary) parameters. For gradient-based optimisations remains, of course, the space convexity-dependence when making the route towards a minimum besides the importance of the initial point. However, the industrial optimisation problem we are aiming to solve remains a mathematical formulation that has to deal with topological and dimensional restrictions, whatever the algorithms is, whatever its type is there are always *pros&cons*. In this contexts, the adjoint method presents a strong advantage which is the decrease of computational cost necessary for sensitivity analysis. In addition, this information can be exploitable by both local algorithms -mainly- and global

algorithms, offering a better local knowledge of the design space without requiring a high computational cost.

The adjoint developments within the software *elsA* are presented in the next chapter.

3

From aerodynamic design to aero-structural design using the adjoint method

3.1 Preamble

As introduced in the previous chapter, the design process is often faced with the compromise on the number of decision parameters and, possibly, several disciplinary objectives. Needless to say that there is no certitude on the direct link between design space dimension and design optimality. But the idea of exploring a design space, often constrained, aiming to find better configurations or understand why others are worse is challenging for both research and industry.

Some algorithms rely on the information of the gradient to solve the optimization problem and drive their search toward a candidate optimal configuration. This explains directly the invested efforts aiming at the reduction of the sensibility analysis cost. These sensitivities are of tremendous importance to the valuable information required in a design process.

The heart of this work is the aero-structural adjoint method and its attractive cost efficient sensitivity analysis in multidisciplinary high dimensional design spaces. Gradient-

based algorithms use this sensitivity information to drive the search in the design space toward an optimum in the objective/constraint space. There are two different ways to compute the gradients, *purely numerical methods* which consider the analysis code as a black box and more *intrusive methods* that differentiate the analysis code. The most common and widespread purely numerical is finite difference scheme. The application of this method is straightforward and this is a major attractive characteristic. However it has two drawbacks: the computational cost directly depends to the number of design variables and the necessity of choosing the right perturbation magnitude. Analytical methods are subdivided into direct and adjoint approaches. In the direct approach, the flow is linearised with respect to (w.r.t) each design parameter, which gives a direct dependence of the cost of the gradient evolution to the number of design parameters. This approach was initiated in early nineties by Sobieszcanski-Sobieski (78). In the other approach, the dual problem is solved instead of the primary problem (i.e "adjoining" the problem). This allows a cost-efficient evaluation of the functional sensitivities w.r.t the design space.

With the adjoint method, the cost of the gradient computation is determined by the number of objectives/constraints instead of the number of design variables. The choice of the approach therefore depends on whether a high number of design parameters is necessary to achieve optimal design or not. In many cases the answer is positive, consequently the adjoint approach is to be preferred to the linearized approach, see for example the work of Méheut *et al* (63), Brézillon *et al* (14). Brézillon and his co-authors performed two optimizations on a 3-D configuration (DLR-F6) using a coarse parametrisation and a fine parametrisation. Their conclusion is that, although the results depend on the parametrization methods, the adjoint method seems to be essential since there is a substantial advantage to large number of variables. The coarse parametrisation did even deteriorate the objective while the fine parametrization provided an optimal design.

A good indicator for the degree of maturity of a subject is to evaluate its integration in an industrial context. If the multidisciplinary analysis has reached a mature point

and is used in a daily basis in the industry, considerable efforts are still being invested for multidisciplinary numerical design processes development and integration.

A realistic design is a multidisciplinary design and corresponds to a high dimensional design and. High dimensional because, as said previously, of the need for a rich design space. Multidisciplinary because numerous shape and planform modifications are meaningful only if other important disciplines are taken into account to interact with aerodynamics. In some case, sequential discipline optimization were unable to converge to the true optimum of a coupled system.

The adjoint method is all the more justified in gradient-based multidisciplinary optimization. In an optimization that considers the interactions of n disciplines, a gradient-based optimization requires the gradient information of each cost function that represents the discipline $i \in [1, n]$ w.r.t private design parameters and public design parameters. The definition of public and private parameters was given by Masmoudi (60). He defines a private parameter one that has a direct influence limited to the state equations of one discipline, and public parameter one that influences the state equation of all the disciplines taken into account. Adjoint methods offer an attractive approach to compute efficiently the sensitivities w.r.t all parameters, be it private or public.

In this work we extend the adjoint method (the aeroelastic version c.f. section 3.4) to cover both planform (public) and structural (private) modifications aiming at aerodynamics performance without structural penalization.

The remainder of this chapter summarizes the achievements performed at ONERA to integrate the adjoint method, for sensitivity analysis, in the context of multidisciplinary design. In section 3.2 we overview how we *adjoint* the aerodynamic flow equations. Then we describe in section 3.4 the extension performed by Marcelet (59) to solve the adjoint equations of aero-elastic structures -where the structural model is not alterable- and we describe the approach used for fluid/structure coupling. The last section 3.5 introduces the heart of this work, the adjoint equations of an aero-structural system that requires differentiated models for both aerodynamics and structures.

3.2 Numerical method for solving the governing flow equations

In this section we present, in a summarized version, the governing flow equations and their discretisation inside the ONERA CFD flow solver *elsA* (25). There is no new contribution to this part in this work however the presentation of the numerical schemes choices within the adjoint method context, is meant to present to the reader the discrete residual associated to the flow equations that we consider, and for which differentiation is necessary when computing the aerodynamic adjoint, the aero-elastic adjoint or the aero-structural adjoint resolution.

3.2.1 Governing flow equations

Let us consider a compressible viscous flow around an aircraft embedded within a sufficiently large fluid domain \mathcal{D} bounded by the surface Γ of outward unit normal $n = (n_x, n_y, n_z)^T$. The integral form of the conservative flow equations is given by:

$$\frac{d}{dt} \int_{\mathcal{D}} \mathcal{W} d\mathcal{D} + \oint_{\Gamma} (F_c(\mathcal{W}, n) - F_d(\mathcal{W}, \nabla \mathcal{W}, n)) d\Gamma = 0 \quad (3.1)$$

where:

- \mathcal{W} is the vector of the conservative variables: $\mathcal{W} = (\rho, \rho u, \rho v, \rho w, \rho E)^T$

- $\vec{V} = (u, v, w)^T$ is the flow velocity vector expressed in an absolute frame of reference

- F_c is the convective flux vector in the direction \vec{n} :

$$F_c(\mathcal{W}, \vec{n}) = \begin{bmatrix} \rho \vec{V} \cdot \vec{n} \\ \rho u \vec{V} \cdot \vec{n} + p n_x \\ \rho v \vec{V} \cdot \vec{n} + p n_y \\ \rho w \vec{V} \cdot \vec{n} + p n_z \\ \rho E \vec{V} \cdot \vec{n} + p \vec{V} \cdot \vec{n} \end{bmatrix} \quad (3.2)$$

F_d is the diffusive flux vector in the direction \vec{n} :

$$F_d(\mathcal{W}, \nabla \mathcal{W}, \vec{n}) = \begin{bmatrix} 0 \\ \underline{\tau} \vec{n} \\ \underline{\tau} \vec{V} \cdot \vec{n} - \Phi \cdot \vec{n} \end{bmatrix} \quad (3.3)$$

where:

- $\underline{\tau}$ is the viscous stress tensor, the fluid is considered newtonian under the hypothesis of Stokes that is :

$$\underline{\tau} = -\frac{2}{3}\mu(\nabla \cdot V)\underline{I} + \mu(\nabla V + \nabla V^T) \quad (3.4)$$

where

- μ ($kg.m^{-1}.s^{-1}$) is the dynamic viscosity depending on the temperature of the fluid by the Sutherland law.

- Φ is the heat flux vector ;

When considering the Reynolds average process leading to the RANS equations that solve the mean flow quantities evolution, the process of averaging add two new contributions in the diffusive flux vector namely: the Reynolds stress tensor $\underline{\tau}_R$ and a turbulent heat flux vector Φ_T . Because we have considered only inviscid computation we will not present the details of the modelling of these terms that are central aspects of the field of turbulence modelling. The reader may refer to the *elsA* theoretical manual for the different models that are available within *elsA* (25). For an inviscid fluid, the diffusive flux F_d vanishes and we end up with the Euler equation for the behaviour of the flow. We will now present the discretization of the conservative equations considering the finite volume method.

3.2.2 Finite Volume Discretization

Within the CFD code *elsA*, a finite-volume method on structured grids is used to solve the conservative equations. This method consists in discretizing the computational domain \mathcal{D} into hexahedral cells where on each of them, we compute mass, momentum

and energy fluxes balance considering the contribution of each face of the cell. Considering one cell Ω of volume \mathcal{V} and surfaces Σ_i with $i = [1, \dots, 6]$, the mean value \overline{W}_Ω of the conservative variables computed from the fluxes balance is stored at the center of the cell. The residual form of the finite-volume approach in structured meshes can be written as:

$$R_\Omega = \frac{d}{dt}(\mathcal{V}(\Omega)\overline{W}_\Omega) + \sum_{i=1}^6 (F_{c\Sigma_i}^{num} - F_{d\Sigma_i}^{num}) \quad (3.5)$$

R_Ω , called the explicit residual, is a function of the numerical convective flux $F_{c\Sigma_i}^{num}$ and the diffusive flux $F_{d\Sigma_i}^{num}$, both of them evaluated at the interfaces Σ_i with $i = [1, \dots, 6]$. These fluxes are evaluated thanks to the metric and the value of the conservative variables estimated on a given set of neighbouring cells which depends on the selected scheme.

For RANS computation, depending on the chosen turbulence model, transport equations of quantities defining the characteristics of turbulence (energy, dissipation, eddy length...) are written in residual form and are solved separately from the mean flow. For this quantities, convective, diffusive fluxes and source terms (introducing the production and destruction phenomenon for turbulence) are defined. The two system, of conservative variables for the mean flow and of transported turbulence quantities are coupled via the turbulent eddy viscosity. In fact, this variable is in the mean time defined from the field of turbulent quantities and appears in the definition of the Reynolds stress tensor τ_R under the Boussinesq assumption.

3.2.3 Choice of scheme in space and time

The CFD software *elsA* implements a wide variety of available schemes for the evaluation of the numerical fluxes (both convective and diffusive). As we have considered most of the time the steady Euler equations during this thesis work, we present here the spatial discretisation of the convective fluxes. It is worth mentioning that at the start of this Ph.D the only linearised scheme for the convective fluxes compatible with the adjoint solver was the Roe scheme extended to the order two with the MUSCL approach (33) using Van Albada limiting function (25). RANS computation can be run

with the adjoint, but an appropriate scheme for the viscous fluxes, compatible with the adjoint solver is required. An important difficulty arises with the differentiation of the turbulence model. In the *elsA* CFD code, k-w, k-l, and Spalart-Allmaras models have been linearised but they can be source of convergence difficulties for the adjoint system. There are new ways however that have recently been explored to provide improvement of the convergence of fully linearised RaNS adjoint equations. To alleviate convergence difficulties RaNS adjoint system, there is also the option to make the approximation of a “frozen” eddy viscosity. If this approximation improve convergence of the adjoint system, the accuracy of gradients is most of the time deteriorated. The constraints here were a short time of response for the aerodynamic flow solution and a good accuracy of the gradient what make us decided to considered the Euler equations. However, one must mentions that all the development made in this thesis work are compatible with RaNS adjoint solver.

In a second part we will briefly present the integration in time.

Discretization of convective fluxes using the Roe scheme

Let us consider an interface Σ , of vector surface $S = (S_x, S_y, S_z)^T$ between the adjacent cells Ω_i and Ω_{i+1} . W_i and W_{i+1} are, respectively, the numerical value of conservative variables evaluated at the center of the cells Ω_i and Ω_{i+1} . The expression for the evaluation of the convective flux F_c with a Roe scheme is given by :

$$F_{c\Sigma}^{Roe}(W_i, W_{i+1}) = \frac{F_c(W_i, S) + F_c(W_{i+1}, S)}{2} - \frac{1}{2} |\mathcal{A}_{Roe}(\hat{Q}, S)| W_{i+1} - W_i \quad (3.6)$$

where $\mathcal{A}_{Roe}(\hat{Q}, S)$ is the Jacobian of the convective flux with respect to the conservative variables estimated in a specific average of W_i and W_{i+1} defined by Roe. This average is estimated for the set of variables ρ, u, v, w and $h = e + p/\rho$ in bijection with the conservative variables. The characteristics of the matrix $\mathcal{A}_{Roe}(\hat{Q}, S)$ and its computation within *elsA* is detailed in (24).

The Roe scheme is extended to a second order scheme in space using the piecewise linear rebuilding of the approximate solution introduced by Van Leer and known as the MUSCL approach. This approach extrapolates the so called *primitive* variables given by $\mathbf{P} = (\rho, u, v, w, p)$. The vector \mathbf{P} is obtained owing to a bijective transformation of conservative variables \mathcal{W} . This bijective transformation can be found in (24). For the interface $\sum_{i+\frac{1}{2},j,k}$ of the cell (i, j, k) of the structured grid. The left and right states (the direction left to right is associated with an increase of topological index i in this case) at this interface are defined as:

$$\left\{ \begin{array}{l} \mathbf{P}_{i+\frac{1}{2},j,k}^{left} = \mathbf{P}_{i,j,k} + \frac{1}{2} * Slope_i(i, j, k) \\ \mathbf{P}_{i+\frac{1}{2},j,k}^{right} = \mathbf{P}_{i+1,j,k} - \frac{1}{2} * Slope_i(i+1, j, k) \end{array} \right. \quad (3.7)$$

where $Slope_i(i, j, k)$ indicates the variation of primitive variable in the direction of the grid index i computed at cell (i, j, k) . It is given by

$$Slope_i(i, j, k) = \psi(\mathbf{P}_{i,j,k} - \mathbf{P}_{i-1,j,k}, \mathbf{P}_{i+1,j,k} - \mathbf{P}_{i,j,k}) \quad (3.8)$$

Where ψ is the limiting function. It has been chosen in our case as the function proposed by Van Albada [ADDRE] and whose expression is given by:

$$\psi(a, b) = \frac{(b^2 + \epsilon)a + (a^2 + \epsilon)b}{a^2 + b^2 + \epsilon} \quad (3.9)$$

where ϵ is a very small number to avoid the denominator to become null.

One can notice that thanks to its differentiable expression, this limiting function is compatible with the resolution of the adjoint system implemented in *elsA*.

For diffusive fluxes because velocity gradients and temperature gradients need to be evaluated. One need to choose a discretization scheme to evaluate these gradients. Their are several possibilities in *elsA* ((24),(25)).

Time integration

The steady state computation introduced a pseudo time integration to make as low as possible the residual presented in (3.5). To realize this process of convergence, the Backward-Euler time integration scheme proposed initially by Beam and Warming is used (24). It is based on a Taylor development keeping only the one order term of the evaluation of the residual at time step $n + 1$. The expression of the Backward-Euler scheme is given by:

$$\left(\frac{\underline{I}}{\Delta t} + \frac{1}{\mathcal{V}} \frac{dR}{d\mathcal{W}^{(app)}} \right) (\mathcal{W}^{(n+1)} - \mathcal{W}^{(n)}) = -\frac{1}{\mathcal{V}} R(\mathcal{W}^{(n)}) \quad (3.10)$$

where $\frac{dR}{d\mathcal{W}^{(app)}}$ is an approximate jacobian of the residual w.r.t. to the conservative variable and $\mathcal{W}^{(n+1)}$ is the evaluation of the conservative variable at time step $n + 1$. The system defined above is rewritten on the form of bloc matrix with lower (\underline{L}), upper (\underline{U}), and diagonal (\underline{D}) blocs.

$$(\underline{L} + \underline{D} + \underline{U})\Delta\mathcal{W} = rhs \quad (3.11)$$

For each time step, this system is solved using a relaxation technic:

$$\begin{cases} \Delta\mathcal{W}^0 = 0 \\ (\underline{L} + \underline{D})\Delta\mathcal{W}^1 = rhs \\ (\underline{U} + \underline{D})\Delta\mathcal{W}^2 = rhs - \underline{L}\Delta\mathcal{W}^1 \\ (\underline{L} + \underline{D})\Delta\mathcal{W}^3 = rhs - \underline{U}\Delta\mathcal{W}^2 \\ \dots \end{cases} \quad (3.12)$$

Most of the time only two step of relaxation are used. (one with the matrix ($\underline{L} + \underline{D}$), and the other with the matrix ($\underline{U} + \underline{D}$))

As we are looking for a steady state solution, we defined for each cell a local time step from the relation:

$$\Delta t^{ref} = \min \left(\frac{dist}{(|V| + c)} \right) \quad (3.13)$$

where $dist$ is a characteristic length of the hexahedral cell defined by:

$$dist = \frac{\Delta x \Delta y \Delta z}{\sqrt{\Delta x^2 \Delta y^2 + \Delta x^2 \Delta z^2 + \Delta y^2 \Delta z^2}} \quad (3.14)$$

with Δx , Δy et Δz are the lenght of the hexahedra in x, y, z directions and $\frac{dist}{(|V|+c)}$ is the fasted wave speed encoutered in the cell (this is the highest eigenvalue of the jacobian dR/dW) where $|V|$ is the norm of the fluid velocity and c is the sound speed velocity defined with the state of the flow in the cell.

Usually, for steady state computations the time step imposed in every cell is the product of the local Δt^{ref} define above and the CFL number.

This numerical scheme is coupled with a multigrid method to accelerate the convergence. It is not possible to give a brief description of this method here but the reader may refer to (24) for a detailed presentation.

3.3 Sensitivity analysis using the discrete aerodynamic adjoint method

In this section we present, synthetically, how the pure aerodynamic adjoint equations are derived and solved under the hypothesis of a rigid structure. These equations are the starting point from which the extension to aero-elasticity and aero-structure is developed.

We consider the CFD volume mesh \mathcal{X} as a C^1 -differentiable function of the design parameters α_{geom}^* (aerodynamic planform parameters). We assume that the residual R_f , of the equations governing the flow, is C^1 -differentiable and that to a unique given geometry corresponds a unique flow field. Be \mathcal{X}^* the CFD mesh that corresponds to a design vector α_{geom}^* and W^* the flow field computed on the CFD mesh. The residual form of the finite volume discretization of the flow equation is given by:

$$R_f(W^*, \mathcal{X}^*) = 0 \quad (3.15)$$

if the jacobian of R_f is invertible, then

$$\det\left[\frac{\partial R_f}{\partial W}(W^*, \mathcal{X}^*)\right] \neq 0 \quad (3.16)$$

The implicit function theorem states that one can solve $R_f(W, \mathcal{X}) = 0$ for \mathcal{X} in a neighbourhood¹ of \mathcal{X}^* . \mathcal{X} is a continuous and a regular function of α_{geom} thus, the flow field W is defined as a C^1 function of α_{geom} in the neighbourhood of α_{geom}^* . $R_f(W, \mathcal{X}) = 0$ can be solved for α_{geom} in the neighbourhood of α_{geom}^* . We extend the validity of this statement to all design space points, thus:

$$R_f(W(\alpha_{geom}), \mathcal{X}(\alpha_{geom})) = 0 \quad (3.17)$$

From(3.17) one can state that:

$$\frac{dR_f}{d\alpha_{geom}} = \frac{\partial R_f}{\partial \mathcal{X}} \frac{d\mathcal{X}}{d\alpha_{geom}} + \frac{\partial R_f}{\partial W} \frac{dW}{d\alpha_{geom}} = 0 \quad (3.18)$$

This zero quantity can be multiplied by any non-zero vector λ_f of dimension $5 * n_{ncell}$ -or $7 * n_{ncell}$ for RaNS equations with two equations turbulence models- and added to the gradient of a functional wrt to α_{geom} . Let us consider $\mathcal{J}_{aero}(W, \mathcal{X})$ a function of interest such as drag, lift, or many other scalar functions. The sensitivity of \mathcal{J}_{aero} w.r.t. α_{geom} can be expressed as:

$$\left(\frac{d\mathcal{J}_{aero}}{d\alpha_{geom}} \right)_{rigid} = \left(\frac{\partial \mathcal{J}_{aero}}{\partial \mathcal{X}} + \lambda_f^T \frac{\partial R_f}{\partial \mathcal{X}} \right) \frac{d\mathcal{X}}{d\alpha_{geom}} + \left(\frac{\partial \mathcal{J}_{aero}}{\partial W} + \lambda_f^T \frac{\partial R_f}{\partial W} \right) \frac{dW}{d\alpha_{geom}} \quad (3.19)$$

An appropriate choice of the vector λ_f frees the computation of $\left(\frac{d\mathcal{J}_{aero}}{d\alpha_{geom}} \right)_{rigid}$ from the expensive computation of the flow sensitivity wrt α_{geom} , $\frac{dW}{d\alpha_{geom}}$. Then the following system, called aerodynamic adjoint system, is solved for λ_f

$$\lambda_f^T \frac{\partial R_f}{\partial W} = - \left(\frac{\partial \mathcal{J}_{aero}}{\partial W} \right) \quad (3.20)$$

The computation of the final gradient requires the resolution of a linear system, for this purpose equation (3.20) is expressed in an incremental iterative form, very similar to the iterative used to solve the flow equations. Thus the expensive matrix inversion necessary to access the Jacobian $\frac{\partial R_f}{\partial W}$ is avoided. The set of linear equations is solved by an implicit method also identical to the one uses to solve the flow equations.

¹ $p \in \mathcal{E}$, \mathcal{E} is a topological space, the neighbourhood of p is a set \mathcal{N} , which includes an open set \mathcal{O} containing p , $p \in \mathcal{O} \subset \mathcal{N}$

Computation of the term $\frac{\partial R_f}{\partial \mathcal{X}} \frac{d\mathcal{X}}{d\alpha_{geom}}$:

Once the adjoint vector λ_f is computed, the gradient of the functional is available at a cost equivalent to the estimation of the geometrical sensitivity of the explicit residual: $\frac{\partial R_f}{\partial \mathcal{X}} \frac{d\mathcal{X}}{d\alpha_{geom}}$. In the CFD software this term is linearised and used with aerodynamic adjoint formulation. It can also be computed via second order finite differences:

$$\frac{\partial R_f}{\partial \mathcal{X}} \frac{d\mathcal{X}}{d\alpha_{geom}} = \frac{R_f(\mathcal{X}, \mathcal{X} + \frac{d\mathcal{X}}{d\alpha_{geom}} \delta\alpha_{geom}) - R_f(\mathcal{X}, \mathcal{X} - \frac{d\mathcal{X}}{d\alpha_{geom}} \delta\alpha_{geom})}{2\delta\alpha_{geom}} \quad (3.21)$$

For discrete adjoint formulation, there is another way much more elegant introduced by Nielsen and Park (67) to eliminate the metric sensitivity $\frac{d\mathcal{X}}{d\alpha_{geom}}$ using the adjoint method of the mesh deformation equations. Thus the computation of $n_{\alpha_{geom}}$ metric sensitivities is eliminated. This design-dimension free gradient procedure was used by Mavriplis in (61) when he formulates the adjoint of the entire optimization process, flow equations and mesh motion equations. He successfully applied it to the optimization of the DLR-F6 wing body. The time saving benefit from the adjoint formulation for the mesh linearization was shown by Nielsen and Park in (67) on several large-scale configurations, resulting in some cases in a time saving equivalent to tenth of flowfield solutions time.

In the current work, when the design parameter is a planform parameter, the mesh sensitivity calculation is performed analytically by the fully linearised code SeAnDef for mesh deformation, with a derisory computation cost of these sensitivities.

3.3.1 Accuracy of the gradients

In the following parts the assumptions linked to the resolution of the adjoint system are briefly summarized, since these assumptions affect the solution of the adjoint system, regardless of the nature of the adjoint (aerodynamic, aero-elastic or aero-structural), so that the obtained gradient may be incorrect, approximated or exact. The natural question raised by Dwight and Peter in(69), is how accurate must gradients be for the application under consideration? They illustrated the robustness of steepest-descent algorithms and conjugate-gradient algorithms even with a poor quality gradient. In

fact the objective function will be improved as long as the search direction makes a negative inner product with the gradient. The use of algorithms that approximate the Hessian matrix with a poor quality gradient will hardly converge to the optimal solution found with accurate gradients.

The main source of inexactitude of the gradients comes from the evaluation of the discrete Jacobian $\frac{\partial R_f}{\partial W}$. Although the residual R_f is an explicit function of the flow variables W , its linearisation depends on the complexity of the CFD code and on the operators involved in its computation. The most common approximation in the computation of the Jacobian is to maintain the turbulent eddy viscosity constant and independent on the state variables W . This assumption is quite common in industrial application of aerodynamic adjoint, however many teams have invested significant efforts in turbulence models linearisation. Nielsen and Anderson presented in (2) the one-equation turbulence model of Spalart-Allmaras fully differentiated and coupled into the solution of the adjoint equation. They have examined the accuracy of the gradients computed with several assumptions. It is important to note that in the validations they have presented (on the ONERA M6 wing), when the parameter is associated with vertical changes, the obtained derivative can even show an opposite sign if the complete linearisation is not performed. Obviously such a behaviour may mislead the optimization algorithm. At ONERA, Renac *et al.* linearised the two-equation transport models $k - \epsilon$ (72) and Pham linearized the algebraic Michel model (52) and both applied it to the context of turbo-machinery. An exhaustive list of the successful turbulence models linearisations can be found in (69).

Despite those consequent efforts, it is still the norm to linearise only the mean-flow equations and keep the frozen eddy viscosity hypothesis. However the use of linearised models has not been widely applied. Dwight and Brezillon in (12) affiliate this lack of application to complex configuration to the ill-conditioned character of the resulting linear system of the adjoint equations including the turbulence models linearisation. With a focus on the aero-structural adjoint problem formulation, in this work the aerodynamic terms depend on the former developments in the field, and with the aim of computational time saving and simplification, the flow is modelled with the Euler

equations and when the RANS equations are considered to solve the coupled problem, the frozen eddy viscosity hypothesis is maintained.

3.4 Adjoint equations of the aero-elastic problem

The aero-elastic adjoint equations presented in this section, developed by Marcelet (59), is the starting point toward the aero-structural adjoint developed in this work and introduced in section 3.5 and detailed in section 5.2.

The aero-elastic adjoint method, extension of the aerodynamic adjoint, computes the sensitivities of any aerodynamic function such as aerodynamic coefficients, considering an elastic wing structure of frozen mechanical characteristics (stiffness), with respect to a set of decision parameters. The adjoint state is solved at the convergence of the static aero-elastic coupling process used to solve the aeroelastic equilibrium equations. During the aero-elastic coupling, the structure is assumed not to store any kinetic energy. Such as, an equilibrium position is reached after a number of iterations where the fluid and the structure exchange aerodynamic loads and structural displacements. Precisely, this is the information of this position, under the flexibility effects, which is taken into account in the process of aero-elastic gradient computation. A beam of an Euler Bernoulli type models the wing structural behaviour. The choice of this model is discussed in Chapter 4.1 and the assumption of linear elasticity finds its justification in the small deformation approximation at cruise condition.

We first explain the fluid/structure interaction process as it is used with the aero-elastic adjoint.

3.4.1 Flexibility matrix approach

According to the principle of superposition (8) which states that, if several loads are applied to a linearly elastic structure, the displacement at given point of the discretized geometry of the structure equals the sum of the displacements induced at this point by the loads applied individually at any point. Thus, when a discrete number of forces and

moments acts on the structure (in opposition with distributed loads), the displacement can be expressed as a linear function of the forces:

$$D_i = \sum_{j=1}^n F_{ij} L_j \quad (3.22)$$

where D_i is the displacement of the i^{th} discrete node ². The displacement D_i due to the forces $L_{j_{1 \leq j \leq n}}$ applied at the n load nodes.

The coefficients F_{ij} that describe the behaviour of the structure under the aerodynamic loading L , are organised in a matrix called the flexibility matrix. Thus this set of linear equations can be expressed as a linear matrix system:

$$D = FL \quad (3.23)$$

where L is the vector of applied aerodynamic forces and F , the global flexibility matrix of the structure. F transforms aerodynamic forces and moments acting on the surface mesh into deflection and twist of these elements. These deformations will be then propagated in the volume mesh used to solve the flow equations. F is reciprocal to the stiffness matrix K for which $L = KD$ (when the structure is subject to distributed loads, the equivalent of the flexibility matrix is called influence function). Equation 3.23 means that the work done by the external force during application is transformed completely into strain energy in the structure ($U = \frac{1}{2}D.L$). The fluid structure interactions are exposed in the next section.

3.4.2 Numerical method for fluid and structure coupling

The aero-elastic problem is solved by an aero-elastic module of the CFD software *elsA* named *elsA BAG* (Beam Aero-elastic Gradient). As the acronym *BAG* indicates, it is based on the Euler-Bernoulli beam equation and has been developed and oriented for gradient computation with the adjoint method. This module is independent on the flow modelling, it can be used whether the flow is described by Euler equations or by the Reynolds Averaged Navier-Stokes equations (RANS). The process of the aero-elastic

²Displacement nodes are not necessarily coincident with load nodes

equilibrium computation, presented in this section, still stands for the aero-structural adjoint methods (introduced in section 3.5).

In our work, the initial configuration to which is applied the iterative aero-elastic process is called the *jig-shape*. The *jig-shape* is the shape of the wing in absence of any kind of loads. For example, the original geometry of our test-case is given at the cruise point. It includes already twist deformation under aerodynamic loads, then a twist correction of the opposite magnitude corresponding to the design point is performed. The obtained CFD mesh is the one corresponding to the *jig-shape*. Working with the *jig-shape* presents the advantage of working with a unique reference geometry in multi-points optimization processes in which a different aeroelastically deformed geometry is defined for each flight condition.

To perform a static aero-elastic analysis, a number of coupling iterations is defined during which the fluid and the structure exchange information. At each iteration step of the coupling process, the aerodynamic loads are extracted and applied on the beam model at the beam load nodes.

A beam deformation calculation is performed and the structural displacement field is transferred to the fluid domain. For static coupling this is done through mesh motion. We call \mathcal{X} the CFD mesh used during the current aero-elastic coupling process. The mesh \mathcal{X} is dependent on the initial *jig-shape* mesh \mathcal{X}_{rig} , the structural mesh \mathcal{X}_b and the beam deformation. These dependencies operate in the differentiation process of the aero-structural adjoint method detailed in section 5.2 while the dependency to \mathcal{X}_b is neglected for the aero-elastic adjoint formulation. Due to small deformation approximation, \mathcal{X}_b remains constant during the coupling process, and correspond to the *jig-shape*.

3.4.2.1 Aerodynamic load transfer to the structural mesh

The generic, global coordinates system of the airplane are denoted (x,y,z) .

At each coupling step of the aero-elastic computation, the aerodynamic loads are extracted from the CFD mesh and transferred to the beam node n_{b_i} , $1 \leq i \leq n_b$ of the structural mesh. This procedure has been proven to be consistent i.e. force and moment resultants are conserved. This section summarizes this process.

\vec{F}_i and \vec{M}_i denote, respectively, the aerodynamic force and the moment at the beam-load- point n_{b_i} , they are given by:

$$\begin{cases} \vec{F}_i = \sum_{l=1}^{n_{surf}^I} S_l^i (p_l - p_\infty) \vec{n}_l + S_l^i \mu_l \frac{\partial \gamma_l^i}{\partial n_l} \vec{t}_l \\ \vec{M}_i = \sum_{l=1}^{n_{surf}^I} n_{b_i} \overrightarrow{G_{infl_{n_{b_i}}}} \wedge (S_l^i (p_l - p_\infty) \vec{n}_l + S_l^i \mu_l \frac{\partial \gamma_l^i}{\partial n_l} \vec{t}_l) \end{cases}$$

where n_{surf}^I is the number of surface mesh cells within the influence zone $infl_{n_{b_i}}$ of the beam point n_{b_i} [Fig.3.1]. S_l^i is the intersection of the area of a cell and the influence zone.

The viscous part $S_l^i \mu_l \frac{\partial \gamma_l^i}{\partial n_l} \vec{t}_l$ is omitted when the fluid is modelled by the Euler equations. The computation of \vec{F}_i and \vec{M}_i considers surface mesh points that belongs to the area $S_{n_{b_i}}$ of the influence zone, such as:

$$S_{n_{b_i}} = \mathcal{X}_{surf} \cap infl_{n_{b_i}} = \cup_{n_f^I} S_l^i$$

3.4.2.2 Structural displacement transfer to the CFD volume mesh

Under the Euler-Bernoulli hypothesis, we denote the bending displacement field $d = (d_x, d_y, d_z)$ and the angular twist displacement $\theta = (\theta_x, \theta_y, \theta_z)$.

Once the aerodynamic forces are integrated at the aerodynamic surface mesh, they are transferred to the points of the structural mesh, called the load nodes. To each displacement node of the structural mesh, is associated a vertical movement d_z and a spanwise rotational movement θ_y . These quantities are computed by the structural solver **Beam** (cf A). The z-deflection and θ_y rotation are both expressed in the global

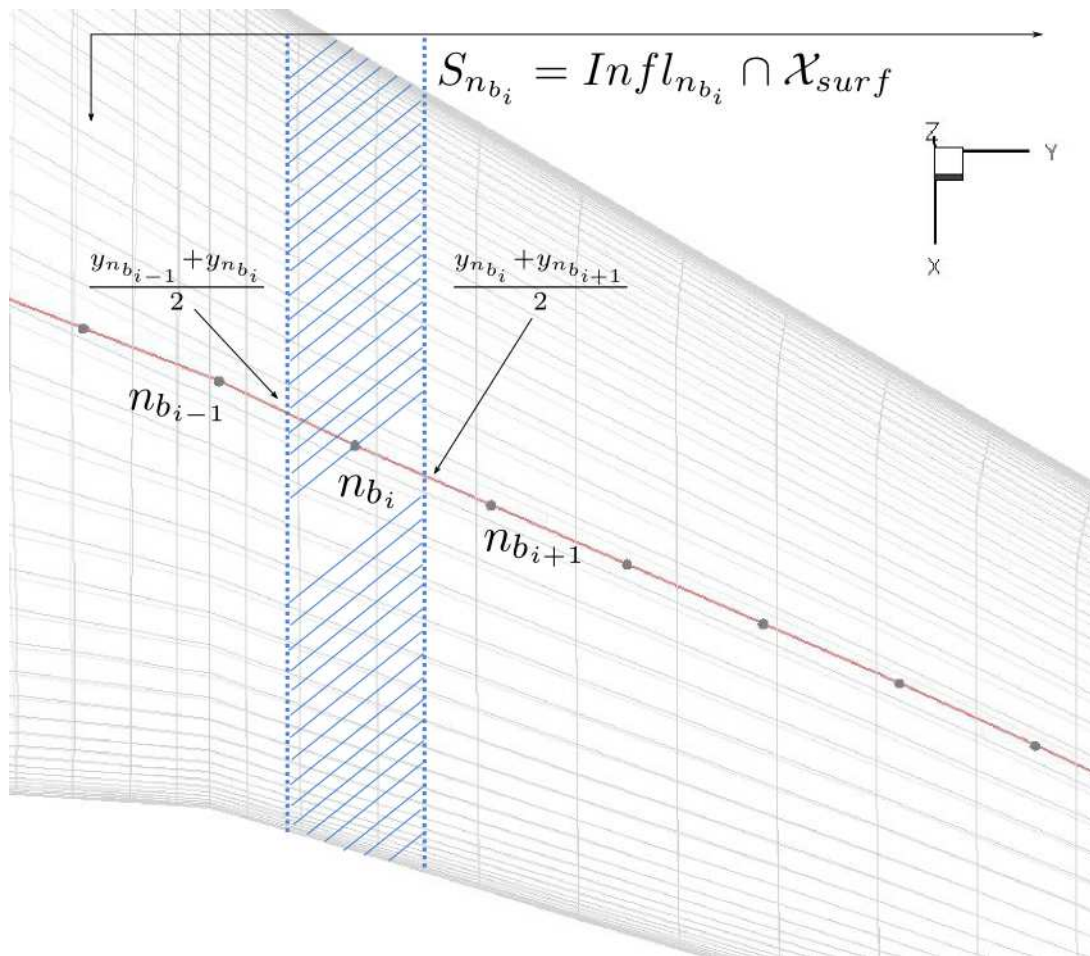


Figure 3.1: Load transfer at beam nodes.

coordinate system associated to the aircraft. To transfer this displacement to the rest of the fluid domain, solid mechanics analogy is used. We introduce

- \mathcal{X}_{rig_j} a point of the mesh corresponding to the *jig-shape*
- \mathcal{X}_j is the position of this point at an iteration of the aero-elastic coupling
- \mathcal{X}'_{b_j} is the projection of \mathcal{X}_j on the structural mesh \mathcal{X}_b

$$\mathcal{X}_j = \mathcal{X}_{rig_j} + d(\mathcal{X}'_{b_j})\vec{z} + \overrightarrow{\mathcal{X}_{rig_j}\mathcal{X}'_{b_j}} \wedge \theta(\mathcal{X}'_{b_j})\vec{y} \quad (3.24)$$

The elastic motion field is available at structural displacement mesh nodes. The projection \mathcal{X}'_{b_i} is unlikely to coincide with a structural mesh node, thus the structural deformation, at this point, is linearly interpolated from the computed value at the neighbouring structural mesh points.

Our interest is on high aspect-ratio aircraft wings, therefore this method may not be applicable for low aspect-ratio wings (supersonic wing for example).

3.4.3 Flexibility matrix computation for aero-elastic analysis

The displacement of structure is defined through the flexibility matrix approach defined as:

$$F = \begin{bmatrix} F^{zz} & F^{z\theta_y} & F^{z\theta_x} \\ F^{\theta_y z} & F^{\theta_y \theta_y} & F^{\theta_y \theta_x} \\ F^{\theta_x z} & F^{\theta_x \theta_y} & F^{\theta_x \theta_x} \end{bmatrix} \quad (3.25)$$

The nine blocks of F , introduced above, are matrices of size $n_b * n_b$, thus F is of dimension $3n_b * 3n_b$. For $1 \leq i, j \leq n_b$:

- the coefficient F_{ij}^{zz} is the linear vertical deflection d_z at the displacement point P_i due to unit vertical force f_z applied at the load node P_j
- the coefficient $F_{ij}^{z\theta_y}$ is the linear vertical deflection d_z at the displacement point P_i due to unit moment M_y applied at the load node P_j

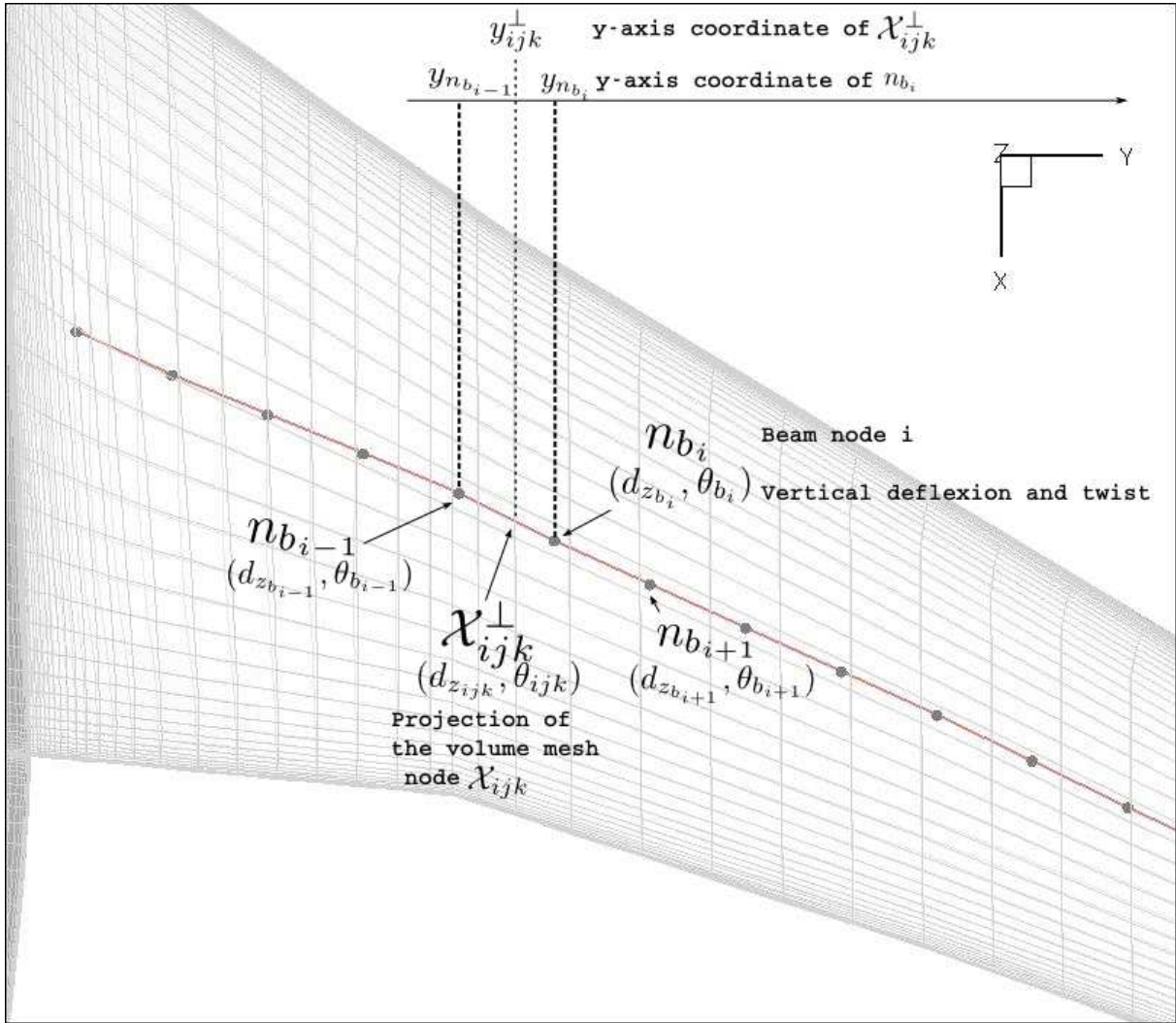


Figure 3.2: Deflection and twist allocation to the CFD volume mesh points

- the coefficient $F_{ij}^{z\theta_x}$ is the linear vertical deflection d_z at the displacement point P_i due to unit moment M_x applied at the load node P_j
- the coefficient $F_{ij}^{\theta_y z}$ is the angular deflection θ_y at the displacement point P_i due to unit vertical force f_z applied at the load node P_j
- the coefficient $F_{ij}^{\theta_y \theta_y}$ is the angular deflection θ_y at the displacement point P_i due to unit moment M_y applied at the load node P_j
- the coefficient $F_{ij}^{\theta_y \theta_x}$ is the angular deflection θ_y the displacement point at P_i due to unit moment M_x applied at the load node P_j
- the coefficient $F_{ij}^{\theta_x z}$ is the angular deflection θ_x at the displacement point P_i due to unit vertical force f_z applied at the load node P_j
- the coefficient $F_{ij}^{\theta_x \theta_y}$ is the angular deflection θ_x at the displacement point P_i due to unit moment M_y applied at the load node P_j
- the coefficient $F_{ij}^{\theta_x \theta_x}$ is the angular deflection θ_x at the displacement point P_i due to unit moment M_x applied at the load node P_j

The kinematics of the structure, which we assume linear elastic, is modelled by an Euler Bernoulli beam. There is no possible lead and lag motions according to the x-axis and lengthening movement according to the y-axis.

The structure of the wing takes up flexural loads f_z and M_x and torsional loads M_y , but it does transfer to the fluid domain, through the fluid-structure interface, only the bending displacement d_z and the twist θ_y . Because there is no transfer of angular deflection θ_x to the fluid domain (according to (3.24)), the dimension of the flexibility matrix is reduced to $2n_b * 3n_b$:

$$F = \begin{bmatrix} [F^{zz}]_{(1 \leq i, j \leq n_b)} & [F^{z\theta_y}]_{(1 \leq i, j \leq n_b)} & [F^{z\theta_x}]_{(1 \leq i, j \leq n_b)} \\ [F^{\theta_y z}]_{(1 \leq i, j \leq n_b)} & [F^{\theta_y \theta_y}]_{(1 \leq i, j \leq n_b)} & [F^{\theta_y \theta_x}]_{(1 \leq i, j \leq n_b)} \end{bmatrix} \quad (3.26)$$

The strain energy conservation in a body implies the symmetry of the complete $9n_b \times 9n_b$ flexibility matrix (a complete proof can be found in (8))

$$[F^{\theta d}]_{(1 \leq i, j \leq n_b)} = [F^{d\theta}]_{(1 \leq i, j \leq n_b)}$$

The direct simplifications resulting from the property of symmetry of F are that only the computation of the upper side of F^{zz} and $F^{\theta_y \theta_y}$ is needed and either $F^{\theta_y z}$ or $F^{z \theta_y}$ is computed. The coefficients $F^{z \theta_x}$ and $F^{\theta_y \theta_x}$ are fully computed.

The computation of the flexibility matrix coefficients, when the wing beam model is available, meaning that both the elastic axis geometry and the spanwise stiffness distribution are known, was performed by Marcelet for the purpose of aero-elastic adjoint development. It is detailed in (59) for simplified wings (rectilinear) and for wings like the configuration used in this work, with a positive sweep angle and positive dihedral angle that cannot be assimilated to a rectilinear beam and must be treated as piecewise linear.

The following section lays out the flexibility matrix coefficients in a summarized form. Their computation for a discretized beam model, of n_b points, is either identifies from a structural finite element model of the wing or computed by the structural module developed in this work and presented in chapter 4.1. These coefficients are linearised for the resolution of the aero-structural adjoint problem, their differentiation w.r.t. aero-structural design parameters is presented in Section 5.2.

At these stage, the bending stiffness EI and the torsion stiffness GJ spanwise distribution are supposed to be known and constants and provided with the extracted model. Such as, the resolution of the aero-elastic adjoint problem for the computation of the gradient of an aerodynamic cost function, do not take into account the sensitivities wrt EI and GJ . In an optimization process this means that these coefficients remain constant during the entire optimization process: The internal wing structure is frozen and do not evolve with the planform parameter changes.

We define the beam section $P_{i-1}P_i$ in the local coordinate system (X_i, Y_i, Z_i) , we assume that the beam deformation is known at displacement node P_{i-1} and we compute the induced deformation of the section $P_{i-1}P_i$. The loads at the beam point P_j , expressed in the global coordinate system (x, y, z) , are:

$$\begin{pmatrix} 0 & M_{x_j} \\ 0 & M_{y_j} \\ f_{z_j} & 0 \end{pmatrix}_{(x,y,z)} \quad (3.27)$$

Where M_{x_j} , M_{y_j} and f_{z_j} are, respectively, the flexural moment, the torsion moment and the vertical force per unit span. The moment induced at P_i by the loading at P_j , expressed in the global coordinate system, is:

$$\vec{M}(P_i)_{x,y,z} = \vec{M}(P_j) + \overrightarrow{P_iP_j} \times f_{z_j} \vec{z} \quad (3.28)$$

$$= M_x \vec{x} + M_y \vec{y} + \overrightarrow{P_iP_j} \times f_{z_j} \vec{z} \quad (3.29)$$

We project $\vec{M}(P_i)_{x,y,z}$ in the local coordinate system associated to the beam section $P_{i-1}P_i$:

$$\vec{M}(P_i) = M_{X_i} \vec{X}_i + M_{Y_i} \vec{Y}_i + M_{Z_i} \vec{Z}_i \quad (3.30)$$

With the assumption of the Euler-Bernoulli Beam model, only flexural moments M_{X_i} and torsional moments M_{Y_i} at the beam point P_i are considered for the deformation calculation. The structural deformation, expressed in the local coordinate system is the combination of d_{Z_i} the linear deflection according to the axis Z_i , θ_{X_i} the angular deflection according to the axis X_i and θ_{Y_i} the angular deflection according to the axis Y_i .

We denote:

- $(\theta_{X_i})_i$, respectively $(\theta_{X_i})_{i-1}$, is the angular deflection according to the local beam axis X_i at P_i , respectively P_{i-1}
- $(M_{X_i})_i$, respectively $(M_{X_i})_{i-1}$, is the flexural moment according to the local beam axis X_i , at P_i , is respectively P_{i-1}

- $(M_{Y_i})_i$, respectively $(M_{Y_i})_{i-1}$, is the flexural moment according to the local beam axis Y_i , at P_i , respectively P_{i-1}
- J_i , respectively J_{i-1} , is the torsional stiffness of the wing section at P_i , respectively P_{i-1}
- I_i and I_{i-1} , respectively, is the bending stiffness of the wing section at P_i , respectively P_{i-1}

If the loaded point P_j is located beyond the point P_i , meaning at a spanwise location closer to the wing tip, the deformation induced by the loads at P_i :

$$(\theta_{X_i})_i = (\theta_{X_i})_{i-1} + \frac{1}{2} \left(\frac{(M_{X_i})_i}{EI_i} + \frac{(M_{X_i})_i}{EI_i} \right) \|P_{i-1}P_i\| \quad (3.31)$$

$$(\theta_{Y_i})_i = (\theta_{Y_i})_{i-1} + \frac{1}{2} \left(\frac{(M_{Y_i})_i}{GJ_i} + \frac{(M_{Y_i})_{i-1}}{GJ_{i-1}} \right) \|P_{i-1}P_i\| \quad (3.32)$$

$$(d_{Z_i})_i = (d_{Z_i})_{i-1} + \frac{1}{2} \left((\theta_{X_i})_i + (\theta_{X_i})_{i-1} \right) \|P_{i-1}P_i\| \quad (3.33)$$

If the loaded point P_j is located before the point P_i :

$$(\theta_{X_i})_i = (\theta_{X_i})_j \quad (3.34)$$

$$(\theta_{Y_i})_i = (\theta_{Y_i})_j \quad (3.35)$$

$$(d_{Z_i})_i = (d_{Z_i})_j - (\theta_{X_i})_j \|P_{i-1}P_i\| \quad (3.36)$$

To go further

The previous deformations are the discrete formulation of the integral form of the classical formulation for beam deflections. Let d and θ denote the deflection and the elastic twist. The bending curvature is related to a unitary bending moment M through the relation

$$\frac{d^2 d}{dz^2} = \frac{M}{EI} \quad (3.37)$$

And St. Venant theory states for a unitary twist moment T

$$\frac{d\theta}{dy} = \frac{T}{GJ} \quad (3.38)$$

Then $(\theta_{X_i})_i$, $(\theta_{Y_i})_i$ and $(d_{Z_i})_i$ are projected in the global coordinate system of the aircraft (x,y,z) :

$$\begin{pmatrix} (\theta_{x_i})_i \\ (\theta_{y_i})_i \\ (d_{z_i})_i \end{pmatrix} = \mathcal{P}_{global/local} \begin{pmatrix} (\theta_{X_i})_i \\ (\theta_{Y_i})_i \\ (d_{Z_i})_i \end{pmatrix}_{(x,y,z)} \quad (3.39)$$

where $\mathcal{P}_{global/local}$ is the transfer matrix from the local coordinate system of the beam structural node to the global coordinate system of the aircraft.

The loading computed according to relation 3.27 is a generalisation case of the admitted loads on the point P_j . For example to compute the flexibility matrix coefficients $[F^{z\theta_x}]_{(1 \leq i, j \leq n_b)}$ that represent the deflection d_z along the axis z induced by the unit moment aligned with the x -axis, then only the flexural moment M_x is considered:

$$\tau = \begin{pmatrix} 0 & M_{x_j} \\ 0 & 0 \\ 0 & 0 \end{pmatrix}_{(x,y,z)} \quad (3.40)$$

Once the flexibility matrix is fully computed, the structural deformation it is multiplied by the aerodynamic loads according to the relation (3.22). The corresponding

deflection d_z according to the z -axis and the angular deflection (θ_y) according to the y -axis are propagated to the fluid domain, yielding a deformed CFD mesh in which a new iteration of the aero-elastic coupled simulation can be started.

To sum up, the aero-elastic equilibrium -a prerequisite for aero-structural and aero-elastic adjoints- is performed through a consistent and conservative load/structure iterative procedure, including the following sequence of actions:

- Loads transfer from aerodynamic mesh to the structural mesh;
- Compute displacements with the beam model;
- Transfer aero-elastic displacements from the beam mesh into the CFD mesh;
- Move the CFD volume mesh;
- Solve steady flow equations in the new mesh;
- Evaluate aerodynamic loads;

The number of the aero-elastic cycles depends on the treated configuration and on the initial point (jig-shape or not). For the studied configuration ?? the equilibrium is reached for five iteration of aero-elastic coupling.

3.4.4 Sensitivity analysis using the discrete aero-elastic adjoint method

The gradient computed via the aero-elastic adjoint concerns aerodynamic cost function. Let \mathcal{J}_{aero} denotes the aerodynamic objective -or constraint- function. \mathcal{J}_{aero} is taken to be :

$$\mathcal{J}_{aero} = \mathcal{J}(S_v, D_p), \text{ function of interest}$$

where

$S_v = \begin{pmatrix} S_{vf} \\ S_{vs} \end{pmatrix} = \begin{pmatrix} W \\ D \end{pmatrix}$, the state variables vector

$D_p = \begin{pmatrix} D_{pf} \\ D_{ps} \end{pmatrix} = \begin{pmatrix} \mathcal{X}(\mathcal{X}_{rig}, D) \\ 0 \end{pmatrix}, W^b(W, X)$, the dependencies of \mathcal{J}_{aero}

where W , respectively W^b is the aerodynamic conservative variables field on the CFD mesh \mathcal{X} , respectively on the CFD surface mesh \mathcal{X}_{surf} , and D the displacement field of the structural mesh \mathcal{X}_b nodes.

D_{pf} and D_{ps} are respectively the aerodynamic and the structural dependencies of the cost function taken into account by the differentiation process. In the case of the aero-elastic adjoint, the hypothesis of a constant structural model, the dependency of the function to the structural characteristics and to the structural mesh \mathcal{X}_b is not considered in the sensitivity analysis. The aero-elastic system is described, at the aero-elastic equilibrium, by the following state equation, expressed under residual form

$$R = \begin{pmatrix} R_f(S_{vf}, D_{pf}) \\ R_s(S_{vs}, D_{ps}) \end{pmatrix} = \begin{pmatrix} 0 \\ 0 \end{pmatrix}; \text{ governing equations}$$

R_f and R_s are respectively the aerodynamic and the structural residual form of the state equations. The adjoint of the aero-elastic problem, in opposition to the adjoint of the aero-structural problem, assumes an unchanged structure for the calculation of the gradient. In other words material and structural properties of the structure remain constant. The displacement $D = FL$ of the structure depends only on the transferred loads, so that differentiating the state equations w.r.t. α_{geom} gives:

$$\begin{bmatrix} \frac{\partial R_f}{\partial D_{pf}} & 0 \\ \frac{\partial R_s}{\partial D_{ps}} & 0 \end{bmatrix} \begin{bmatrix} dD_{pf} \\ d\alpha_{geom} \end{bmatrix} + \begin{bmatrix} \frac{\partial R_f}{\partial S_{vf}} & \frac{\partial R_f}{\partial S_{vs}} \\ \frac{\partial R_s}{\partial S_{vf}} & \frac{\partial R_s}{\partial S_{vs}} \end{bmatrix} \begin{bmatrix} dS_{vf} \\ dS_{vs} \\ d\alpha_{geom} \end{bmatrix} = \begin{pmatrix} 0 \\ 0 \end{pmatrix} \quad (3.41)$$

With the assumption of a constant structural model, are accessible only gradients of aerodynamic function with respect to aerodynamic shape parameters:

$$\frac{d\mathcal{J}_{aero}}{d\alpha_{geom}} = \begin{bmatrix} \frac{\partial \mathcal{J}_{aero}}{\partial D_{pf}} \\ 0 \end{bmatrix}^T \begin{bmatrix} dD_{pf} \\ d\alpha_{geom} \end{bmatrix} + \begin{bmatrix} \frac{\partial \mathcal{J}_{aero}}{\partial S_{vf}} \\ \frac{\partial \mathcal{J}_{aero}}{\partial S_{vs}} \end{bmatrix}^T \begin{bmatrix} dS_{vf} \\ dS_{vs} \\ d\alpha_{geom} \end{bmatrix} \quad (3.42)$$

As for the pure aerodynamic adjoint formulation, two arbitrary vectors which multiply the derivatives of the state equations are introduced to factorize out the expensive terms one wants to avoid calculation:

$$\begin{aligned}
\frac{d\mathcal{J}_{aero}}{d\alpha_{geom}} &= \begin{bmatrix} \frac{\partial \mathcal{J}_{aero}}{\partial D_{pf}} \\ 0 \end{bmatrix}^T \begin{bmatrix} dD_{pf} \\ d\alpha_{geom} \\ 0 \end{bmatrix} + \begin{bmatrix} \frac{\partial \mathcal{J}_{aero}}{\partial S_{vf}} \\ \frac{\partial \mathcal{J}_{aero}}{\partial S_{vs}} \end{bmatrix}^T \begin{bmatrix} dS_{vf} \\ d\alpha_{geom} \\ dS_{vs} \end{bmatrix} \\
&+ \begin{bmatrix} \lambda_f^T \\ \lambda_s^T \end{bmatrix}^T \begin{bmatrix} \frac{\partial R_f}{\partial D_{pf}} & 0 \\ \frac{\partial R_s}{\partial D_{pf}} & 0 \end{bmatrix} \begin{bmatrix} dD_{pf} \\ d\alpha_{geom} \\ 0 \end{bmatrix} + \begin{bmatrix} \lambda_f^T \\ \lambda_s^T \end{bmatrix}^T \begin{bmatrix} \frac{\partial R_f}{\partial S_{vf}} & \frac{\partial R_f}{\partial S_{vs}} \\ \frac{\partial R_s}{\partial S_{vf}} & \frac{\partial R_s}{\partial S_{vs}} \end{bmatrix} \begin{bmatrix} dS_{vf} \\ d\alpha_{geom} \\ dS_{vs} \end{bmatrix} \\
&= \begin{bmatrix} \frac{\partial \mathcal{J}_{aero}}{\partial D_{pf}} \\ 0 \end{bmatrix}^T \begin{bmatrix} dD_{pf} \\ d\alpha_{geom} \\ 0 \end{bmatrix} + \begin{bmatrix} \lambda_f^T \\ \lambda_s^T \end{bmatrix}^T \begin{bmatrix} \frac{\partial R_f}{\partial D_{pf}} & 0 \\ \frac{\partial R_s}{\partial D_{pf}} & 0 \end{bmatrix} \begin{bmatrix} dD_{pf} \\ d\alpha_{geom} \\ 0 \end{bmatrix} \\
&+ \left(\begin{bmatrix} \lambda_f^T \\ \lambda_s^T \end{bmatrix}^T \begin{bmatrix} \frac{\partial R_f}{\partial S_{vf}} & \frac{\partial R_f}{\partial S_{vs}} \\ \frac{\partial R_s}{\partial S_{vf}} & \frac{\partial R_s}{\partial S_{vs}} \end{bmatrix} + \begin{bmatrix} \frac{\partial \mathcal{J}_{aero}}{\partial S_{vf}} \\ \frac{\partial \mathcal{J}_{aero}}{\partial S_{vs}} \end{bmatrix}^T \right) \begin{bmatrix} dS_{vf} \\ d\alpha_{geom} \\ dS_{vs} \end{bmatrix}
\end{aligned} \tag{3.43}$$

Then the following system is solved for $\lambda = (\lambda_f^T, \lambda_s^T)$ using an iterative fixed-point like scheme

$$\begin{bmatrix} \frac{\partial R_f}{\partial S_{vf}} & \frac{\partial R_f}{\partial S_{vs}} \\ \frac{\partial R_s}{\partial S_{vf}} & \frac{\partial R_s}{\partial S_{vs}} \end{bmatrix}^T \begin{bmatrix} \lambda_f^T \\ \lambda_s^T \end{bmatrix} = - \begin{bmatrix} \frac{\partial \mathcal{J}_{aero}}{\partial S_{vf}} \\ \frac{\partial \mathcal{J}_{aero}}{\partial S_{vs}} \end{bmatrix} \tag{3.44}$$

When a converged solution is reached for the system (3.44), the sensitivity of $\frac{\mathcal{J}_{aero}}{d\alpha_{geom}}$ is assembled according to:

$$\frac{d\mathcal{J}_{aero}}{d\alpha_{geom}} = \left(\begin{bmatrix} \frac{\partial \mathcal{J}_{aero}}{\partial D_{pf}} \\ 0 \end{bmatrix}^T + \begin{bmatrix} \lambda_f^T \\ \lambda_s^T \end{bmatrix}^T \begin{bmatrix} \frac{\partial R_f}{\partial D_{pf}} & 0 \\ \frac{\partial R_s}{\partial D_{pf}} & 0 \end{bmatrix} \right) \begin{bmatrix} dD_{pf} \\ d\alpha_{geom} \\ 0 \end{bmatrix} \tag{3.45}$$

3.5 Extension of the aeroelastic adjoint method to an aerostructural adjoint method

In the previous section we presented the adjoint of the state equations for aeroelastic structures. The computations of the sensitivities with the aeroelastic adjoint are performed under the hypothesis of objective functions independent of the structural properties. In this case the structure is parametrized with wisely selected aerodynamic shape parameters and both objectives and constraints are aerodynamic functions.

In this section the objective function represents aerodynamics or structural performances, and likewise the constraint(s). The design parameters concern both disciplines so that the gradient computed allows the optimizer to shape both the aerodynamic envelop and the internal structure. The objective function -objective or constraint- is taken to be:

$$\mathcal{J} = \mathcal{J}(S_v, D_p), \text{ function of interest}$$

where

$$S_v = \begin{pmatrix} S_{vf} \\ S_{vs} \end{pmatrix} = \begin{pmatrix} W \\ D \end{pmatrix}, \text{ state variables vector}$$

$$D_p = \begin{pmatrix} D_{pf} \\ D_{ps} \end{pmatrix}$$

D_{pf} and D_{ps} are the dependencies of the functional \mathcal{J} -be it aerodynamic or structural- unlike the case of the aero-structural adjoint, these dependencies are coupled via W^b , the conservative variables at the fluid/structure interface, and via the structural mesh \mathcal{X}_b . The latter is a an explicite structural dependency D_{ps} and an implicite aerodynamic dependency D_{pf} , via the aero-elastic CFD mesh. All these terms are detailed in chapter 5.2.

The aeroelastic system is described by:

$$R = \begin{pmatrix} R_f(S_{vf}, D_{pf}) \\ R_s(S_{vs}, D_{ps}) \end{pmatrix} = \begin{pmatrix} 0 \\ 0 \end{pmatrix}; \text{ governing equations}$$

R_f and R_s are the discrete residual form of the RANS or the Euler equations and the structural equilibrium equation. Gradient based optimization requires the information of the sensitivity of the objective function with respect to the design variables:

$$\frac{d\mathcal{J}}{d\alpha} = \begin{bmatrix} \frac{\partial \mathcal{J}}{\partial D_{p_f}} \\ \frac{\partial \mathcal{J}}{\partial D_{p_s}} \end{bmatrix}^T \begin{bmatrix} \frac{dD_{p_f}}{d\alpha} \\ \frac{dD_{p_s}}{d\alpha} \end{bmatrix} + \begin{bmatrix} \frac{\partial \mathcal{J}}{\partial S_{v_f}} \\ \frac{\partial \mathcal{J}}{\partial S_{v_s}} \end{bmatrix}^T \begin{bmatrix} \frac{dS_{v_f}}{d\alpha} \\ \frac{dS_{v_s}}{d\alpha} \end{bmatrix} \quad (3.46)$$

To compute the total variation of \mathcal{J} with this formula, $\frac{dS_v}{d\alpha}$ would be necessary for each α . The increase of computation cost with the increase of design space dimension is obvious. Because the variation of the residuals is zero, the variation of the cost function with respect to the design variable can be expressed again:

$$\begin{aligned} \frac{d\mathcal{J}}{d\alpha} = & \begin{bmatrix} \frac{\partial \mathcal{J}}{\partial D_{p_f}} \\ \frac{\partial \mathcal{J}}{\partial D_{p_s}} \end{bmatrix}^T \begin{bmatrix} \frac{dD_{p_f}}{d\alpha} \\ \frac{dD_{p_s}}{d\alpha} \end{bmatrix} + \begin{bmatrix} \frac{\partial \mathcal{J}}{\partial S_{v_f}} \\ \frac{\partial \mathcal{J}}{\partial S_{v_s}} \end{bmatrix}^T \begin{bmatrix} \frac{dS_{v_f}}{d\alpha} \\ \frac{dS_{v_s}}{d\alpha} \end{bmatrix} \\ & + \begin{bmatrix} \lambda_f^T \\ \lambda_s^T \end{bmatrix}^T \begin{bmatrix} \frac{\partial R_f}{\partial D_{p_f}} & \frac{\partial R_f}{\partial D_{p_s}} \\ \frac{\partial R_s}{\partial D_{p_f}} & \frac{\partial R_s}{\partial D_{p_s}} \end{bmatrix} \begin{bmatrix} \frac{dD_{p_f}}{d\alpha} \\ \frac{dD_{p_s}}{d\alpha} \end{bmatrix} + \begin{bmatrix} \lambda_f^T \\ \lambda_s^T \end{bmatrix}^T \begin{bmatrix} \frac{\partial R_f}{\partial S_{v_f}} & \frac{\partial R_f}{\partial S_{v_s}} \\ \frac{\partial R_s}{\partial S_{v_f}} & \frac{\partial R_s}{\partial S_{v_s}} \end{bmatrix} \begin{bmatrix} \frac{dS_{v_f}}{d\alpha} \\ \frac{dS_{v_s}}{d\alpha} \end{bmatrix} \end{aligned} \quad (3.47)$$

where λ_s and λ_f are two arbitrary vectors called the adjoint vectors and

- $\frac{\partial \mathcal{J}}{\partial D_{p_f}} \frac{dD_{p_f}}{d\alpha}$: the change in the cost function due to design variable perturbation through the aerodynamic dependencies: the metric \mathcal{X} and the conservative variable W_b at the fluid/structure interface.
- $\frac{\partial \mathcal{J}}{\partial D_{p_s}} \frac{dD_{p_s}}{d\alpha}$: the change in the cost function due to design variable perturbation through the explicit structural dependencies: $\mathcal{X}_b, F(\mathcal{X}_b, I, J)$
- $\frac{\partial R_f}{\partial D_{p_f}} \frac{dD_{p_f}}{d\alpha}$: the sensitivity of the flow equations residual w.r.t design variable changes through the aerodynamic dependencies: the metric \mathcal{X} and the conservative variable W_b at the fluid/structure interface.

- $\frac{\partial R_f}{\partial D_{p_s}} \frac{dD_{p_s}}{d\alpha}$: the -implicite- sensitivity of the flow equations residual w.r.t the structural dependencies (effect of structural mesh changes on the aero-elastic mesh, and thus on R_f).
- $\frac{\partial R_s}{\partial D_{p_f}} \frac{dD_{p_f}}{d\alpha}$: the sensitivity of structural equations residual w.r.t design variable changes through the aerodynamic dependencies. In other words, this term quantifies the effect of design space perturbation on the loads L and on the flexibility matrix F through D_{p_f} .
- $\frac{\partial R_s}{\partial D_{p_s}} \frac{dD_{p_s}}{d\alpha}$: the sensitivity of structural equations residual w.r.t design variable changes through wing box geometry and flexibility modifications. It represents the effect of design variables perturbation on aerodynamic loads and on the flexibility matrix F through \mathcal{X}_b , the conservative variable W^b at the interface and the structural characteristics I and J .

In equation 3.48 below, the total variation of the cost function is reorganized, the first term represents the dependencies of \mathcal{J} and the second term is the dependence on the state variables:

$$\begin{aligned} \frac{d\mathcal{J}}{d\alpha} = & \left(\begin{bmatrix} \frac{\partial \mathcal{J}}{\partial D_{p_f}} \\ \frac{\partial \mathcal{J}}{\partial D_{p_s}} \end{bmatrix}^T + \begin{bmatrix} \lambda_f^T \\ \lambda_s^T \end{bmatrix}^T \begin{bmatrix} \frac{\partial R_f}{\partial D_{p_f}} & \frac{\partial R_f}{\partial D_{p_s}} \\ \frac{\partial R_s}{\partial D_{p_f}} & \frac{\partial R_s}{\partial D_{p_s}} \end{bmatrix} \right) \begin{bmatrix} \frac{dD_{p_f}}{d\alpha} \\ \frac{dD_{p_s}}{d\alpha} \end{bmatrix} \\ & + \left(\begin{bmatrix} \frac{\partial \mathcal{J}}{\partial S_{v_f}} \\ \frac{\partial \mathcal{J}}{\partial S_{v_s}} \end{bmatrix}^T + \begin{bmatrix} \lambda_f^T \\ \lambda_s^T \end{bmatrix}^T \begin{bmatrix} \frac{\partial R_f}{\partial S_{v_f}} & \frac{\partial R_f}{\partial S_{v_s}} \\ \frac{\partial R_s}{\partial S_{v_f}} & \frac{\partial R_s}{\partial S_{v_s}} \end{bmatrix} \right) \begin{bmatrix} \frac{dS_{v_f}}{d\alpha} \\ \frac{dS_{v_s}}{d\alpha} \end{bmatrix} \end{aligned} \quad (3.48)$$

Similarly to the aerodynamic adjoint, to eliminate the dependency of the total variation of the cost function on the state variables sensitivities, we solve for λ_s and λ_f :

$$\begin{bmatrix} \frac{\partial R_f}{\partial S_{v_f}} & \frac{\partial R_f}{\partial S_{v_s}} \\ \frac{\partial R_s}{\partial S_{v_f}} & \frac{\partial R_s}{\partial S_{v_s}} \end{bmatrix}^T \begin{bmatrix} \lambda_f^T \\ \lambda_s^T \end{bmatrix} = - \begin{bmatrix} \frac{\partial \mathcal{J}}{\partial S_{v_f}} \\ \frac{\partial \mathcal{J}}{\partial S_{v_s}} \end{bmatrix} \quad (3.49)$$

The aero-structural adjoint system, is solved using an iterative fixed-point like scheme by the software *elsA* (25). Once the adjoint vectors are computed, they are injected in

the expression of the final aero-structural gradient given by:

$$\frac{d\mathcal{J}}{d\alpha} = \left(\begin{bmatrix} \frac{\partial \mathcal{J}}{\partial D_{p_f}} \\ \frac{\partial \mathcal{J}}{\partial D_{p_s}} \end{bmatrix}^T + \begin{bmatrix} \lambda_f^T \\ \lambda_s^T \end{bmatrix}^T \begin{bmatrix} \frac{\partial R_f}{\partial D_{p_f}} & \frac{\partial R_f}{\partial D_{p_s}} \\ \frac{\partial R_s}{\partial D_{p_f}} & \frac{\partial R_s}{\partial D_{p_s}} \end{bmatrix} \right) \begin{bmatrix} \frac{dD_{p_f}}{d\alpha} \\ \frac{dD_{p_s}}{d\alpha} \end{bmatrix} \quad (3.50)$$

The gathering of the final aero-structural gradient requires the computation of the terms appearing in (3.48) and (3.50). These terms involve the sensitivities of the structural residuals or the sensitivities through the structural dependencies. These sensitivities are supplied by a structural solver developed in this work. The same module supplies the structural model for the aero-elastic computation step. The structural module InAirSsi, is presented chapter 4.1.

3.6 Outcome

In this chapter, we reviewed the aerodynamic adjoint equations, then the aero-elastic adjoint equations and finally introduced its extension: the aero-structural adjoint method. The aero-structural adjoint development relaxes the problem from the frozen flexibility hypothesis assumed for the development of the aero-elastic adjoint. This aims at accessing to the adjoint-based sensitivity analysis of the drag and structural weight, in order to solve a design problem: $C_D + \omega W$.

For the aero-structural adjoint resolution and gradient gathering, it is necessary to provide some sensitivities (partial or total) of the structural model w.r.t material characteristics, planform parameters α_{geom} and internal structure parameters α_{struct} . The aero-structural adjoint method has been introduced in section 3.5, it will be detailed in section 5.2, but before this, we present in section 4.1, the differentiated analytical structural model.

4

Development of an adjoint-compatible structural model of the wing

4.1 Preamble

In Chapter 3 we presented the extension of the adjoint method toward the consideration of the structure as an additional degree of freedom of the wing optimization problem. Our work is motivated by the search of the best compromise between aerodynamics and structures for optimal performance. For that we need the capability, for a given wing planform, to size the different structural components (for example spars...) in a way that minimizes the wing structural weight. The formulation of such a problem defines an aero-structural optimization framework. It requires the consideration of fluid and structure interactions and evolution not only of the wing shape parameters but also of the so called internal structural parameters. The structural decision parameters shape the geometry and/or topology of the internal wing. Aerodynamic loads are transferred to the rest of the aircraft via these components.

A gradient-based MDO process requires sensitivity information of the different functions involved in the multidisciplinary design problem. In the bi-disciplinary context

of this work, the sensitivities are those of aerodynamic and structural cost functions w.r.t. aero-structural design parameters. The aero-structural adjoint provides these sensitivities independently of the number of decision parameters. However, calculating these sensitivities requires the use of a parametric structural model which provides analytical derivatives of its internal routines. Indeed, the adjoint solver module and the final gradient gathering module of the CFD software *elsA*, must be supplied with the structural sensitivities appearing in the gradient expression (Sections 3.5, 5.2).

This chapter presents the linearised structural module that has been developed in this work: InAirSsi (Internal Aircraft Structural sizing) for structural and sensitivity analysis.

Powerful, commercial off-the-shelf tools for structural analysis, with fully featured finite elements models, exist and can be coupled to the ONERA CFD software *elsA*, but at the cost of high complexity in the preprocessing (data preparation) and actual use. Our approach derives from the idea that a tool used in conceptual and/or preliminary design needs to converge in a short time to a feasible solution and to be easy to use. We expect the methods, tools and solvers developed in research context for optimization purposes to be used by industry. In this context, if multidisciplinary tools are nested with a varying degree of fidelity, it is first because of the attractive ease of use linked to the current model complexity. Secondly, because the necessity of multidisciplinary interactions in preliminary design stage implies an elaborate convergence process toward a solution. The last point is all the more applicable when each of the intervening disciplines is modelled with the highest degree of fidelity. In addition, when the optimization does not lie simply on black box strategy to evaluate the performance of each discipline, the proposed methods for design space investigation, such as the adjoint method, should allow an effective adaptability, regardless of the studied configuration. It is not desirable to have complex set-up processes in early design phases where the reduction of time/cost is a target.

For the previous given reasons, we chose to model the wing structure behaviour by an Euler-Bernoulli beam ¹.

An important distinction between design processes and analysis processes must be done, understood and highlighted. At an early stage, when the objective is to explore the design space, the modelling of the physics can be, legitimately, kept simple. All the more since in a multidisciplinary context, the adjoint approach cannot be build upon black box software components, since its development is intrusive and requires full control on the entire process.

Beam models provide a valuable insight into slender structures. They are reliable and simple -yet physically meaningful- tools to take into account the aero-elasticity interactions that cannot be neglected even in a pre-design or optimization process. However, one must remember that a critical evaluation of the results is as important as the analysis itself. The beam model is and remains a low fidelity model with a high number of assumptions.

At ONERA, numerous works cover the high-fidelity structural modelling for optimization (25). The last example, to date, of high-fidelity modelling in a MDO context, is the work of Blondeau *et al.* (9). The authors computed aerodynamic and structural response using a CFD/CSM simulation with the *elsA* and MSC NASTRAN software to solve an aero-structural optimization problem implemented using the BLISS (Bi-level Integrated System Synthesis) (75) MDO formulation.

The work presented here is intended to extend the purely aerodynamic adjoint-based capability towards aero-structural design with simplified structural modelling. The developed aero-structural adjoint solver constitutes a step forward compared to the aero-elastic adjoint method. As said previously, the need to compute the objectives of both disciplines as well as their gradients drove us to develop a tool for structural modelling compatible with adjoint-based sensitivity analysis.

¹The Euler beam theory was established around 1750 by Leonard Euler, Daniel Bernoulli and Jacob Bernoulli

The first step for the adjoint formulation of an aero-structural problem is to perform an analysis at the aero-elastic equilibrium. This is performed via a coupled fluid/structure simulation, with the structural model computed by InAirSsi. The second step is the resolution of the dual problem for the gradient computation which requires the computation of derivatives w.r.t the dependencies of both disciplines. The resulting structural module, InAirSsi, is an input-output system [Fig 4.1] that interacts with the other pre-processing, analysis and post-processing modules composing the design process. The capabilities of the structural module InAirSsi can be summarised as:

- Structural modelling capability
- Weight computation capability
- Load application capability
- Material stress computation capability
- Sensitivity analysis capability
- Gradient-based optimization compatibility

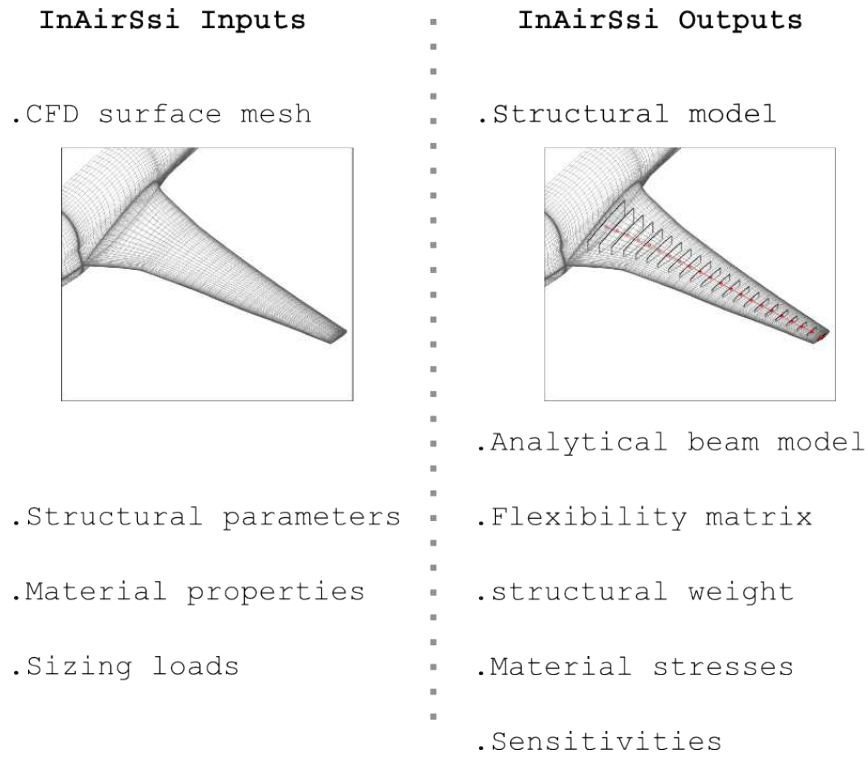


Figure 4.1: Input-Output system of the structural module InAirSsi

4.2 Structural model extraction

The wing is modelled as a cantilevered Euler Bernoulli beam with linear coupled bending and twist motions.

The equivalent beam model could be derived from a structural finite element model. During an optimization process, this would mean the generation of a CSM model for each configuration, but then the complexity and cost of such approach is debatable. The alternative is an identical structural model during the entire optimization process. This implies a design space restricted to parameters that do not affect both the mechanical properties of the wing and the structural weight. However, such a restricted design for an elastic wing would not benefit from the adjoint method capacity to over-

come the dimension of the design space.

The coupling of the aerodynamics and the structure passes through the nodes of the discretized beam model. These nodes can be either displacement nodes or load nodes. These nodes are the points where the aerodynamic forces are extracted and transferred to the structure, and where the structural displacement is transferred back into the aerodynamic mesh during the aero-elastic coupling.

The consideration of an Euler-Bernoulli beam as a wing model is driven by the importance of sections deformations under the efforts that the internal structure of the wing takes up. The internal structure of the wing (Fig 4.2) is assumed to be composed of elements of a closed section that do not warp under loads. Two key assumptions are implied with the Euler-Bernoulli beam model: the material is elastic according to Hook's law and the cross-section remains planar and perpendicular to the neutral axis during bending. The latter is known as Navier's hypothesis. Timoshenko's beam theory relaxes the Navier's hypothesis and allows shear deformation. This type of deformations, in the context of fluid/structure coupling, requires special care for mesh deformation, since at the fluid/structure interface a sheared cell will be propagated into the volume. In fact, the no-shear hypothesis is an additional virtual rigidity to the structure that we accept to take into account in the context of aero-structural adjoint method development.

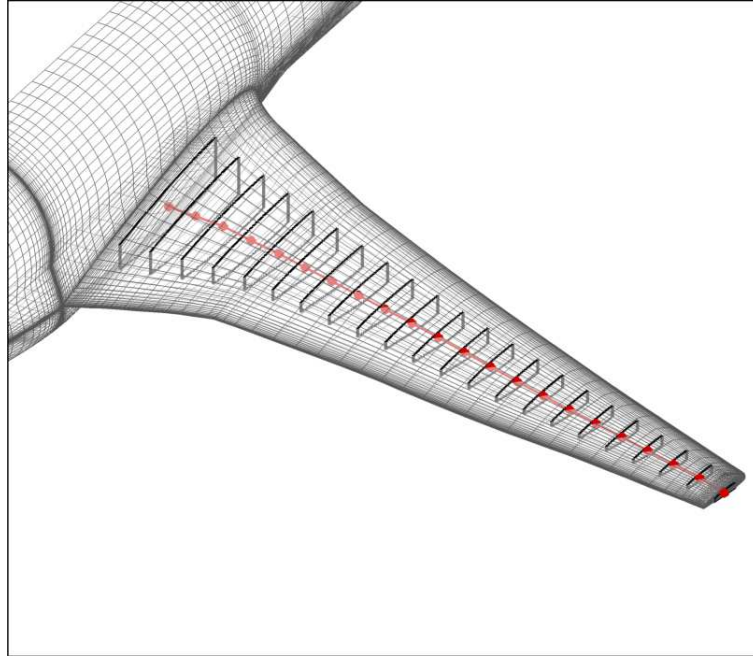


Figure 4.2: The structural model of the wing

4.2.1 Primary structure elements

Airworthiness requirements classify structures as load-bearing and non load-bearing structures. The former are called primary structures and are those that will endanger the aircraft upon failure. The latter are called secondary structures and are those that do not cause immediate danger upon failure.

The primary structure of the wing consists of spars, stringers and ribs. The secondary structure gathers the leading edge part and the trailing edge part and represents the main place for high lift devices. Both structures are embedded in the aerodynamic envelope of the wing.

In this work we have made the choice to model only the primary structure of the wing, since it is the part of the internal wing with the highest influence on the structural performances and the most sensitive to the external aerodynamic loads. The spars are major structural elements of the wing and the most heavily loaded structure of an air-

craft. Spars consist in a simple beam with usually an I-shaped cross section composed of a vertical part, the web and a horizontal part, the cap. The role of the spar caps is to increase the torsion resistance and to resist mostly bending loads and axial loads. The skin, as part of the torsion box, takes up the torsion loads. It links the caps of the front spar to the one of the rear spar and serves to resist bending. In addition, the skin of the upper wing and the lower wing resist shearing loads, and transmit the aerodynamic loads to the longitudinal part of the structure (spars) and the transverse part of the structure (ribs). The applied loads are then transferred to the rest of the structure via the spar elements. Finally, the skin operates with the spar caps to resist applied bending loads.

InAirSsi assumes a wing structure composed of two spars which are joined by a strengthened skin, forming the so-called torsion box. We assume that the longitudinal elements (skin and spar caps) are lumped into a single effective longitudinal element, forming a unique body. The spanwise wing box sections are assumed to remain rigid within their own plane [Fig.4.3].



Figure 4.3: Primary structure elements in a wing cross section

The components of the wing box elements are defined by the following geometrical properties, which form the structural parameters α_{struct} :

- t_{fs} : Thickness of the front spar web
- t_{rs} : Thickness of the rear spar web
- p_{fs} : Position of the front spar web

- p_{rs} : Position of the rear spar web
- t_{clow} : Thickness of the lower surface spar cap
- t_{cupp} : Thickness of the upper surface spar cap
- t_{slow} : Thickness of the lower surface skin
- t_{supp} : Thickness of the upper surface skin

4.2.2 Elastic axis of the structural model

For k spanwise control sections, we define $k * 8$ -where 8 is the number of structural parameters defined above- structural degrees of freedom to shape and size the wing box, and represented by the vector α_{struct} . InAirSsi takes as input α_{struct} and the aerodynamic wing envelope defined by α_{geom} . At each control section, each of the eight input values actually represents a percentage of the local airfoil thickness (for the upper and lower wing thicknesses) or a percentage of the local chord (for the front and rear thicknesses).

This geometrical characteristics are interpolated in the spanwise direction at the beam discretization nodes. This interpolation is performed considering the distribution of the thickness-to-chord ratio [Fig. 4.4].

The elastic axis [Fig.4.3] is located at the centroid of the cross-sections. To determine the centroid X_{b_iG} of a cross-section i , the wing box section is split into j common geometric shapes of centroid X_{jG} and area \mathcal{A}_j . The beam node, in the discrete form, is given by:

$$X_{b_iG} = \frac{\sum X_{jG}\mathcal{A}_j}{\sum \mathcal{A}_j}$$

The beam axis, piecewise linear, is oriented towards the wing tip and is noted y-axis. The x-axis is aligned with the fuselage axis and is oriented towards the empennage. The z-axis completes the system of axes [Fig.4.7].

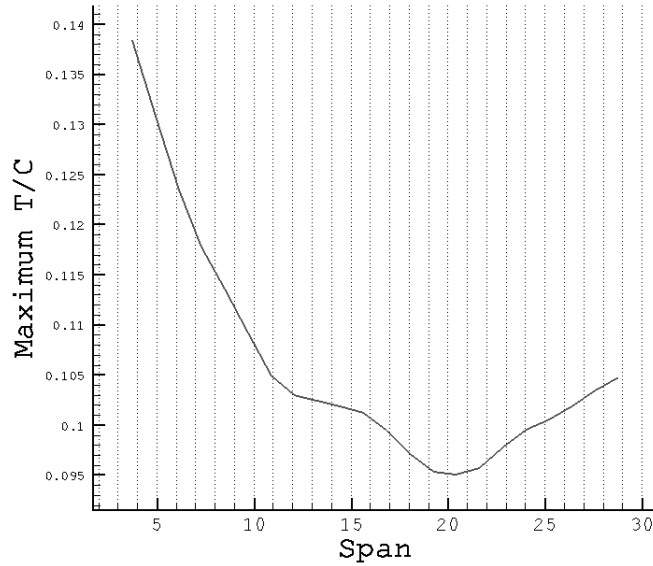


Figure 4.4: Maximal thickness to chord ratio distribution on the AIRBUS XRF1 configuration

During the structural sizing process or during the aero-structural optimization process, the wing box elements thickness, represented by α_{struct} , are controlled so that the weight or the aero-structural objective function is minimized while the stresses in the different elements material never exceed the elastic limit. The wing-box candidate, to sizing or MDO, must withstand maximum force of both stress components, the normal and the shearing stress. The response of the wing structure to the aerodynamic loads, depends on the mechanical properties of the wing. The computation of these properties via InAirSsi is presented in the next section.

4.3 Wing box mechanical properties

The flexibility matrix, presented in Section 3.4.3, transforms a loading field on the structure into a displacement field of the structure. The wing undergoes distributed

pressure forces which can be decomposed and represented through two spanwise distribution of integrated loads, namely a bending (or flexion, or flexural) load and a torsion (or twist, or torsional) loads. The intensity of the structural response is a function of the flexibility matrix coefficients, which depend on the structural, material and geometrical characteristics. The wing bending and twist resistance are measured, respectively, by the so called bending stiffness EI and torsion stiffness GJ along the beam axis. The key factor for flexion is the EI factor, the flexural stiffness that is simply the product of the young's modulus E that reflects the material properties and the I factor, named the second moment of area. E has the dimension of a force per square length, EI is thus expressed in term of force times squared length ($N.m^2$). The torsional response is controlled by the GJ factor. G is the shear modulus of elasticity and J the torsional constant of the cross -section

As explained previously, the aero-structural adjoint is developed to take into account flexibility changes. These changes are direct results of geometrical modifications (plan-form and geometrical). The need is then to evaluate EI and GJ as well as their sensitivities.

Bending stiffness

When a slender object of finite thickness is placed under bending loads, a part of this object is stretched and the other is compressed. The plane in between that is neither under tension nor compression is called the neutral plan. The amount of bending is controlled by EI . The bending stiffness of a section can be efficiently increased by placing the material away from the neutral plan (i.e., increasing the moment of inertia I). For the same amount of material, a full rectangle section is less stiff than an I-beam. At first this informs us on how the components considered to model the primary structure of the wing behave under bending loads. Secondly, it tells that the upper and lower longitudinal components of the wing structure drive the sizing of the wing box in flexion. As it is the case for metallic material (steel, aluminium...) the wing material is considered to be isotropic, this means that all the planes that pass through the wing

components are planes of elastic symmetry and thus $E_{xx} = E_{yy} = E_{zz} = E$.

To go further

Let S be a wing cross-section perpendicular to the beam axis oriented from the wing root toward the wing tip. The moment of inertia about the x-axis I_{xx} , the moment of inertia about the z-axis I_{zz} and the product of inertia I_{xz} , are defined as

$$I_{xx} = \iint_{\text{section}} z^2 dA \quad I_{zz} = \iint_{\text{section}} x^2 dA$$

$$I_{xz} = \iint_{\text{section}} xz dA$$

The structural elements are decomposed into symmetric elements about the x-axis or the z-axis, then we have $I_{xz} = 0$. The general bending equation is then given by

$$\sigma_{yy} = \frac{M_x}{I_{xx}}z + \frac{M_z}{I_{zz}}x$$

where σ_{yy} is the normal stress (defined in section 4.4.2). M_x and M_z are, respectively, the bending moments according to the x-axis and z-axis. The only bending moment that the wing box structure is subject to is the one according to the x-axis (see section 3.4.2). Thus only the moment of inertia about the x axis is computed.

The moment of inertia I_{xx} of the sections located at beam node discretization number j , $1 \leq j \leq n_b$, is formulated in a discretized form:

$$I_{xx_j} = \sum_{i=1}^6 \text{surf}_i (Z_{G_i} - Z_{b_j})^2 + \frac{w_i t_i^3}{12} \quad (4.1)$$

where

- surf_i is the area of the wing box i^{th} element $1 \leq i \leq 6$ (6 thicknesses: upper wing=spar caps+skin , lower wing=spar caps+skin , front spar web, rear spar web)
- Z_{G_i} is the z-coordinate of the centroid of the i^{th} element
- Z_{b_j} is the z coordinate of the displacement node at the j^{th} section $1 \leq j \leq n_b$
- w_i is the width of the i^{th} element

- t_i is the thickness of the i^{th} element

To validate the second moment of area calculation, we consider a wing box geometry represented by a set of random α_{struct} (without sizing), based on the aerodynamic envelope of a reference wing geometry. Then we compare the second moment of inertia extracted from the commercial CAD software CATIA to the one computed by the structural module InAirSsi:

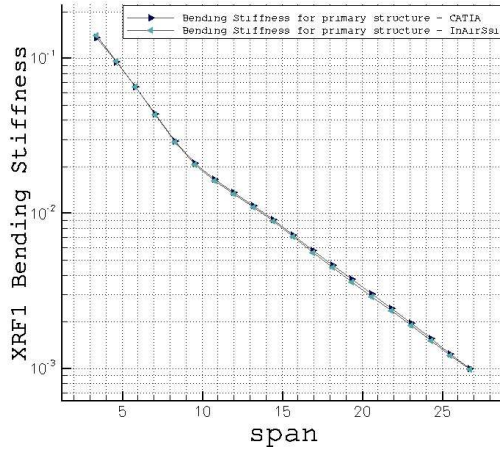


Figure 4.5: CATIA vs InAirSsi for I_{xx} of the XRF1 constructed primary structure

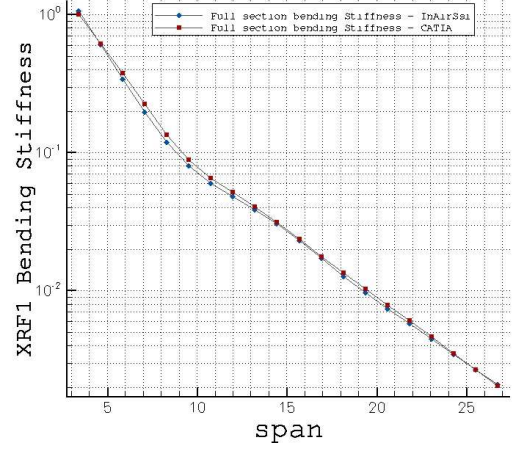


Figure 4.6: CATIA vs InAirSsi for I_{xx} of the full geometrical section of the XRF1 aerodynamic envelope

Torsional Stiffness

GJ , called the torsional stiffness, is the analogous variable to EI for torsional stiffness. G , the shear modulus, represents the resistance of the material to shearing, and is equal to the Young's modulus with a correction for Poisson ratio, $G = \frac{E}{2(1+\nu)}$. J , the torsional constant, should not be confused with the polar moment of inertia that is also described by the same variable J and defined as the sum of the main axis moments of Inertia. The only case where these two entities are numerically equal is for a circular member.

In our case, when we consider a linear elastic material, G is constant. For an isotropic material of centroidal axes x and z , $G_{zx} = G_{yx} = G_{yz} = G$.

To go further

Shear flow in an element of thickness t subject to shear stress τ is $\tau_f = \tau t$. Bredt-Bahto formula defines the torsion T of closed section beams with a constant shear flow:

$$T = 2\mathcal{A}\tau_f$$

where \mathcal{A} is the area enclosed by the cross section. The rate of twist for a constant shear flow is given by

$$2\mathcal{A}\frac{d\theta}{dy} = \oint \frac{\tau_f(s)}{Gt} ds = \tau_f \oint \frac{ds}{Gt}$$

s being the distance along the cross-section. The torsion moment resisted by the cross-section is:

$$T = GJ\frac{d\theta}{dy}$$

From the previous formulas we approach J by the so-called Bredt formula, given by:

$$J = \frac{4\mathcal{A}^2}{\oint_s \frac{ds}{t}} \quad (4.2)$$

The structural module InAirSsi uses the discretized form of formula 4.2:

$$J = \frac{4\mathcal{A}^2}{\sum_{i=1}^6 \frac{w_i}{t_i}} \quad (4.3)$$

The mechanical properties of the wing box, I and J , are presented as they are implemented in the structural module InAirSsi. They quantify the response of the loaded structure and the next section presents the method used to calculate the inner stress in each structural element for a given load case.

4.4 Primary structure elements stress analysis

The object of the present section is to present the computation of the stresses undergone by the wing structural elements.

During flight, any manoeuvre that causes accelerations or deceleration increases the forces and the stresses on the wing and fuselage. The stress, defined as load per area, quantifies the force intensity at any point in the structure and produces deformations in the material that are called strain. The integrity of the airplane depends on how the structure is loaded and how the resulting stresses are distributed in the structural elements. Thus, the role of the structural sizing is to keep the stress below a threshold level to prevent critical deformation that imperil the structural integrity of the airplane. The design process of the wing must provide a saving in structural weight while satisfying a minimum strength. This loss of strength is quantified by computing the maximum stress induced by the selected sizing load cases for each set of design parameters of the design space describing the aerodynamic shape and the geometry of the primary structure. The loading condition used to size the wing structure are defined by airworthiness FAR or JAR regulations (c.f. appendix C).

The stress field acting on the wing box is determined from the loading case given as input to the structural module InAirSsi. The structure resists to these solicitations and its response is given as a function of the mechanical characteristics of the beam model.

4.4.1 Load type on the wing box

The role of the primary structure of the wing is to carry and transmit all aerodynamic loads through the parts of the airplane: loads are taken up first by the wing skin, then transmitted to the ribs and finally to the spars.

There exist two distinct types of stress, normal and shear stress. The normal stress is associated with a relative change in length and the stress component associated to relative changes in angles is called shear stress. The normal stress component is induced by axial (y -axis) and bending moments. The shear stress component is induced by torsional moments and shear forces.

As stated previously, the wing aero-elastic behaviour is considered in this work as a linear system, the response of the structure to aerodynamic loads is calculated using the relation 3.22.

With the assumption of an Euler-Bernoulli beam-like structural behaviour, the wing box takes up the following loads:

- Vertical force F_z (bending action)
- Flexural moment M_x (bending action)
- Torsional moment M_y (twist action)

The wing is assumed to behave as a perfectly elastic material -i.e. the structure regains its initial form when external forces are removed-.

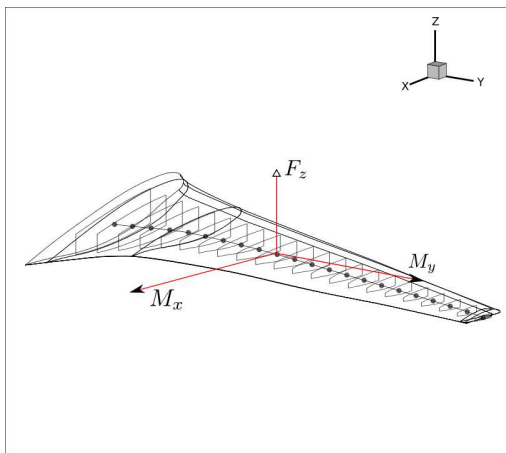


Figure 4.7: Bending and twist actions on primary wing box structure

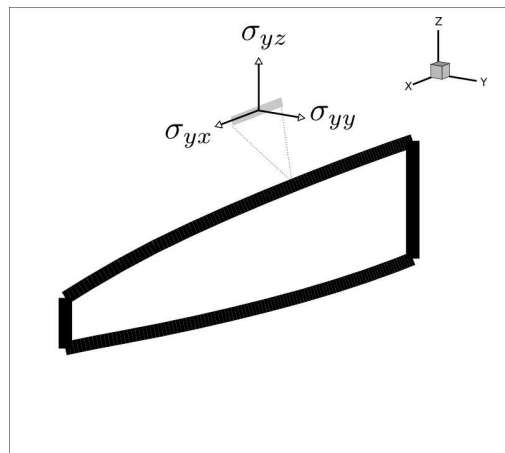


Figure 4.8: Stress solicitation on primary wing box structure

The force F_z is normal to the elastic axis. The torque moment M_y induces torsional shearing stress σ_{yz} and the bending moment M_x causes normal stress σ_{yy} . The stresses are related to the force resultant through the following relations

$$F_z = \int_{section} \sigma_{yz} dS \quad (4.4)$$

$$M_x = \int_{section} z\sigma_{yy}dS \quad (4.5)$$

$$M_y = \int_{section} x\sigma_{yz}dS \quad (4.6)$$

4.4.2 Bending normal stress on wing box elements

The x and z axes are the principal axes of the wing box cross-section. Thus, the product moment of inertia of cross-section $I_{zx} = \int_{section} zxdS$ is zero. In the case where no axial force F_y is acting on the structure and the bending occurs only along the centroidal x-axis, the general expression of the normal stress¹ reduces to the strength of material equation:

$$\sigma_{yy_i}(y) = \frac{M_{x_i}(z_i - z_{b_i})}{I_{xx_i}} \quad (4.7)$$

Where I_{xx_i} is the moment of inertia about the y-axis (section 4.3) of the cross-section i and $(z_i - z_{b_i})$ the distance of a point of vertical coordinate z_i to the neutral axis. M_{x_i} is the integrated bending moment of all aerodynamic forces acting on the wing, from the tip to the current beam node i :

$$M_{x_i} = \sum_{k=n_b}^i (M_{x_k} + \overrightarrow{P_i P_k} \wedge \overrightarrow{F^i})$$

where $\overrightarrow{F^i} = \begin{pmatrix} 0 \\ 0 \\ f_{z_j} \end{pmatrix}_{(x,y,z)}$.

The flexural loads are principally carried by the spar caps. For positive lift, bending moments produce compressive stresses on the upper part and tensile stresses on the lower part. The maximum compressive and the maximum tensile stress are located at the upper wing and lower wing interface, given by

$$\begin{cases} \sigma_{max}^u = \frac{M_x(z_{upp} - z_b)}{I_x} \\ \sigma_{max}^l = \frac{M_x(z_{low} - z_b)}{I_x} \end{cases}$$

¹ See reference (70) for detailed proof

The normal stress under sizing loads is computed by the structural module and must be kept below the elastic limit of the material in tension and compression.

4.4.3 Torsional shear stress on wing box elements

When the wing is aerodynamically loaded, the structural response induces a certain amount of twist. This angular-deflection is caused by a torsional action that induces shearing stress on the wing box. For thin-walled² closed cross-sections we assume that the torsional response can be determined without warping consideration. In fact, the warping is minimized because the relative displacement along the longitudinal line is minimized for closed-sections. By neglecting warping, the cross-section remains plane and torsion is resisted by torsional shear stresses. The level of torsional shear stress at the section i is given by:

$$\tau = \frac{M_{y_i}}{2\mathcal{A}_i t} \quad (4.8)$$

where t is the thickness of the bounding element and where M_{y_i} is the integrated torsional moment of all aerodynamic forces acting on the wing from the tip to the current beam node i :

$$M_{y_i} = \sum_{k=n_b}^i M_{y_k} + \overrightarrow{P_i P_k} \wedge \overrightarrow{F}$$

4.4.4 Shear stress in Euler-Bernoulli beam

The integral of lift forces from the wing tip to current cross section i , introduced as the vertical force F_z is mainly taken up by the spar webs. F_z produces bending normal stress, presented above, and transverse shear stress. Shear stress component in Euler-Bernoulli beam are equal to zero if the beam is under pure bending moment. If the cross-section is subject to both shear force (F_{z_i}) and bending moment (M_{x_i}) we cannot assume zero shear stress component. Under these conditions, Navier's hypothesis is still assumed to be valid and the level of shear stress³ at each component of the wing

²A cross-section of thickness t and width w is considered thin walled when $10 \leq \frac{w}{t}$

³The shear stress is established via the Saint-Venant assumption and the equations of equilibrium

$$\frac{\partial \sigma_{yy}}{\partial y} + \frac{\partial \sigma_{xy}}{\partial x} + \frac{\partial \sigma_{zy}}{\partial z} = 0$$

box of thickness t is given by

$$\tau_i = \frac{F_{z_i} \int_{area} z dA_i}{I_{xx_i} t} \quad (4.9)$$

Unlike the maximum stress, $\sigma_{yy_{max}}$ induced by bending action that is located at the edges of the section (skin), the maximum shearing stress, τ_{max} is located at the neutral axis of the cross section. The computed shearing stress under sizing loads must be kept below the elastic limit of the material in shear solicitation.

4.5 Analytical wing structural weight estimation

An optimal configuration has, among other characteristics, a low structural weight. From an overall point of view, we can say that the structural weight control implies the control of both payload, fuel-burn and range, three key indicators for airliners and aircraft manufacturers. Having said this, it is recalled that our work is to be used in an early design stage, and therefore it does not aim at developing a structural performance predicting tool providing a high level of accuracy of the absolute wing weight value, but rather a tool which predicts the sensitivity of this weight with respect to the different parameters involved in the present aero-structural design context.

Indeed, the aero-structural adjoint method which is the approach selected in this research to perform efficient design space exploration requires the calculation of wing weight sensitivity. What is considered as fundamental in this work, is not so much the high fidelity weight estimation as the evaluation of trade-off variations between aerodynamic and structures via a simple, but representative model. This section reviews briefly the state of the art in wing weight estimation and then presents its computation approach in InAirSsi.

To estimate the wing weight, three clusters of methods are commonly used. The first method relies on empirical regression, the second method on analytical equations and finally the third on accurate detailed multidisciplinary structural analysis.

4.5.1 Empirical methods

Empirical methods are the simplest methods to estimate the wing weight. They are based on the extrapolation of the structural data computed on existing and similar aircraft. It is obvious that the accuracy of such methods depends on the quality and quantity of available data. When innovative technologies are integrated or new concept evaluated, the physics-based methods are more suitable. E. Roux give in (73) a detailed and analysed selection of the existing statistical-based methods.

4.5.2 Analytical methods

In analytical methods, the weight evaluation is based on fundamental structural principles. Analytical methods are the intermediate approach between the empirical methods and the detailed, but time-consuming, FEM-based methods. The most widely cited model is developed by Ardema *et al.* (6), where *“the ideal weight of the carrythrough structure is computed from a summation of the bending shear and torsion material”*:

$$W = W_{bend} + W_{shear} + W_{torsion}$$

each of these terms is calculated from analytical formulae.

4.5.3 Physics based methods

In physics-based methods for wing weight estimation, the physics is modelled according to the phase of the design considered and the acceptable computation cost. The highest available degree of modelling is the finite element method. The structure is discretized into "finite" elements that have physical and geometrical properties, connected to the adjacent elements at nodal or displacement points. Beam and shell-elements are common physical-based methods in aeronautical structure representation. Dorbath *et al.* made in (23) a comparative study between the analysis with a beam model and the analysis with a shell theory in preliminary aircraft design. They show that the bending computation with a beam model presents a difference of $\pm 5\%$ in comparison with the deflection obtained with the shell theory. This difference is assimilated to the neglected

shear effects induced by the beam theory hypothesis. Torsion effects differ for configurations with quasi-rectangular wing boxes, where the shear center cannot be assimilated to the beam axis. They also conclude that beam approaches tend to underestimate the structural weight, due to the manner of computing the element thicknesses under the maximum stress value at each spanwise strip. Because the local effects are better represented in the shell computation, the highest stress level per section is higher in the shell computation, leading to a difference up to 19% for high swept wings.

Sometimes the simplicity of the purely analytical methods and the exactitude of physics-based methods can be combined for their respective profitable aspects of speed and fidelity. The wing can for example be divided into regions where the weight is estimated based on statistics and physically modelled regions. These methods are integrated to be used in frameworks which gather all mandatory steps to converge toward a correct mass estimation. Hürlimann presents rigorously in (37) a selection of the most popular existing tools and frameworks for mass estimation in use in the European aircraft industry. The tool Fame-W (Fast and Advanced Mass Estimation-Wing) developed by Airbus Germany (85), uses the effects of static aero-elasticity to size analytically the wing box modelled by a beam model. A key indicator for these tools is the way they are managing the complexity at all the steps. MDCAD is another mass estimation tool, developed by *QinetiQ*, which is based on CAD to generate the FEM for structural modelling and the CFD mesh for aerodynamic analysis.

This work aims at developing a tool compatible with the use of an adjoint solver which can be integrated in the preliminary design stage to form a physics based tool enabling multidisciplinary optimizations including structural sizing. In the framework of aero-structural adjoint method development, both methods (analytical and empirical) are not suitable. Empirical methods, besides the fact that they are not applicable to unconventional wings, are not suited to model the impact of structural characteristics of the model on the overall performance, and therefore are not suitable in the present context of aero-structural adjoint design. Finite element based-methods would present higher computational cost, and require much larger efforts to prepare the structural

model and data in an iterative optimization process. It is more suitable for detailed design and could represents an extension of this work.

4.5.4 Wing weight estimation with InAirSsi

As introduced in this chapter, each control section is defined by 6 thicknesses (see section 4.2.1. These thicknesses are then linearly interpolated in the spanwise direction . We first compute the structural weight of each element (skin, spar caps,etc...). Let us call W_i the structural weight of the element i , the total structural weight of the wing box is given by:

$$W_{wbox} = \sum_{i=1}^6 W_i \quad (4.10)$$

Let us exemplify the computation of W_i when the element i is the upper wing spar:

$$W_{c_{upp}} = 2\rho_{c_{upp}} \int_0^{span} h_{c_{upp}} l_{c_{upp}} dy \quad (4.11)$$

where

$\rho_{c_{upp}}$ is the material density of the upper wing spar cap elements,

$h_{c_{upp}}$ and $l_{c_{upp}}$ are the spar cap element dimensions,

As explained in section 4.2, all the decision variables computed in InairSsi are given as a function of the local chord for longitudinal elements or as a function of the local thickness for transverse elements. The spar caps thickness is a function of the local chord, then:

$$W_{c_{upp}} = 2\rho_{c_{upp}} \int_0^{span} Interp_{c_{upp}} \delta C(y) (\alpha_{rs} C(y) - \alpha_{fs} C(y)) dy \quad (4.12)$$

where

$C(y)$ is the local chord at the span location y ,

δ is the factor such as $h_{c_{upp}} = \delta(y)C(y)$,

α_{fs} and α_{rs} are, respectively, the front spar location and the rear spar location adimensioned by the local chord,

$Interp_{c_{upp}}(y)$ is the interpolating function between two control sections C_{s_i} and $C_{s_{i+1}}$ of upper wing thickness, respectively, $t_{c_{upp}^i}$ and $t_{c_{upp}^{i+1}}$, then for $y_{C_{s_i}} \leq y \leq y_{C_{s_{i+1}}}$:

$$Interp_{c_{upp}}(y) = y \left(\frac{t_{c_{upp}^{i+1}} - t_{c_{upp}^i}}{y_{C_{s_{i+1}}} - y_{C_{s_i}}} \right) + \frac{t_{c_{upp}^i} y_{C_{s_{i+1}}} - t_{c_{upp}^{i+1}} y_{C_{s_i}}}{y_{C_{s_{i+1}}} - y_{C_{s_i}}} \quad (4.13)$$

The local chord is expressed as a piecewise linear function, assuming a double-trapezoidal wing planform:

$$\begin{cases} \text{if } y \leq y_{crank} & C(y) = f(y_{root}, y_{crank}) + g(y_{root}, y_{crank})y \\ \text{if } y_{crank} \leq y & C(y) = f(y_{tip}, y_{crank}) + g(y_{tip}, y_{crank})y \end{cases}$$

where

$f(y_{root}, y_{crank})$ and $g(y_{root}, y_{crank})$ are the interpolation coefficients for the inner wing chord distribution function

$f(y_{tip}, y_{crank})$ and $g(y_{tip}, y_{crank})$ are the interpolation coefficients for the outer wing chord distribution function

We deduce the total weight of the spar caps distributed spanwise from 4.12,4.13,:

$$W_{c_{upp}} = 2\rho_{c_{upp}}\delta \sum_{i=root,tip} \left(y_i^4 \times \frac{f(y_i, y_{crank})^2 \alpha}{4} + y_i^3 \times \frac{2\alpha f(y_i, y_{crank})g(y_i, y_{crank}) + \beta g(y_i, y_{crank})^2}{3} + y_i^2 \times \frac{2\beta f(y_i, y_{crank})g(y_i, y_{crank}) + \alpha f(y_i, y_{crank})^2}{3} + y_i \times g(y_i, y_{crank})^2 \beta \right) \quad (4.14)$$

The structural computed weight $W_{c_{upp}}$ is unsized. The next step is then to provide to the sizing process the necessary constraints to converge toward a wing box structure that does not fail under the selected load cases.

InAirSsi takes the design load cases as inputs. These loads are given in the discrete form at the beam nodes. The structural module InAirSsi can take as many load cases as the user can provide. However, in the context of gradient computation with the aero-structural adjoint method, we choose to simplify the sizing loads computation:

the validation of the aero-structural gradients does not depend on the fidelity of sizing loads computation nor on the number of design load cases.

We select the $2.5g$ manoeuvre as the wing sizing load and we simply extrapolate the aerodynamic data at $2.5g$ from data measured for steady flow condition at the design point for simplicity reasons and for the present work validation purposes. The corresponding bending moment M_x , torsion moment M_y and vertical effort F_z are extracted for the purpose of stress analysis (section 4.4). Each primary structure element is sized for both flexural and torsional loads. In more complex structural modelling, the choice can be done to size an element only according to the load that it transfers to the rest of the structure. This results in a reduction of both analysis cost and number of structural constraints for the optimization. In our case the stress analysis, performed analytically, is straightforward and the structural constraints are managed by the analytical composite KS function, presented in the next section.

4.5.4.1 Constrained sizing for wing weight computation

There are different approaches to manage the large number of constraints when solving a structural optimization. These constraints -in an optimization perspective- are imposed to the structure, enabling it to support the sizing loads. The material constraints -that are the constraints of the optimization problem- can be all considered individually, or one can consider only the maximum of these constraints. The first approach may be seen as robust, but if we are not able to support it with a robust algorithm that will manage a fast convergence enabling a daily-use possibility, then it is judicious to explore other approaches. In the second approach the problem is solved by satisfying the most *urgent* constraint, useful when solving an aerodynamic optimisation problem without structural deterioration but not the most efficient for aero-structural optimization. These methods were compared by Poon and Martins in (71) with another approach based on constraints aggregation. This approach is the one used in this work and, as a numerical method, has also its *pros & cons*.

The Kreisselmeier-Steinhauser function was first introduced by G. Kreisselmeier and R. Steinhauser (106). It is an elegant manner to define a composite function for constraint aggregation: the constraints are aggregated into one or few composite functions reducing a multi-constraints problem into a single-constrained one.

The adjoint formulation is a direct answer to optimization problems with high number of design parameters and few objective functions. But there is no known method to compute the sensitivity of a high number of functions with respect to high number of design parameters at a low cost.

Structural weight minimisation problems are highly constrained problems, each stressed element of the structure being designed to withstand critical loads. When adjoint-based sensitivity is combined with gradient-based algorithms -local or global- to explore the solution space of such problem, the *KS* function presents a full potential by relaxing the optimization problem from the number of constraints.

The *KS* function was initially applied to the aggregation into a single composite function of both objective and constraint functions. It is defined as:

$$KS(g_i(\alpha)_{i \in [1, n_g]}) = \frac{1}{\rho} \ln \left[\sum_i^{n_g} e^{\rho g_i(\alpha)} \right] \quad (4.15)$$

Where $g_i(\alpha)_{i \in [1, n_g]}$ is a set of n_g constraints. An alternate formulation, that allows to avoid the computation of high exponential values and thus offers a better numerical behaviour is:

$$KS(g_i(\alpha)_{i \in [1, n_g]}) = g_{max}(\alpha) + \frac{1}{\rho} \ln \left[\sum_i^{n_g} e^{\rho(g_i(\alpha) - g_{max}(\alpha))} \right] \quad (4.16)$$

The parabolic *KS* function is the envelope surface of all the local stresses computed on the structural wing box. These stresses are the constraints of the structural sizing. The *KS* function, which is continuously differentiable, is defined as the maximum of local stresses. The *KS* function also allows to have less discontinuities at the constraints “intersections” in an optimisation problem. This induces a smooth transition from one

constraint surface to another.

However, the KS function presents drawbacks that must be understood, criticized and analysed in order to fully benefit from the great advantages that it offers in a adjoint-based optimization framework.

The KS function approaches the maximum of the constraints set. The parameter ρ controls the distance from the envelope surface to the surface of maximum constraint $\|g_i(\alpha)\|_\infty$. A high value of ρ draws the KS bound closer to the maximum constraint. A straightforward remark concerns the influence of this parameter in highly non-convex spaces. It follows that the efficiency of the KS function depends on the parameter ρ and the convergence may become more difficult when numerous constraints are active at an optimum. Martins et al. analysed in (94) the effect impacting the optimality of the KS function and proposed an alternative to the classical formulation which relies on the constraint sensitivity to update the value of the parameter ρ .

The constraint aggregation is implemented in the structural module InAirSsi. It comes with different options and formulations with a numerical interest, and thus will not be exposed in this manuscript.

The next section presents, as a validation, the sizing of 4 configurations followed by a comparative analysis of the parameters ρ .

4.6 Validation of InAirSsi

Let us recall that InAirSsi is a structural module developed, in the context of adjoint based optimization, InAirSsi computes analytically all the structural variables, as well as their sensitivities (see 5.2) w.r.t. α_{geom} and α_{struct} .

As a validation of InAirSsi, we present in section 4.6.2 the structural sizing of 4 configurations. These test cases are based on one original configuration modified by application of deformation of the spanwise thickness-to-chord distribution aiming at impacting the structural weight and analysing the behaviour of InAirSsi.

In section 4.6.3 is analysed the effect of the aggregation parameter on the convergence of the structural optimization.

4.6.1 Computation with InAirSsi of the derivatives required for the adjoint formulation

Any variable or function computed by InAirSsi is derived with respect to α_{geom} and α_{struct} .

Let us recall the main outputs of InAirSsi:

- \mathcal{W}_{wbox} , the structural weight;
- The material stresses (c.f. section 4.4) and their composite function KS ;
- \mathcal{X}_b the structural mesh (beam);
- $I(y)$ and $J(y)$ material characteristic distribution along the y-axis.

The derivatives of these outputs w.r.t the design variables are available besides the sensitivities of some of these outputs w.r.t the others. For example the sensitivities of $I(y)$ and $J(y)$ wrt to \mathcal{X}_b or the sensitivity of KS w.r.t to $I(y)$ and $J(y)$.

The gradient computed via the adjoint requires both explicit and implicit derivatives as introduced in section 3.5 and as it will be detailed in chapter 5.2.

The sensitivities -total and partial- of the flexibility matrix, assembled by the **Beam** class of the *elsA-BAG* solver (cf Appendix A) are also computed by InAirSsi.

Structural weight and KS function sensitivity validation

For sensitivity analysis -global and thus partial- validation purpose, we consider the aerodynamic envelope of our test case [Fig. 4.2]. The wing box is defined by an initial design vector α_{struct} . Before the sizing process, we compute the sensitivities of the initial structural weight, and the sensitivities of the KS function w.r.t to a selection of parameters. The validation of the KS sensitivities validates at the same time those of the material constraints, the material properties $I(y)$ and $J(y)$ and all the internal function of the module InAirSsi.

We control the geometry of the internal structure by using 42 variables driving the thicknesses of structural elements located at seven spanwise control sections (six parameters by section). Each section is then fully defined by 6 thicknesses. The validation is performed w.r.t the following variables, selected randomly among the total 42 variables:

- $t_{s_{low_1}}$: the thickness of the lower skin surface defined at the control section located at 16.6% of span
- $t_{s_{upp_2}}$: the thickness of the upper skin surface defined at the control section located at 20.9% of span
- $t_{c_{upp_3}}$: the thickness of the lower spar cap defined at the control section located at 28.22% of span
- $t_{c_{low_4}}$: the thickness of the upper spar cap defined at the control section located at 34.72% of span
- $t_{f_{s_5}}$: the thickness of the front spar web defined at the control section located at 52.15% of span
- $t_{r_{s_6}}$: the thickness of the rear spar web defined at the control section located at 75.2% of span

Figures 4.9 and 4.10 presents the exact match between the sensitivities computed analytically with InAirSsi and those computed by FD. These validations are the least that we can ask a derived code, the high valued interest is the -low cost- sensitivity analysis that in little CPU time we access rich informations corresponding to stress distribution over the structural elements [Fig 4.11]. An exploitable information for the aero-structural optimization, that can even be used to select a starting point for the gradient-based search algorithm by helping the user to know when and how the constraint is activated.

In Appendix B are presented additional sensitivity comparisons (differentiation with InAirSsi vs FD). These sensitivities are those of the internal functions and outputs of InAirSsi w.r.t to the design parameters α_{geom} et α_{struct} . These terms appear in the adjoint-based gradient formulation, detailed in the next chapter.

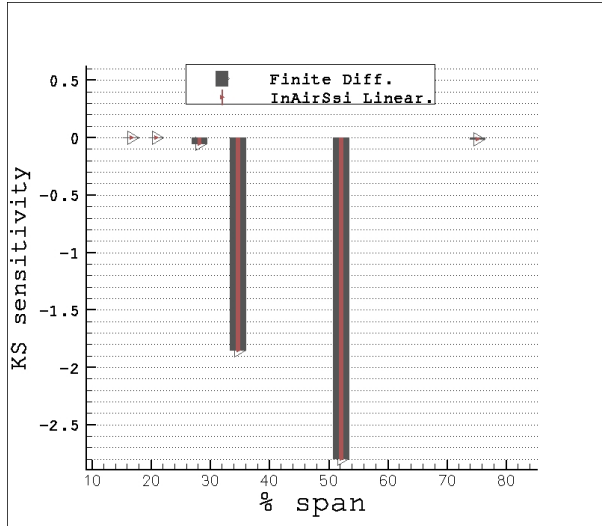


Figure 4.9: Finite difference vs differentiation with InAirSsi for *KS* function

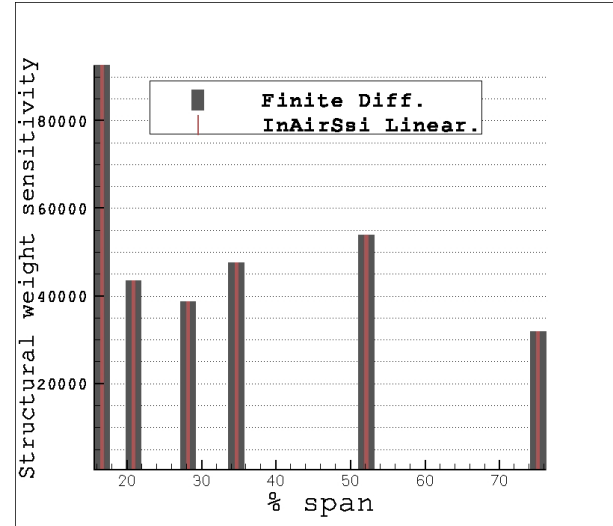


Figure 4.10: Finite difference vs differentiation with InAirSsi for the structural weight

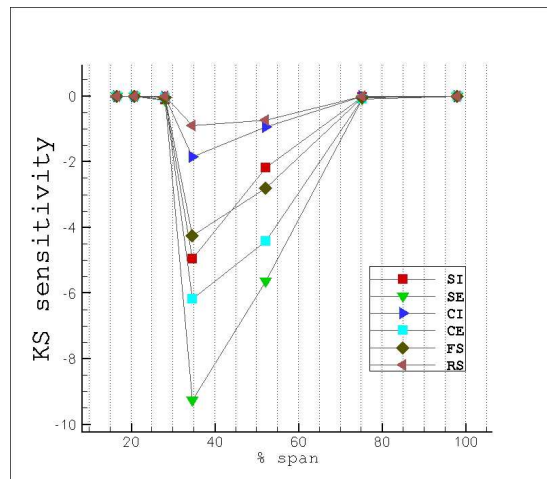


Figure 4.11: Spanwise sensitivity of *KS* at the initial design point function with respect to the 42 ticknesses

4.6.2 Comparative sizing of four XRF1-based configurations coupling InAirSsi with gradient-based algorithm

One of the most weight-impacting planform parameter is the thickness to chord ratio. This section presents, in the framework of validation, the structural sizing of 4 configurations. All derived from the initial test case by introducing thickness-to-chord and twist modifications.

We aim at evaluating, through gradient-based optimization, how the beam model implemented in the module InAirSsi behaves when an important parameter such as the thickness varies. The introduction of high fidelity analysis, may sometimes introduce numerical noise that makes the analysis difficult. Of course one may say that this noise is introduced because of complex phenomena. However, with an identical physical modelling, we should be able to predict behaviour such as an increase of the structural weight when the wing thickness is decreased (at constant loading). If not we should be able to provide a physical explanation.

The optimization problem is described as follows for a given aerodynamic loading:

$$\begin{aligned} & \text{minimize: } W_{wb}(\alpha_{struct}) \\ & \text{w.r.t. } \alpha_{struct} \in \mathbb{R}^n \\ & \text{subject to } KS(g_i(\alpha_{struct})_{i \in [1, n_g]}) \leq 0 \end{aligned}$$

where $g_i(\alpha_{struct}) = \frac{\sigma_i}{\sigma_{yield}} - 1$, σ_i is the material stress (bending normal stress, torsional shear stress, shear stress for Euler-Bernoulli beam) and σ_{yield} the yield stress of each type of stress. The wing box is parametrized by six thicknesses at seven control sections distributed spanwise (=42 parameters).

(a) Geometries

Tables 4.1 and 4.2 compare the parameters of the four configurations which differ in the spanwise wing airfoils thickness-to-chord ratio distribution and in the twist distribution.

	conf 10/10	conf 8/8	conf 4/4	conf 4/0
Wing root TTC ratio	+5%	+4%	+2%	+2%
Wing Crank TTC ratio	+10%	+8%	+4%	+4%
Wing tip TTC ratio	+10%	+8%	+4%	0%

Table 4.1: Thickness distribution of the candidate configurations expressed as variations w.r.t. to the reference wing (0%)

	conf 10/10	conf 8/8	conf 4/4	conf 4/0
Wing root section twist	0.38°	0.38°	0.36°	0.24°
Wing tip section twist	4°	4°	3.8°	2.86°

Table 4.2: Twist distribution of the candidate configurations

(b) Load cases calculation

When each of the four configurations reaches the aero-elastic equilibrium, as presented in section 3.4, the aerodynamic forces are extracted on the load nodes. The flexural force represented by the vertical effort F_z and the moment M_x as well as the torsional moment M_y are integrated from the wing tip to the wing root (Fig. 4.12) and extrapolated to generate the sizing load corresponding to a manoeuvre of 2.5g.

To extrapolate the aero-loads at 2.5g manoeuvre condition from the results of a calculation near design condition (1g), we apply to the integrated loads a factor of $= \frac{1.25}{C_L}$, 1.25 being the lift coefficient of the test case configuration under a load factor of 2.5g. In this case, after extrapolation, the four configurations have the same total integrated lift as presented in Fig.4.13.

(c) Structural sizing

The initial wing box is defined by a random set of structural parameters α_{struct} . This set of parameters corresponds to a light structural weight with a positive KS function,

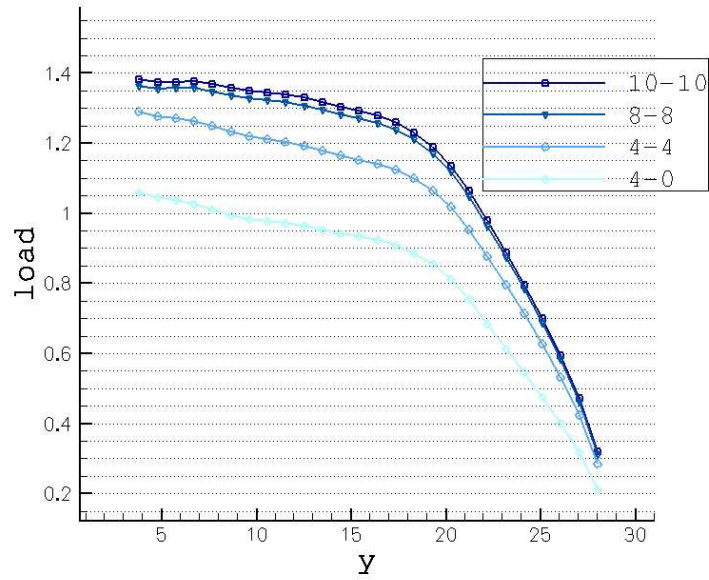


Figure 4.12: Integrated aerodynamic load distributions on the four configurations (calculation at forced angle of attack corresponding to the cruise condition)

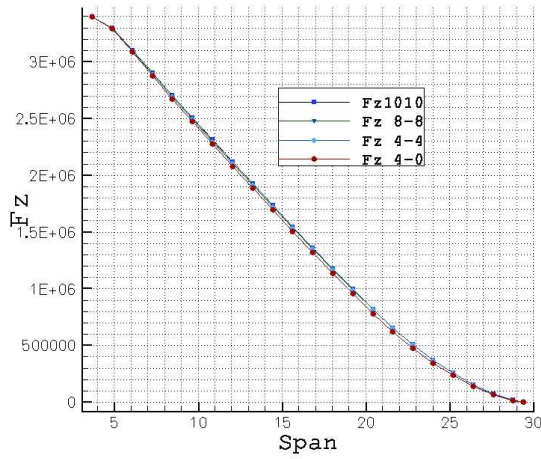


Figure 4.13: Cumulated F_z effort from the wing tip to the root at each spanwise position

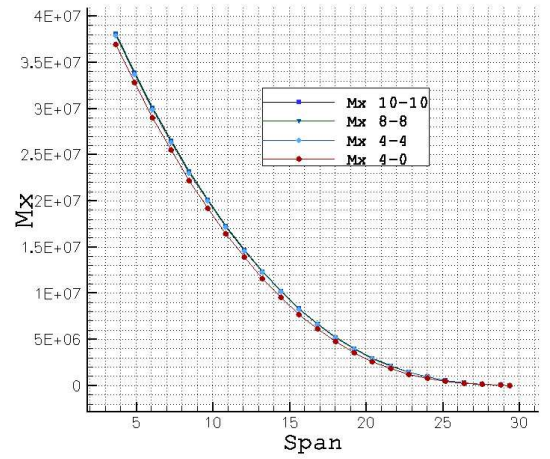


Figure 4.14: Cumulated M_x moment from the wing tip to the root at each spanwise position

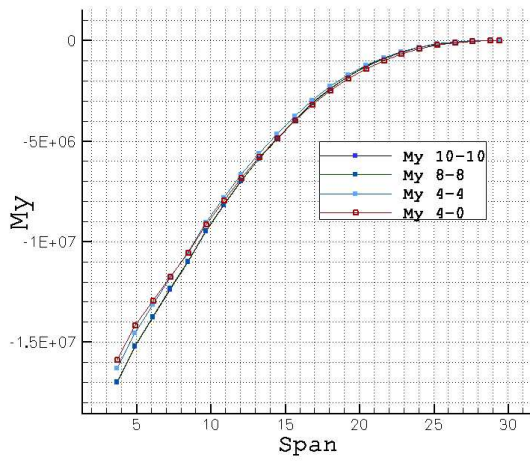


Figure 4.15: Cumulated M_y moment from the wing tip to the root at each spanwise position

which means that the structure is over-stressed under the imposed sizing loads. Table 4.3 lists the initial structural performance of the four configurations

	conf 10/10	conf 8/8	conf 4/4	conf 4/0
$W_{wb}(Kg)$	19,221	19,214	19,215	19,222
KS	1.83	1.90	2.00	1.891

Table 4.3: Initial structural weight and structural constraints aggregation

For a constant aerodynamic envelope we optimize the structural wing box to obtain a minimum structural weight while satisfying that the stress in the material does not exceed the limits of stress (through the aggregated stress constraint). Three algorithms were tested to solve this problem: CONMIN, DOT and CFSQP. The results with CFSQP (16) a sequential quadratic programming based algorithm were the most efficient in reaching the constraint although the convergence speed is relatively low [Fig. 4.16,4.17,4.18,4.19].

Table 4.4 summarizes the obtained structural performances at the convergence of the optimization. The configurations conf 10/10, conf 8/8 and conf 4/4 present the expected increase of structural weight of the wing box with the decrease of thickness to chord ratio. The last configuration conf 4/0 that approaches the initial test case presents however a lighter wing box than the configuration conf 4/4. This is explained through the cumulated loads F_z and the integrated moments M_x of this case, which are lower than the loads acting on the other configurations and thus producing lower material stresses.

A complementary test has been performed by sizing the four configurations under the same loading. In this case the configuration conf 4/0 has the heaviest wing box and the conf 10/10 the lightest wing box as expected.

There is also the fact that the aero-elastic computation, to produce the sizing loads, was performed with the initial wing box -unsized- geometry used for the optimization. This choice is probably not optimal and would require a loopback: the sizing of the optimal wing box under the sizing loads computed with the optimal parameter set.

However, the goal of this section is not to perform structural sizing but rather validate the derivation of the module InAirSsi, which has been successfully done.

	conf 10/10	conf 8/8	conf 4/4	conf 4/0
$W_{wb}(Kg)$	24.702	25.197	25.826	25.302
KS	-9.17E-04	-9.05E-04	-9.05E-04	-9.03E-04

Table 4.4: Structural weight and structural constraints aggregation at optimization convergence

Actually, these four configurations were issued from a MDO work using the BLISS method conducted by Blondeau, Dumont and Salah el Din in (9). There is no aim at comparing the results of this work with those of the BLISS approach based on finite elements structural modelling with NASTRAN. The topology and the structural characteristics used in InAirSsi differ from the ones used in the BLISS process (metallic vs composite). The sizing loads, for the FE model, were computed by Doublet Lattice Method (DLM) of NASTRAN, while InAirSsi computes the sizing loads obtained by extrapolating the discrete loads from the *elsA-BAG* (c.f Appendix A) aero-elastic computation at the design points. In addition, the high-fidelity FE-based procedure sizes the composite component of the wing box in terms of structural deformation while InAirSsi performs sizing by stress analysis. The expectation of this analysis is therefore not to obtain a perfect match of the two structural procedures, but rather to see how InAirSsi is able to predict the structural weight variation when basic parameters like wing thickness vary.

4.6.3 Analysis of the effect of the parameter ρ for constraint aggregation

The aggregation parameter ρ influences the behaviour of the algorithm by modifying the lower bound envelope of the constraints. The effect of this parameter is tested on a configuration that has more span and sweep angle than the original configuration. Of

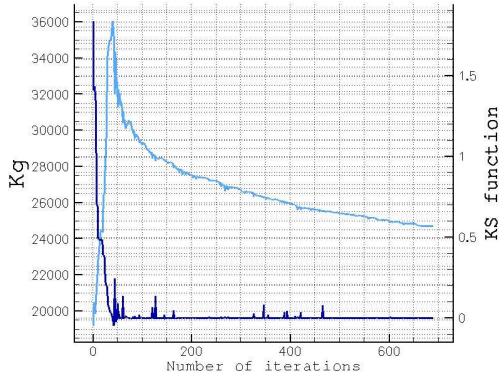


Figure 4.16: Structural weight optimization history for the case conf 10/10

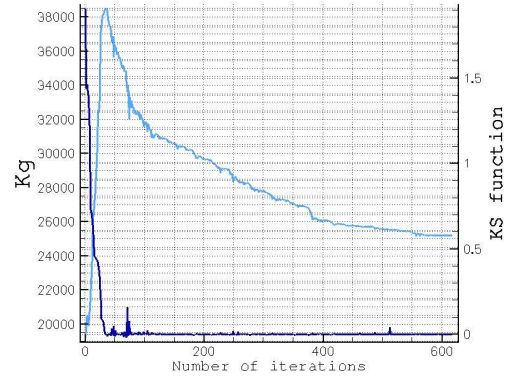


Figure 4.17: Structural weight optimization history for the case conf 8/8

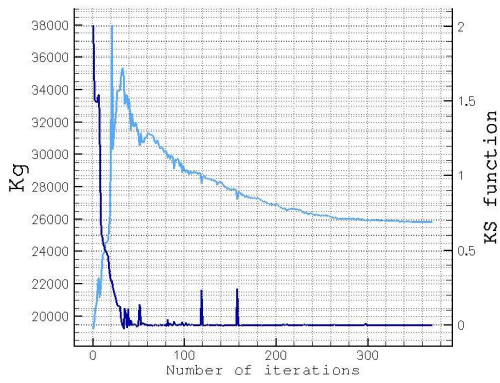


Figure 4.18: Structural weight optimization history for the case conf 4/4

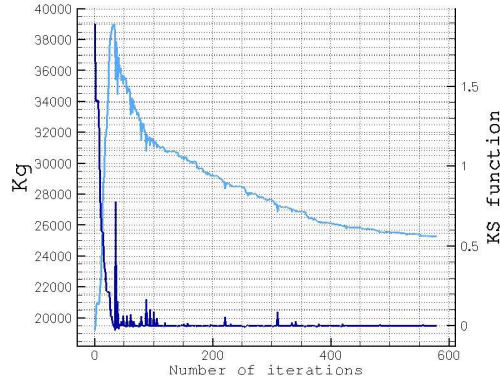


Figure 4.19: Structural weight optimization history for the case conf 4/0

course, this choice does not seek any particular effect, it is simply a demonstration of the capabilities of InAirSsi and the inhouse mesh deformation tools.

We solve the following problem with different aggregation factors:

$$\begin{aligned} & \text{minimize: } W_{wb}(\alpha_{struct}) \\ & \text{w.r.t. } \alpha_{struct} \in \mathbb{R}^n \\ & \text{subject to } KS(g_i(\alpha_{struct})_{i \in [1, n_g]}) \leq 0 \end{aligned}$$

where $g_i(\alpha_{struct}) = \frac{\sigma_i}{\sigma_{yield}} - 1$, σ_i is the material stress and σ_{yield} the yield stress.

Identical parametrisation to the sizing of the four previous wing boxes is used, i.e. 42 parameters (6 thicknesses at 7 control sections). The material stresses are computed at the section corresponding to the y-coordinate of the beam node elements.

For 23 beam elements, the structural sizing is constrained by 184 material constraints. Each section being constrained by 8 stress components (4 of bending type, 2 of torsion type and 2 of shear type).

According to its formulation, when the parameter ρ increases, the KS function approaches the maximum constraint. Wrenn shows in (89) that for the minimization problem of a one-dimensional case with two constraints, larger values of ρ results in a smaller optimum objective function. This cannot be generalized. In our case, the optimum improves with smaller values of ρ . In fact as it is shown in table 4.5 the lightest configuration is obtained for $\rho = 50$.

ρ	Initial wing box	Wing box after sizing
50	KS=0.139 & W=4.38e+04	KS=-0.0007 & W=3.02e+04
100	KS=0.121 & W=4.38e+04	KS=-0.0009 & W=3.08e+04
200	KS=0.115 & W=4.38e+04	KS=-0.0004 & W=3.22e+04

Table 4.5: Redesign results with different values of KS function parameter ρ

The weight breakdown, detailed in table 4.6, shows that the increase of the parameter ρ comes with a decrease of the structural weight of the elements sized mainly in bending

(the longitudinal elements), and with an increase of the structural weight of the vertical elements (spar webs).

	Initial WB	Opt. $\rho = 50$	Opt. $\rho = 100$	Opt. $\rho = 200$
Upper wing skin (kg)	3,611	3,924	3,602	3,441
Lower wing skin (kg)	4,352	4,001	3,691	3,518
Upper wing caps (kg)	11,559	7,587	7,497.47	7,449
Lower wing caps (kg)	10,574	7,652	7,511.13	7,457
Front spar web (kg)	6,903	3,543	4,359.39	5,240
Rear spar web (kg)	6,802	3,522	4,164.96	5,159

Table 4.6: Redesign results with different values of the aggregation parameter ρ

To understand this behaviour, we now plot the spanwise distribution of:

- the normal bending stress distribution acting on the set $\{t_{c_{upp}} + t_{s_{upp}}\}$;
- the torsion stress distribution acting on the set $= \{t_{c_{upp}}\}$;
- the torsion stress distribution acting on the set $= \{t_{s_{low}}\}$;
- the torsion stress distribution acting on the set $= \{t_{fs}\}$;

in both initial and optimal configurations for 3 values of the aggregation parameter: $\rho = 50, 100$ and 200 .

The left side of the figures represents the spanwise stress distribution at the start of the optimization. The right side the stress distribution at the convergence of the optimization.

Let us first focus on the bending stress distribution in the longitudinal elements: The value of σ_i tends toward σ_{yield} when ρ increases [set of Figures 4.20,4.21, 4.22, 4.23, 4.24 & 4.25].

The stress augmentation concerns the sections located before 70% of the span. Beyond, the elements are not more stressed because the lower bounds -defined as input for the optimization- of the design variables were reached.

It is important also to note that the initial stress distribution is homogeneous. The yield bending stress is not reached in any section. While we remark that the initial torsion stress distribution in the front spar webs is not uniform [Fig. 4.38,4.40 and 4.42]

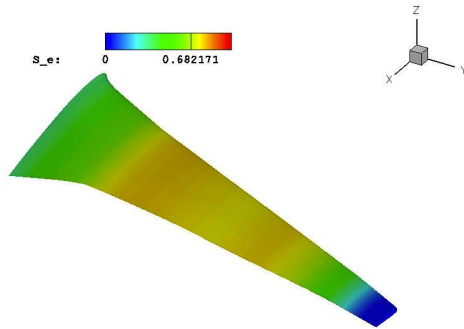


Figure 4.20: $\rho = 50$: Initial span distribution of the ratio of the bending stress in $\{t_{c_{upp}} + t_{s_{upp}}\}$ to σ_{yield} .

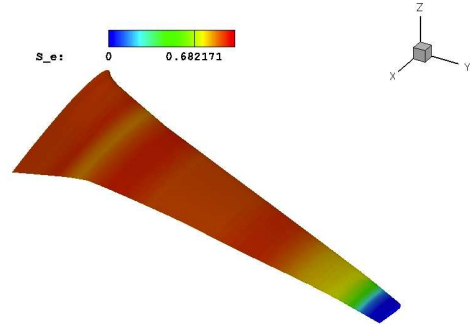


Figure 4.21: $\rho = 50$: Optimized span distribution of the ratio of the bending stress in $\{t_{c_{upp}} + t_{s_{upp}}\}$ to σ_{yield} .

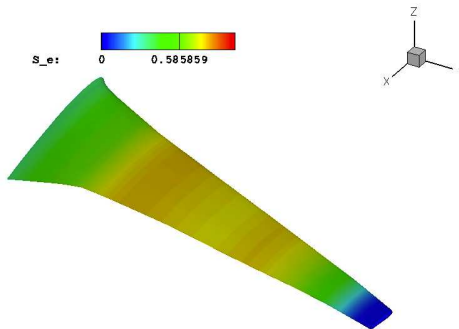


Figure 4.22: $\rho = 100$: Initial span distribution of the ratio of the bending stress in $\{t_{c_{upp}} + t_{s_{upp}}\}$ to σ_{yield} .

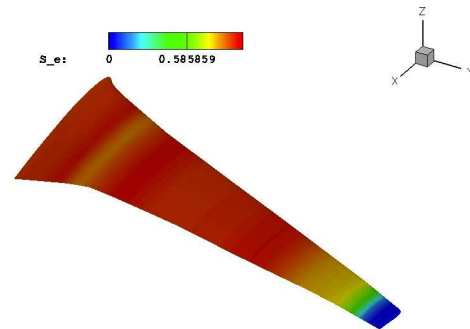


Figure 4.23: $\rho = 100$: Optimized span distribution of the ratio of the bending stress in $\{t_{c_{upp}} + t_{s_{upp}}\}$ to σ_{yield} .

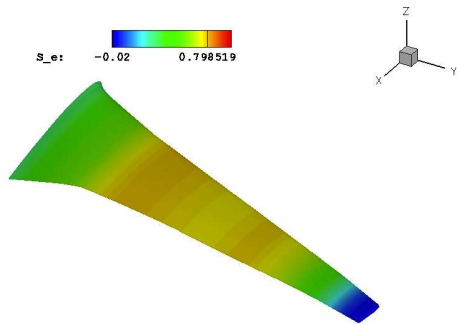


Figure 4.24: $\rho = 200$: Initial span distribution of the ratio of the bending stress in $\{t_{c_{upp}} + t_{s_{upp}}\}$ to σ_{yield} .

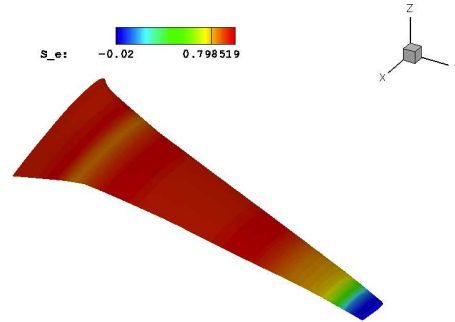


Figure 4.25: $\rho = 200$: Optimized span distribution of the ratio of the bending stress in $\{t_{c_{upp}} + t_{s_{upp}}\}$ to σ_{yield} .

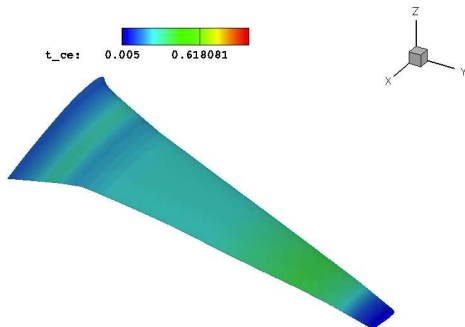


Figure 4.26: $\rho = 50$: Initial span distribution of the ratio of the torsion stress in $t_{c_{upp}}$ to τ_{yield} .

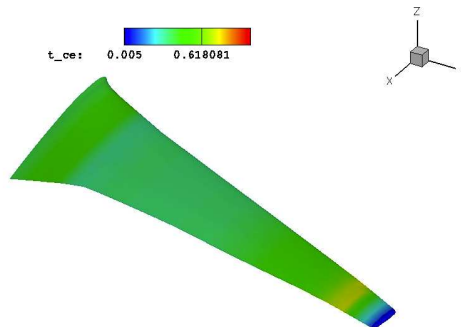


Figure 4.27: $\rho = 50$: Optimized span distribution of the ratio of the torsion stress in $t_{c_{upp}}$ to τ_{yield} .

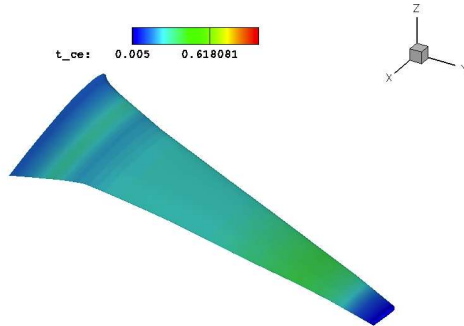


Figure 4.28: $\rho = 100$: Initial span distribution of the ratio of the torsion stress in $t_{c_{upp}}$ to τ_{yield} .

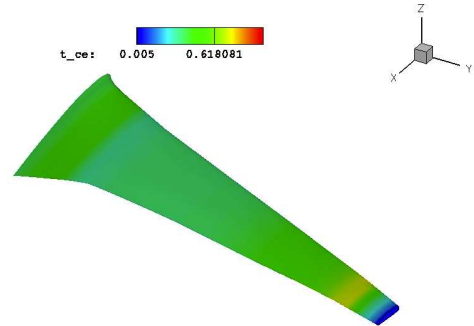


Figure 4.29: $\rho = 100$: Optimized span distribution of the ratio of the torsion stress in $t_{c_{upp}}$ to τ_{yield} .

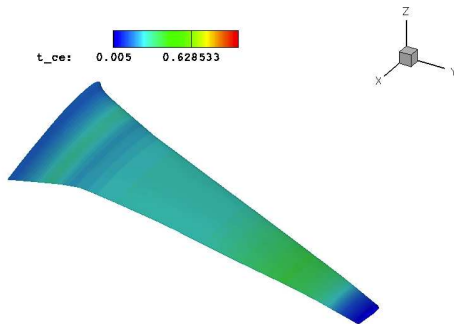


Figure 4.30: $\rho = 200$: Initial span distribution of the ratio of the torsion stress in $t_{c_{upp}}$ to τ_{yield} .

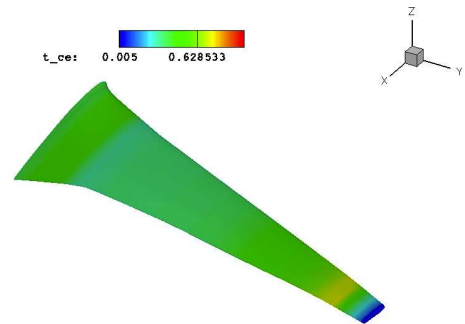


Figure 4.31: $\rho = 200$: Optimized span distribution of the ratio of the torsion stress in $t_{c_{upp}}$ to τ_{yield} .

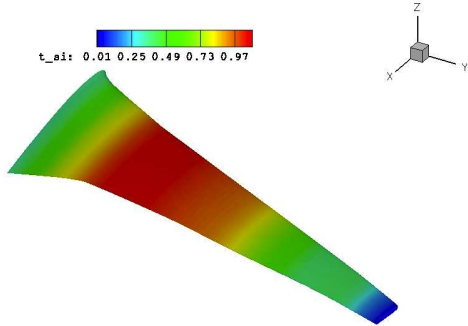


Figure 4.32: $\rho = 50$: Initial span distribution of the ratio of the torsion stress in $t_{s_{low}}$ to τ_{yield} .

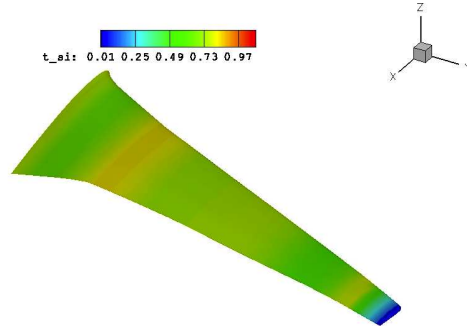


Figure 4.33: $\rho = 50$: Optimized span distribution of the ratio of the torsion stress in $t_{s_{low}}$ to τ_{yield} .

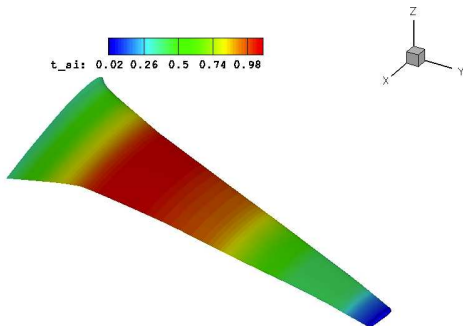


Figure 4.34: $\rho = 100$: Initial span distribution of the ratio of the torsion stress in $t_{s_{low}}$ to τ_{yield} .

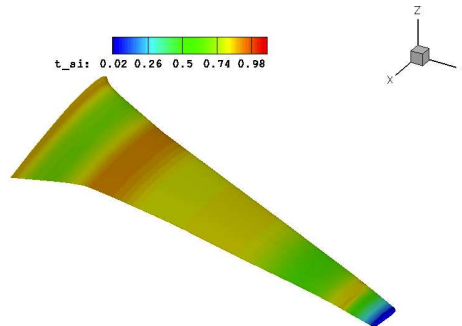


Figure 4.35: $\rho = 100$: Optimized span distribution of the ratio of the torsion stress in $t_{s_{low}}$ to τ_{yield} .

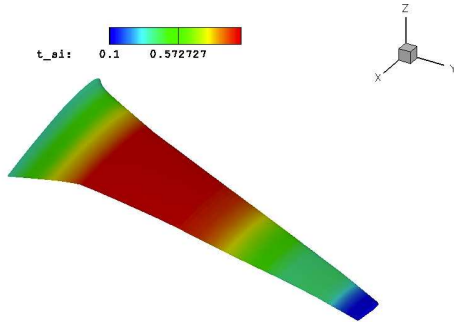


Figure 4.36: $\rho = 200$: Initial span distribution of the ratio of the torsion stress in t_{slow} to τ_{yield} .

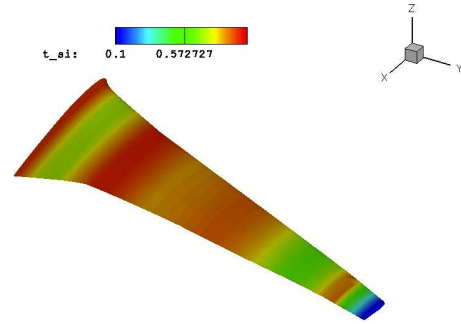


Figure 4.37: $\rho = 200$: Optimized span distribution of the ratio of the torsion stress in t_{slow} to τ_{yield} .

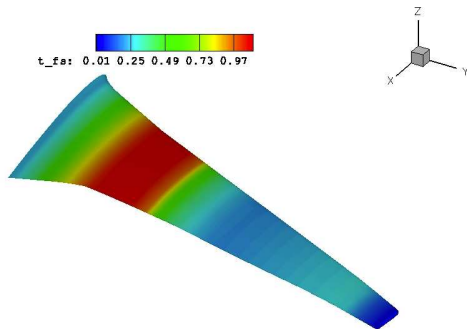


Figure 4.38: $\rho = 50$: Initial span distribution of the ratio of the torsion stress in t_{fs} to τ_{yield} .

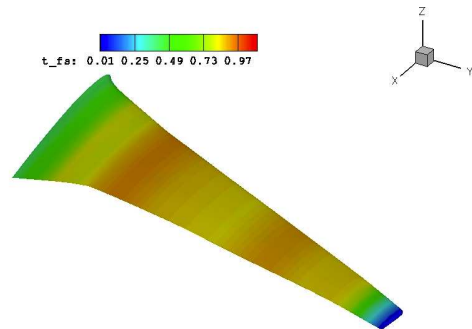


Figure 4.39: $\rho = 50$: Optimized span distribution of the ratio of the torsion stress in t_{fs} to τ_{yield} .

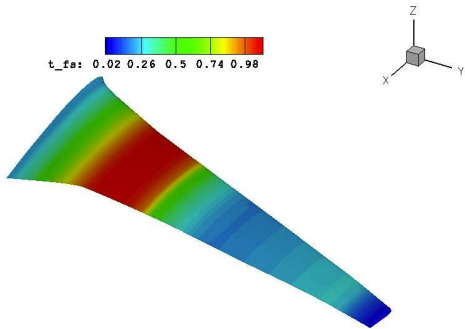


Figure 4.40: $\rho = 100$: Initial span distribution of the ratio of the torsion stress in t_{fs} to τ_{yield} .

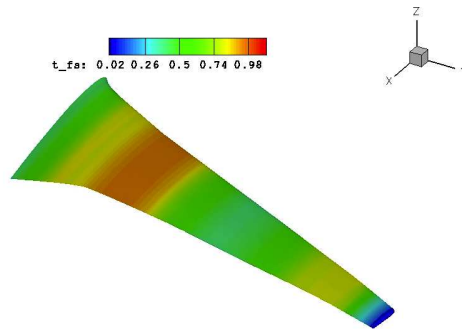


Figure 4.41: $\rho = 100$: Optimized span distribution of the ratio of the torsion stress in t_{fs} to τ_{yield} .

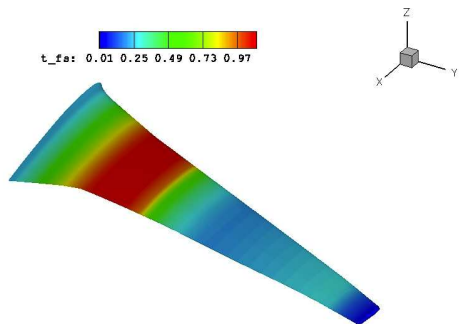


Figure 4.42: $\rho = 200$: Initial span distribution of the ratio of the torsion stress in t_{fs} to τ_{yield} .

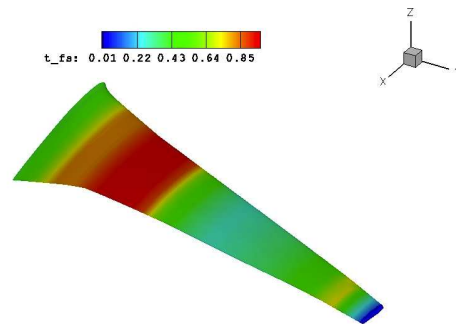


Figure 4.43: $\rho = 200$: Optimized span distribution of the ratio of the torsion stress in t_{fs} to τ_{yield} .

. The analysis of optimal stress distribution in the front spar [Fig. 4.39,4.41 and 4.43] show that with the chosen initial geometry the maximal stress value is reached in the wing portion located between the crank and 40% of the span ($\tau_{yield} \leq \tau$). If we analyse what are the regions most affected by the modifications of the aggregation parameter ρ , then it appears that it is particularly these regions, initially severely stressed. They drive mostly the sizing, unbalancing the sizing of the vertical element located before the crank and after 40% of the span. One can make the hypothesis that the aggregation parameter plays the role of a weighting parameter for the most violated constraints. The smallest the aggregation parameter the more the aggregated functions are treated equally.

The torsion stress, as expected, do not drive the sizing of spar caps elements. The optimal span distribution of the torsional stress [Fig. 4.27,4.29 and 4.31] is almost unaffected by the value of the aggregation parameter indicating a hierarchy of the different aggregated constraints. The torsion stress distribution on the lower skin is also not uniformly distributed along the span [Fig. 4.32,4.34 and 4.36], however the sizing for these elements is mainly driven by the bending stress.

The important points that this section meant to highlight, beside being a validation of the structural module, is that special care has to be taken when numerous constraint functions are lumped into one aiming at capitalising the full potential of the adjoint method.

The different nature of the stress components acting on the structure makes this function composition *non-physical*. In addition, the aggregation parameter is problem-dependant or constraint-dependant, and requires a pre-analysis. This is specifically where the low-cost sensitivity analysis of the structural module InAirSsi presents a full potential. Another remark concerns the decomposition of the KS function. The wing is far from being uniformly stressed, and thus lumping high and low stress values may lead to a suboptimal results. One can then introduce two or three KS functions by separating the outer and the inner regions, or by introducing an upper and a lower lumping.

In other words, a compromise has to be found between the number of constraints and the efficiency of the design exploration.

4.7 Outcome

This chapter details the development of the adjoint-oriented structural module InAirSsi.

This module enables aero-elastic computations by providing a model (geometry and flexibility) of the wing structure straightforwardly, without any effort by the designer. But the most important thing concerning the structural approach used by InAirSsi is that it enables the sensitivity analysis used for the design space exploration in a preliminary design phase. The required information at these stages of the design is not necessary complex or high-fidelity based, but still requires efficient physical modelling and mathematical tools, since the exploration of a design space of dimension higher than 100, cannot be done neither by hand, nor by empirical methods.

Dedicating a considerable effort to evaluate an exact structural weight, knowing that the structure is subject to changes and modifications is not the strategy for optimisation at early design stages, but rather for latter detailed analysis stages. But having the sensitivities, w.r.t. planform changes, of both aerodynamic and structural performances is a valuable information.

The development of InAirSsi was oriented according to this strategy: enabling a cost-effective access to the adjoint-based gradients of an aero-structural system by providing all the sensitivities that appear in the adjoint formulation that are detailed in the next chapter.

5

From aero-elastic to aero-structural adjoint-based gradients: Detailed description

5.1 Preamble

In chapter 3 we introduced the extension of the aero-structural adjoint formulation from the aero-elastic adjoint formulation, itself extended from the aerodynamic adjoint. This extension requires a derived structural model that supplies the adjoint solver with:

- sensitivities related to the evolution of the structural model and its mechanical characteristics;

- sensitivities linked to the impact that structural geometry modifications has on the aero-elastic equilibrium.

The module implementing this structural and its functionalities were presented in the chapter 4 p. 69.

The aim of this chapter is to detail the formulation of the aero-structural adjoint and highlight the origin and the physical meaning of each term it introduces.

5.2 Mathematical formulation

As explained in Section 3.4.2 p. 51, the aero-elastic equilibrium is found by iteratively updating the fluid grid according to the displacements prescribed by the beam solver. The aerodynamic load is transferred to the beam through the pairing of each beam node with a part of the wetted wing surface. Conversely, the displacement of each CFD node is deduced from the displacement of its orthogonal projection on the beam aero-elastic axis. The coupled sensitivity calculation is performed in a similar iterative coupled fashion.

Let R_f be the residual of the equations governing the flow field W in a domain discretised by the mesh $s\mathcal{X}$. R_s the residual of the beam equations providing the displacement field D of the structure represented by the mesh \mathcal{X}_b . At the aero-elastic equilibrium W and D satisfy:

$$\begin{cases} R_f(W, \mathcal{X}) = 0 \\ R_s(D(\vec{\alpha}), F, L) = D - FL = 0 \end{cases}$$

where $\vec{\alpha} = (\vec{\alpha}_{geom}, \vec{\alpha}_{struct}) \in \mathcal{D}_{design} \subset \mathbb{R}^{n_\alpha}$ is the design variable vector and F the flexibility matrix.

These equations represent a set of n_a non-linear discrete equations governing the fluid and $2 * n_{\mathcal{X}_b}$ linear discrete equations governing the structure, where

- $n_a = 5 * n_{cell}$ for Euler equations
- $n_a = 7 * n_{cell}$ for RANS equations with two equations turbulence models)
- $n_{\mathcal{X}_b} =$ number of displacement nodes

The elastic equilibrium is expressed as:

$$\forall \vec{\alpha} \in \mathcal{D}_{design} \quad \begin{cases} R_f(W(\vec{\alpha}), \mathcal{X}(\vec{\alpha})) = 0 \\ R_s(D(\vec{\alpha}), \mathcal{X}_b, W^b, \mathcal{X}, F) = D(\vec{\alpha}) - F(I(\vec{\alpha}), J(\vec{\alpha}))L = 0 \end{cases}$$

5.2.1 Gradient of an aerodynamic cost function w.r.t. α_{geom} :

An aerodynamic function \mathcal{J}_{aero} (drag, lift, etc) is a function of the CFD volume mesh at the aero-elastic equilibrium, and the flow state at the interface fluid-structure (W^b) and in the volume (W)

$$\mathcal{J}_{aero} = \mathcal{J}_{aero}(\mathcal{X}, W^b, W)$$

Thus the gradient of \mathcal{J}_{aero} with respect to a shape design parameter α_{geom} can then be expressed as:

$$\frac{d\mathcal{J}_{aero}}{d\alpha_{geom}} = \frac{\partial\mathcal{J}_{aero}}{\partial\mathcal{X}} \frac{d\mathcal{X}}{d\alpha_{geom}} + \frac{\partial\mathcal{J}_{aero}}{\partial W^b} \frac{dW^b}{d\alpha_{geom}} + \frac{\partial\mathcal{J}}{\partial W} \frac{dW}{d\alpha_{geom}} \quad (5.1)$$

The first term $\frac{\partial \mathcal{J}_{aero}}{\partial \mathcal{X}} \frac{d\mathcal{X}}{d\alpha_{geom}}$ is the partial derivative of \mathcal{J}_{aero} w.r.t. α_{geom} through the influence of the design parameters on the CFD mesh \mathcal{X} . \mathcal{X} is the CFD mesh obtained from the initial mesh \mathcal{X}_{rig} on which we apply the structural deformations D computed at the load nodes of \mathcal{X}_b , $\mathcal{X} = \mathcal{X}(\mathcal{X}_{rig}, \mathcal{X}_b, D)$ thus

$$\frac{d\mathcal{X}}{d\alpha_{geom}} = \frac{\partial \mathcal{X}}{\partial \mathcal{X}_{rig}} \frac{d\mathcal{X}_{rig}}{d\alpha_{geom}} + \frac{\partial \mathcal{X}}{\partial \mathcal{X}_b} \frac{\partial \mathcal{X}_b}{\partial \mathcal{X}_{surf}} \frac{d\mathcal{X}_{surf}}{d\alpha_{geom}} + \frac{\partial \mathcal{X}}{\partial D} \frac{dD}{d\alpha_{geom}} \quad (5.2)$$

where

$\mathcal{X}_{surf} = \mathcal{X}_{surf}(\mathcal{X}_{rig}(\alpha_{geom}))$ is the surface mesh of the wing skin in the CFD mesh of the *jig-shape*

The influence of the shape parameters on the flow field W^b at the fluid-structure interface is shown in the 2nd term. W^b depends on the flow field in the volume and the volume CFD mesh \mathcal{X} , thus:

$$\frac{dW^b}{d\alpha_{geom}} = \frac{\partial W^b}{\partial W} \frac{dW}{d\alpha_{geom}} + \frac{\partial W^b}{\partial \mathcal{X}} \left(\frac{\partial \mathcal{X}}{\partial \mathcal{X}_{rig}} \frac{d\mathcal{X}_{rig}}{d\alpha_{geom}} + \frac{\partial \mathcal{X}}{\partial \mathcal{X}_b} \frac{\partial \mathcal{X}_b}{\partial \mathcal{X}_{surf}} \frac{d\mathcal{X}_{surf}}{d\alpha_{geom}} + \frac{\partial \mathcal{X}}{\partial D} \frac{dD}{d\alpha_{geom}} \right) \quad (5.3)$$

The third part of (5.1) is the more tedious and computationally expensive contribution due to the sensitivity of the volume flow field with respect to the design variables.

The completely developed expression of the gradient of an aerodynamic function with respect to a design parameter that controls the planform shape can therefore be written as:

$$\begin{aligned} \frac{d\mathcal{J}_{aero}}{d\alpha_{geom}} = & \frac{\partial \mathcal{J}_{aero}}{\partial \mathcal{X}} \left(\frac{\partial \mathcal{X}}{\partial \mathcal{X}_{rig}} \frac{d\mathcal{X}_{rig}}{d\alpha_{geom}} + \frac{\partial \mathcal{X}}{\partial \mathcal{X}_b} \frac{\partial \mathcal{X}_b}{\partial \mathcal{X}_{surf}} \frac{d\mathcal{X}_{surf}}{d\alpha_{geom}} + \frac{\partial \mathcal{X}}{\partial D} \frac{dD}{d\alpha_{geom}} \right) \\ & + \frac{\partial \mathcal{J}_{aero}}{\partial W^b} \left(\frac{\partial W^b}{\partial W} \frac{dW}{d\alpha_{geom}} + \frac{\partial W^b}{\partial \mathcal{X}} \left(\frac{\partial \mathcal{X}}{\partial \mathcal{X}_{rig}} \frac{d\mathcal{X}_{rig}}{d\alpha_{geom}} + \frac{\partial \mathcal{X}}{\partial \mathcal{X}_b} \frac{\partial \mathcal{X}_b}{\partial \mathcal{X}_{surf}} \frac{d\mathcal{X}_{surf}}{d\alpha_{geom}} + \frac{\partial \mathcal{X}}{\partial D} \frac{dD}{d\alpha_{geom}} \right) \right) \\ & + \frac{\partial \mathcal{J}}{\partial W} \frac{dW}{d\alpha_{geom}} \end{aligned} \quad (5.4)$$

5.2.2 Gradient of an aerodynamic cost function w.r.t. α_{struct} :

The gradient of \mathcal{J}_{aero} with respect to a structural parameter α_{struct} that controls the design of the wing box is expressed as

$$\frac{d\mathcal{J}_{aero}}{d\alpha_{struct}} = \frac{\partial\mathcal{J}_{aero}}{\partial\mathcal{X}} \frac{d\mathcal{X}}{d\alpha_{struct}} + \frac{\partial\mathcal{J}_{aero}}{\partial W^b} \frac{dW^b}{d\alpha_{struct}} + \frac{\partial\mathcal{J}}{\partial W} \frac{dW}{d\alpha_{struct}} \quad (5.5)$$

The mesh of the configuration under the aero-elastic equilibrium depends on the structural variables through the elastic deformation. The first term translates this dependency.

$$\frac{d\mathcal{X}}{d\alpha_{struct}} = \frac{\partial\mathcal{X}}{\partial\mathcal{X}_b} \frac{d\mathcal{X}_b}{d\alpha_{struct}} + \frac{\partial\mathcal{X}}{\partial D} \frac{dD}{d\alpha_{struct}} \quad (5.6)$$

The influence of the structural parameters on the flow field W^b at the fluid-structure interface is shown in the 2nd term. W^b depends on the flow field in the volume and the volume CFD mesh, thus

$$\frac{dW^b}{d\alpha_{struct}} = \frac{\partial W^b}{\partial W} \frac{dW}{d\alpha_{struct}} + \frac{\partial W^b}{\partial\mathcal{X}} \left(\frac{\partial\mathcal{X}}{\partial\mathcal{X}_b} \frac{d\mathcal{X}_b}{d\alpha_{struct}} + \frac{\partial\mathcal{X}}{\partial D} \frac{dD}{d\alpha_{struct}} \right) \quad (5.7)$$

The third part of (5.5) is the computationally expensive contribution of the sensitivity of the volume flow field with respect to the design variables.

The explicit expression of the gradient of an aerodynamic function w.r.t. a design parameter that controls the internal wing structure is finally:

$$\begin{aligned} \frac{d\mathcal{J}_{aero}}{d\alpha_{struct}} = & \frac{\partial\mathcal{J}_{aero}}{\partial\mathcal{X}} \left(\frac{\partial\mathcal{X}}{\partial\mathcal{X}_b} \frac{d\mathcal{X}_b}{d\alpha_{struct}} + \frac{\partial\mathcal{X}}{\partial D} \frac{dD}{d\alpha_{struct}} \right) \\ & + \frac{\partial\mathcal{J}_{aero}}{\partial W^b} \left(\frac{\partial W^b}{\partial W} \frac{dW}{d\alpha_{struct}} + \frac{\partial W^b}{\partial\mathcal{X}} \left(\frac{\partial\mathcal{X}}{\partial\mathcal{X}_b} \frac{d\mathcal{X}_b}{d\alpha_{struct}} + \frac{\partial\mathcal{X}}{\partial D} \frac{dD}{d\alpha_{struct}} \right) \right) \\ & + \frac{\partial\mathcal{J}}{\partial W} \frac{dW}{d\alpha_{struct}} \end{aligned} \quad (5.8)$$

5.2.3 Gradient of a structural cost function w.r.t. α_{geom} :

The dependency of a structural function \mathcal{J}_{struct} (structural weight, structural constraint, etc.) is expressed as:

$$\mathcal{J}_{struct} = \mathcal{J}_{struct}(\mathcal{X}_{surf}, \mathcal{X}_b, D, \alpha_{struct})$$

The gradient of \mathcal{J}_{struct} wr.t. shape parameter α_{geom} is

$$\frac{d\mathcal{J}_{struct}}{d\alpha_{geom}} = \frac{\partial\mathcal{J}_{struct}}{\partial\mathcal{X}_{surf}} \frac{d\mathcal{X}_{surf}}{d\alpha_{geom}} + \frac{\partial\mathcal{J}_{struct}}{\partial\mathcal{X}_b} \frac{d\mathcal{X}_b}{d\alpha_{geom}} + \frac{\partial\mathcal{J}_{struct}}{\partial D} \frac{dD}{d\alpha_{geom}} \quad (5.9)$$

The sensitivity of a structural function to a wing aerodynamic shape change is expressed through the mesh before the aero-elastic coupling and the surface mesh. A structural function can only be influenced by the surfacic mesh that defines the aerodynamic envelope.

$$\frac{d\mathcal{X}_{surf}}{d\alpha_{geom}} = \frac{\partial\mathcal{X}_{surf}}{\partial\mathcal{X}_{rig}} \frac{d\mathcal{X}_{rig}}{d\alpha_{geom}} \quad (5.10)$$

α_{geom} shapes the aerodynamic envelope of the jig shape and influences the elastic axis, this is shown through

$$\frac{d\mathcal{X}_b}{d\alpha_{geom}} = \frac{\partial\mathcal{X}_b}{\partial\mathcal{X}_{surf_{rig}}} \frac{d\mathcal{X}_{surf_{rig}}}{d\alpha_{geom}} \quad (5.11)$$

The third part of (5.9) is the computationally expensive contribution of the sensitivity of the displacement field with respect to the planform design variables.

5.2.4 Gradient of a structural cost function w.r.t. α_{struct} :

The gradient of \mathcal{J}_{struct} with respect to a structural parameter α_{struct} is

$$\frac{d\mathcal{J}_{struct}}{d\alpha_{struct}} = \frac{\partial\mathcal{J}_{struct}}{\partial\mathcal{X}_b} \frac{d\mathcal{X}_b}{d\alpha_{struct}} + \frac{\partial\mathcal{J}_{struct}}{\partial D} \frac{dD}{d\alpha_{struct}} + \frac{\mathcal{J}_{struct}}{\partial\alpha_{struct}} \quad (5.12)$$

The first term is the direct dependency of the elastic axis to the design of the wing box. The second term is the computationally expensive contribution of the sensitivity of the displacement field with respect to the wing box design variables.

The last term is the direct dependence of \mathcal{J}_{struct} (for instance the weight) to α_{struct} .

5.3 Implementation of the aero-structural adjoint method

In the previous section we detailed the sensitivities of the functions, involved in the aero-structural optimization problem, according to their nature and according to the nature of the design parameter. The purpose of the current section is to establish the equation of the aero-structural adjoint system to be solved to calculate the previous sensitivities without having to evaluate the derivatives of the state variables W and D w.r.t. the design parameters.

In the scenario of static fluid and structure interactions, when the aero-elastic equilibrium of the wing is reached, the residual form of the state equations $R_f = 0$ and $R_s = 0$ are satisfied over the CFD grid nodes and the structural beam nodes for all values of the design parameters $\vec{\alpha}$. Thus, according to eq (3.16), the residual is equal to zero and so is its variation:

$$\begin{cases} \frac{dR_f(W, \mathcal{X})}{d\alpha} = 0 \\ \frac{dR_s(D(\alpha), \mathcal{X}_b, W^b, \mathcal{X}, I, J)}{d\alpha} = 0 \end{cases}$$

Therefore, one can write, $\forall(\lambda_f^T, \lambda_s^T) \in (\mathbb{R}^{n_a}, \mathbb{R}^{2*n_p})$:

$$\frac{d\mathcal{J}}{d\alpha} = \frac{d\mathcal{J}}{d\alpha} + \lambda_f^T \frac{dR_f(W, \mathcal{X})}{d\alpha} + \lambda_s^T \frac{dR_s(D(\alpha), \mathcal{X}_b, W^b, \mathcal{X}, I, J)}{d\alpha} \quad (5.13)$$

λ_f^T and λ_s^T are at this time two arbitrary vectors. The following equations are the developed expression of (5.13) when \mathcal{J} describes either structural or aerodynamic performance and α either the wing aerodynamic shape parameters α_{geom} or the wing

box parameters α_{struct} . The next paragraphs present in a condensed and in detailed manner the step toward the establishment of the adjoint equations for the different combinations between function type and design parameter type.

5.3.1 Gradient of an aerodynamic cost function w.r.t. α_{geom} :

$$\begin{aligned}
\frac{d\mathcal{J}_{aero}}{d\alpha_{geom}} &= \frac{\partial\mathcal{J}_{aero}}{\partial\mathcal{X}} \left(\frac{\partial\mathcal{X}}{\partial\mathcal{X}_{rig}} \frac{d\mathcal{X}_{rig}}{d\alpha_{geom}} + \frac{\partial\mathcal{X}}{\partial\mathcal{X}_b} \frac{\partial\mathcal{X}_b}{\partial\mathcal{X}_{surf}} \frac{d\mathcal{X}_{surf}}{d\alpha_{geom}} + \frac{\partial\mathcal{X}}{\partial D} \frac{dD}{d\alpha_{geom}} \right) \\
&+ \frac{\partial\mathcal{J}_{aero}}{\partial W^b} \left(\frac{\partial W^b}{\partial W} \frac{dW}{d\alpha_{geom}} + \frac{\partial W^b}{\partial\mathcal{X}} \left(\frac{\partial\mathcal{X}}{\partial\mathcal{X}_{rig}} \frac{d\mathcal{X}_{rig}}{d\alpha_{geom}} + \frac{\partial\mathcal{X}}{\partial\mathcal{X}_b} \frac{\partial\mathcal{X}_b}{\partial\mathcal{X}_{surf}} \frac{d\mathcal{X}_{surf}}{d\alpha_{geom}} + \frac{\partial\mathcal{X}}{\partial D} \frac{dD}{d\alpha_{geom}} \right) \right) \\
&+ \frac{\partial\mathcal{J}_{aero}}{\partial W} \frac{dW}{d\alpha_{geom}} \\
&+ \lambda_f^T \frac{dR_f}{d\alpha_{geom}} \\
&+ \lambda_s^T \frac{dR_s}{d\alpha_{geom}}
\end{aligned} \tag{5.14}$$

The terms appearing in the sensitivity of state equations residuals for both disciplines,

$\frac{dR_s}{d\alpha_{geom}} = \frac{d(D-FL)}{d\alpha_{geom}}$ and in $\frac{dR_f}{d\alpha_{geom}}$, are detailed in the next paragraphs:

5.3.1.1 Sensitivity of R_f w.r.t. α_{geom}

The residual of the flow equations is linearised through the field of conservative flow variables W and the CFD mesh \mathcal{X}

$$\frac{dR_f}{d\alpha_{geom}} = \frac{\partial R_f}{\partial W} \frac{dW}{d\alpha_{geom}} + \frac{\partial R_f}{\partial\mathcal{X}} \frac{d\mathcal{X}}{d\alpha_{geom}} \tag{5.15}$$

where

$$\frac{d\mathcal{X}}{d\alpha_{geom}} = \left(\frac{\partial\mathcal{X}}{\partial\mathcal{X}_{rig}} \frac{d\mathcal{X}_{rig}}{d\alpha_{geom}} + \frac{\partial\mathcal{X}}{\partial\mathcal{X}_b} \frac{\partial\mathcal{X}_b}{\partial\mathcal{X}_{surf}} \frac{d\mathcal{X}_{surf}}{d\alpha_{geom}} + \frac{\partial\mathcal{X}}{\partial D} \frac{dD}{d\alpha_{geom}} \right) \tag{5.16}$$

5.3.1.2 Sensitivity of R_s w.r.t. α_{geom}

The aero-structural adjoint takes into account the changes of both loads and structural characteristics with the changes in design:

$$\frac{dR_s}{d\alpha_{geom}} = \frac{d(D - FL)}{d\alpha_{geom}} = \left(\frac{dD}{d\alpha_{geom}} - F \frac{dL}{d\alpha_{geom}} - \frac{dF}{d\alpha_{geom}} L \right) \quad (5.17)$$

Aerodynamic loads extracted on the current mesh \mathcal{X} depend on the structural mesh and the conservative variables at the fluid/structure interface:

$$F \frac{dL}{d\alpha_{geom}} = F \left(\frac{\partial L}{\partial \mathcal{X}} \frac{d\mathcal{X}}{d\alpha_{geom}} + \frac{\partial L}{\partial \mathcal{X}_b} \frac{d\mathcal{X}_b}{d\alpha_{geom}} + \frac{\partial L}{\partial W^b} \frac{dW^b}{d\alpha_{geom}} \right) \quad (5.18)$$

where:

$$\frac{\partial L}{\partial \mathcal{X}} \frac{d\mathcal{X}}{d\alpha_{geom}} = \frac{\partial L}{\partial \mathcal{X}} \left(\frac{\partial \mathcal{X}}{\partial \mathcal{X}_{rig}} \frac{d\mathcal{X}_{rig}}{d\alpha_{geom}} + \frac{\partial \mathcal{X}}{\partial \mathcal{X}_b} \frac{\partial \mathcal{X}_b}{\partial \mathcal{X}_{surf}} \frac{d\mathcal{X}_{surf}}{d\alpha_{geom}} + \frac{\partial \mathcal{X}}{\partial D} \frac{dD}{d\alpha_{geom}} \right) \quad (5.19)$$

$$\frac{\partial L}{\partial \mathcal{X}_b} \frac{d\mathcal{X}_b}{d\alpha_{geom}} = \frac{\partial L}{\partial \mathcal{X}_b} \frac{\partial \mathcal{X}_b}{\partial \mathcal{X}_{surf}} \frac{d\mathcal{X}_{surf}}{d\alpha_{geom}} \quad (5.20)$$

$$\frac{\partial L}{\partial W^b} \frac{dW^b}{d\alpha_{geom}} = \frac{\partial L}{\partial W^b} \left(\frac{\partial W^b}{\partial W} \frac{dW}{d\alpha_{geom}} + \frac{\partial W^b}{\partial \mathcal{X}} \frac{d\mathcal{X}}{d\alpha_{geom}} \right) \quad (5.21)$$

We linearise the flexibility matrix F w.r.t. the structural beam stiffness distribution vectors $I(y)$ and $J(y)$ as well as the structural mesh \mathcal{X}_b

$$\frac{dF}{d\alpha_{geom}} L = \left(\frac{\partial F}{\partial I} \frac{dI}{d\alpha_{geom}} + \frac{\partial F}{\partial J} \frac{dJ}{d\alpha_{geom}} + \frac{\partial F}{\partial \mathcal{X}_b} \frac{d\mathcal{X}_b}{d\alpha_{geom}} \right) L \quad (5.22)$$

α_{geom} influences the structural parameters through the CFD surface mesh \mathcal{X}_{surf} from which the structural mesh is extracted:

$$\frac{\partial F}{\partial I} \frac{dI}{d\alpha_{geom}} = \frac{\partial F}{\partial I} \left(\frac{\partial I}{\partial \mathcal{X}_b} \frac{\partial \mathcal{X}_b}{\mathcal{X}_{surf}} + \frac{\partial I}{\partial \mathcal{X}_{surf}} \right) \frac{d\mathcal{X}_{surf}}{d\alpha_{geom}} \quad (5.23)$$

$$\frac{\partial F}{\partial J} \frac{dJ}{d\alpha_{geom}} = \frac{\partial F}{\partial J} \left(\frac{\partial J}{\partial \mathcal{X}_b} \frac{\partial \mathcal{X}_b}{\mathcal{X}_{surf}} + \frac{\partial J}{\partial \mathcal{X}_{surf}} \right) \frac{d\mathcal{X}_{surf}}{d\alpha_{geom}} \quad (5.24)$$

The coefficients of the flexibility matrix correspond to vertical and angular deflections due to unit vertical force and moment at the different points of the structural mesh \mathcal{X}_b , thus F is linearised with respect to the coordinates of the structural mesh according to:

$$\frac{\partial F}{\partial \mathcal{X}_b} \frac{d\mathcal{X}_b}{d\alpha_{geom}} = \frac{\partial F}{\partial \mathcal{X}_b} \frac{\partial \mathcal{X}_b}{\partial \mathcal{X}_{surf}} \frac{d\mathcal{X}_{surf}}{d\alpha_{geom}} \quad (5.25)$$

5.3.2 Gradient of an aerodynamic cost function w.r.t. α_{struct} :

$$\begin{aligned} \frac{d\mathcal{J}_{aero}}{d\alpha_{struct}} &= \frac{\partial \mathcal{J}_{aero}}{\partial \mathcal{X}} \left(\frac{\partial \mathcal{X}}{\partial \mathcal{X}_b} \frac{d\mathcal{X}_b}{d\alpha_{struct}} + \frac{\partial \mathcal{X}}{\partial D} \frac{dD}{d\alpha_{struct}} \right) \\ &+ \frac{\partial \mathcal{J}_{aero}}{\partial W^b} \left(\frac{\partial W^b}{\partial W} \frac{dW}{d\alpha_{struct}} + \frac{\partial W^b}{\partial \mathcal{X}} \left(\frac{\partial \mathcal{X}}{\partial \mathcal{X}_b} \frac{d\mathcal{X}_b}{d\alpha_{struct}} + \frac{\partial \mathcal{X}}{\partial D} \frac{dD}{d\alpha_{struct}} \right) \right) \\ &+ \frac{\partial \mathcal{J}_{aero}}{\partial W} \frac{dW}{d\alpha_{struct}} \\ &+ \lambda_f^T \frac{dR_f}{d\alpha_{struct}} \\ &+ \lambda_s^T \frac{dR_s}{d\alpha_{struct}} \end{aligned} \quad (5.26)$$

5.3.2.1 Sensitivity of R_f w.r.t. α_{struct}

$$\frac{dR_f}{d\alpha_{struct}} = \left(\frac{\partial R_f}{\partial W} \frac{dW}{d\alpha_{struct}} + \frac{\partial R_f}{\partial \mathcal{X}} \frac{d\mathcal{X}}{d\alpha_{struct}} \right) \quad (5.27)$$

we recall that when the design parameter is a structural parameter, there is no intervention of the CFD volume mesh of the jig shape:

$$\frac{d\mathcal{X}}{d\alpha_{struct}} = \left(\frac{\partial \mathcal{X}}{\partial \mathcal{X}_b} \frac{d\mathcal{X}_b}{d\alpha_{struct}} + \frac{\partial \mathcal{X}}{\partial D} \frac{dD}{d\alpha_{struct}} \right) \quad (5.28)$$

5.3.2.2 Sensitivity of R_s w.r.t. α_{struct}

$$\frac{dR_s}{d\alpha_{geom}} = \frac{d(D - FL)}{d\alpha_{geom}} = \left(\frac{dD}{d\alpha_{geom}} - F \frac{dL}{d\alpha_{geom}} - \frac{dF}{d\alpha_{geom}} L \right) \quad (5.29)$$

where

$$F \frac{dL}{d\alpha_{struct}} = F \left(\frac{\partial L}{\partial \mathcal{X}} \frac{d\mathcal{X}}{d\alpha_{struct}} + \frac{\partial L}{\partial \mathcal{X}_b} \frac{d\mathcal{X}_b}{d\alpha_{struct}} + \frac{\partial L}{\partial W^b} \frac{dW^b}{d\alpha_{struct}} \right) \quad (5.30)$$

The full expression of the sensitivity of the flow field at the interface fluid/structure $\frac{dW^b}{d\alpha_{struct}}$ is given in (5.7).

The structural model is computed starting from the surface mesh jig shape and so are the sensitivities of the structural properties. Thus, for a parameter that has no influence on the aerodynamic envelope:

$$\frac{dF}{d\alpha_{struct}}L = \left(\frac{\partial F}{\partial I} \frac{dI}{d\alpha_{struct}} + \frac{\partial F}{\partial I} \frac{dJ}{d\alpha_{struct}} + \frac{\partial F}{\partial X_b} \frac{dX_b}{d\alpha_{struct}} \right) L \quad (5.31)$$

$$\frac{\partial F}{\partial I} \frac{dI}{d\alpha_{struct}} = \frac{\partial F}{\partial I} \left(\frac{\partial I}{\partial X_b} \frac{dX_b}{d\alpha_{struct}} + \frac{dI}{d\alpha_{struct}} \right) \quad (5.32)$$

$$\frac{\partial F}{\partial J} \frac{dJ}{d\alpha_{struct}} = \frac{\partial F}{\partial J} \left(\frac{\partial J}{\partial X_b} \frac{dX_b}{d\alpha_{struct}} + \frac{dJ}{d\alpha_{struct}} \right) \quad (5.33)$$

$\frac{\partial I}{\partial X_b}$ and $\frac{\partial I}{\partial X_b}$ express the dependence of the stiffness coefficient expression to the position of the elastic axis in the formula of the first and second order moment of inertia of the wing box sections.

$\frac{dI}{d\alpha_{geom}}$ and $\frac{dJ}{d\alpha_{geom}}$ come from the dependence of the moment of inertia of wing box cross sections to structural thicknesses.

5.3.3 Gradient of a structural cost function w.r.t. α_{geom} :

$$\begin{aligned} \frac{d\mathcal{J}_{struct}}{d\alpha_{geom}} &= \frac{\partial \mathcal{J}_{struct}}{\partial X_{surf}} \frac{\partial X_{surf}}{\partial X_{rig}} \frac{dX_{rig}}{d\alpha_{geom}} + \frac{\partial \mathcal{J}_{struct}}{\partial X_b} \frac{\partial X_b}{\partial X_{surf}} \frac{dX_{surf}}{d\alpha_{geom}} + \frac{\partial \mathcal{J}_{struct}}{\partial D} \frac{dD}{d\alpha_{geom}} \\ &+ \lambda_f^T \left(\frac{\partial R_f}{\partial W} \frac{dW}{d\alpha_{geom}} + \frac{\partial R_f}{\partial X} \frac{dX}{d\alpha_{geom}} \right) \\ &+ \lambda_s^T \left(\frac{dD}{d\alpha_{geom}} - \frac{dF}{d\alpha_{geom}}L - F \frac{dL}{d\alpha_{geom}} \right) \end{aligned} \quad (5.34)$$

The sensitivity of the residuals (5th and 6th terms) are identical to those computed in the set of equations from(5.15) to (5.25)

5.3.4 Gradient of a structural cost function w.r.t. α_{struct} :

$$\begin{aligned}
\frac{d\mathcal{J}_{struct}}{d\alpha_{struct}} &= \frac{\partial\mathcal{J}_{struct}}{\partial\mathcal{X}_b} \frac{d\mathcal{X}_b}{d\alpha_{struct}} + \frac{\partial\mathcal{J}_{struct}}{\partial D} \frac{dD}{d\alpha_{struct}} + \frac{\partial\mathcal{J}_{struct}}{\partial\alpha_{struct}} \\
&+ \lambda_f^T \left(\frac{\partial R_f}{\partial W} \frac{dW}{d\alpha_{struct}} + \frac{\partial R_f}{\partial \mathcal{X}} \frac{d\mathcal{X}}{d\alpha_{struct}} \right) \\
&+ \lambda_s^T \frac{d(D - FL)}{d\alpha_{struct}}
\end{aligned} \tag{5.35}$$

The sensitivity of the residuals (5th and 6th terms) are identical to those computed in the set of equations from(5.27) to (5.33)

5.3.5 Introduction of adjoint equations

Now that we established the detailed expression of the objective function gradients and the gradients of the residuals of the governing equations of fluid and structure, we can rearrange the complete gradient expression to factorize the terms:: $\frac{dW}{d\alpha_{geom}}$, $\frac{dW}{d\alpha_{struct}}$, $\frac{dD}{d\alpha_{geom}}$ and $\frac{dD}{d\alpha_{struct}}$. These factorisations introduce the aero-structural adjoint systems that must be solved for the unknowns λ_s^T and λ_f^T in order to avoid the expensive resolution of the primal problem that could provide $\frac{dW}{d\alpha}$ and $\frac{dD}{d\alpha}$. λ_s^T and λ_f^T are the so-called adjoint vectors, respectively the aerodynamic and the structural adjoint vectors, solution of the dual problem. After rearranging the different terms and factorizing $\frac{dW}{d\alpha}$

and $\frac{dD}{d\alpha}$, we obtain:

$$\begin{aligned}
\frac{d\mathcal{J}_{aero}}{d\alpha_{geom}} &= \frac{\partial\mathcal{J}_{aero}}{\partial\mathcal{X}} \left(\frac{\partial\mathcal{X}}{\partial\mathcal{X}_{rig}} \frac{d\mathcal{X}_{rig}}{d\alpha_{geom}} + \frac{\partial\mathcal{X}}{\partial\mathcal{X}_b} \frac{\partial\mathcal{X}_b}{\partial\mathcal{X}_{surf}} \frac{d\mathcal{X}_{surf}}{d\alpha_{geom}} \right) \\
&+ \frac{\partial\mathcal{J}_{aero}}{\partial W^b} \frac{\partial W^b}{\partial\mathcal{X}} \left(\frac{\partial\mathcal{X}}{\partial\mathcal{X}_{rig}} \frac{d\mathcal{X}_{rig}}{d\alpha_{geom}} + \frac{\partial\mathcal{X}}{\partial\mathcal{X}_b} \frac{\partial\mathcal{X}_b}{\partial\mathcal{X}_{surf}} \frac{d\mathcal{X}_{surf}}{d\alpha_{geom}} \right) \\
&+ \lambda_f^T \frac{\partial R_f}{\partial\mathcal{X}} \left(\frac{\partial\mathcal{X}}{\partial\mathcal{X}_{rig}} \frac{d\mathcal{X}_{rig}}{d\alpha_{geom}} + \frac{\partial\mathcal{X}}{\partial\mathcal{X}_b} \frac{\partial\mathcal{X}_b}{\partial\mathcal{X}_{surf}} \frac{d\mathcal{X}_{surf}}{d\alpha_{geom}} \right) \\
&+ \lambda_s^T \left(-F \left(\frac{\partial L}{\partial\mathcal{X}} \left(\frac{\partial\mathcal{X}}{\partial\mathcal{X}_{rig}} \frac{d\mathcal{X}_{rig}}{d\alpha_{geom}} + \frac{\partial\mathcal{X}}{\partial\mathcal{X}_b} \frac{\partial\mathcal{X}_b}{\partial\mathcal{X}_{surf}} \frac{d\mathcal{X}_{surf}}{d\alpha_{geom}} \right) \right. \right. \\
&+ \left. \left. \frac{\partial L}{\partial\mathcal{X}_b} \frac{d\mathcal{X}_b}{d\alpha_{geom}} + \frac{\partial L}{\partial W^b} \frac{\partial W^b}{\partial\mathcal{X}} \left(\frac{\partial\mathcal{X}}{\partial\mathcal{X}_{rig}} \frac{d\mathcal{X}_{rig}}{d\alpha_{geom}} + \frac{\partial\mathcal{X}}{\partial\mathcal{X}_b} \frac{\partial\mathcal{X}_b}{\partial\mathcal{X}_{surf}} \frac{d\mathcal{X}_{surf}}{d\alpha_{geom}} \right) \right) - \frac{dF}{d\alpha_{geom}} L \right) \\
&+ \left[\frac{\partial\mathcal{J}_{aero}}{\partial\mathcal{X}} \frac{\partial\mathcal{X}}{\partial D} + \frac{\partial\mathcal{J}_{aero}}{\partial W^b} \frac{\partial W^b}{\partial\mathcal{X}} \frac{\partial\mathcal{X}}{\partial D} \right. \\
&+ \left. \lambda_f^T \frac{\partial R_f}{\partial\mathcal{X}} \frac{\partial\mathcal{X}}{\partial D} + \lambda_s^T \left(I_d - F \left(\frac{\partial L}{\partial\mathcal{X}} \frac{\partial\mathcal{X}}{\partial D} + \frac{\partial L}{\partial W^b} \frac{\partial W^b}{\partial\mathcal{X}} \frac{\partial\mathcal{X}}{\partial D} \right) \right) \right] \frac{dD}{d\alpha_{geom}} \\
&+ \left[\frac{\partial\mathcal{J}_{aero}}{\partial W^b} \frac{\partial W^b}{\partial W} + \frac{\partial\mathcal{J}_{aero}}{\partial W} + \lambda_f^T \frac{\partial R_f}{\partial W} - \lambda_s^T F \frac{\partial L}{\partial W^b} \frac{\partial W^b}{\partial W} \right] \frac{dW}{d\alpha_{geom}}
\end{aligned} \tag{5.36}$$

$$\begin{aligned}
\frac{d\mathcal{J}_{aero}}{d\alpha_{struct}} &= \frac{\partial\mathcal{J}_{aero}}{\partial\mathcal{X}} \frac{\partial\mathcal{X}}{\partial\mathcal{X}_b} \frac{d\mathcal{X}_b}{d\alpha_{struct}} \\
&+ \frac{\partial\mathcal{J}_{aero}}{\partial W^b} \frac{\partial W^b}{\partial\mathcal{X}} \frac{\partial\mathcal{X}}{\partial\mathcal{X}_b} \frac{d\mathcal{X}_b}{d\alpha_{struct}} + \lambda_f \frac{\partial R_f}{\partial\mathcal{X}} \frac{\partial\mathcal{X}}{\partial\mathcal{X}_b} \frac{d\mathcal{X}_b}{d\alpha_{struct}} \\
&+ \lambda_s^T \left(-F \left(\frac{\partial L}{\partial\mathcal{X}} \frac{\partial\mathcal{X}}{\partial\mathcal{X}_b} \frac{d\mathcal{X}_b}{d\alpha_{struct}} + \frac{\partial L}{\partial\mathcal{X}_b} \frac{d\mathcal{X}_b}{d\alpha_{struct}} + \frac{\partial L}{\partial W^b} \frac{\partial W^b}{\partial\mathcal{X}} \frac{\partial\mathcal{X}}{\partial\mathcal{X}_b} \frac{d\mathcal{X}_b}{d\alpha_{struct}} \right) - \frac{dF}{d\alpha_{struct}} L \right) \\
&+ \left[\frac{\partial\mathcal{J}_{aero}}{\partial\mathcal{X}} \frac{\partial\mathcal{X}}{\partial D} + \frac{\partial\mathcal{J}_{aero}}{\partial W^b} \frac{\partial W^b}{\partial\mathcal{X}} \frac{\partial\mathcal{X}}{\partial D} + \lambda_f^T \frac{\partial R_f}{\partial\mathcal{X}} \frac{\partial\mathcal{X}}{\partial D} \right. \\
&\left. + \lambda_s^T \left(I_d - F \left(\frac{\partial L}{\partial\mathcal{X}} \frac{\partial\mathcal{X}}{\partial D} + \frac{\partial L}{\partial W^b} \frac{\partial W^b}{\partial\mathcal{X}} \frac{\partial\mathcal{X}}{\partial D} \right) \right) \right] \frac{dD}{d\alpha_{struct}} \\
&+ \left[\frac{\partial\mathcal{J}_{aero}}{\partial W^b} \frac{\partial W^b}{\partial W} + \frac{\partial\mathcal{J}_{aero}}{\partial W} + \lambda_f^T \frac{\partial R_f}{\partial W} - \lambda_s^T F \frac{\partial L}{\partial W^b} \frac{\partial W^b}{\partial W} \right] \frac{dW}{d\alpha_{struct}}
\end{aligned} \tag{5.37}$$

$$\begin{aligned}
\frac{d\mathcal{J}_{struct}}{d\alpha_{geom}} &= \frac{\partial\mathcal{J}_{struct}}{\partial\mathcal{X}_{surf}} \frac{\partial\mathcal{X}_{surf}}{\partial\mathcal{X}_{rig}} \frac{d\mathcal{X}_{rig}}{d\alpha_{geom}} + \frac{\partial\mathcal{J}_{struct}}{\partial\mathcal{X}_b} \frac{\partial\mathcal{X}_b}{\partial\mathcal{X}_{rig}} \frac{d\mathcal{X}_{rig}}{d\alpha_{geom}} \\
&+ \lambda_f^T \frac{\partial R_f}{\partial\mathcal{X}} \left(\frac{\partial\mathcal{X}}{\partial\mathcal{X}_{rig}} \frac{d\mathcal{X}_{rig}}{d\alpha_{geom}} + \frac{\partial\mathcal{X}}{\partial\mathcal{X}_b} \frac{\partial\mathcal{X}_b}{\partial\mathcal{X}_{surf}} \frac{d\mathcal{X}_{surf}}{d\alpha_{geom}} \right) \\
&+ \lambda_s^T \left(-F \left(\frac{\partial L}{\partial\mathcal{X}} \left(\frac{\partial\mathcal{X}}{\partial\mathcal{X}_{rig}} \frac{d\mathcal{X}_{rig}}{d\alpha_{geom}} + \frac{\partial\mathcal{X}}{\partial\mathcal{X}_b} \frac{\partial\mathcal{X}_b}{\partial\mathcal{X}_{surf}} \frac{d\mathcal{X}_{surf}}{d\alpha_{geom}} \right) \right. \right. \\
&\left. \left. + \frac{\partial L}{\partial\mathcal{X}_b} \frac{d\mathcal{X}_b}{d\alpha_{geom}} + \frac{\partial L}{\partial W^b} \frac{\partial W^b}{\partial\mathcal{X}} \left(\frac{\partial\mathcal{X}}{\partial\mathcal{X}_{rig}} \frac{d\mathcal{X}_{rig}}{d\alpha_{geom}} + \frac{\partial\mathcal{X}}{\partial\mathcal{X}_b} \frac{\partial\mathcal{X}_b}{\partial\mathcal{X}_{surf}} \frac{d\mathcal{X}_{surf}}{d\alpha_{geom}} \right) \right) - \frac{dF}{d\alpha_{geom}} L \right) \\
&+ \left[\frac{\partial\mathcal{J}_{struct}}{\partial D} + \lambda_f^T \frac{\partial R_f}{\partial\mathcal{X}} \frac{\partial\mathcal{X}}{\partial D} + \lambda_s^T \left(I_d - F \left(\frac{\partial L}{\partial\mathcal{X}} \frac{\partial\mathcal{X}}{\partial D} + \frac{\partial L}{\partial W^b} \frac{\partial W^b}{\partial\mathcal{X}} \frac{\partial\mathcal{X}}{\partial D} \right) \right) \right] \frac{dD}{d\alpha_{geom}} \\
&+ \left[\lambda_f^T \frac{\partial R_f}{\partial W} - \lambda_s^T F \frac{\partial L}{\partial W^b} \frac{\partial W^b}{\partial W} \right] \frac{dW}{d\alpha_{geom}}
\end{aligned} \tag{5.38}$$

$$\begin{aligned}
\frac{d\mathcal{J}_{struct}}{d\alpha_{struct}} &= \frac{\partial\mathcal{J}_{struct}}{\partial\mathcal{X}_b} \frac{d\mathcal{X}_b}{d\alpha_{struct}} + \frac{\partial\mathcal{J}_{struct}}{\partial\alpha_{struct}} \\
&+ \lambda_f^T \frac{\partial R_f}{\partial\mathcal{X}} \frac{\partial\mathcal{X}}{\partial\mathcal{X}_b} \frac{d\mathcal{X}_b}{d\alpha_{struct}} \\
&+ \lambda_s^T \left(-F \left(\frac{\partial L}{\partial\mathcal{X}} \frac{\partial\mathcal{X}}{\partial\mathcal{X}_b} \frac{d\mathcal{X}_b}{d\alpha_{struct}} + \frac{\partial L}{\partial\mathcal{X}_b} \frac{d\mathcal{X}_b}{d\alpha_{struct}} + \frac{\partial L}{\partial W^b} \frac{\partial W^b}{\partial\mathcal{X}} \frac{\partial\mathcal{X}}{\partial\mathcal{X}_b} \frac{d\mathcal{X}_b}{d\alpha_{struct}} \right) - \frac{dF}{d\alpha_{struct}} L \right) \\
&+ \left[\frac{\partial\mathcal{J}_{struct}}{\partial D} + \lambda_f^T \frac{\partial R_f}{\partial\mathcal{X}} \frac{\partial\mathcal{X}}{\partial D} + \lambda_s^T \left(I_d - F \left(\frac{\partial L}{\partial\mathcal{X}} \frac{\partial\mathcal{X}}{\partial D} + \frac{\partial L}{\partial W^b} \frac{\partial W^b}{\partial\mathcal{X}} \frac{\partial\mathcal{X}}{\partial D} \right) \right) \right] \frac{dD}{d\alpha_{struct}} \\
&+ \left[\lambda_f^T \frac{\partial R_f}{\partial W} - \lambda_s^T F \frac{\partial L}{\partial W^b} \frac{\partial W^b}{\partial W} \right] \frac{dW}{d\alpha_{struct}}
\end{aligned} \tag{5.39}$$

In equations (5.36), (5.37), (5.38) and (5.39) appear term-factors of the sensitivities of the displacement field and the conservative variables. For a type of an objective function, these term-factors do not depend on the nature of the design variable. These systems describing the dual problem are called the aero-structural adjoint systems. They are solved iteratively to find the adjoint vectors λ_s^T and λ_f^T . For an aerodynamic function J_{aero} (e.g. drag, pitching moment, etc.) the aero-structural adjoint system to be solved is:

$$\begin{aligned}
\frac{\partial\mathcal{J}_{aero}}{\partial\mathcal{X}} \frac{\partial\mathcal{X}}{\partial D} + \frac{\partial\mathcal{J}_{aero}}{\partial W^b} \frac{\partial W^b}{\partial\mathcal{X}} \frac{\partial\mathcal{X}}{dD} + \lambda_f^T \frac{\partial R_f}{\partial\mathcal{X}} \frac{\partial\mathcal{X}}{\partial D} + \lambda_s^T \left(I_d - F \left(\frac{\partial L}{\partial\mathcal{X}} \frac{\partial\mathcal{X}}{\partial D} + \frac{\partial L}{\partial W^b} \frac{\partial W^b}{\partial\mathcal{X}} \frac{\partial\mathcal{X}}{\partial D} \right) \right) &= 0 \\
\frac{\partial\mathcal{J}_{aero}}{\partial W^b} \frac{\partial W^b}{\partial W} + \frac{\partial J}{\partial W} + \lambda_f^T \frac{\partial R_f}{\partial W} - \lambda_s^T F \frac{\partial L}{\partial W^b} \frac{\partial W^b}{\partial W} &= 0
\end{aligned} \tag{5.40}$$

and for a structural function \mathcal{J}_{struct} (e.g. material stress), the aero-structural adjoint to be solved is:

$$\frac{\partial\mathcal{J}_{struct}}{\partial D} + \lambda_f^T \frac{\partial R_f}{\partial\mathcal{X}} \frac{\partial\mathcal{X}}{\partial D} + \lambda_s^T \left(I_d - F \left(\frac{\partial L}{\partial\mathcal{X}} \frac{\partial\mathcal{X}}{\partial D} + \frac{\partial L}{\partial W^b} \frac{\partial W^b}{\partial\mathcal{X}} \frac{\partial\mathcal{X}}{\partial D} \right) \right) = 0 \tag{5.41}$$

$$\lambda_f^T \frac{\partial R_f}{\partial W} - \lambda_s^T F \frac{\partial L}{\partial W^b} \frac{\partial W^b}{\partial W} = 0 \tag{5.42}$$

Once the vector λ_f and λ_s are computed they are reintroduced in the final expression of the gradients, yielding the following expressions for the different gradients:

$$\begin{aligned}
\frac{d\mathcal{J}_{aero}}{d\alpha_{geom}} &= \frac{\partial\mathcal{J}_{aero}}{\partial\mathcal{X}} \left(\frac{\partial\mathcal{X}}{\partial\mathcal{X}_{rig}} \frac{d\mathcal{X}_{rig}}{d\alpha_{geom}} + \frac{\partial\mathcal{X}}{\partial\mathcal{X}_b} \frac{\partial\mathcal{X}_b}{\partial\mathcal{X}_{surf}} \frac{d\mathcal{X}_{surf}}{d\alpha_{geom}} \right) \\
&+ \frac{\partial\mathcal{J}_{aero}}{\partial W^b} \left(\frac{\partial W^b}{\partial\mathcal{X}} \left(\frac{\partial\mathcal{X}}{\partial\mathcal{X}_{rig}} \frac{d\mathcal{X}_{rig}}{d\alpha_{geom}} + \frac{\partial\mathcal{X}}{\partial\mathcal{X}_b} \frac{\partial\mathcal{X}_b}{\partial\mathcal{X}_{surf}} \frac{d\mathcal{X}_{surf}}{d\alpha_{geom}} \right) \right) \\
&+ \lambda_f^T \frac{\partial R_f}{\partial\mathcal{X}} \left(\frac{\partial\mathcal{X}}{\partial\mathcal{X}_{rig}} \frac{d\mathcal{X}_{rig}}{d\alpha_{geom}} + \frac{\partial\mathcal{X}}{\partial\mathcal{X}_b} \frac{\partial\mathcal{X}_b}{\partial\mathcal{X}_{surf}} \frac{d\mathcal{X}_{surf}}{d\alpha_{geom}} \right) \\
&+ \lambda_s^T \left(-F \left(\frac{\partial L}{\partial\mathcal{X}} \left(\frac{\partial\mathcal{X}}{\partial\mathcal{X}_{rig}} \frac{d\mathcal{X}_{rig}}{d\alpha_{geom}} + \frac{\partial\mathcal{X}}{\partial\mathcal{X}_b} \frac{\partial\mathcal{X}_b}{\partial\mathcal{X}_{surf}} \frac{d\mathcal{X}_{surf}}{d\alpha_{geom}} \right) \right. \right. \\
&\left. \left. + \frac{\partial L}{\partial\mathcal{X}_b} \frac{d\mathcal{X}_b}{d\alpha_{geom}} + \frac{\partial L}{\partial W^b} \frac{\partial W^b}{\partial\mathcal{X}} \left(\frac{\partial\mathcal{X}}{\partial\mathcal{X}_{rig}} \frac{d\mathcal{X}_{rig}}{d\alpha_{geom}} + \frac{\partial\mathcal{X}}{\partial\mathcal{X}_b} \frac{\partial\mathcal{X}_b}{\partial\mathcal{X}_{surf}} \frac{d\mathcal{X}_{surf}}{d\alpha_{geom}} \right) \right) - \frac{dF}{d\alpha_{geom}} L \right)
\end{aligned} \tag{5.43}$$

$$\begin{aligned}
\frac{d\mathcal{J}_{aero}}{d\alpha_{struct}} &= \frac{\partial\mathcal{J}_{aero}}{\partial\mathcal{X}} \frac{\partial\mathcal{X}}{\partial\mathcal{X}_b} \frac{d\mathcal{X}_b}{d\alpha_{struct}} \\
&+ \frac{\partial\mathcal{J}_{aero}}{\partial W^b} \left(\frac{\partial W^b}{\partial W} + \frac{\partial W^b}{\partial\mathcal{X}} \left(\frac{\partial\mathcal{X}}{\partial\mathcal{X}_b} \frac{d\mathcal{X}_b}{d\alpha_{struct}} + \frac{\partial\mathcal{X}}{\partial D} \right) \right) + \lambda_f^T \frac{\partial R_f}{\partial\mathcal{X}} \frac{\partial\mathcal{X}}{\partial\mathcal{X}_b} \frac{d\mathcal{X}_b}{d\alpha_{struct}} \\
&+ \lambda_s^T \left(-F \left(\frac{\partial L}{\partial\mathcal{X}} \frac{\partial\mathcal{X}}{\partial\mathcal{X}_b} \frac{d\mathcal{X}_b}{d\alpha_{struct}} + \frac{\partial L}{\partial\mathcal{X}_b} \frac{d\mathcal{X}_b}{d\alpha_{struct}} + \frac{\partial L}{\partial W^b} \frac{dW^b}{d\alpha_{struct}} \right) - \frac{dF}{d\alpha_{struct}} L \right)
\end{aligned} \tag{5.44}$$

$$\begin{aligned}
\frac{d\mathcal{J}_{struct}}{d\alpha_{geom}} &= \frac{\partial\mathcal{J}_{struct}}{\partial\mathcal{X}_{surf}} \frac{\partial\mathcal{X}_{surf}}{\partial\mathcal{X}_{rig}} \frac{d\mathcal{X}_{rig}}{d\alpha_{geom}} + \frac{\partial\mathcal{J}_{struct}}{\partial\mathcal{X}_b} \frac{\partial\mathcal{X}_b}{\partial\mathcal{X}_{rig}} \frac{d\mathcal{X}_{rig}}{d\alpha_{geom}} \\
&+ \lambda_f^T \frac{\partial R_f}{\partial\mathcal{X}} \left(\frac{\partial\mathcal{X}}{\partial\mathcal{X}_{rig}} \frac{d\mathcal{X}_{rig}}{d\alpha_{geom}} + \frac{\partial\mathcal{X}}{\partial\mathcal{X}_b} \frac{\partial\mathcal{X}_b}{\partial\mathcal{X}_{surf}} \frac{d\mathcal{X}_{surf}}{d\alpha_{geom}} \right) \\
&+ \lambda_s^T \left(-F \left(\frac{\partial L}{\partial\mathcal{X}} \frac{d\mathcal{X}}{d\alpha_{geom}} + \frac{\partial L}{\partial\mathcal{X}_b} \frac{d\mathcal{X}_b}{d\alpha_{geom}} + \frac{\partial L}{\partial W^b} \frac{dW^b}{d\alpha_{geom}} \right) - \frac{dF}{d\alpha_{geom}} L \right)
\end{aligned} \tag{5.45}$$

$$\begin{aligned}
\frac{d\mathcal{J}_{struct}}{d\alpha_{struct}} &= \frac{\partial\mathcal{J}_{struct}}{\partial\mathcal{X}_b} \frac{d\mathcal{X}_b}{d\alpha_{struct}} + \frac{\partial\mathcal{J}_{struct}}{\partial\alpha_{struct}} + \lambda_f^T \frac{\partial R_f}{\partial\mathcal{X}} \frac{\partial\mathcal{X}}{\partial\mathcal{X}_b} \frac{d\mathcal{X}_b}{d\alpha_{struct}} \\
&+ \lambda_s^T \left(-F \left(\frac{\partial L}{\partial\mathcal{X}} \frac{d\mathcal{X}}{d\alpha_{struct}} + \frac{\partial L}{\partial\mathcal{X}_b} \frac{d\mathcal{X}_b}{d\alpha_{struct}} + \frac{\partial L}{\partial W^b} \frac{\partial W^b}{\partial\mathcal{X}} \frac{\partial\mathcal{X}}{\partial\mathcal{X}_b} \frac{d\mathcal{X}_b}{d\alpha_{struct}} \right) \right. \\
&\quad \left. - \frac{dF}{d\alpha_{struct}} L \right) \quad (5.46)
\end{aligned}$$

5.4 Implementation of the derivatives appearing in the gradient of an aerodynamic cost function \mathcal{J}_{aero} and or structural cost function \mathcal{J}_{struct}

To solve the aero-structural adjoint system and assemble the final gradient of a function, 5 software components are involved:

- the CFD software *elsA* and its associated adjoint solver *elsA/Opt* and beam aero-elastic module *elsA/Bag* ;
- the linearised structural module *InAirSsi*;
- the post-processing code for drag extraction & breakdown *ffd72*;
- the python implementation of the beam equation solver *Beam*;
- the mesh deformation tool *SeAnDef*.

The following table summarises the physical meaning of each term, the computing software by which it is computed and the size of the matrix-term.

5.4.1 Terms appearing only in structural functions gradient

Term	Meaning	Computing program and Size
$\frac{\partial \mathcal{J}_{struct}}{\partial \mathcal{X}_{surf}}$	Sensitivity of a structural function w.r.t. the rigid CFD surface mesh	InAirSsi $3n_{\mathcal{X}_{surf}}$
$\frac{\partial \mathcal{J}_{struct}}{\partial \mathcal{X}_b}$	Sensitivity of a structural function w.r.t. the structural mesh	InAirSsi $3n_{\mathcal{X}_b}$

5.4.2 Terms appearing only in aerodynamic functions gradient

Term	Meaning	Computing program and Size
$\frac{\partial \mathcal{J}_{aero}}{\partial \mathcal{X}}$	Sensitivity of aerodynamic function w.r.t. the current CFD mesh	<i>ffd72</i> $3n_{\mathcal{X}}$
$\frac{\partial \mathcal{J}_{aero}}{\partial W^b}$	Sensitivity of the aerodynamic function w.r.t. the state variables at the fluid structure interface	<i>ffd72</i> $5n_{cell}^I$ or $7n_{cell}^I$
$\frac{\partial \mathcal{J}_{aero}}{\partial W}$	Sensitivity of the aerodynamic function w.r.t. the state variables	<i>ffd72</i> $5n_{cell}$ or $7n_{cell}$
$\frac{\partial W^b}{\partial W}$	Sensitivity of the state variables at the interface \mathcal{J}^{FS} w.r.t. the flow field in the computational domain	<i>elsA</i> $5n_{cell}^I * 5n_{cell}$ or $7n_{cell}^I * 7n_{cell}$
$\frac{\partial W^b}{\partial \mathcal{X}}$	Sensitivity of the state variables at the interface \mathcal{J}^{FS} w.r.t. the current mesh	<i>elsA</i> $5n_{cell}^I * 3n_{\mathcal{X}}$ or $7n_{cell}^I * 3n_{\mathcal{X}}$

5.4.3 Terms appearing in the gradient formulation independently on the nature of the cost function

5.4.3.1 Sensitivities of \mathcal{X} , \mathcal{X}_{rig} , \mathcal{X}_{surf} , \mathcal{X}_b :

Term	Meaning	Computing program and Size
$\frac{\partial \mathcal{X}}{\partial \mathcal{X}_{rig}}$	Sensitivity of the aero-elastic CFD mesh w.r.t. the rigid mesh (mesh before aero-elastic effects)	<i>elsA</i> $3n_{\mathcal{X}} * 3n_{\mathcal{X}}$
$\frac{d\mathcal{X}_{rig}}{d\alpha_{geom}}$	Sensitivity of the rigid mesh w.r.t. to aerodynamic shape parameters	SeanDef $3n_{\mathcal{X}} * n_{\alpha_{geom}}$
$\frac{\partial \mathcal{X}}{\partial \mathcal{X}_b}$	Sensitivity of the aero-elastic CFD mesh w.r.t. beam mesh nodes	<i>elsA</i> $3n_{\mathcal{X}} * 3n_{\mathcal{X}_b}$
$\frac{\partial \mathcal{X}_b}{\partial \mathcal{X}_{surf}}$	Sensitivity of beam mesh nodes w.r.t. the surface CFD mesh	InAirSsi $3n_{\mathcal{X}_b} * 3n_{surf}$
$\frac{\partial \mathcal{X}_{surf}}{\partial \mathcal{X}_{rig}}$	Sensitivity of the surface CFD mesh w.r.t. rigid mesh	InAirSsi $3n_{surf} * 3n_{\mathcal{X}}$
$\frac{\partial \mathcal{X}}{\partial D}$	Sensitivity of the aero-elastic CFD mesh w.r.t. structural displacements	<i>elsA</i> $3n_{\mathcal{X}} * 2n_{\mathcal{X}_b}$
$\frac{d\mathcal{X}_b}{d\alpha_{struct}}$	Sensitivity of the beam mesh w.r.t. the structural design parameters	InAirSsi $3n_{\mathcal{X}_b} * n_{\alpha_{struct}}$

5.4.3.2 Sensitivities of aerodynamic loads L:

Term	Meaning	Computing program and Size
$\frac{\partial L}{\partial \mathcal{X}}$	Sensitivity of the wing aerodynamic loads w.r.t. the current mesh	<i>elsA</i> $3n_{x_b} * 3n_{\mathcal{X}}$
$\frac{\partial L}{\partial x_b}$	Sensitivity of the wing aerodynamic loads w.r.t. the current mesh	<i>elsA</i> $3n_{x_b} * 3n_{x_b}$
$\frac{\partial L}{\partial W^b}$	Sensitivity of the wing aerodynamic loads w.r.t. the state variable at the fluid/structure interface	<i>elsA</i> $3n_{x_b} * 5n_{cell}$ or $n_{x_b} * 7n_{cell}$

Example of differentiation: $\frac{\partial L}{\partial x_b}$

At each step of the aero-elastic computation, the aerodynamic loads extracted from the CFD mesh and transferred to the beam nodes B_i , $1 \leq i \leq n_{x_b}$ of the structural grid are:

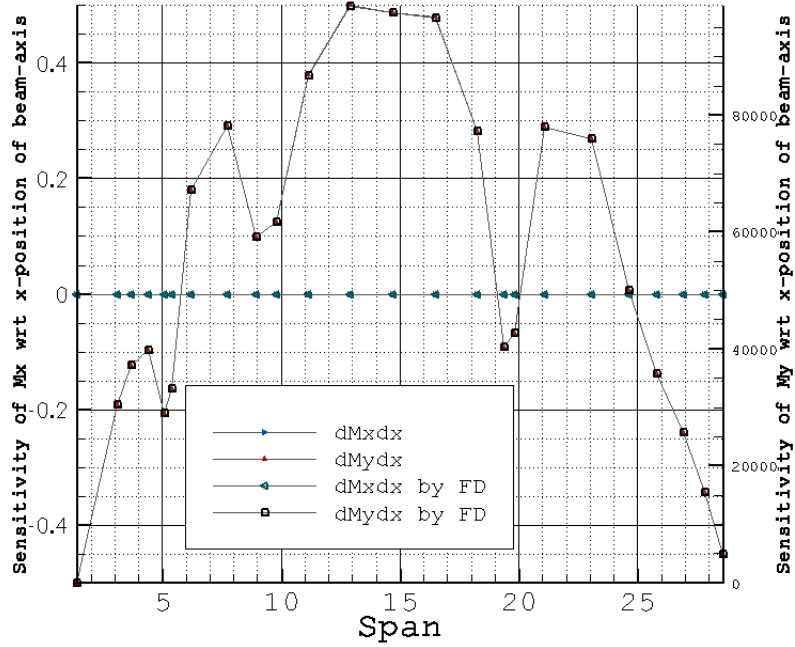
$$\left\{ \begin{array}{l} \vec{F}_i = \sum_{l=1}^{n_f^i} S_l^i (p_l - p_\infty) \vec{n}_l \\ \vec{M}_i = \sum_{l=1}^{n_f^i} \vec{B}_i \vec{G}_l \wedge S_l^i (p_l - p_\infty) \vec{n}_l \end{array} \right.$$

Where S_l^i is the intersection between the influence area V_i of the node B_i and the interface I_l of the surface mesh. For a fixed span configuration, the influence area V_i of each node B_i of the beam axis X_{beam} remains constant and so does S_l^i . The partial derivative of the static pressure p_l with respect to the beam axis position is zero. Hence the dependence of the aerodynamic loads to the beam axis is expressed through the sensitivity of the lever arm $\vec{B}_i \vec{G}_l$ to the x and z coordinates of the X_{beam} .

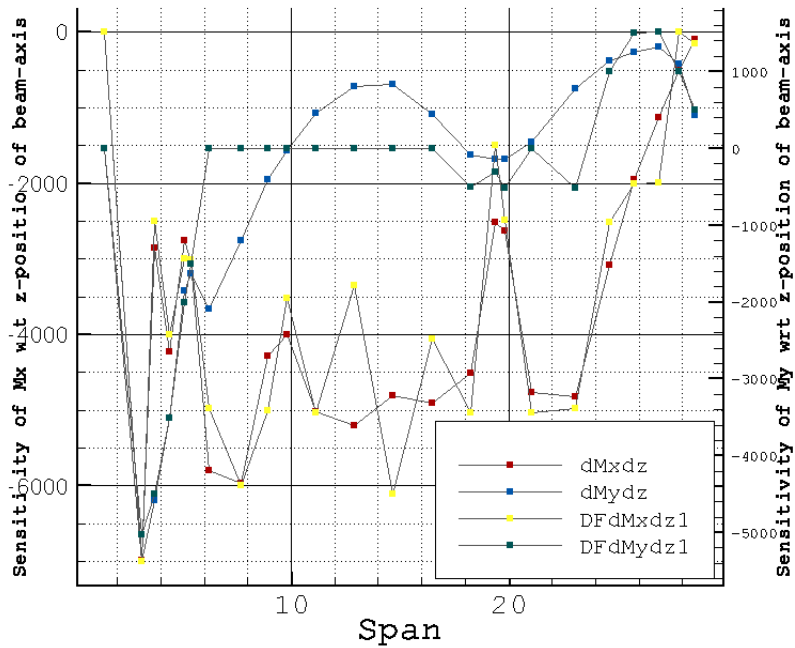
The integrated load transferred to the structure depends on the elastic axis position which with α_{geom} and α_{struct} . Under the Euler-Bernoulli assumptions, only flexural and torsional loads $\vec{F}_i \cdot \vec{z}$, $\vec{M}_i \cdot \vec{x}$ and $\vec{M}_i \cdot \vec{y}$ are transferred to the beam axis. The vertical component \vec{F}_i depends only on the slice on which aerodynamic loads are integrated. If the latter remains constant, the sensitivity of \vec{F}_i with respect to the coordinate of the load node(s) framed in the slice is zero. The lever arm of the bending moment and the torsion moment applied to the structure are the terms affected by the beam axis position:

$$\left\{ \begin{array}{l} \frac{\partial F_{iz}}{\partial x} = 0 ; \quad \frac{\partial F_{iz}}{\partial y} = 0; \quad \frac{\partial F_{iz}}{\partial z} = 0 \\ \frac{\partial M_{ix}}{\partial x} = 0 ; \quad \frac{\partial M_{ix}}{\partial y} = 0; \quad \frac{\partial M_{ix}}{\partial z} = F_{iy} \\ \frac{\partial M_{iy}}{\partial x} = F_{iz} ; \quad \frac{\partial M_{iy}}{\partial y} = 0; \quad \frac{\partial M_{iy}}{\partial z} = -F_{ix} \end{array} \right.$$

The computation of the term $\frac{\partial L}{\partial \mathcal{X}_b}$ is implemented in the module BAG of the CFD code *elsA*. This linearisation is independent on the equations that model the fluid behaviour since the only term that is influenced by the beam axis position is the lever arm of the torsion and flexural moment.



(a) Partial derivatives of flexion M_x and torsion M_y moments with respect to x-coordinate of the beam axis position



(b) Partial derivatives of flexion M_x and torsion M_y moments with respect to z-coordinate of the beam axis position

Figure 5.1: Evaluation of $\frac{\partial L}{\partial x_b}$ by finite differences VS linearization

5.4.3.3 Sensitivities of the flexibility matrix:

Term	Meaning	Computing program and Size
$\frac{\partial F}{\partial I}$	Sensitivity of the flexibility matrix w.r.t. the second moment of area $I(y)$	Beam $3n_{x_b} * 3n_{x_b} * n_{x_b}$
$\frac{\partial F}{\partial J}$	Sensitivity of the flexibility matrix w.r.t. the torsion constant $J(y)$	Beam $3n_{x_b} * 3n_{x_b} * n_{x_b}$
$\frac{\partial F}{\partial \mathcal{X}_b}$	Sensitivity of the flexibility matrix w.r.t. the structural mass \mathcal{X}_b	Beam $3n_{x_b} * 3n_{x_b} * 3n_{x_b}$

5.4.3.4 Sensitivities of the structural properties I and J :

Term	Meaning	Computing program and Size
$\frac{\partial I}{\partial \mathcal{X}_b}$	Sensitivity of the bending constant w.r.t. the structural mess \mathcal{X}_b	InAirSsi $3n_{\mathcal{X}_b} * 3n_{\mathcal{X}_b} * 3n_{\mathcal{X}_b}$
$\frac{\partial J}{\partial \mathcal{X}_b}$	Sensitivity of the torsion constant w.r.t. the structural mess \mathcal{X}_b	InAirSsi $9n_{\mathcal{X}_b} * 9n_{\mathcal{X}_b} * 3n_{\mathcal{X}_b}$
$\frac{\partial I}{\partial \alpha_{geom}}$	Sensitivity of the second moment of area w.r.t. aerodynamic shape parameters \mathcal{X}_b	InAirSsi $n_{\mathcal{X}_b} n_{\alpha_{geom}}$
$\frac{\partial J}{\partial \alpha_{geom}}$	Sensitivity of the torsion constant w.r.t. aerodynamic shape parameters \mathcal{X}_b	InAirSsi $n_{\mathcal{X}_b} * n_{\alpha_{geom}}$
$\frac{\partial I}{\partial \alpha_{struct}}$	Sensitivity of the second moment of area w.r.t. structural parameters parameters \mathcal{X}_b	InAirSsi $n_{\mathcal{X}_b} * n_{\alpha_{struct}}$
$\frac{\partial J}{\partial \alpha_{struct}}$	Sensitivity of the torsion constant w.r.t. structural parameters \mathcal{X}_b	InAirSsi $n_{\mathcal{X}_b} * n_{\alpha_{struct}}$

5.5 Outcome

The aero-structural adjoint development has been detailed in this chapter. The meaning and the computation of the new terms appearing with this extension have been explained.

The aero-structural adjoint is now implemented and available in *elsA/BAG* and can

be used in combination of the linearised structural module InAirSsi. The validation of the aero-structural adjoint is presented in the next chapter.

6

Aerodynamic, aero-elastic and aero-structural adjoint-based gradients: results and comparison

6.1 Preamble

Now that the development of the aero-structural adjoint has been presented and the derived structural module validated, this chapter is intended to validate the aero-structural adjoint method.

The aim of this work is to access the aero-structural sensitivities, however much work has been done to prepare the stage for this extension and validate the common part to the aerodynamic, aero-elastic and aero-structural adjoints. This work is presented in this chapter through the gradient validation -adjoint vs finite Difference(FD)- of the three adjoint methods, all available now in the ONERA CFD software *elsA-BAG*.

6.2 Test case description

The gradient computation and validation as well as the structural optimization exercises presented in chapter 4 p. 69 and in what follows are performed for the wing of the

AIRBUS configuration XRF1¹ 6.1 p. 143.

The Euler grid has 1.378.895 points and 1.189.584 cells and it is composed of 143 structured blocks.

The CFD mesh corresponding to the *jig-shape*, used for aero-elastic computation, has first been constructed from the available CFD mesh of the cruise flight condition shape by applying the inverse of the aero-elastic deformations induced by aerodynamic loads at the design point. All calculations presented in this section have been performed for the cruise conditions defined as $C_L = 0.5$, $Mach = 0.83$, $Altitude = 35000ft$. The structural members used for the purpose of aero-structural adjoint validation are issued from an initial sizing according to the methodology presented in section 4.6.2.

6.3 Problem parametrization

For the aerodynamic shape parametrisation, the in-house analytical tool for mesh deformation SeAnDef (Sequential Analytical Deformation) is used. SeAnDef is coded in C++ and can perform nine deformation modes are available:

- chord deformation;
- twist deformation;
- sweep deformation;
- span modification (according to the y-axis);
- dihedral modification (according to the z-axis);
- thickness deformation;
- camber deformation;
- airfoils shape by chordwise B-spline based deformation;

¹eXternal Research Forum: comprising Airbus, DLR, ONERA, QinetiQ (then EADS/IW from 2009)

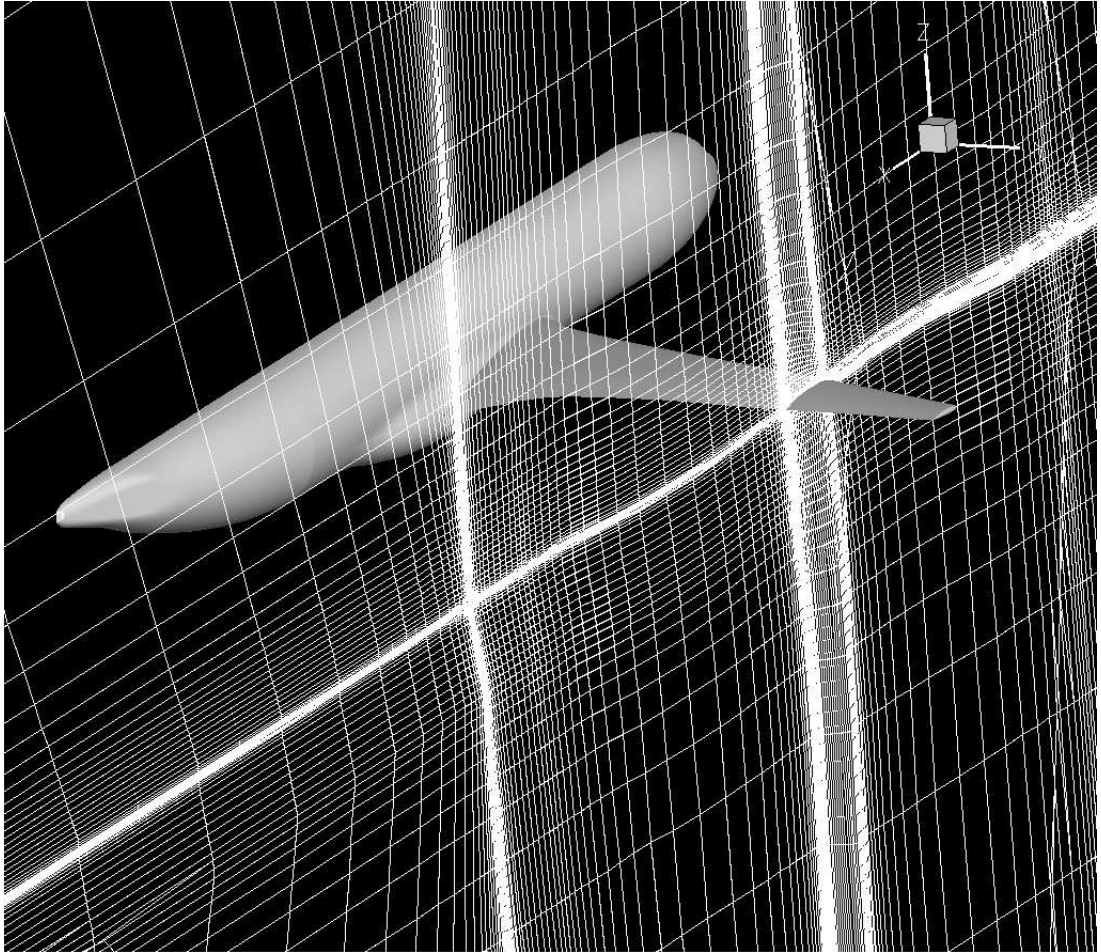


Figure 6.1: Euler grid of the Airbus XRF1 wing-fuselage configuration

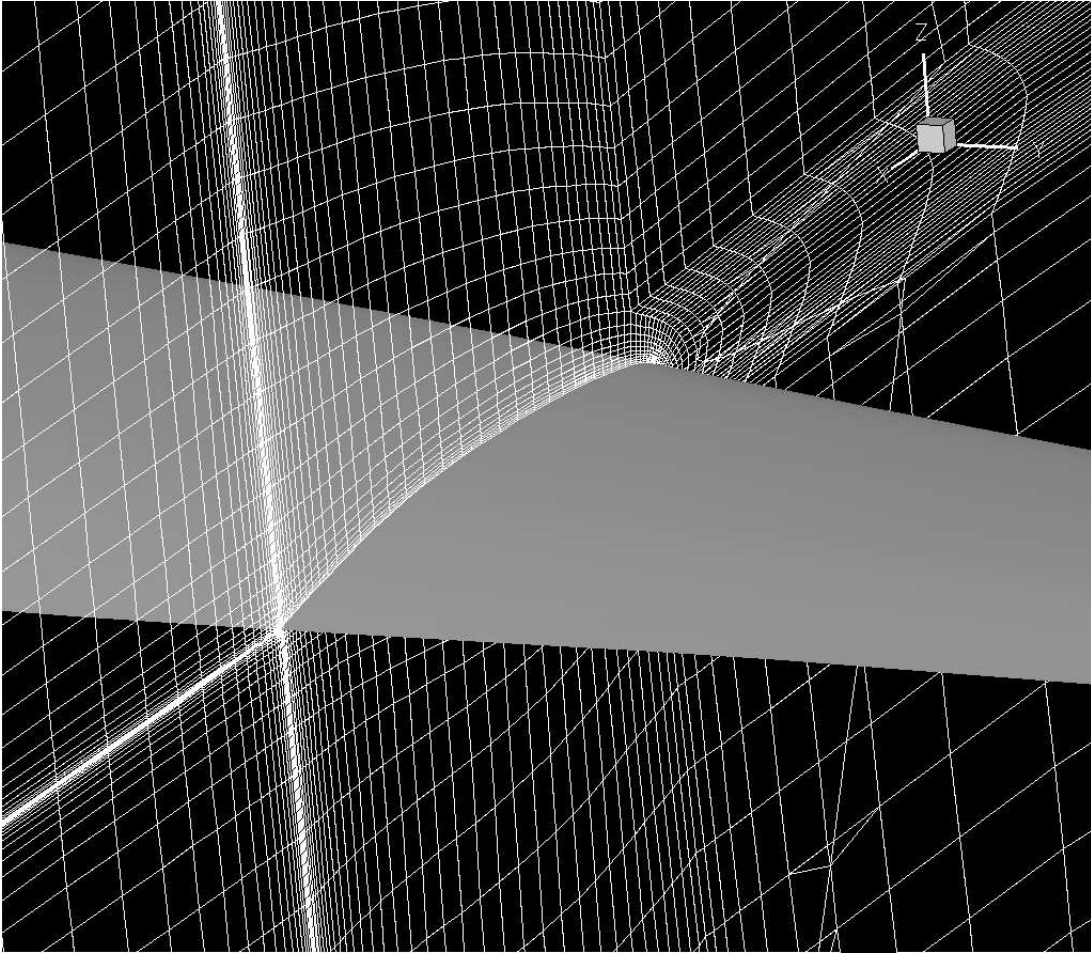


Figure 6.2: Zoom on the Euler grid of the Airbus XRF1 wing-fuselage configuration

- geometrical angle of attack.

It is possible to access the combination of these deformation modes to realise complex deformation modes. For example the sweep angle or the span with a constant reference area. In this case an automatic adjustment of the chord at the wing root, the crank and the wing tip is performed.

The deformation laws are defined using control sections along the span, at which deformations parameters are defined by the user or by the optimiser and interpolated in between the framed sections. The geometrical angle of attack actually corresponds to a rigid rotation of the complete CFD grid around the span axis. The interpolation between two control sections can be performed using different laws. Linear interpolation and cubic spline are defined as direct laws, since in this case the parameter controlling the law correspond exactly to the deformation induced in the mesh. For the second category that gather Bezier curves, B-spline curves and Nurbs, the input values are not the parameters that directly shape the aerodynamic envelop of the wing but the control points of the parametric deformation law.

The deformations can be damped far away from the body. A control volume is defined such as the deformation is fully applied in this volume, and progressively damped to become null far away. It is interesting to mention that, the same deformation method is used to introduce the aero-elastic deformations in the CFD mesh during the aero-elastic coupling. Let us recall that the authorised aero-elastic deformations, under the Euler Bernoulli hypothesis, are wing vertical deflection and twist.

The different variables which can be used in the three different wing design problems: aerodynamic, aero-elastic and aero-structural are given in table 6.1 p. 146. Obviously the structural parameters (handled with InAirSsi) are only meaningful in the case of an aero-structural design optimisation. Moreover, wing planform and wing thickness parameters can only be reasonably treated in the case of an aero-structural design, since these parameters have a strong impact on the structure behaviour and on the structural weight.

	Aerodynamic adjoint	Aero-elastic adjoint	Aero-structural adjoint
α_{geom}			
Twist	possible	possible	possible
Camber	possible	possible	possible
Profil control point	possible	possible	possible
AOA	possible	possible	possible
Thickness	possible but no physical meaning	possible but no physical meaning	possible
Chord	possible but no physical meaning	possible but no physical meaning	possible
Span	possible but no physical meaning	possible but no physical meaning	possible
α_{struct}			
Front spar web	impossible	impossible	possible
Rear spar web	impossible	impossible	possible
Lower surface spar cap	impossible	impossible	possible
Upper surface spar cap	impossible	impossible	possible
Lower surface skin	impossible	impossible	possible
Upper surface skin	impossible	impossible	possible

Table 6.1: Parametrisation dependency on the design problem: aerodynamic, aero-elastic or aero-structure

6.4 Aerodynamic functions evaluation, decomposition and partial sensitivities of these functions with *ffd72*

One important component of the adjoint is the software *ffd72* for drag decomposition and breakdown. It is based on the near-field and far-field drag balance carried out by van der Vooren and Destarac (22) (36) (82). This theory ensures the balance between the sum of pressure and friction drag (near-field) and the sum of viscous, wave and induced drag.

This means that the effect of geometrical modifications can be analysed over any drag component. In addition, *ffd72* provides the partial derivatives of all aerodynamic function (including the lift coefficient and the pitching moment) with respect to the metric and the flow variables, as detailed in chapter 5.2 p. 116 and needed for all adjoint computations.

6.5 Aerodynamic adjoint-based optimisations

The aerodynamic adjoint method is introduced in section 3.2. This work does not make further contribution to this part, however it is the common part to the three types of adjoint formulations and thus serves as a comparison baseline to the introduction of flexibility effects.

6.5.1 Gradient validation

As a validation of the aerodynamic gradients calculated by the adjoint method, we compare in Table 6.2 the gradient of the lift coefficient C_L and pressure drag C_{D_p} , calculated with the adjoint method and by FD (2nd order), w.r.t. to five twist parameters defined at five control sections along the span.

α_{geom}	Aerodynamic adjoint		Finite Differences		Relative error	
	$\frac{dC_L}{d\alpha_i}$	$\frac{dC_{Dp}}{d\alpha_i}$	$\frac{dC_L}{d\alpha_i}$	$\frac{dC_{Dp}}{d\alpha_i}$	$\frac{dC_L}{d\alpha_i}$	$\frac{dC_{Dp}}{d\alpha_i}$
α_{twist_1}	2.185e-02	2.04e-03	2.202e-02	2.014e-03	0.7%	1.2%
α_{twist_2}	3.653e-02	3.829e-03	3.728e-02	3.94e-03	2%	2.8%
α_{twist_3}	3.806e-02	4.862e-03	3.888e-02	5.066e-03	2.1%	4%
α_{twist_4}	2.010e-02	3.387e-03	2.038e-02	3.493e-03	1.3%	3%
α_{twist_5}	5.687e-03	9.891e-04	5.713e-03	1.005e-04	0.45%	8.8%
AoA	1.559e-01	1.416e-02	1.577e-01	1.855e-02	0.01%	23.6%

Table 6.2: C_L and C_{D_p} gradient computation: aerodynamic adjoint and FD

6.5.2 Application of the aerodynamic adjoint method to the optimisation of the test-case wing

To initiate the application of the aerodynamic adjoint solver, we employ an inviscid design strategy. The optimisation process, performed at Mach=0.83, is constrained by the lift coefficient. The constraint is reached by adjusting the angle of attack.

The inviscid redesign at cruise condition for transonic wings is common and our choice to solve the flow via the Euler equations concerns first the need of fast access to results during validation steps. Secondly because in a validation step the gradients must be unruffled by the modelling hypothesis. The RaNS computations although very fast are still subject to some inconsistencies due to the non-exact linearisation of viscosity terms. Of course, inviscid computation are unable to predict flow separation, but the C_p distribution constitutes a reliable indicator by analysing the gradient in the trailing edge region, where the flow is suppose to decelerate. A steeper gradient in this region may count as a flow separation indicator. No need also to expand on the valuable low cost aspect of the Euler computations that remains desirable in both preliminary design and detailed design. The development of the aero-structural adjoint method is not intrinsic and remains valid regardless of the flow modelling .

This section presents, by mean of gradient-based algorithms, the purely aerodynamic optimisation of the wing of the selected test case. Before going further, let us say already that this configuration is twist-optimized configuration. Four optimisation scenarios are

presented aiming at exploring the rigid design space. The pressure drag is used as the objective function which is constrained by the lift coefficient. The optimum is analysed in terms of drag components but also in terms of spanwise lift distribution².

6.5.2.1 Optimisation with first wing parametrisation: 5 twist control section + angle of attack

The results presented in this section are selected from a set of several optimisation, performed with three algorithms CONMIN (83), DOT-MMFD (84) and CFSQP (16). The effects of both the optimisation algorithm and the starting point were investigated: far or close from the lift constraint, yielding with active or non-active constraint at the starting point. Needless to say that for an objective such as the pressure drag with a complex behaviour producing a non-convex, possibly multi-modal design space, the variety of results goes with the creativity of the algorithm... It is important then to remember that the optimisation results may depend on the gradient optimisation algorithm as well as the starting point.

The strategy of the optimizer raises some questions. In fact, the algorithm chose to twist negatively all the sections and increase the angle of attack. The initial fuselage incidence $+1.9^\circ$ is increased to $+2.7^\circ$ while the one of the wing is combined with a dominant negative twist. Actually the final value of the angle of attack is the upper bound of this variable given to the optimizer. One may wonder if this result is dependant on the gradient order of magnitude since the angle of attack gradient is dominant -at least at the optimisation start- or simply on the starting point. Tables 6.3 and 6.4 compare the initial and the optimized designs in terms of aerodynamic performance and design parameters. The most important drag reduction concerns the wave drag

² Both lift distribution and load distribution (the distribution of the lift coefficient times the sectional chord) are key indicators for the optimality analysis. In the 30's, the common vision was that to obtain an elliptical load distribution, the planform must be elliptical... Mythical aircraft were constructed under this assumption, the *Hawker Sea Fury* is one of these extraordinary planes. Since the 50's, wings look far from elliptical. In fact, load distribution depends explicitly on the relative importance of drag and weight. And Elliptical load distribution is first of all a target for aerodynamic design.

	Reference configuration	Optimized conf. with quadratic programming (CFSQP)	Optimized conf. with Method of Feasible directions (CONMIN, DOT)
C_{D_p} (Drag Counts)	100 %	95.39 %	96.36%
C_{D_w} (DC)	10.42%	6.45	11.21%
C_{D_i} (DC)	63.28 %	62.56%	62.36 %
$C_{D_{sp}}$ (DC)	26.27%	17.78%	38.94%
C_L	0.5	0.5	0.5

Table 6.3: Drag extraction and decomposition for both initial and optimised -in terms of C_{D_p} - configurations, $\alpha_{geom} \in \mathbb{R}^6$ (first wing parametrization)

α_{geom}	Reference configuration	Sequential algorithms CFSQP
α_{twist_1}	0	-2.4°
α_{twist_2}	0	-2.11°
α_{twist_3}	0	-1.62°
α_{twist_4}	0	-3.51°
α_{twist_5}	0	-2.36°
α_{AoA}	+1.9°	+2.7°

Table 6.4: Design parameters for the Initial point and optimized configuration by the CFSQP algorithm using the first parametrisation ($\alpha_{geom} \in \mathbb{R}^6$)

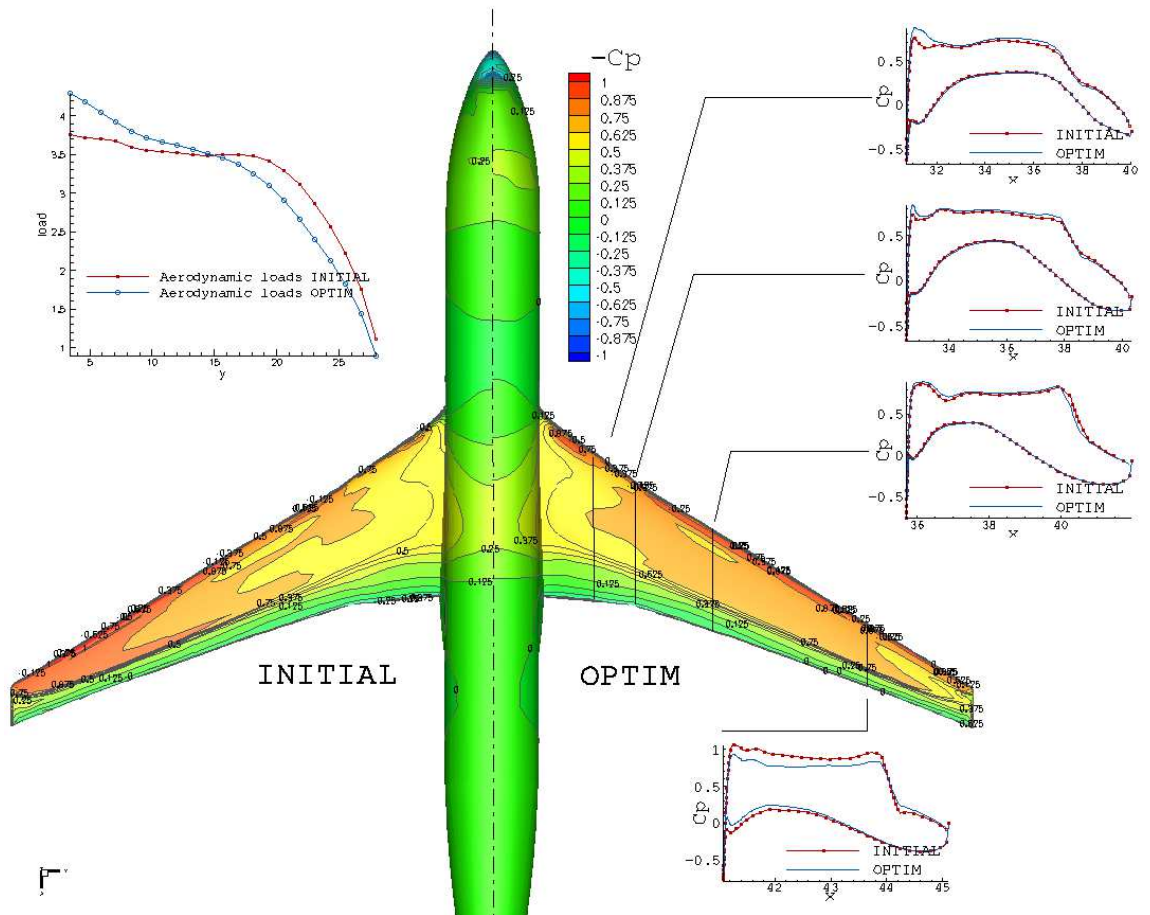


Figure 6.3: Pressure distribution of the rigid configuration optimized for the C_{D_p} with CFDSQP algorithm. Parametrization with 5 twist control sections and the angle of attack

	Reference configuration	Optimised con. with 5 twist sections (CFSQP)	Optimised con. with 10 twist sections (CFSQP)
C_{D_p} (DC)	100%	95.39%	95.22%
C_{D_w} (DC)	10.42%	6.45%	6.38%
C_{D_i} (DC)	63.28%	62.56%	62.45%
$C_{D_{sp}}$ (DC)	26.27%	26.37%	26.38%
C_L (DC)	0.5	0.5	0.5

Table 6.5: Design parameters for the Initial point and optimized configuration by the CFSQP algorithm using the first parametrisation ($\alpha_{geom} \in \mathbb{R}^{11}$) (second parametrisation)

component. Actually, the induced drag cannot be significantly improved because of the already nearly optimal lift distribution of the initial design. Can this results obtained with only 5 twist control sections and the angle of attack be significantly improved if we further enrich the design space by adding more twist control sections?

6.5.2.2 Optimisation with the second wing parametrisation: 10 twist control section + angle of attack

Five additional control sections are introduced to the design space and optimisation were conducted with this new parametrisation. The results are listed in table 6.5 and compared to the results obtained with previous parametrisation. The drag reduction is still mostly achieved through the reduction of the wave drag component, however this does not result in a significantly better design than the results of the previous optimization with the coarser optimization. The algorithm (CFSQP) indeed converges to a point close to the one found when $\alpha_{geom} \in \mathbb{R}^6$. Enriching the design space with more twist control section did not significantly improve the results found with coarser parametrisation, indicating that the twist control with few control sections is physically pertinent.

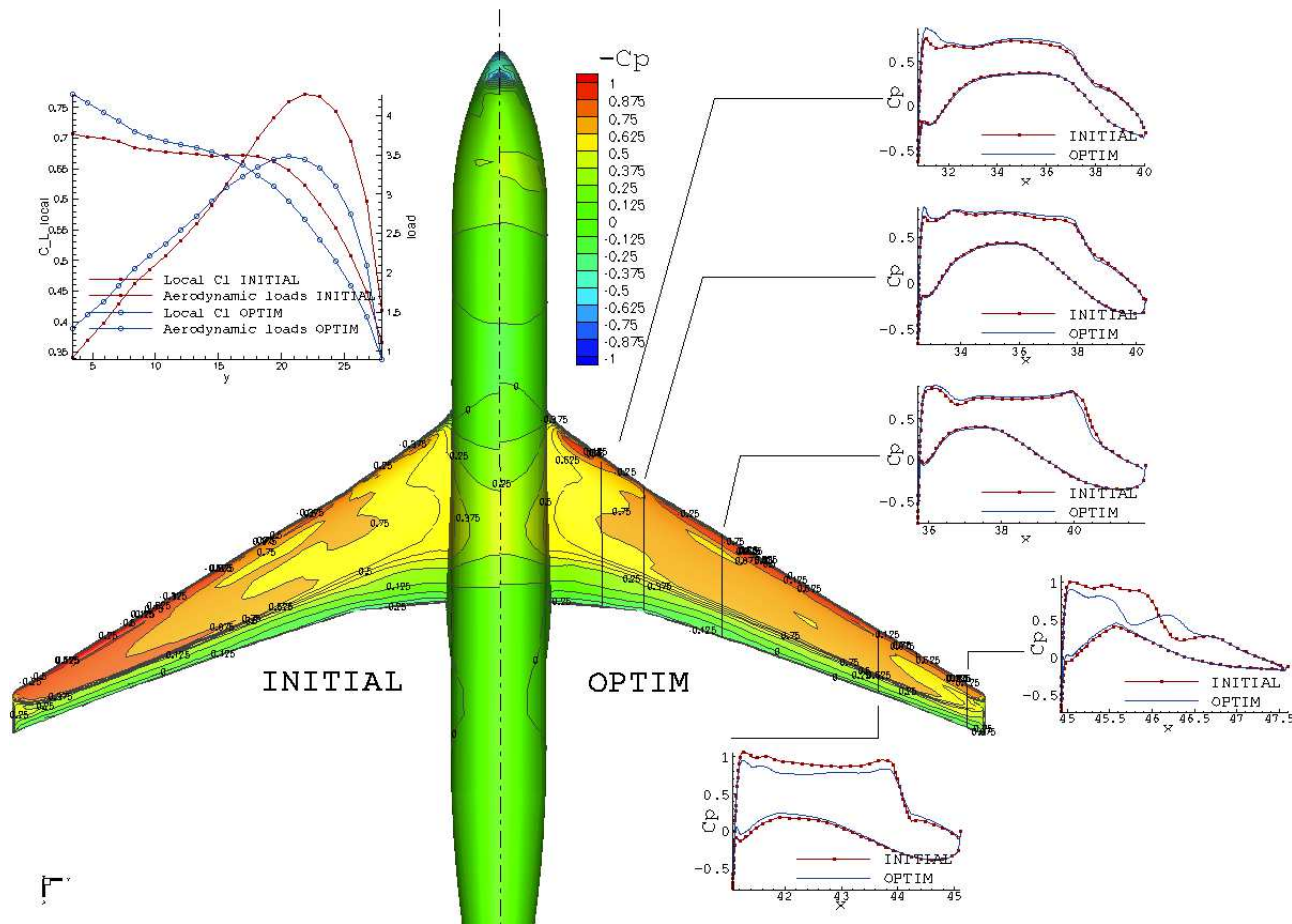


Figure 6.4: Pressure distribution of the rigid configuration optimized for the C_{D_p} with CFDSQP algorithm. Parametrization with 10 twist control sections and the angle of attack

α_{geom}	Reference configuration	Sequential algorithms CFSQP
α_{twist_1}	0	-1.130
α_{twist_2}	0	-2.262
α_{twist_3}	0	-2.150
α_{twist_4}	0	-1.858
α_{twist_5}	0	-1.472
α_{twist_6}	0	-2.944
α_{twist_7}	0	-3.227
α_{twist_8}	0	-3.099
α_{twist_9}	0	-2.758
$\alpha_{twist_{10}}$	0	-2.268
α_{AoA}	1.9	+2.7

Table 6.6: Design parameters for the initial point and the optimized configuration by the CFSQP $\alpha_{geom} \in \mathbb{R}^{11}$

(second parametrisation)

6.5.2.3 Optimization with the third wing parametrisation: 5 twist control section + 25 airfoil control points + angle of attack

Aiming at evaluating the effect of parametrisation enrichment, we introduce another type of parameters: local airfoil control points of B-splines curves. Twenty five points are distributed over the twist control sections to introduce local smooth bumps over the airfoil. Then, two optimisation scenarios are tested:

- first scenario with a starting point almost satisfying the lift constraint (NC), $C_L = 0.534$;
- second scenario with a starting point far from the lift coefficient constraint (FC), $C_L = 0.664s$;

DOT-MMFD algorithm is selected to perform the optimisation of the drag coefficient under lift constraint which is controlled via the adjustment of the the angle of attack. The optimisation of scenario FC did not converge. There is two possible reasons: the most likely hypothesis can be linked to gradient inaccuracy for high lift coefficients. If the gradient can be validated at the start of the optimization, this does not warranty that during the optimisation process the gradients remain accurate. The second hypothesis concerns the multi-modality of the design space and the potential existence of a local minima.

The case where the starting point has a lift coefficient closer to the design point (scenario (NC)) converged without difficulty. The aerodynamic performance is summarised in Table 6.7 p. 156: drag coefficient breakdown and lift coefficient for the starting point and the optimal point.

This parametrisation gives identical results in comparison with the results presented in subsections 6.5.2.1 and 6.5.2.2 in terms of drag breakdown. The wave drag remains the only improvable far field drag component. However it worth mentioning the difference in lift distribution between twist parametrisation (Fig.6.4) and control point parametrisation (Fig.6.5).

The direct conclusion is that the increase of design space dimension is not correlated with the convergence of the optimization. However the parametrisation (type and dimension) drive the physical behaviour of the configuration (lift distribution). The

	XRF1 Initial con- figuration	DOT-MMFD NC
C_{D_p} (DC)	100%	96.5%
C_{D_w} (DC)	10.42%	7.06%
C_{D_i} (DC)	63.28 %	62.80%
$C_{D_{sp}}$ (DC)	26.27%	26.64%
C_L (DC)	0.5	0.5

Table 6.7: Drag extraction and decomposition: initial configuration, optimised NC (optimal in terms of C_{D_p}), $\alpha_{geom} \in \mathbb{R}^{31}$
(third parametrisation)

XRF1 configuration could not be more optimised than the obtained results. One can surmise on the high design quality of the initial configuration or on the parametrisation choice and initialization or on the multi-modality of the design space.

Several parametrisations and problem definition were tested including modification of the starting point, scaling of the design variables and normalization of the objective functions/constraints. But no noticeable difference were obtained to justify the presentation of these test in the manuscript. The convergence of the optimisation process was verified via KKT conditions -using a graphical interpretation- but of course these are not sufficient conditions since we do not have any certainty about the convexity of the objective functions.

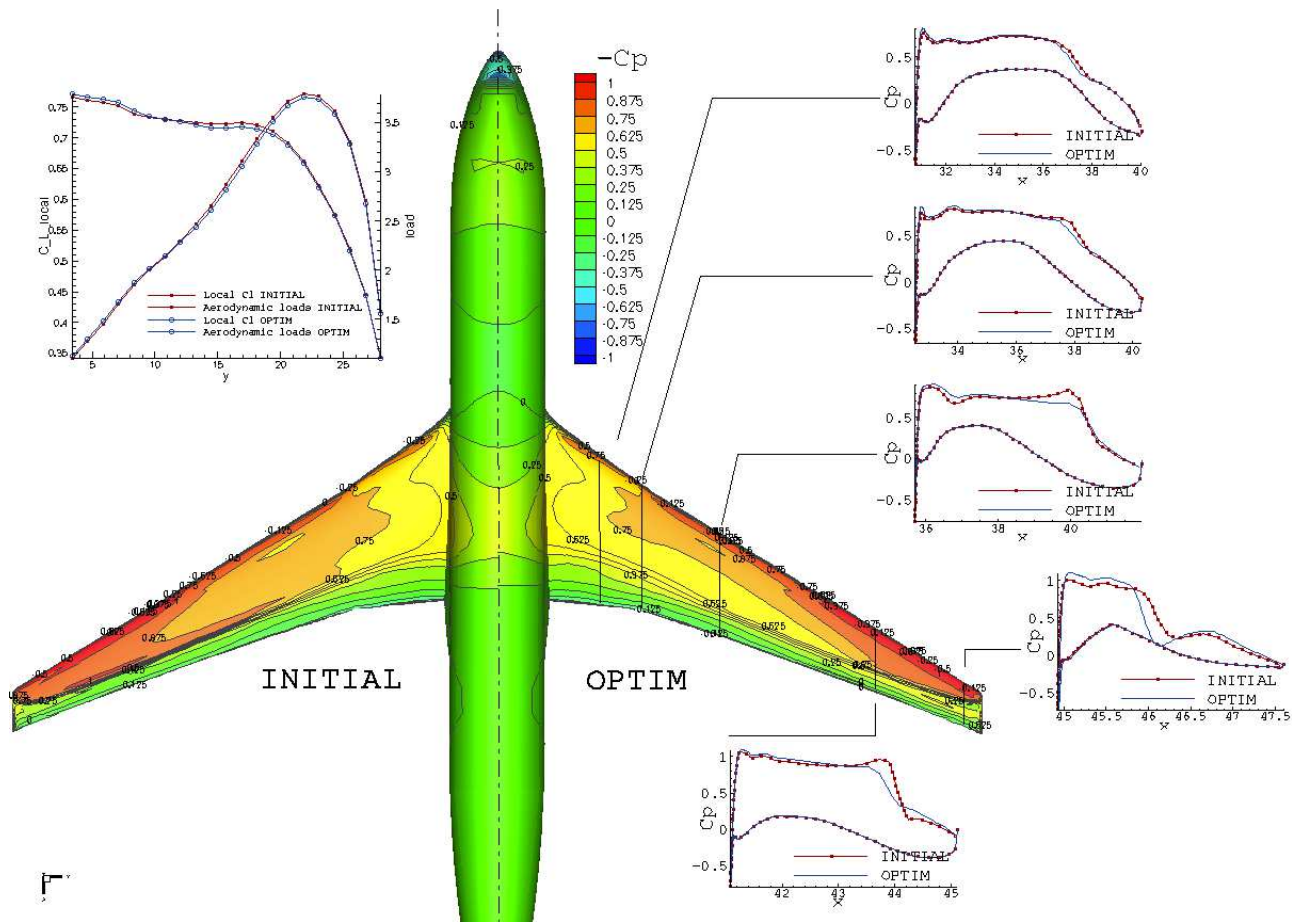


Figure 6.5: Pressure distribution of the rigid configuration optimized for the C_{D_p} with CFDSQP algorithm. Parametrization with 5 twist control sections, 25 airfoil control points and the angle of attack

α_{geom}	Reference configuration	Sequential algorithms CFSQP
α_{twist_1}	-8.633e-02	-1.438e-03
α_{twist_2}	-1.372e-01	-2.601e-03
α_{twist_3}	-2.130e-01	-3.152e-03
α_{twist_4}	-2.352e-01	-2.125e-03
α_{twist_5}	-6.915e-02	-5.428e-04
α_{profil_6}	1.941e-03	1.115e-02
α_{profil_7}	3.330e-02	6.329e-02
α_{profil_8}	-1.422e-03	1.348e-02
α_{profil_9}	5.550e-02	8.330e-02
$\alpha_{profil_{10}}$	6.369e-03	1.436e-02
$\alpha_{profil_{11}}$	9.134e-02	9.349e-02
$\alpha_{profil_{12}}$	-6.562e-03	7.285e-03
$\alpha_{profil_{13}}$	6.364e-02	6.914e-02
$\alpha_{profil_{14}}$	-1.289e-02	-2.677e-03
$\alpha_{profil_{15}}$	6.907e-03	1.540e-02
$\alpha_{profil_{16}}$	-1.951e-02	-5.612e-02
$\alpha_{profil_{17}}$	-1.303e-01	-9.256e-02
$\alpha_{profil_{18}}$	-4.888e-02	-9.246e-02
$\alpha_{profil_{19}}$	-9.693e-02	-1.151e-01
$\alpha_{profil_{20}}$	-1.829e-01	-7.800e-02
$\alpha_{profil_{21}}$	-7.056e-02	-1.003e-01
$\alpha_{profil_{22}}$	-1.920e-01	-1.150e-01
$\alpha_{profil_{23}}$	-2.667e-01	-4.831e-02
$\alpha_{profil_{24}}$	-1.025e-01	-9.004e-02
$\alpha_{profil_{25}}$	-2.291e-01	-8.400e-02
$\alpha_{profil_{26}}$	-8.526e-02	1.462e-03
$\alpha_{profil_{27}}$	3.839e-02	-2.620e-02
$\alpha_{profil_{28}}$	-4.467e-02	-2.725e-02
$\alpha_{profil_{29}}$	6.161e-02	1.200e-02
$\alpha_{profil_{30}}$	3.582e-02	-1.177e-04
$\alpha_{profil_{31}}$	1.102e+00	1.578e+00

Table 6.8: Design parameters for the initial point and the optimized configuration by the CFSQP $\alpha_{geom} \in \mathbb{R}^{31}$

(third parametrisation)

6.6 Aero-elastic adjoint-based optimizations

The aero-elastic adjoint, presented in chapter 3 gives the sensitivities of aerodynamic functions w.r.t aerodynamic shape parameters of a flexible wing. It is a baseline to be compared with the aero-structural adjoint gradient. A comparison available, of course, only when the parameter is an aerodynamic shape parameter.

6.6.1 Aero-elastic gradient validation

The convergence of the aero-elastic adjoint equations depends highly on several numerical ingredients: first on the convergence of the direct aero-elastic equations. The adjoint system is solved for the shape at the aero-elastic equilibrium. Secondly, because the aero-elastic adjoint is based on the existing aerodynamic adjoint. It is subject to the same difficulties in solving the aerodynamic part of the coupled aero-elastic adjoint system, which sometimes requires the use of artificial dissipation to stabilise the iterative scheme used to solve the adjoint system.

As we did for the aerodynamic adjoint, we present in table 6.9 p. 160 the gradients of aerodynamic functions w.r.t. some aerodynamic shape parameters: five twist control sections. Of course, the FD-based gradients are obtained after a full step convergence. However one may notice that some gradients obtained with FD are still inconsistent with the adjoint-based value. In fact, it is inevitable that each aerodynamic function sensitivity requires a FD convergence step. It is intuitive that the impact of twist changes will not affect the drag coefficient and the lift coefficient in the same manner. Thus, when performing a drag optimization constrained by lift, a unique step to evaluate the gradient of both function will not be appropriate. This is another point that must not be forgotten when using FD for evaluating gradient along local optimization.

6.6.2 Application of the aero-elastic adjoint method to the elastic optimization of the test case wing

In this section, we use the aero-elastic adjoint to perform the elastic optimization of the test case wing and we compare the results to the aerodynamic -rigid- optimization.

α_{geom}	Aero-elastic adjoint		Finite Differences		Relative error	
	$\frac{dC_{Lp}}{d\alpha_i}$	$\frac{dC_{Dp}}{d\alpha_i}$	$\frac{dC_{Lp}}{d\alpha_i}$	$\frac{dC_{Dp}}{d\alpha_i}$	$\frac{dC_{Lp}}{d\alpha_i}$	$\frac{dC_{Dp}}{d\alpha_i}$
α_{twist_1}	2.259e-02	1.476e-03	2.262e-02	1.373e-03	0.1%	7.5%
α_{twist_2}	3.712e-02	2.369e-03	3.716e-02	2.152e-03	0.1%	10%
α_{twist_3}	3.656e-02	2.401e-03	3.660e-02	2.088e-03	0.1%	14.9%
α_{twist_4}	1.532e-02	1.149e-03	1.528e-02	8.641e-04	0.2 %	32.97%
α_{twist_5}	2.341e-03	1.703e-04	2.278e-03	7.258e-05	2.7%	>100%
AoA	1.426e-01	4.947e-03	1.423e-01	8.218e-03	0.2%	39.8%

Table 6.9: C_{Lp} and C_{Dp} gradient computation: aero-elastic adjoint and FD

As explained above, when a *frozen* structural model is used all along the optimization process and when the flexibility effect modifications are neglected, then the parametrisation choices have to be restricted. We aim at ameliorating the aerodynamic drag, at the design point ($C_L = 0.5$) via the control of five twist sections, distributed along the span, and 5 camber points located at the mid chord of each twist section. A degree of freedom is given to the angle of attack to reach the lift constraint.

The design exploration for both aerodynamic and aero-elastic adjoint start from a point that has a lift coefficient higher than the design point.

The optimization process is supervised by DOT algorithm. Each step of the gradient-based algorithm necessitates the computation of the aerodynamic flow on the elastic wing configuration and the resolution of the aero-elastic adjoint system for each function when the gradient is required.

The aero-elastic equilibrium of the wing is reached for 5 fluid/structure coupling iterations.

Of course, both rigid and elastic optimisation have the same degrees of freedom to control the aerodynamic wing shape. Table 6.10 list, at $C_L = 0.5$, C_{Dp} for the initial and the optimised configuration. The design space is not large, but enough to highlight the difference of design space exploration of a rigid or elastic wing. In fact, the pressure drag of the optimal elastic configuration has 7.09% less drag than the baseline

Table 6.10: Drag extraction and decomposition for initial, rigid and elastic optimal -in terms of C_{D_p} - configurations, $\alpha_{geom} \in \mathbb{R}^{11}$

	Baseline	Aerodynamic	Aero-elastic
C_{D_p} (Drag Counts)	100 %	96.01%	92.91%
C_{D_w} (Drag Counts)	10.43 %	6.94%	4.52%
C_{D_i} (Drag Counts)	63.29 %	62.76%	62.14%
$C_{D_{sp}}$ (Drag Counts)	26.27 %	26.27%	26.27%

configuration, while the rigid optimal configuration has 3.98% less drag count. Thus a difference of 3.1% of total drag reduction is resulting from the consideration of elastic effects. The straight forward conclusion to this, is that if we do increase the design space dimension it can be expectable that more differences between the rigid and elastic optimization process rise. This does not mean that elastic considerations warranty optimality for any case, but this will certainly give more physical meaning to the results.

The drag breakdown shows that for both scenarios, the total drag decrease is due to the wave drag component. In fact, the flow is modelled by the Euler-Bernoulli flow equations, thus the only expected component to be modified with a twist and camber p[arametrisation is either the wave drag or the induced drag. The analysis of the load distribution on for both scenarios (Figures. 6.8 164 and 6.9 165) and the optimal set of design parameters presents an elastic optimised wing with a negative twist for the five control sections and a negative camber at the exception of the mid-span section. The elastic optimum design shows a optimised configuration slightly loaded in the region between 50% to 72% of the span. The loading decrease in the regio and unloaded between the wing and the wing crank.

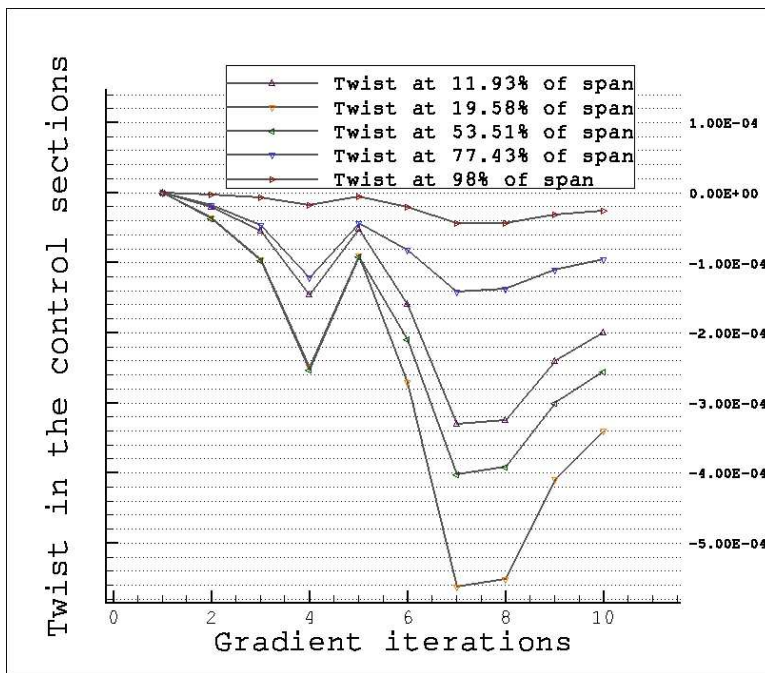


Figure 6.6: Twist angle on the control sections of the optimal elastic configuration

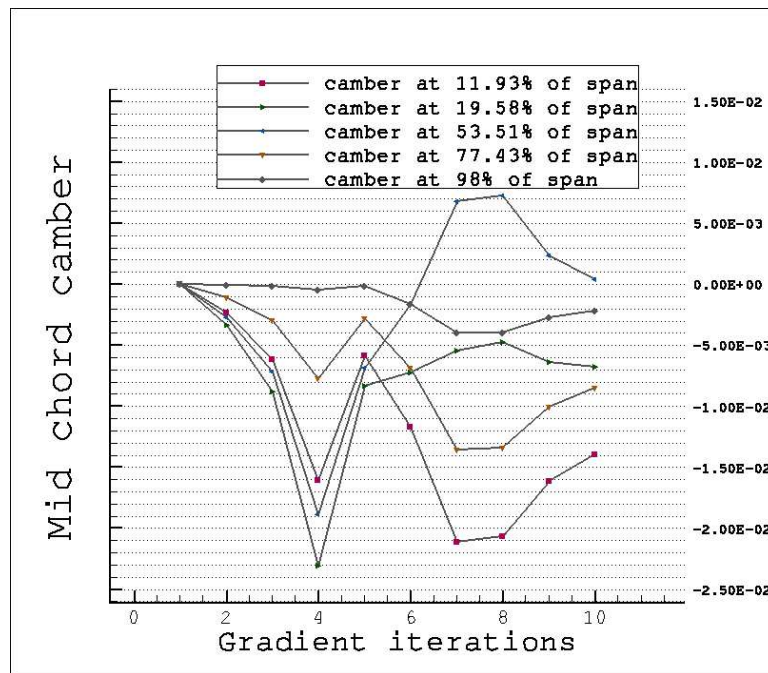


Figure 6.7: Mid-chord camber of control sections of the optimal elastic configuration

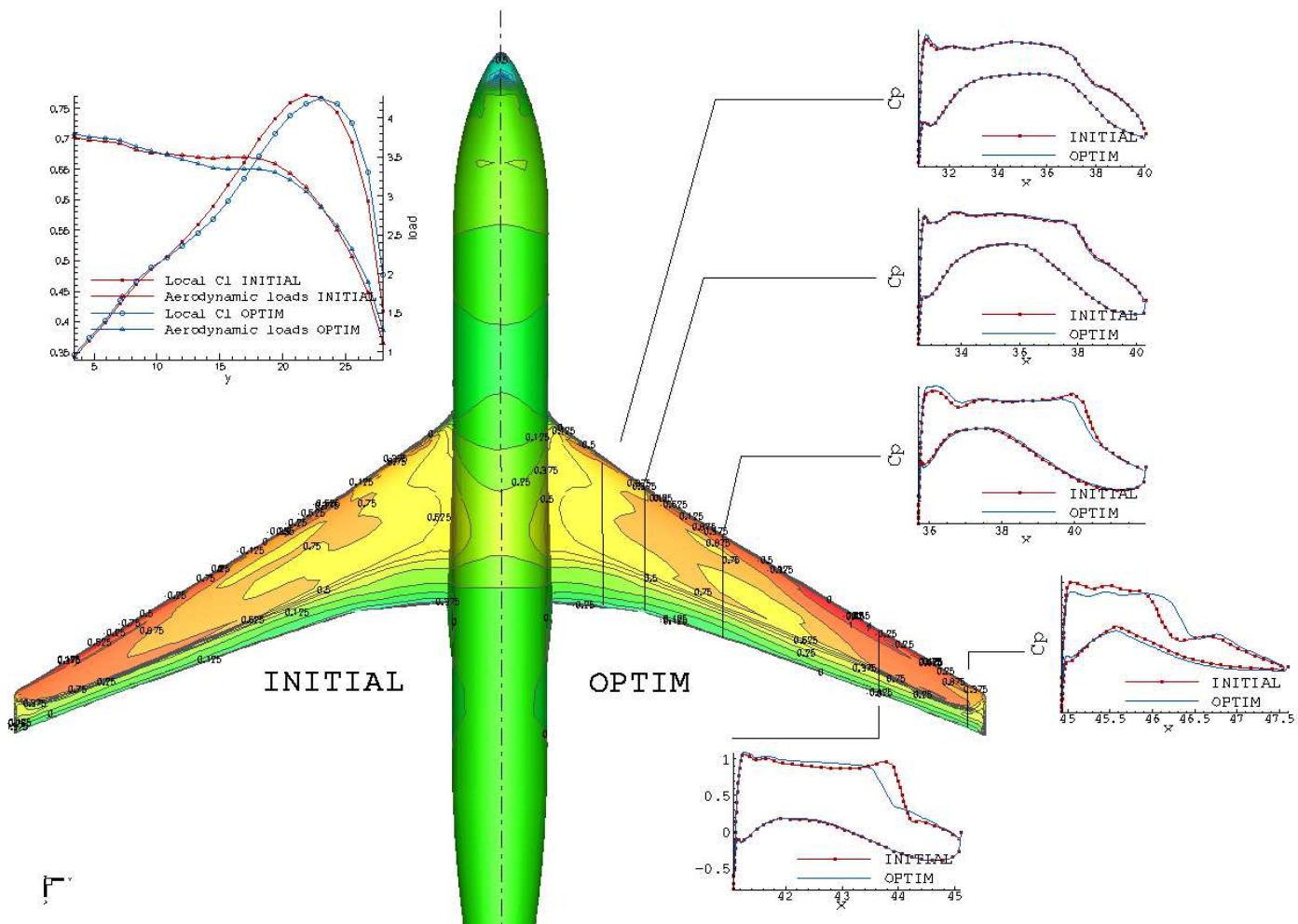


Figure 6.8: Summary of C_{D_p} aerodynamic optimization, performed with DOT algorithm. Parametrization with 5 control twist section, 5 camber sections and the angle of attack

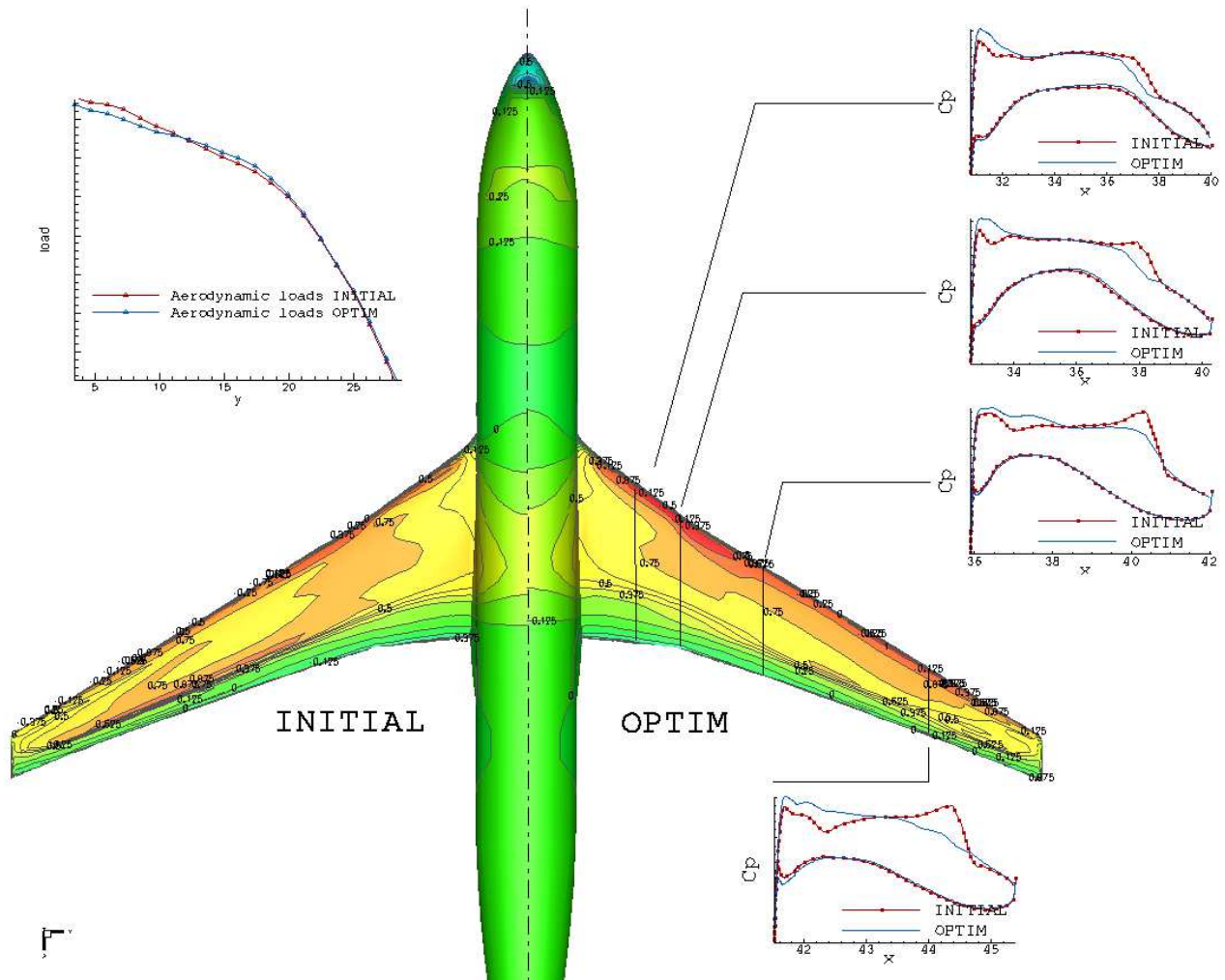


Figure 6.9: Summary of C_{Dp} aero-elastic optimization, performed with DOT algorithm. Parametrization with 5 control twist section, 5 camber sections and the angle of attack

6.7 Aero-structural adjoint gradients

The computation of the aero-structural adjoint-based gradient requires the intervention of several software components. All these elements are embedded into a python framework (Fig 6.10, 167). The steps performed to obtain the final gradient may be summarized as follows:

- produce the *jig-shape* CFD mesh of the configuration;
- compute, on the *jig-shape*, the sensitivities of the metric w.r.t. the design variables;
- compute the structural model of the wing and its characteristics (this stage may require a sizing step if no aero-structural optimization process is performed);
- solve the coupled flow equations and compute the aero-elastic equilibrium;
- supply the adjoint solver of *elsA* with the necessary terms computed by InAirSsi;
- solve the aero-structural adjoint problem at the aero-elastic equilibrium of the wing.

6.7.1 Aero-structural gradient validation

This section validates the gradients computed by the aero-structural via a comparison with finite differences gradient. The adjoint method is of course independent of the number of parameters and one may access to hundreds of gradient componenets, however we present the validation only on a selection of parameters: seven aerodynamic shape parameters (α_{geom}) and 10 structural parameters (α_{struct}). The only reason to this restriction is the, often, necessary step convergence of finite differences. In particular, the FD step is dependant not only on the nature of the parameter but also on the nature and the behaviour of the function as we will present in table 6.11.

6.7.2 Remarks on difficulties linked to finite difference step convergence

During the validation of the gradient, it was necessary to perform a step convergence for each of the parameter and at least for one of the two evaluated function (C_{l_p} , C_{D_p}).

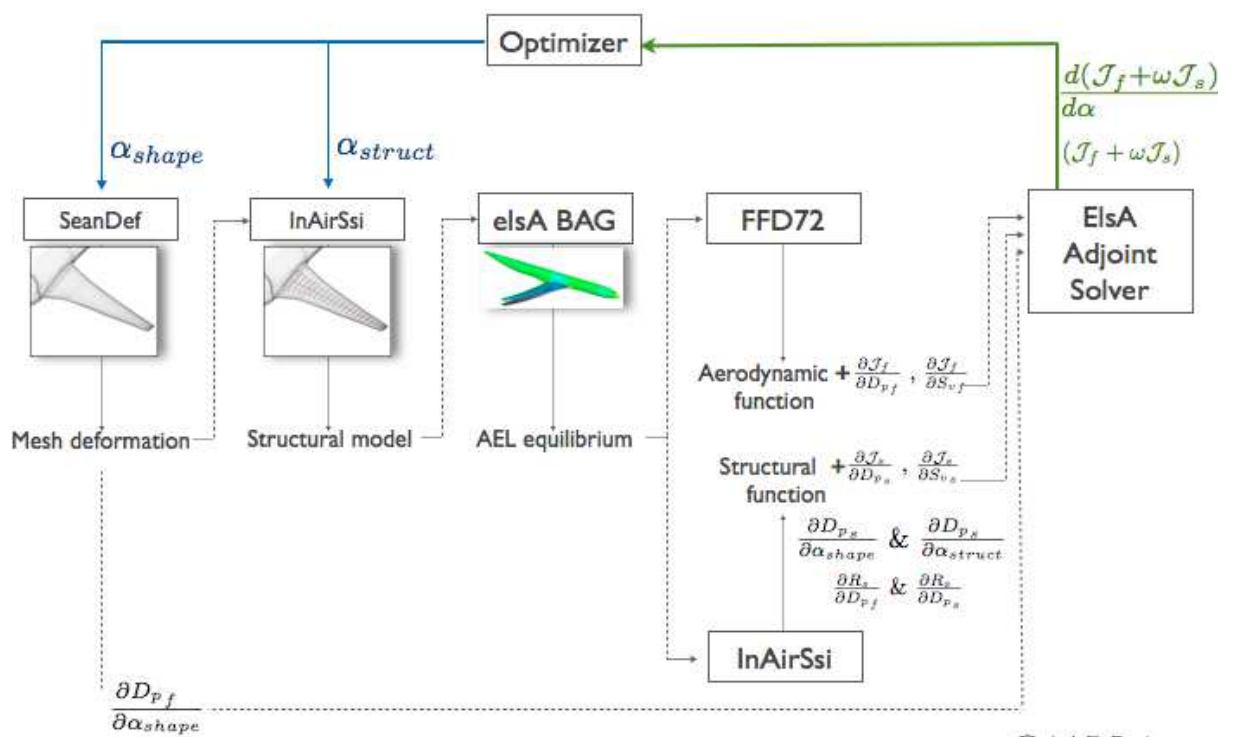


Figure 6.10: aero-structural adjoint-based gradient computation process

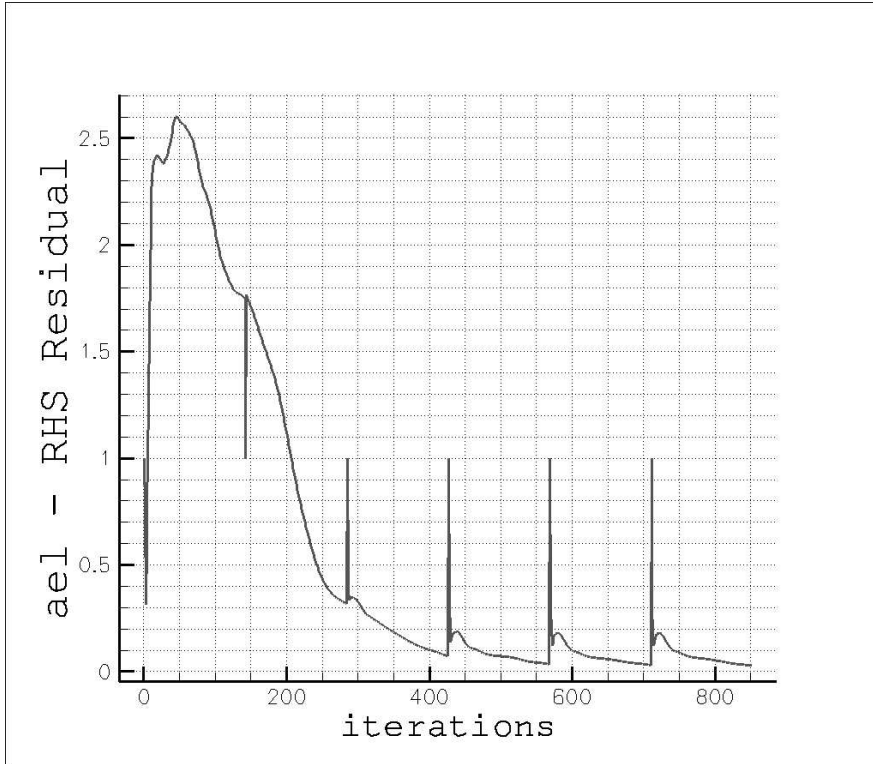


Figure 6.11: Convergence of the norm L_2 of the residual of first equation of the system 3.44 p. 64 (aero-elastic adjoint)

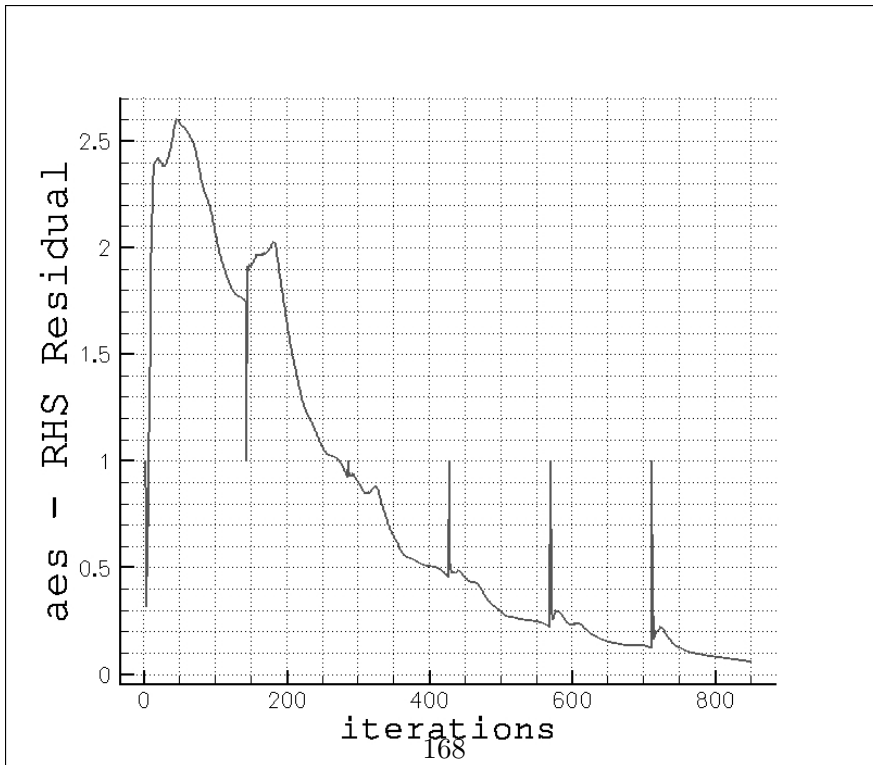


Figure 6.12: Convergence of the norm L_2 of the residual of first equation of the system 5.40 p. 129 (aero-structural adjoint)

α_{geom}	Aero-structural adjoint		Finite Differences		Relative error	
	$\frac{dCl_p}{d\alpha_i}$	$\frac{dCd_p}{d\alpha_i}$	$\frac{dCl_p}{d\alpha_i}$	$\frac{dCd_p}{d\alpha_i}$	$\frac{dCl_p}{d\alpha_i}$	$\frac{dCd_p}{d\alpha_i}$
α_{twist_1}	2.21e-02	1.17e-03	2.21e-02	1.12e-03	0.0%	4.0%
α_{twist_2}	3.49e-02	1.80e-03	3.52e-02	1.69e-03	0.8%	6.5%
α_{twist_3}	3.99e-02	2.05e-03	4.02e-02	1.71e-03	0.7%	19%
$\alpha_{thickness_1}$	7.76e-02	4.20e-03	7.76e-02	4.77e-03	0.0%	11%
$\alpha_{thickness_2}$	2.05e-01	8.77e-03	2.06e-01	1.12e-02	0.4%	21%
$\alpha_{thickness_3}$	2.60e-01	1.23e-02	2.59e-01	1.37e-02	0.3%	10%
t_{slow} at 16.6% span	7.12e-02	-7.28e-05	6.89e-02	requires a step con- vergence (r.s.c)	3.3%	-
$t_{c_{low}}$ at 16.6% span	7.13e-02	-8.00e-05	6.89e-02	r.s.c	3.4%	-
$t_{s_{upp}}$ at 20.9% span	6.12e-02	-1.71e-04	6.05e-02	r.s.c	1.1%	-
t_{f_s} at 20.9% span	-4.671e-02	-3.39e-03	-4.00e-02	r.s.c	16%	-
$t_{c_{upp}}$ at 28.1% span	1.20e-01	1.63e-04	1.18e-01	1.87e-04	0.1%	12%
$t_{s_{upp}}$ at 34.7% span	3.12e-01	1.52e-03	3.04e-01	r.s.c	2.6%	-
t_{r_s} at 52.1% span	1.07e-01	2.24e-03	6.0e-02	r.s.c	78%	-
$t_{s_{upp}}$ at 75.2% span	1.88e-01	3.18e-03	1.67e-01	r.s.c	12.5%	-
$t_{c_{upp}}$ at 75.2% span	1.19e-01	6.60e-04	1.6e-01	r.s.c	25%	-
t_{f_s} at 98% span	5.9e-02	-8.61e-04	1.00e-01	r.s.c	41%	-

Table 6.11: C_{l_p} and C_{D_p} gradient computation: **aero-structural** adjoint and FD

	$\frac{dCl_p}{d\alpha_i}$: Aes adjoint	$\frac{dCl_p}{d\alpha_i}$: FD					
Step	-	1.e-05	5.e-05	1.e-06	1.e-07	1.e-08	1.e-09
$t_{c_{upp}}$ 28.1%	1.20e-01	1.18e-01	1.16e-01	1.25e-01	1.00e-01	0	0

Table 6.12: FD step convergence for $\frac{dCl_p}{d\alpha_i}$ computation

	$\frac{dC_{D_p}}{d\alpha_i}$: Aes adjoint	$\frac{dC_{D_p}}{d\alpha_i}$: FD					
Step	-	5.e-05	1.e-06	1.e-07	1.e-08	5.e-09	1.e-09
$t_{c_{upp}}$ 28.1%	1.63e-04	4.50e-03	4.77e-03	3.03e-04	2.39e-04	1.87e-04	1.14e-04

Table 6.13: FD step convergence for $\frac{dC_{D_p}}{d\alpha_i}$ computation

We present in tables 6.13 p. 170 and 6.12 p. 170 the convergence step of the sensitivity to the perturbations of the upper cap thickness located at 28.1% of the span. While the step giving the lift coefficient sensitivity with good accuracy is rapidly evaluated, the one for the pressure drag evaluation is not straightforward.

6.7.3 Aero-structural gradient vs aero-elastic gradient

In this section we present a comparison of the gradient computed with the aero-elastic adjoint method and the aero-structural adjoint method. This comparison can only be meaningful on aerodynamic shape parameters, since without a structural model, the aero-elastic adjoint cannot compute the sensitivity of a cost function to the modifications of internal structural thicknesses.

For this comparison, we select two types of parameters: three twist control sections and three airfoil thickness control sections. The control sections are located at 19.09%, 26.16% and 52.43% of the span.

As said previously the gradients of the lift coefficient is rapidly aligned with the value given by the 2nd order finite differences. For example, the perturbation applied to obtain the gradient with respect to thickness is 1% of the local thickness. This value was ideal to give a perfect match for the lift gradient while it results in a relative error up to 21% in the pressure drag gradient. In fact the post-processing of the computation used

α_{geom}	Aero-structural adjoint		Aero-elastic adjoint	
s	$\frac{dC_L}{d\alpha_i}$	$\frac{dCdp}{d\alpha_i}$	$\frac{dClp}{d\alpha_i}$	$\frac{dCdp}{d\alpha_i}$
α_{twist_1}	2.21e-02	1.17e-03	2.45e-02	1.15e-03
α_{twist_2}	3.49e-02	1.80e-03	3.95e-02	1.75e-03
α_{twist_3}	3.99e-02	2.05e-03	5.23e-02	1.95e-03
$\alpha_{thickness_1}$	7.76e-02	4.20e-03	6.31e-02	4.26e-03
$\alpha_{thickness_2}$	2.05e-01	8.77e-03	1.36e-01	8.66e-03
$\alpha_{thickness_3}$	2.60e-01	1.23e-02	1.93e-01	1.19e-02

Table 6.14: Comparison of aero-elastic adjoint-based gradient and aero-structural adjoint-based gradient

α_{geom}	Aero-elastic adjoint		Finite Differences		Relative error	
	$\frac{dClp}{d\alpha_i}$	$\frac{dCdp}{d\alpha_i}$	$\frac{dClp}{d\alpha_i}$	$\frac{dCdp}{d\alpha_i}$	$\frac{dClp}{d\alpha_i}$	$\frac{dCdp}{d\alpha_i}$
α_{twist_1}	2.45e-02	1.15e-03	2.21e-02	1.11e-03	10%	3.06 %
α_{twist_2}	3.95e-02	1.75e-03	3.52e-02	1.70e-03	12%	2.9%
α_{twist_3}	5.23e-02	1.95e-03	4.08e-02	1.73e-03	28%	12%
$\alpha_{thickness_1}$	6.31e-02	4.26e-03	5.50e-02	3.92e-03	15%	8.6%
$\alpha_{thickness_2}$	1.36e-01	8.66e-03	1.13e-01	7.91e-03	20%	9.4%
$\alpha_{thickness_3}$	1.93e-01	1.19e-02	1.15e-01	9.40e-03	67%	26%

Table 6.15: Comparison of **aero-elastic** adjoint-based gradient and finite difference with a fixed structural model (to match the aero-elastic hypothesis)

for FD, shows that a perturbation of 1% of the local thickness is enough to produce an increase of 3 d.c. which is too large to give accurate FD gradients. Indeed, the thickness increase at a control section is propagated toward the tip and the wing root where it is dumped and even if this value is small, it is enough to increase both wave and induced drag. A new step convergence study would then be mandatory to evaluate the gradient of the pressure drag. For these reasons, it has been decided to concentrate on $\frac{dC_L}{d\alpha_i}$. We performed two 2nd order finite differences computations. The first one to be compared with the aero-structural adjoint-based gradient and the other one to be compared with the aero-elastic adjoint-based gradient. For the first one, a different structural model is generated for the different values of thickness perturbation and for the second the same structural mesh and characteristics are used. Each type of FD is then consistent with the hypothesis of the adjoint method to be compared with.

Table 6.14 confronts the aero-elastic and the aero-structural gradients. The parameter for which the aero-structural adjoint presents the larger differences (justifying the aero-structural adjoint) on the aero-elastic adjoint concerns the parameters that impact the most the structural behaviour, i.e. airfoil thickness. If the aero-structural adjoint-based lift sensitivity w.r.t. thickness presents a perfect match with the FD (less than 0.4)% , aero-elastic FD gradients (with identical step) present differences from 15% to 67%. In addition, the impact of thickness modification on lift coefficient is underestimated when aero-elastic adjoint method is used.

6.8 Outcome

This section presented a sensitivity analysis on the 3D test case XRF1 with the three adjoint formulations available in the CFD software *elsA*:

the aerodynamic adjoint;

the aero-elastic adjoint;

and the aero-structural adjoint;

The contributions of this work is the development of the aero-structural adjoint approach which introduces flexibility effects through sensitivity analysis. The terms that

reflect those effects are, mainly, computed via the structural module presented in chapter 4 p. 69. The aero-structural adjoint-based gradients are compared to those obtained by finite difference. We say compared and not validated, because it turned out that sometimes establishing a reference value of the gradient by FD is hardly possible and a step convergence was necessary depending on the nature of the parameters and the cost function. All that indicating in certain cases the gradient computed by the aero-structural adjoint method as a reference point...!

In the first section of this chapter, the aerodynamic adjoint and the aero-elastic adjoint were validated on the test case XRF1, and an application to aerodynamic design of both rigid wing and elastic wing were presented and compared. The common design space for these optimisations was of dimension 11, and thus of course did not exploit the full potential of the dual formulation from which the adjoint is derived and which relaxes the dependency on the design space dimension. But, it is well known that the optimisation do not depend only on the way the function or their gradient are computed but also on the way the exploration algorithm deals with high dimensional design spaces. Gradient algorithms represent by themselves a separate subject in the optimization (if not the most important...). However, this parametrisation is enough to show that a significant difference can be achieved when flexibility effect are included. What we want to highlight with this difference is not much the obtained results in terms of drag reduction, because having a good gradient does not meant obtaining a zero-drag flying configuration but converging toward the correct physical interpretation and thus providing explanations whether or not drag performances are increased.

The confrontation of rigid (flight shape) and elastic wing optimizations proved that the same parametrisation (twist + airfoil shapes) leads to different results, because the cost function(s) and/or the constraint function(s) do not have the same sensitivity response with or without flexibility effects. From this point we see that the introduction of aero-structural effects will bring even more physical interpretation to the gradients and to the optimisation process. This was shown, for example, through the gradient computation of the thickness parameter with the aero-elastic adjoint and the aero-structural adjoint. The latter understates the impact on the aerodynamic functions, and if in

preliminary design stages we are not aiming at evaluating the absolute performance, the sensitivity analysis necessary for a preliminary design stage must be as physically-accurate as possible.

Finally the validated aero-structural gradient set the stage for near future aero-structural optimisation or structural sizing with flexible load cases.

7

Conclusion and perspectives

Through this work, the aero-elastic adjoint, available in the ONERA CFD software *elsA*, was extended to an aero-structural adjoint method.

The aero-elastic adjoint was developed, at ONERA, by Marcelet (59). Her work has enabled the access to the sensitivities of aerodynamic functions with respect to (w.r.t.) aerodynamic shape parameter, for the wing in aero-elastic equilibrium with a frozen structural model. Marcelet forecasts that *[...it can be interesting to take into account the effect of planform parameter modifications on structural characteristics...]* and that *[...structural functions gradients could be considered...]*.

These perspectives are part of the capabilities of the aero-structural adjoint. Indeed, it is now possible through the developments achieved in this work to access the sensitivity of both aerodynamic and structural functions w.r.t. changes of the aerodynamic shape or w.r.t. a change of the internal structural geometry.

To achieve these targets the first step was to enable the calculation of structural characteristics and their sensitivities to evaluate their impact on cost functions of the aero-structural optimization problem. For that, a dedicated wing structural model InAirSsi has been developed. It allows the computation of structural functions: structural weight and material constraints. Indeed, via the development of the aero-structural adjoint, the target is to perform aero-structural optimizations.

The modelling of the aero-elastic behaviour of the wing, as it was already available at

the beginning of this work, lays on a Euler-Bernoulli beam theory for the structural modelling. The displacements of the structural model nodes are then computed by considering the aerodynamic flexural and torsional loads under the hypothesis dictated by the beam type as it is explained in chapter 4 p. 69. The structural mesh has to be available to perform the aero-elastic coupling and the aero-elastic adjoint solution. Without the availability of a structural model, this process requires the call of high-fidelity tools to derive the equivalent beam model mesh on which the aerodynamic loads are extracted and structural displacements computed. The first step of this work has been to develop a fully linearised structural module. This module (InAirSsi) constructs the structural model of the wing by fitting into the aerodynamic envelope, extracted from the surface CFD mesh, the wing primary structure built upon 4 structural components (2 spars, upper and lower skin) and 8 degrees of freedom (6 for thicknesses and 2 for positions cf. 4 p. 69). The first type of InAirSsi outputs are those necessary to compute the aero-elastic equilibrium, namely the structural mesh and the spanwise distribution of bending and torsion stiffnesses. These stiffnesses are necessary to calculate the flexibility matrix that explicitly relates the aerodynamic loads and the structural displacements. The second type of InAirSsi outputs are the sensitivity terms developed in section 5.2 p. 116. These terms depends on both the nature of the cost function (aerodynamic or structural) and on the nature of the design parameters (aerodynamic shape parameters or internal structural parameters).

Based on the structural outputs of this module InAirSsi and on the developments made in the *elsA* code, the gradients can be computed via the aero-structural adjoint. These gradients have been compared with Finite Differences-based gradients. It is also important to note that these developments do not depend on the flow equations used in the flow solver. The aero-structural adjoint extension remains valid for both inviscid and viscous flows, although it has been validated and applied only to inviscid flow for the sake of simplicity in this work.

This work aims at adding more physical meaning into the computation of the cost function gradients, however when it comes to modelling the physics, thinking of enhancement and improvement is self-evident. This is what we name *degree of fidelity*.

Yet, it is still important to define the framework of application and analyse how the hypothesis may affect the results and the interpretation or help in reducing the cost of analysis. The real focus of this work being on proposing methods to deal with the intrinsically multidisciplinary nature of wing design, the modelling of each discipline could be improved to be applied in more advanced design stages -one day, when numerical optimization will be applied in early design stages- thus one may think that the structural behaviour must be upgraded and elevated to the state of the art fidelity available for the analysis through: structural degrees of freedom, diversification of material and thus of structural behaviour, sizing criteria, etc...For the aerodynamic modelling, the most important challenge -ongoing at ONERA- is related to the improvement of the RaNS adjoint system solution.

The adjoint formulation has presented challenges since almost 40 years now. More than four decades have passed since the first adjoint formulation for aerodynamic problems and still difficulties to penetrate “real world”. If numerous teams, in the optimization community still work actively on this subject, it is because of the unquestionable potential such technique presents.

The applicability of high-fidelity optimization in the industrial conceptual design process is of course linked to its computational cost. However if we note that today a full aircraft configuration can be analysed in a matter of minutes -using approximately 128 cores- we will be able to do this in seconds 10 years from now. But this gain will only be beneficial to aircraft design innovation if the increase of computational capability is accompanied by development within aero-structural optimization framework and conceptual design tools.

When numerical optimization techniques will penetrate intensively the industrial world (one day!) then, the high potential of the adjoint is that it can be exploited by partisans of both local and global algorithms. For the *unconverted* -to numerical optimization- it presents a cost-effective and information-valuable sensitivity analysis (yet multidisciplinary).

Appendix A

For the users of *elsA* BAG: module modifications

This appendix describes the modification incorporated into the module Bag (Beam Aeroelastic gradient) created to manage the fluid/structure interactions through a beam model.

The module Bag computes the aerodynamic loads that will be transferred to the structure, it is also in charge of the CFD volume mesh deformation according to structural displacements. *elsA*/Bag contains three directories : Descp, Deform and Sio

***elsA*/Bag/Deform**

The deformation of the CFD volumic mesh is piloted by two C++ classes defined in this directory: -DeformationAxis -BlkTwistbendDeformator -MeshDeform

The structural displacements computed by the external python class "Beam" are transferred to the object described by the C++ class DeformationAxis.

The C++ class BlkTwistbendDeformator supervises the deformation process. The C++ class interferes when $\frac{dR_f}{dx}$ is computed by finite difference.

***elsA*/Bag/Sio**

This directory contains the class SioBeamLoads in charge of aerodynamic load transfer

elsA/Bag/Descp

This directory make possible the access to the C++ classes of elsA/Bag/Deform and elsA/Bag/Sio directly through the python script that drive the aeroelastic computation. It contains the descriptor objects of the C++ classes contained in elsA/Bag/Deform and elsA/Bag/Sio:

- DesDeformationAxis, descriptor of DeformationAxis
- DesBlkTwistbendDeformator, descriptor of BlkTwistbendDeformator
- DesSioBeamLoads, descriptor of SioBeamLoads

```
# *****
# *****
# *****

#-----
#InAirSsi
#-----
inairssi.readInputFile("InAirSsi.in", "./INAIRSSI/" )
inairssi.BuildWingBox(0,"linear", "./ADJCOMPUTATION/", "./MAIL-JIG/" )
# 0 => Beam nodes are different from control section
inairssi.ComputeBeam("WBox") #full=WB+LE+TE , WBox
inairssi.ComputeStructParam("WBox") #full=WB+LE+TE , WBox
inairssi.ComputeSensStructParam("WBox") #full=WB+LE+TE , WBox
inairssi.WriteModel()
if couplingType=="aerostructural":
    dIdgeom=inairssi.ComputedXbdXsurfdalpha()[0]
    dJdgeom=inairssi.ComputedXbdXsurfdalpha()[1]
    dIdstruct=inairssi.ComputedXbdXsurfdalpha()[2]
    dJdstruct=inairssi.ComputedXbdXsurfdalpha()[3]

# Initialisation du DesShapeOpt:
# -----
```

```

eqadj.submit()

# initialisation:
# -----
beam.setNbFunctions(3)
beam.setNbAlphas(4,2) # Nbgeom , Nbstruct
beam.initLambdaS()
beamloads.initFlexMatTransposLambdaS(3)
deform.createTwistAndBendRhs(3)

if couplingType=="aeroelastic":
    beamloads.initdEdXrigdAlpha(0,0) #Nbgeom , Nbstruct

if couplingType=="aerostructural":
    beamloads.initdEdXrigdAlpha(4,2)
    beamloads.initdEdXbdAlpha(4,2) #Nbgeom , Nbstruct

deform.setBeamInfoToOpt()
beam.computedDefAxisdBeam(defaxis)

loads = beamloads.extract_Fld(0)
beam.applyLoading(loads)

# Boucle de resolution du systeme lineaire:
# -----
nCIter =5

for iii in (range(nCIter)):

    print "*****"

```

```

print "Iterative Resolution of the Coupled Adjoint Discrete Equations"
print " ----- iteration number " + repr(iii+1)
print"*****"

if (iii==0):
    eqadj.compute_Aeroelast(1,0) # isFirstIteration, isLastIteration
    deform.computeRhsToBeam(1) # isFirstIteration
elif (iii==nCIter-1):
    eqadj.compute_Aeroelast(0,1) # isFirstIteration, isLastIteration
    #Pb.extract()
else:
    eqadj.compute_Aeroelast(0,0) # isFirstIteration, isLastIteration
    deform.computeRhsToBeam(0) # isFirstIteration

if (iii != nCIter-1):

    twistRHS = deform.returnTwistRhs()
    bendRHS = deform.returnBendRhs()
    beam.applydDefAxisTransposRHS(twistRHS, bendRHS, defaxis)

    dRdTwiSt = deform.computedRdTwiStLambdaA()
    dRdBend = deform.computedRdBendLambdaA()

    beam.applydRdDefAxisTransposLambdaA(dRdTwiSt,dRdBend,defaxis)

    beam.computeLambdaS(defaxis)
    beam.computeFlexMatTransposLambdaS(beamloads)

    beamloads.createAndSetListdEdFTransposRhs(0)
# choixMaillage (0=flexible, 1=rigide)
    beamloads.createAndSetListdEdXTransposRhs(0)
# choixMaillage (0=flexible, 1=rigide)

```

```

# assemblage du gradient:
if (iii==nCIter-2):

    if couplingType=="aeroelastic":
        deform.computeAndsetdnewMeshdXrigdAlpha(4)
        beamloads.computedEdXrigdAlpha(0)
        dFzdXrigda = beamloads.returndFflexiondXrigdAlpha()
        dMxdXrigda = beamloads.returndMflexiondXrigdAlpha()
        dMydXrigda = beamloads.returndMtorsiondXrigdAlpha()
        loadPts = beamloads.returnLoadPts()
        beam.applydEdXrigdAlpha(loadPts, dFzdXrigda, dMxdXrigda, dMydXrigda)
        eqadj.createBeamGradFunc()
        beam.computeAndSetBeamGradFunc(eqadj ,0)
        # 0=aeroelastic 1=aerostructural

    elif couplingType=="aerostructural":
        deform.computeAndsetdXdAlpha(4,2,23)
        #alphageom, alphastruct, discretization

        beamloads.computedEdXrigdXbdAlpha(0)
        # choice of Mesh (0=flexible, 1=jig)

        beamloads.computedEdXbeamdAlpha(0)
        # choice of Mesh (0=flexible, 1=jig)

        dFzdXdXbda = beamloads.returndFflexiondXrigdXbdAlpha()
        dMxdXdXbda = beamloads.returndMflexiondXrigdXbdAlpha()
        dMydXdXbda = beamloads.returndMtorsiondXrigdXbdAlpha()

        dFzdXbda = beamloads.returndFflexiondXbdAlpha()
        dMxdXbda = beamloads.returndMflexiondXbdAlpha()
        dMydXbda = beamloads.returndMtorsiondXbdAlpha()

```

```

loadPts = beamloads.returnLoadPts()

beam.applydEdXrigdXbdAlpha(loadPts,dFzdXdbda,dMxdXdbda,dMydXdbda)

beam.applydEdXbdAlpha(loadPts, dFzdXbda, dMxdXbda, dMydXbda)

eqadj.createBeamGradFunc()

beam.computedFlexdIJdIJdalpha(dIIdgeom,dJdgeom,dIdstruct,dJdstruct)
beam.computeAndSetBeamGradFunc(eqadj ,1)
# 0=aeroelastic 1=aerostructural

# *****
# *****
# *****

```

computeAndsetdXdAlpha

Replace computeAndsetdnewMeshdXrigdAlpha when the aerostructural adjoint is called. This routine is defined in the class BlkTwistBendDeformator (*elsA/Bag/Deform/*) and it is accessible via the descriptor Desdeformator (*elsA/Bag/Descp/*).

The computed term depends on the nature of the design variable, the first argument is the number of aerodynamic design variables, the second one is the number of the structural design parameters and the last argument is the number of displacement nodes.

When the design variable $\in \alpha_{geom}$, the returned value is

$$\left(\frac{\partial \mathcal{X}}{\partial \mathcal{X}_{rig}} \frac{d\mathcal{X}_{rig}}{d\alpha_{geom}} + \frac{\partial \mathcal{X}}{\partial \mathcal{X}_b} \frac{\partial \mathcal{X}_b}{\partial \mathcal{X}_{surf}} \frac{d\mathcal{X}_{surf}}{d\alpha_{geom}} \right)$$

When the design variable is $\in \alpha_{struct}$, the returned value is

$$\frac{\partial \mathcal{X}}{\partial \mathcal{X}_b} \frac{d\mathcal{X}_b}{d\alpha_{struct}}$$

computedEdXrigdXbdAlpha

This routine is accessible via the descriptor *Desdeformator* (*elsA/Bag/Descp/*) and it is defined in *BlkTwistBendDeformator* (*elsA/Bag/Deform/*), it supervises the computation of

$$\frac{\partial L}{\partial \mathcal{X}} \left(\frac{\partial \mathcal{X}}{\partial \mathcal{X}_{rig}} \frac{d\mathcal{X}_{rig}}{d\alpha_{geom}} + \frac{\partial \mathcal{X}}{\partial \mathcal{X}_b} \frac{\partial \mathcal{X}_b}{\partial \mathcal{X}_{surf}} \frac{d\mathcal{X}_{surf}}{d\alpha_{geom}} \right) + \frac{\partial L}{\partial W^b} \frac{\partial W^b}{\partial \mathcal{X}} \left(\frac{\partial \mathcal{X}}{\partial \mathcal{X}_{rig}} \frac{d\mathcal{X}_{rig}}{d\alpha_{geom}} + \frac{\partial \mathcal{X}}{\partial \mathcal{X}_b} \frac{\partial \mathcal{X}_b}{\partial \mathcal{X}_{surf}} \frac{d\mathcal{X}_{surf}}{d\alpha_{geom}} \right)$$

The first term is calculated by the routine *computedEdFdXrigdAlpha* and the second term is computed by *computedFdXdXrigdAlpha*. The difference between the aeroelastic adjoint and the structural adjoint lays on the attribut of the C++ class *elsA/Blk/ComposeBlkBaseBlock: _dNewMeshdXrigdAlpha*.

This term is divided into three parts related to the type of loading transferred to the structure, the force of flexion F_z , the moment of flexion M_x and the moment of torsion M_y , these three part are stored as attributes of the *SioBeamLoads* C++ class (*elsA/Bag/Sio/*)

- *_dFlexiondXrigdXbdAlpha*
- *_dMflexiondXrigdXbdAlpha*
- *_dMtorsiondXrigdXbdAlpha*

This terms are accessible from the *elsA* script via the three routines of the descriptor object *elsA/Bag/Descp/DesSioBeamLoads*:

- *returndFflexiondXrigdXbdAlpha*
- *returndMflexiondXrigdXbdAlpha*
- *returndMtorsiondXrigdXbdAlpha*

computedEdXbeamdAlpha

This routine is accessible via the descriptor *Desdeformator* (*elsA/Bag/Descp/*) and it is defined in *BlkTwistBendDeformator* (*elsA/Bag/Deform/*). It computes the sensitivity of the aerodynamic loads wrt to the design variable (α_{geom} or α_{struct}) through the coordinates of the structural mesh:

$$\frac{\partial L}{\partial X_b} \frac{\partial X_b}{\partial X_{surf}} \frac{dX_{surf}}{d\alpha_{geom}}$$

This term is also divided into three part, each one is of dimension $n_b \times n_\alpha$:

- *_dFflexiondXbdAlpha*
- *_dMflexiondXbdAlpha*
- *_dMtorsiondXbdAlpha*

This terms are accessible from the *elsA* script via the three routines of the descriptor object *elsA/Bag/Descp/DesSioBeamLoads*:

- *returndFflexiondXbdAlpha*
- *returndMflexiondXbdAlpha*
- *returndMtorsiondXbdAlpha*

applydEdXrigdXbdAlpha

This routine, contained in the python class *Beam*, transfers to the *Beam* object the returned attributes of *computedEdXrigdXbdAlpha* :

- *_dFflexiondXrigdXbdAlpha*
- *_dMflexiondXrigdXbdAlpha*
- *_dMtorsiondXrigdXbdAlpha*

applydEdXbdAlpha

The role of this python class *Beam* routine is to transfers to the *Beam* object the returned attributes of *computedEdXbeamAlpha*:

- *.dFlexiondXbdAlpha*
- *.dMflexiondXbdAlpha*
- *.dMtorsiondXbdAlpha*

computedFlexdIJdIJdalpa(dIdgeom,dJdgeom,dIdstruct,dJdstruct)

This routine returns to the python class *Beam* the sensitivity of the structural parameters *I* and *J* with respect to the design variables α_{struct} and α_{geom} computed value of the python class *inairssi*

$$-L \left(\frac{\partial F}{\partial I} \left(\frac{\partial I}{\partial X_b} \frac{\partial X_b}{X_{surf}} + \frac{\partial I}{\partial X_{surf}} \right) \frac{dX_{surf}}{d\alpha_{geom}} + \frac{\partial F}{\partial J} \left(\frac{\partial J}{\partial X_b} \frac{\partial X_b}{\partial X_{surf}} + \frac{\partial J}{\partial X_{surf}} \right) \frac{dX_{surf}}{d\alpha_{geom}} \right)$$

computeAndSetBeamGradFunc

This routine of the *Beam* python class assembles:

$$\lambda_s^T \left(- \frac{dF}{d\alpha_{geom}} L - F \frac{dL}{d\alpha_{geom}} \right)$$

And transferred directly to the *elsA* object of description *elsA/Bag/Descp/DesShapeOpt*

Appendix B

Structural sensitivity with INAIIRSSI

B.0.1 Calculation and validation of $\frac{dChord_{law}}{d\alpha_{geom}}$

Definition:

$\frac{dChord_{law}}{d\alpha_{geom}}$ is the sensitivity of the law chord distribution with respect to α_{geom} .

The chord law depends on three main parameters, the leading edge, the trailing edge and the local thickness to chord ratio. All these parameters are influenced by the parameters that defines the aerodynamic shape and do change if only the structural parameters are modified. This term drives the interpolation the primary structure element thickness between two control section.

At a constant y-span position, the local chord is defined by two x-coordinates. These coordinates are modified when the wing planform is modified (via the

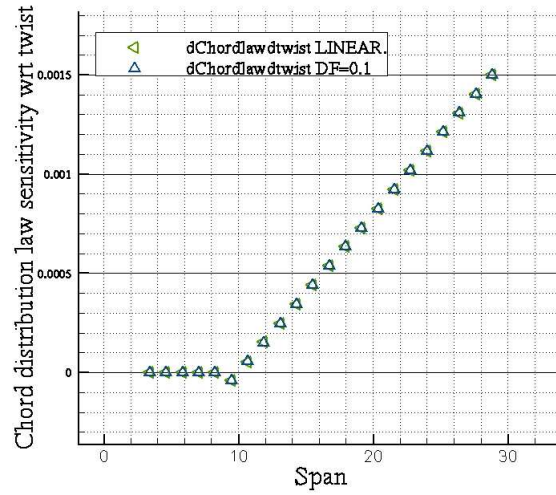


Figure B.1: Sensitivity of chord law with respect to twist

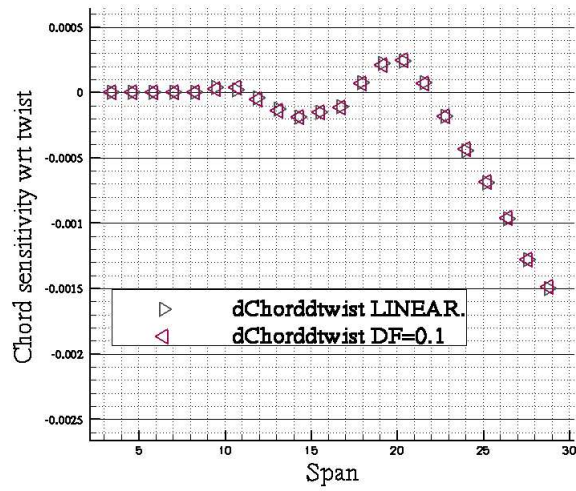


Figure B.2: Sensitivity of the x-coordinates defining the chord law w.r.t twist

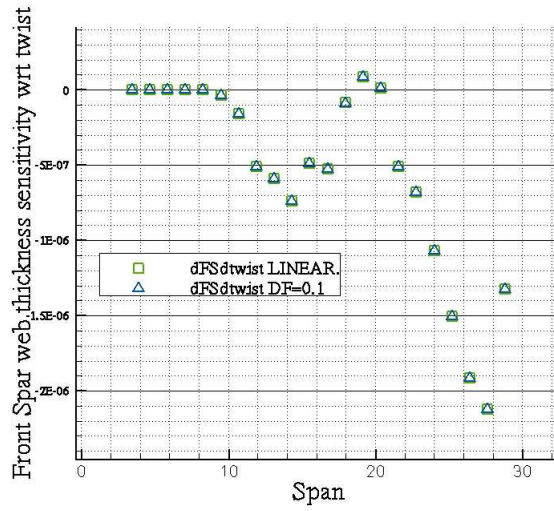


Figure B.3: Sensitivity of the front spar web thickness with respect to twist

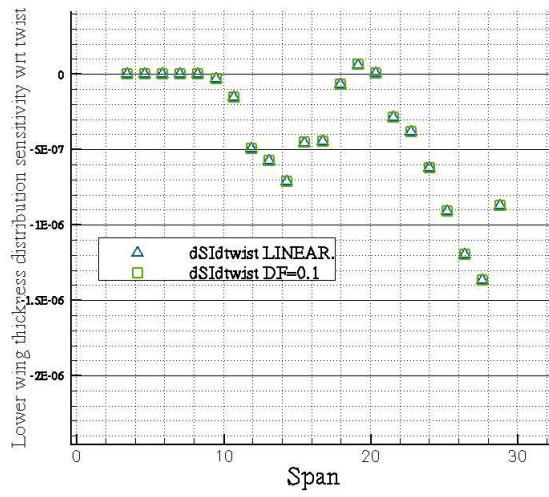


Figure B.4: Sensitivity of lower wing thickness distribution with respect to twist

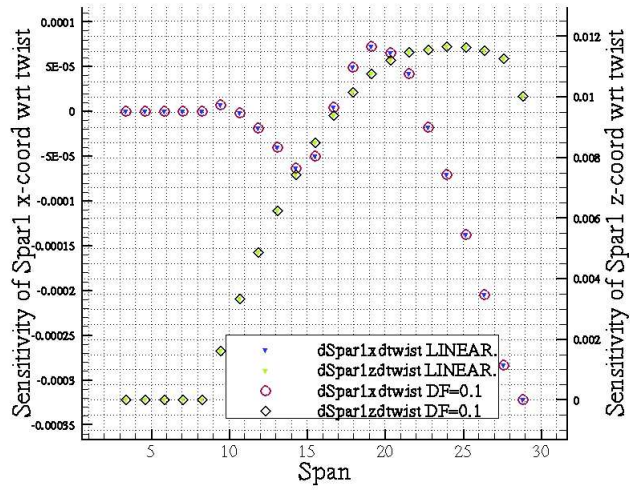


Figure B.5: Sensitivity of first spar x-coordinate with respect to twist

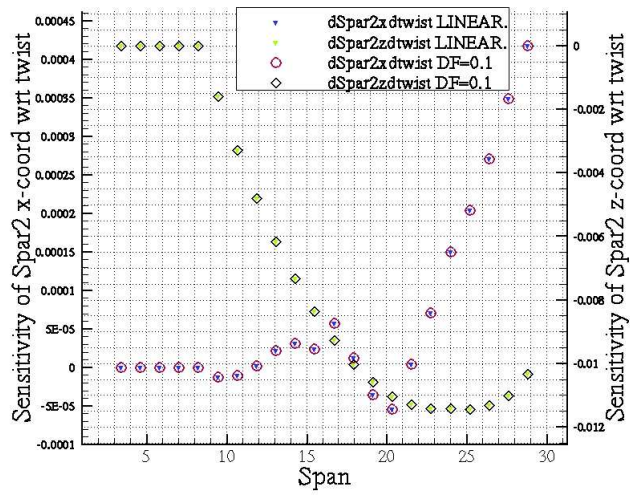


Figure B.6: Sensitivity of second spar x-coordinate with respect to twist

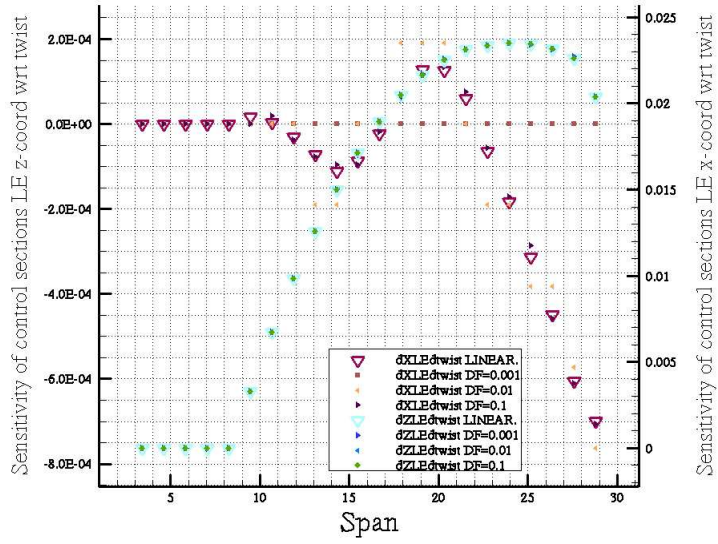


Figure B.7: Sensitivity the leading edge mesh points with respect to twist

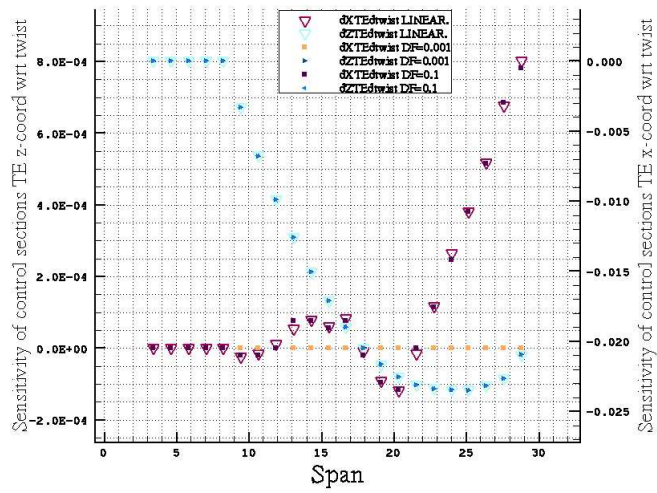


Figure B.8: Sensitivity of the trailing edge mesh points with respect to twist

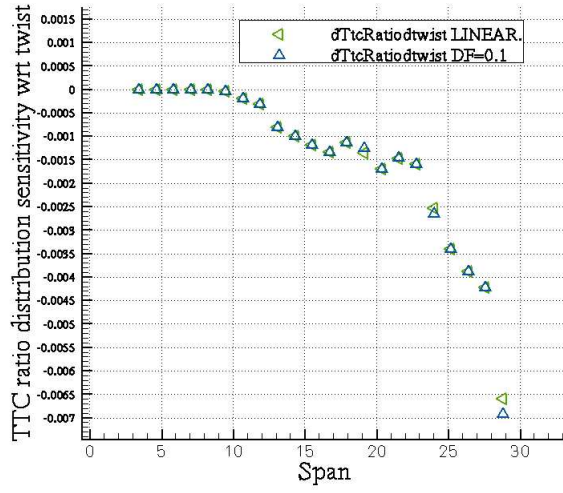


Figure B.9: Sensitivity of thickness to chord ratio with respect to twist

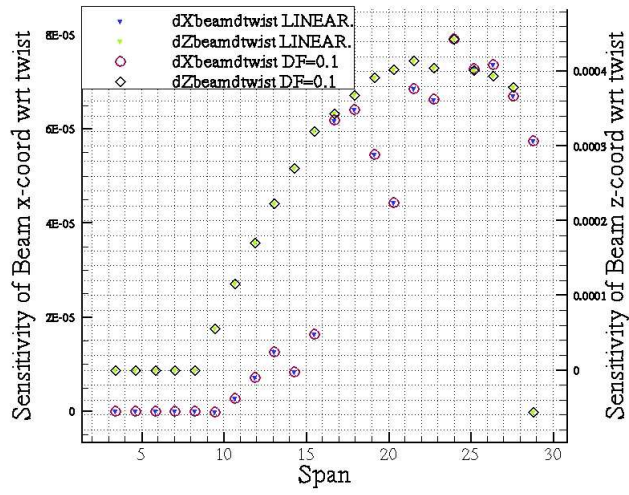


Figure B.10: Sensitivity beam node mesh with respect to twist

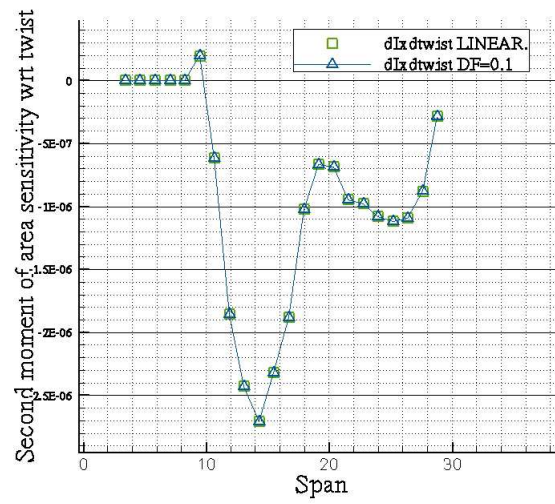


Figure B.11: Sensitivity bending constant w.r.t twist parameter

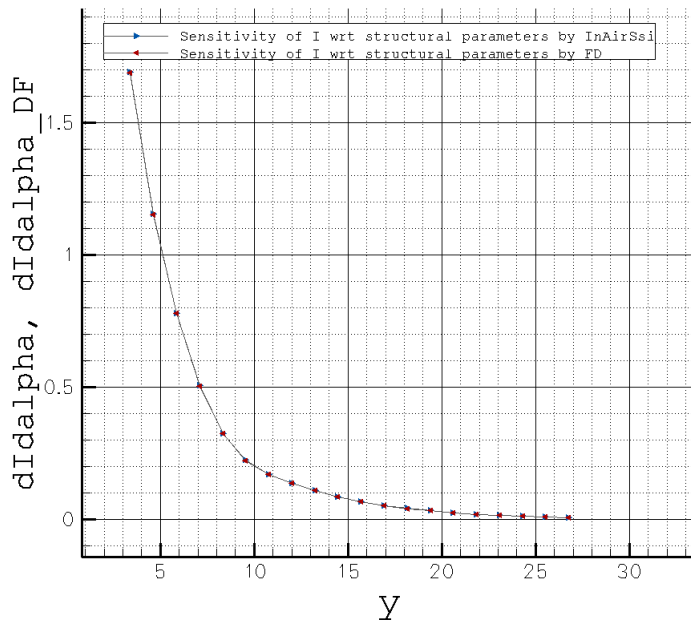


Figure B.12: Gradient of bending stiffness with respect to skin thickness

$$\begin{aligned}
\frac{d\mathcal{J}_{aero}}{d\alpha_{geom}} &= \frac{\partial\mathcal{J}_{aero}}{\partial\mathcal{X}} \left(\frac{\partial\mathcal{X}}{\partial\mathcal{X}_{rig}} \frac{d\mathcal{X}_{rig}}{d\alpha_{geom}} + \frac{\partial\mathcal{X}}{\partial\mathcal{X}_b} \frac{\partial\mathcal{X}_b}{\partial\mathcal{X}_{surf}} \frac{d\mathcal{X}_{surf}}{d\alpha_{geom}} \right) \\
&+ \frac{\partial\mathcal{J}_{aero}}{\partial W^b} \left(\frac{\partial W^b}{\partial X} \left(\frac{\partial\mathcal{X}}{\partial\mathcal{X}_{rig}} \frac{d\mathcal{X}_{rig}}{d\alpha_{geom}} + \frac{\partial\mathcal{X}}{\partial\mathcal{X}_b} \frac{\partial\mathcal{X}_b}{\partial\mathcal{X}_{surf}} \frac{d\mathcal{X}_{surf}}{d\alpha_{geom}} \right) \right) \\
&+ \lambda_f \left(\frac{\partial R_f}{\partial X} \left(\frac{\partial\mathcal{X}}{\partial\mathcal{X}_{rig}} \frac{d\mathcal{X}_{rig}}{d\alpha_{geom}} + \frac{\partial\mathcal{X}}{\partial\mathcal{X}_b} \frac{\partial\mathcal{X}_b}{\partial\mathcal{X}_{surf}} \frac{d\mathcal{X}_{surf}}{d\alpha_{geom}} \right) \right) \\
&+ \lambda_s \left(-F \left(\frac{\partial L}{\partial\mathcal{X}} \left(\frac{\partial\mathcal{X}}{\partial\mathcal{X}_{rig}} \frac{d\mathcal{X}_{rig}}{d\alpha_{geom}} + \frac{\partial\mathcal{X}}{\partial\mathcal{X}_b} \frac{\partial\mathcal{X}_b}{\partial\mathcal{X}_{surf}} \frac{d\mathcal{X}_{surf}}{d\alpha_{geom}} \right) + \frac{\partial L}{\partial\mathcal{X}_b} \frac{\partial\mathcal{X}_b}{\partial\mathcal{X}_{surf}} \frac{d\mathcal{X}_{surf}}{d\alpha_{geom}} \right. \right. \\
&+ \left. \left. \frac{\partial L}{\partial W^b} \frac{\partial W^b}{\partial\mathcal{X}} \left(\frac{\partial\mathcal{X}}{\partial\mathcal{X}_{rig}} \frac{d\mathcal{X}_{rig}}{d\alpha_{geom}} + \frac{\partial\mathcal{X}}{\partial\mathcal{X}_b} \frac{\partial\mathcal{X}_b}{\partial\mathcal{X}_{surf}} \frac{d\mathcal{X}_{surf}}{d\alpha_{geom}} \right) \right) \right) \\
&- L \left(\frac{\partial F}{\partial I} \left(\frac{\partial I}{\partial\mathcal{X}_b} \frac{\partial\mathcal{X}_b}{\mathcal{X}_{surf}} + \frac{\partial I}{\partial\mathcal{X}_{surf}} \right) \frac{d\mathcal{X}_{surf}}{d\alpha_{geom}} + \frac{\partial F}{\partial J} \left(\frac{\partial J}{\partial\mathcal{X}_b} \frac{\partial\mathcal{X}_b}{\partial\mathcal{X}_{surf}} + \frac{\partial J}{\partial\mathcal{X}_{surf}} \right) \frac{d\mathcal{X}_{surf}}{d\alpha_{geom}} \right) \\
&+ \left[\frac{\partial\mathcal{J}_{aero}}{\partial\mathcal{X}} \frac{\partial\mathcal{X}}{\partial D} + \frac{\partial\mathcal{J}_{aero}}{\partial W^b} \frac{\partial W^b}{\partial\mathcal{X}} \frac{\partial\mathcal{X}}{dD} + \lambda_f \frac{\partial R_f}{\partial\mathcal{X}} \frac{\partial\mathcal{X}}{\partial D} \right. \\
&+ \left. \lambda_s \left(I_d - F \left(\frac{\partial L}{\partial\mathcal{X}} \frac{\partial\mathcal{X}}{\partial D} + \frac{\partial L}{\partial W^b} \frac{\partial W^b}{\partial\mathcal{X}} \frac{\partial\mathcal{X}}{\partial D} \right) \right) \right] \frac{dD}{d\alpha_{geom}} \\
&+ \left[\frac{\partial\mathcal{J}_{aero}}{\partial W^b} \frac{\partial W^b}{\partial W} + \frac{\partial\mathcal{J}_{aero}}{\partial W} + \lambda_f \frac{\partial R_f}{\partial W} - \lambda_s F \frac{\partial L}{\partial W^b} \frac{\partial W^b}{\partial W} \right] \frac{dW}{d\alpha_{geom}}
\end{aligned} \tag{B.1}$$

$$\begin{aligned}
\frac{d\mathcal{J}_{aero}}{d\alpha_{struct}} &= \frac{\partial\mathcal{J}_{aero}}{\partial\mathcal{X}} \frac{\partial\mathcal{X}}{\partial\mathcal{X}_b} \frac{d\mathcal{X}_b}{d\alpha_{struct}} \\
&+ \frac{\partial\mathcal{J}_{aero}}{\partial W^b} \frac{\partial W^b}{\partial X} \frac{\partial\mathcal{X}}{\partial\mathcal{X}_b} \frac{d\mathcal{X}_b}{d\alpha_{struct}} + \lambda_f \frac{\partial R_f}{\partial X} \frac{\partial\mathcal{X}}{\partial\mathcal{X}_b} \frac{d\mathcal{X}_b}{d\alpha_{struct}} \\
&+ \lambda_s \left(-F \left(\frac{\partial L}{\partial\mathcal{X}} \frac{\partial\mathcal{X}}{\partial\mathcal{X}_b} \frac{d\mathcal{X}_b}{d\alpha_{struct}} + \frac{\partial L}{\partial\mathcal{X}_b} \frac{d\mathcal{X}_b}{d\alpha_{struct}} + \frac{\partial L}{\partial W^b} \frac{\partial W^b}{\partial X} \frac{\partial\mathcal{X}}{\partial\mathcal{X}_b} \frac{d\mathcal{X}_b}{d\alpha_{struct}} \right) \right. \\
&- L \left(\frac{\partial F}{\partial I} \left(\frac{\partial I}{\partial\mathcal{X}_b} \frac{d\mathcal{X}_b}{d\alpha_{struct}} + \frac{dI}{d\alpha_{struct}} \right) + \frac{\partial F}{\partial J} \left(\frac{\partial J}{\partial\mathcal{X}_b} \frac{d\mathcal{X}_b}{d\alpha_{struct}} + \frac{dJ}{d\alpha_{struct}} \right) \right) \left. \right) \\
&+ \left[\frac{\partial\mathcal{J}_{aero}}{\partial\mathcal{X}} \frac{\partial\mathcal{X}}{\partial D} + \frac{\partial\mathcal{J}_{aero}}{\partial W^b} \frac{\partial W^b}{\partial X} \frac{\partial\mathcal{X}}{\partial D} + \lambda_f \frac{\partial R_f}{\partial X} \frac{\partial\mathcal{X}}{\partial D} \right. \\
&+ \lambda_s \left(I_d - F \left(\frac{\partial L}{\partial\mathcal{X}} \frac{\partial\mathcal{X}}{\partial D} + \frac{\partial L}{\partial W^b} \frac{\partial W^b}{\partial X} \frac{\partial\mathcal{X}}{\partial D} \right) \right) \left. \right] \frac{dD}{d\alpha_{struct}} \\
&+ \left[\frac{\partial\mathcal{J}_{aero}}{\partial W^b} \frac{\partial W^b}{\partial W} + \frac{\partial\mathcal{J}_{aero}}{\partial W} + \lambda_f \frac{\partial R_f}{\partial W} - \lambda_s F \frac{\partial L}{\partial W^b} \frac{\partial W^b}{\partial W} \right] \frac{dW}{d\alpha_{struct}}
\end{aligned} \tag{B.2}$$

$$\begin{aligned}
\frac{d\mathcal{J}_{struct}}{d\alpha_{geom}} &= \frac{\partial\mathcal{J}_{struct}}{\partial\mathcal{X}_{surf}} \frac{\partial\mathcal{X}_{surf}}{\partial\mathcal{X}_{rig}} \frac{d\mathcal{X}_{rig}}{d\alpha_{geom}} + \frac{\partial\mathcal{J}_{struct}}{\partial\mathcal{X}_b} \frac{\partial\mathcal{X}_b}{\partial\mathcal{X}_{rig}} \frac{d\mathcal{X}_{rig}}{d\alpha_{geom}} \\
&+ \lambda_f \left(\frac{\partial R_f}{\partial X} \left(\frac{\partial\mathcal{X}}{\partial\mathcal{X}_{rig}} \frac{d\mathcal{X}_{rig}}{d\alpha_{geom}} + \frac{\partial\mathcal{X}}{\partial\mathcal{X}_b} \frac{\partial\mathcal{X}_b}{\partial\mathcal{X}_{rig}} \frac{d\mathcal{X}_{rig}}{d\alpha_{geom}} \right) \right) \\
&+ \lambda_s \left(-F \left(\frac{\partial L}{\partial\mathcal{X}} \left(\frac{\partial\mathcal{X}}{\partial\mathcal{X}_{rig}} \frac{d\mathcal{X}_{rig}}{d\alpha_{geom}} + \frac{\partial\mathcal{X}}{\partial\mathcal{X}_b} \frac{\partial\mathcal{X}_b}{\partial\mathcal{X}_{rig}} \frac{d\mathcal{X}_{rig}}{d\alpha_{geom}} \right) + \frac{\partial L}{\partial\mathcal{X}_b} \frac{\partial\mathcal{X}_b}{\partial\mathcal{X}_{rig}} \frac{d\mathcal{X}_{rig}}{d\alpha_{geom}} \right) \right. \\
&+ \left. \frac{\partial L}{\partial W^b} \left(\frac{\partial W^b}{\partial X} \left(\frac{\partial\mathcal{X}}{\partial\mathcal{X}_{rig}} \frac{d\mathcal{X}_{rig}}{d\alpha_{geom}} + \frac{\partial\mathcal{X}}{\partial\mathcal{X}_b} \frac{\partial\mathcal{X}_b}{\partial\mathcal{X}_{rig}} \frac{d\mathcal{X}_{rig}}{d\alpha_{geom}} \right) \right) \right) \\
&- L \left(\frac{\partial F}{\partial I} \left(\frac{\partial I}{\partial\mathcal{X}_b} \frac{\partial\mathcal{X}_b}{\mathcal{X}_{surf}} + \frac{\partial I}{\partial\mathcal{X}_{surf}} \right) \frac{d\mathcal{X}_{surf}}{d\alpha_{geom}} + \frac{\partial F}{\partial J} \left(\frac{\partial J}{\partial\mathcal{X}_b} \frac{\partial\mathcal{X}_b}{\partial\mathcal{X}_{surf}} + \frac{\partial J}{\partial\mathcal{X}_{surf}} \right) \frac{d\mathcal{X}_{surf}}{d\alpha_{geom}} \right) \\
&+ \left[\frac{\partial\mathcal{J}_{struct}}{\partial D} + \lambda_f \frac{\partial R_f}{\partial X} \frac{\partial\mathcal{X}}{\partial D} + \lambda_s \left(I_d - F \left(\frac{\partial L}{\partial\mathcal{X}} \frac{\partial\mathcal{X}}{\partial D} + \frac{\partial L}{\partial W^b} \frac{\partial W^b}{\partial X} \frac{\partial\mathcal{X}}{\partial D} \right) \right) \right] \frac{dD}{d\alpha_{geom}} \\
&+ \left[\lambda_f \frac{\partial R_f}{\partial W} - \lambda_s F \frac{\partial L}{\partial W^b} \frac{\partial W^b}{\partial W} \right] \frac{dW}{d\alpha_{geom}}
\end{aligned} \tag{B.3}$$

$$\begin{aligned}
\frac{d\mathcal{J}_{struct}}{d\alpha_{struct}} &= \frac{\partial\mathcal{J}_{struct}}{\partial\mathcal{X}_b} \frac{d\mathcal{X}_b}{d\alpha_{struct}} \\
&+ \lambda_f \frac{\partial R_f}{\partial X} \frac{\partial\mathcal{X}}{\partial\mathcal{X}_b} \frac{d\mathcal{X}_b}{d\alpha_{struct}} \\
&+ \lambda_s \left(-F \left(\frac{\partial L}{\partial\mathcal{X}} \left(\frac{\partial\mathcal{X}}{\partial\mathcal{X}_b} \frac{d\mathcal{X}_b}{d\alpha_{struct}} + \frac{\partial\mathcal{X}}{\partial D} \frac{dD}{d\alpha_{struct}} \right) + \frac{\partial L}{\partial\mathcal{X}_b} \frac{d\mathcal{X}_b}{d\alpha_{struct}} \right. \right. \\
&\quad \left. \left. + \frac{\partial L}{\partial W^b} \frac{dW^b}{d\alpha_{struct}} \right. \right. \\
&\quad \left. \left. - L \left(\frac{\partial F}{\partial I} \left(\frac{\partial I}{\partial\mathcal{X}_b} \frac{\partial\mathcal{X}_b}{d\alpha_{struct}} + \frac{dI}{d\alpha_{struct}} \right) + \frac{\partial F}{\partial J} \left(\frac{\partial J}{\partial\mathcal{X}_b} \frac{d\mathcal{X}_b}{d\alpha} + \frac{dJ}{d\alpha_{struct}} \right) \right) \right) \right) \\
&+ \left[\frac{\partial\mathcal{J}_{struct}}{\partial D} + \lambda_f \frac{\partial R_f}{\partial\mathcal{X}} \frac{\partial\mathcal{X}}{\partial D} + \lambda_s \left(I_d - F \left(\frac{\partial L}{\partial\mathcal{X}} \frac{\partial\mathcal{X}}{\partial D} + \frac{\partial L}{\partial W^b} \frac{\partial W^b}{\partial X} \frac{\partial\mathcal{X}}{\partial D} \right) \right) \right] \frac{dD}{d\alpha_{struct}} \\
&+ \left[\lambda_f \frac{\partial R_f}{\partial W} - \lambda_s F \frac{\partial L}{\partial W^b} \frac{\partial W^b}{\partial W} \right] \frac{dW}{d\alpha_{struct}}
\end{aligned} \tag{B.4}$$

Appendix C

Wing design

The design loads are imposed to the structure to predict its behavior to preserve the integrity and the efficiency of the aircraft during the mission. Far25 specifies two kind of design loads:

- Limit loads, are the maximum loads that a structure can withstand and remains in an elastic domain. i.e no permanent deformation of the structure at limit loads (FAR sec 25.301)
- Ultimate loads, are the limits loads multiplied by a safety factor prescribed by the FAR25 (1.5 for civil aircraft and 1.20 for military aircraft). The structure must be able to support ultimate loads without failure for at least 3 seconds
- Limit maneuvering load factor for any speed up to V_{ne} (never exceed speed) must not be less than 2.5 g and need not be greater than 3.8 g (FAR sec 25.337.b)

Bibliography

- [1] Abou El Majd, Désidéri J.-A., Habbal A. *Optimisation aéro-structurale de la voilure d'un avion d'affaires par un jeu de Nash et un partage adapté des variables* INRIA Equipe-projet OPALE
- [2] Nielsen E. J., Anderson W. K. *Aerodynamic design optimization on unstructured meshes using the Navier-Stokes Equations*, AIAA-98-4809, 1998 14, 49
- [3] Anderson. M.B., *Genetic algorithms in aerospace design: Substantial progress, tremendous potential*, Technical report, Sverdrup Technology Inc. TEAS group, 260 Eglin Air Force Base, FL 32542, USA 2002
- [4] Anderson. M.B., Lawrence W.R., Lopez J.L., *Supplementing gradient search with genetic algorithm in air data estimation system*, AIAA 94 1931, Colorado Springs, CO., June 1994
- [5] Anhalt C., Monner P.H., Breitbach E. *Interdisciplinary Wing Design – Structural Aspects*, SAE International, 03WAC 29
- [6] Ardema M.D., Chambers M.C., Patron A.P., Hahn A.S., Miura H., Moore M.D., *Analytical Fuselage and Wing Weight Estimation of Transport Aircraft*, NASA Technical Memorandum 110392, May 1996 88
- [7] Ashley H., *On Making things the best Aeronautics uses of Optimization*, AIAA 81 1738R 1
- [8] Bisplinghoff R.L., Ashley H., Halfman R.L., *Principles of aeroelasticity*, 1962 50, 58

- [9] Blondeau C., Irisarri F.X., Leroy F.H., Salah El Din I., *A Bi level high fidelity Aero structural integrated design methodology*, RaeS 3rd Aircraft Structural Design Conference, october 2012 71, 103
- [10] Brezillon J., Abu Zurayk M., *Development and evaluation of the adjoint approach for aeroelastic wing optimization*, DLR, Notes on Numerical Fluid Mechanics and Multidisciplinary Design, p. 8. (Unpublished)
- [11] Brezillon J., Dwight R. P., *Aerodynamic shape optimization using the discrete adjoint of the Navier Stokes equations: Applications towards complex 3D configurations*, KATnet II Conference on Key Aerodynamic Technologies paper No.36 1, 12 14 May 2009, Bremen 21
- [12] Dwight R. P., Brezillon J., *Effect of approximations of the discrete adjoint on gradient based optimization*, AIAA Journal 44 (12)(2006) 3022 3071 49
- [13] Dwight R. P., Brezillon J., *Adjoint Algorithms for the Optimization of 3d Turbulent Configurations*, 15th STAB Symposium, 2006
- [14] Brezillon J., Brodersen O., Dwight R. P., Ronzheimer A., Wild J., *Development and application of a flexible and efficient environment for aerodynamic shape optimization* proceedings of the ONERA DLR Aerospace Symposium (ODAS), Toulouse 2006 38
- [15] Carrier G., Marcelet M., Peter J. *Sensitivity analysis of a coupled aero structural system using direct differentiation and adjoint equations* ECCOMAS CFD (2006)
- [16] Lawrence C., Zhou J.L., Tits A.L., *Users's guide for CFSQP Version 2.5: A C code for solving (Large Scale) constrained Nonlinear (Minimax) optimization problems, generating iterates, satisfying all inequality constraints*, Institute for Systems Research TR 94 16 r1 19, 102, 149
- [17] Cusdin P., Müller J D., *On the performance of discrete adjoint CFD codes using automatic differentiation*, Int J Numer Methods Fluids 2005;47(6-7):939-45 27

- [18] Agarwal S., Deb M.K., Pratap A. *Transaction on evolutionary computation* vol 6, n 2. IEEE, 2002
- [19] Pratap A., Agarwal S., Deb M.K., Meyarivan T., *A fast and Elitist Multi objective genetic algorithm NSGA II*. KanGAL, report number 2000001, 2001
- [20] Deb M.K., Zitzler E., Thiele L. *Comparison of multi objective evolutionary algorithms: Empirical results* Massachusetts Institutes of Technology, Evolutionary computation 8(2): 173 195 20
- [21] Desideri J.A., *Multiple Gradient Descent algorithm (MGDA)* research report 6953, INRIA 2009 20
- [22] Destarac D., *Far Field,Near FieldDragBalanceApplicationsofDrag Extraction in CFD*, CFD Based Aircraft Drag Prediction and Reduction, VKI Lecture Series 2003 02, von Karman Institute for Fluid Dynamics, Rhode Saint Genese, Belgium, Nov. 3-7 2003 20
- [23] Dorbath F., Nagel B., Gollnick V., *Comparison of Beam and Shell Theory for Mass Estimation in Preliminary Wing Design*, 2nd Aircraft Structural Design Conference, 26 28 October 2010 12, 147
- [24] Dumont A., *Calculs de gradients pour l'optimisation des performances aerodynamiques d'un rotor d'helicoptère en vol stationnaire*, PhD thesis, ONERA Ecole doctoral de Science et Ingenieurie en Mecanique, Energetique et Aeronautique, Universite de Poitiers 2010 88
- [25] Cambier L., Veuillot J. P., *Status of the elsA Software for Flow Simulation and Multi Disciplinary Applications*, 46th AIAA Aerospace Sciences Meeting and Exhibit, Reno, Nevada, Jan. 2008 21, 43, 44, 45, 46
- [26] Elmihoub, T., Hopgood, A. A., Nolle, L., Battersby, A., *Hybrid genetic algorithms: a review*, Engineering Letters, 13, pp. 124-137, 2006 21, 40, 41, 42, 44, 67, 71

- [27] Drullion F., *Definition et etude de systèmes lineaires pour la simulation d'écoulements et l'optimisation de formes aerodynamiques par methode de gradient*, PhD thesis, ONERA Ecole doctoral de Mathematiques et d'informatique, Université de Bordeaux I 2008
- [28] Giles M.B., Pierce N.A., *Analytic Adjoint Solutions for the Quasi One Dimensional Euler Equations*, Journal of Fluid Mechanics, Vol. 426, 2001, pp. 327–345
- [29] Giles M.B., Pierce N.A., *On the properties of solutions of the adjoint Euler equations*, 6th ICFD Conference on Numerical Methods for Fluid Dynamics, Oxford, UK, 1998 26
- [30] Giles M.B., Larson M.G., Levenstam J.M. and Suli E., *Adaptive error control for finite element approximations of the lift and drag coefficients in viscous flow*, Report NA 97 06, Oxford University Computing Laboratory, 1997 26
- [31] Giunta A. A., *Aircraft multidisciplinary design optimization using design of experiments theory and response surface modeling methods*, Ph.D dissertation, Virginia Polytechnic Institute, May 1997 27
- [32] Green N. S., *Structural Optimization of Joined Wing Beam Model with Bend Twist Coupling Using Equivalent Static Loads*, PhD thesis, Air Force Institute Of Technology 2009 6
- [33] Guillen, P., Borrel, M., Montagne, J. L. *Numerical simulation of unsteady flows using the MUSCL approach* Numerical methods for fluid dynamics III; Proceedings of the Conference, Oxford, England, Mar. 21 24, 1988 (A89 51531 22 34). Oxford, New York, Clarendon Press, Oxford University Press, 1988, p. 296 309
- [34] Hager W.W., Soonchul P. *Mathematics of computation, Global convergence of SSM for minimizing a quadratic over a sphere*, Volume 74, Number 251, Pages 1413 to 1423, S 0025 5718(04)01731 4, Article electronically published on December 30, 2004 42

- [35] Hansen N., Kern S., *Evaluating the CMA Evolution Strategy on Multimodal Test Functions*, 8th International conference on parallel problem solving from nature PPSN VIII, Proceedings, Berlin: Springer pp.282–291, 2004
- [36] Hue D., Esquieu S. *Computational Drag Prediction of the DPW4 Configuration Using the Far Field Approach*, Journal of Aircraft Vol. 48, No. 5, DOI: 10.2514/1.C031337, September–October 2011 15
- [37] Hürlimann F., *Mass estimation of transport Aircraft Wingbox structures with a CAD, CAE based multidisciplinary process*, PhD thesis, ETH Zurich 2010 147
- [38] Jameson A., Leoviriyakit K., Shankaran S., *Multi point Aero structural optimization of wings including planform variations*, AIAA paper 2007-0000, 45th AIAA/ASME, 2007 89
- [39] Sangho K., Alonso J.J., Jameson A., *Two dimensional high lift aerodynamic optimization using the continuous adjoint method*, AIAA paper 2000-4741, 8th AIAA/USAF/NASA/ISSMO, 2000
- [40] Jameson A., *Aerodynamic design via control theory*, Journal of Scientific Computing, 3:233–260, 1988. 21
- [41] Jameson A., Vasseberg J.C., Shankaran S. *Aerodynamic structural design studies of low sweep transonic wings*, Journal of Aircraft, Vol. 47, No.2, March April
- [42] Jameson A., *Aerodynamic design via control theory*, Journal of Scientific Computing 233–260, 1988
- [43] Jameson A., Pierce, N., Martinelli, L. *Optimum aerodynamic design using the Navier Stokes equations*, Theoretical and Computational Fluid Dynamics, 213–237, 1998 27
- [44] Jameson A., Kui O., *50 years of transonic aircraft design*, Progress in Aerospace Sciences, Vol. 47, No. 5, 2011, pp. 308–318. doi:10.1016/j.paerosci.2011.01.001 27

- [45] Leoviriyakit K., *Wing planform optimization via an adjoint method*, PhD thesis, Stanford University 2005
- [46] Kreisselmeier G., Steinhauser R., *Systematic control design by optimizaing a vector control index*, International Federation of active controls symposium on computer aided design of control systems, Zurich, Switzerland, August 29 31, 1979
- [47] Kroo I., *Multidisciplinary optimization methods for aircraft preliminary design*, AIAA 94 4325, 1994 93
- [48] Kroo I., *Distributed multidisciplinary design and collaborative optmization*, VKI lecture series on Optimization Methods and Tools for Multicriteria, Multidisciplinary Design November 15 19, 2004 1
- [49] Liberti L., *Introduction to Global optimization*, Lecture of Ecole Polytechnique, Palaiseau F 91128 12
- [50] Lions J.L., *Optimal control theory of systems governed by partial differential equations*, Springer Verlag, New York 1971 13
- [51] Pironneau, O., *Optimal shape design for elliptic systems*, Springer Verlag New York, 1984 23
- [52] Pham C., *Linearisation du flux visqueux des equations de Navier Stokes et de modeles de turbulence pour l'optimisation aerodynamique en turbomachines*, PhD thesis, L'Ecole National Superieure d'Arts et Metiers, Septembre 2006 23
- [53] Peery J.D., Azar J.J., *Aircraft structures*, McGraw Hill, 1950 49
- [54] Matsuzawa T., Hafez M., *Treatment of Shock Waves in Design Optimization via Adjoint Equation Approach*, AIAA Paper 98 2537, 1998 85
- [55] McNamara A., Treuille A., Popovic Z., Stam J., *Fluid control using the adjoint method*, ACM Transactions on Graphics (ACM SIGGRAPH 2004) 26

- [56] Marcellet M., Peter J., Carrier G., *Sensitivity Analysis of a Strongly Coupled Aeroelastic System Using Direct and Adjoint Methods*, 12th AIAA,ISSMO MDO, Victoria, Canada, Sep. 2008
- [57] Martins J. R. R. A., *A coupled adjoint Method for high fidelity aero structural optimization* PhD Dissertation, University of Stanford, October 2002 8
- [58] Martins J. R. R., Poon N.K. *On Structural Optimization using Constraint Aggregation*, 6th World Congress on Structural and Multidisciplinary Optimization, Rio de Janeiro 2005, Brazil 30
- [59] Marcellet M., *Etude et mise en oeuvre d'une methode d'optimisation de forme couplant simulation numerique en aerodynamique et en calcul de structure*, PhD thesis, ONERA Ecole doctoral de mecanique, ENSAM 2008 94
- [60] Auroux D., Clement J., Hermetz J., Masmoudi M., Parte Y., *Collaborative Design. Multidisciplinary Design Optimization in Computational Mechanics*, Hermes Science Publishing, ISTE Wiley, London, 2009 8, 39, 50, 58, 175
- [61] Mavriplis D., *A Discrete Adjoint Based Approach for Optimization Problems on Three Dimensional Unstructured Meshes*, AIAA 2006.0050, 2006 39
- [62] Mavris D.N., DauLaurentis D. *Methodology for examining the simultaneous impact of requirements vehicle characteristics, and technologies on military aircraft design*, ICAS Congress, 2000 48
- [63] Meheut M., Arntz A., Carrier G., *Aerodynamic Shape Optimizations of a Blended Wing Body Configuration for Several Wing Planforms*, AIAA 10.2514,6.2012 3122 29
- [64] Morrison S.A., *An Economic Analysis of Aircraft Design*, Journal of transport economics and policy, May 1984 38

- [65] Mader C. A., Martins J. R. R. A., Alonso J. J., Van der Weide E., *ADjoint: An Approach for the Rapid Development of Discrete Adjoint Solvers*, AIAA Journal, 46(4):863-873, Apr.2008-3
- [66] Mader C. A., Martins J. R. R. A., *Computation of Aircraft Stability Derivatives Using an Automatic Differentiation Adjoint Approach*, AIAA Journal, 49(12):2737-2750, 2011-27
- [67] *Using An Adjoint Approach to Eliminate Mesh Sensitivities in Computational Design*, AIAA Paper Series, Paper 2003-0272, 2003
- [68] Peter J. *Discrete adjoint method in elsA (part 1) : Method, Theory*, ODAS, Toulouse, October 2006-48
- [69] Peter E.V. J., Dwight R. P., *Numerical sensitivity analysis for aerodynamic optimization: A survey of Approaches*, Computers and Fluids 39:3, 373-391-21
- [70] Peery D. J. *Aircraft structures*, McGraw Hill Book Company, New York, 1950-21, 48, 49
- [71] Poon N. M. K., Martins J. R. R. A., *An adaptive approach to constraint aggregation using adjoint sensitivity analysis*, Journal of Structural and Multidisciplinary Optimization 34(1):61-73, July 2007-85
- [72] Renac F., *Sensitivity Analysis for the RANS Equations Coupled with Linearized Turbulence Model*, AIAA 2002-0262, 2002-92
- [73] Roux E., *Modèle de Masse Voilure*, PhD thesis, ONERA Ecole doctorale de SupAero 2006-21, 49
- [74] Salah El Din I., Carrier G., Mouton S., *Discrete Adjoint Method in elsA (part 2): Application to Aerodynamic Design Optimisation.*, 7th ONERA DLR Aerospace Symposium, ODAS 2006-88

- [75] Sobieszczanski Sobieski J., *Bi Level Integrated System Synthesis*, 7th AIAA,USAF,NASA,ISSMO Symposium on multidisciplinary analysis and optimization, St Louis, September 2 4 1998
- [76] Sobieszczanski Sobieski J., *Structural shape optimization in multidisciplinary system synthesis*, NASA Technical Memorandum 100538, 1988 12, 71
- [77] Sobieszczanski Sobieski J., *Sensitivity analysis and multidisciplinary optimization for aircraft design: Recent advances and result*, NASA Technical Memorandum 100630, 1988
- [78] Sobieszczanski Sobieski J., *Sensitivity of complex, internally coupled systems*, AIAA paper 88 2378
- [79] Sobieszczanski Sobieski J., *Overcoming the Bellman's "Curse of Dimensionality" in large optimization problems*, NASA Technica Memorandum 102662, April 1990 21, 38
- [80] Taasan, S., Kuruvila, G., Salas, M.D., *Aerodynamic design and optimization in one shot*, AIAA Paper 91 005, 1992
- [81] Thevenin D., Janiga G., *Optimization and Computational Fluid Dynamics*, 2008 Springer Verlag Berlin Heidelberg 27
- [82] Van der Vooren, J., and Destarac, D., *Drag,Thrust Analysis of Jet Propelled Transonic Transport Aircraft; Definition of Physical Drag Components*, Aerospace Science and Technology, Vol. 8, No. 6,Sept. 2004, pp. 545–556. doi:10.1016/j.ast.2004.03.004 4
- [83] Vanderplaats G.N., Sugimoto H., *A general purpose optimization program for engineering design*, Computer & Structures, vol.24, 1986 147
- [84] Vanderplaats G.N., *DOT Users Manual, Version*, Vanderplaats Research and Development, Inc., Colorado Springs, CO, 1995.4.20 15, 149

- [85] Van der Velden A., Kelm R., Kokan D., Mertens J., *Application of MDO to a large subsonic transport aircraft*, AIAA 2000 0844, 200 149
- [86] *Response Surface Methods for High Dimensional Structural Design Problems*, PhD thesis, University of Florida, 2000 89
- [87] Wiart L., Carrier G., *Accounting for wing flexibility in the aerodynamic calculation of transport aircraft using equivalent beam model*, AIAA paper 2010 9135, 13th AIAA,ISSMO, 2010
- [88] Wervaecke, C., *Hybrid stochastic gradient based method for aerodynamic shape optimization*, ONERA Technical Report, RT 2,16642 DAAP, August 2012
- [89] G. A. Wrenn, *An Indirect Method for Numerical Optimization Using the Kreiselmeier Steinhauser Function*, Technical report CR 4220, NASA, 1989 15
- [90] Marcelet M., Peter J., Carrier G., *Sensitivity analysis of a coupled aero structural system using direct differentiation and adjoint method*, ECCOMAS CFD 2006. 105
- [91] Bompard M., Renac F., Peter J., Desideri J. A., Dumont A. *Two Dimensional Aerodynamic Optimization Using the Discrete Adjoint Method with and without Parameterization*, AIAA paper to appear in 2011 8
- [92] Brezillon J., Dwight R.P., Wild J., *Numerical aerodynamic optimization of 3D high lift configurations*, 26th ICAS Congress
- [93] Destarac D., Reneaux J., *Transport aircraft aerodynamic improvement by numerical optimization*, ICAS Congress, Septembre 9-14, 1990
- [94] Martins J. R. R., Poon N.K. *On Structural Optimization using Constraint Aggregation*, 6th World Congress on Structural and Multidisciplinary Optimization, May June, Brazil
- [95] Herencia1 J.E., Weaver P.M., Friswel M.I., *Morphing wing design via aeroelastic tailoring*, AIAA paper 2007 2214, 48th AIAA,ISSMO, 2007 94

- [96] Guo S., *Aeroelastic optimization of an aerobatic aircraft wing structure*, Aerospace Science and Technology 11 (2007) 396 404
- [97] Maute K., Nikbay M., Farhat C., *Sensitivity analysis and design optimization of three dimensional non linear aeroelastic system by the adjoint method*, Int. J. Numer. Meth. Engng 2003; 56:911 933
- [98] Jansen P.W., Perez R.E., Martins J.A., *Aerostructural optimization of nonplanar lifting surfaces*, Journal of Aircraft, Vol. 47, No.5, September October 2010
- [99] Carrese R., Winarto H., Watmuff J., Wickramasinghe K., *Benefits of Incorporating Designer Preferences within a multiobjective Airfoil Design Framework*, Journal of Aircraft, Vol. 48, No.3, May June 2011
- [100] Wunderlich T. F., *Multidisciplinary Wing Design and optimization for transport aircraft*, DLR, September 22, 2008
- [101] Schuhmacher G., Murra I., Wang L., Laxander A., Leary O., Herold M., *Multidisciplinary Design Optimization of a Regional Aircraft Wing Box*, AIAA paper 2002 5406,9th AIAA,ISSMO, 2002
- [102] Nagel B., Kintscher M., Streit T., *Active and passive structural measures for aeroelastic winglet design*, 26th International congress of the aeronautical sciences 2008.
- [103] Kriz R., *A Sailplane Wing Constructed of Foam Core and Polyester fiberGlass Skin*, AIAA paper 74 258,10th AIAA, 1974
- [104] Petermeier J., Radtke G., Stohr M., Woodland Aaron, Talahashi T. T., Donovan S., Shubert M., *Enhanced conceptual wing weight estimation through structural optimization and simulation*, AIAA paper 2010 9075,13th AIAA,ISSMO, 2010
- [105] Falco S. A., Rocha de Faria A., *Optimization of a simple aircraft wing*, Worldwide Aerospace Conference and Technology Showcase, April 8-10 2002
- [106] G. A. Wrenn, *An indirect method for numerical optimization using the kreiselmeir Steinhauser function*, Technical report CR 4220, NASA, 1989

- [107] Verstraete T., *Introduction to optimization and multidisciplinary Design*, VKI, lecture Series 2010 07 93
- [108] McNamara A., Treuille A., Popović Z., Stam J., *Fluid control using the adjoint method*, ACM Transactions on Graphics, ACM SIGGRAPH 2004
- [109] Zhou A., Qu B.Y., Li H., Zhao S Z., Suganthan P.N., Zhang Q., *Multiobjective evolutionary algorithms: A survey of the state of the art*, REMN 17,2008. Shape design in aerodynamics, pages 103 126 28
- [110] Zingg D.W., Nemec D., Pulliam T.H., *A comparative evaluation of genetic and gradient based algorithms applied to aerodynamic optimization*, REMN 17,2008. Shape design in aerodynamics, pages 103 126 20

20